The University Of Sheffield.

DEVELOPMENT OF A NOVEL FUNCTIONALLY GRADED GUIDED TISSUE REGENERATIVE MEMBRANE FOR PERIODONTAL LESIONS

Syed Saad Bin Qasim

Submitted for the degree of Doctor of Philosophy

Department of Materials Science and Engineering

2012-2015

Acknowledgements

It gives me immense pleasure to thank the many people who made this thesis possible. Firstly all praise to Almighty Allah (S.W.T) for the countless blessings. I find it difficult to overstate my appreciation yet again to my PhD Supervisor, Dr Ihtesham Ur Rehman. With his inspiration and enthusiasm to explain things clearly, he guided me to make biomaterials interesting and at the same time fun for me. I would have been lost without him. I would also like to extend my gratitude to Prof. Andrew Rawlinson my second supervisor for his interest, faith and constant guidance he provided throughout the course of my degree.

I am deeply indebted to my doctoral colleagues, especially Ceyla, Abdullah, Ahtasham, Peyman, Salman, Munira, Leyla, Ni Armah, Nadir, Sabi, Robin, Mai, Gifty, Lindsey, Tom, Colin, Hammad and all other masters and undergraduate students that helped me throughout my time at the University as a graduate student.

Special thanks to the people who trained me on various machines, specifically, David James for Raman and FTIR Spectroscopy, Chris J Hill for Scanning electron microscopy training and Pete and Ben for UV-Vis spectroscopy training. I would also like to thank our collaborators Dr Tobias Fey (Erlangen University, Germany) for conducting µCT and Dr Maksym Pogorielov (Sumy State University, Ukraine) for in-*vivo* study.

I am grateful to the University of Sheffield, Materials Science and Engineering Department for awarding me partial funding and the learned society for awarding me travel grants to be able to attend conferences.

I also wish to thank my entire family and friends for all the prayers they made for me during this tenure. My wife Sana, daughter Mahdiya have been instrumental in keeping me motivated, and my extended family members, especially my sister, brothers, sister-in-law, brother-in-law, mother and father-in-law who have prayed for me throughout this journey.

Lastly, and most importantly, I wish to thank my parents, Syed Qasim Ali Rizvi and Shehla Qasim Rizvi. They raised me, supported me, taught me, prayed for me during hard times and loved me. To them I owe my entire life.

Syed Saad Bin Qasim

Dedication

Dedicated to the one, Almighty Allah (S.W.T)

My Parents, Syed Qasim Ali Rizvi and Shehla Qasim Rizvi

My Wife Sana Tahir and our loving Daughter Mahdiya Binte Saad

and

The lives of the family members we lost (2012-2015)

Abstract

Periodontal diseases are chronic inflammatory conditions affecting the supporting tissues of teeth caused by the prolonged accumulation of micro-organisms in the biofilm that forms on tooth surfaces. Conventional non-surgical and surgical treatments aim to halt disease progression and repair the lost periodontal tissues. Surgical therapies such as open flap debridement are aimed to replace the lost alveolar bone and guided tissue regeneration (GTR) is also used to treat this disease. Whilst the regeneration of lost support is an aim of periodontal treatment, the outcomes of current approaches to periodontal regeneration (PR) are unpredictable. Consequently, significant laboratory and clinical research has been undertaken to explore the possibilities of improving the outcomes of treatment over the past few decades. In this respect chitosan (CH), a well-known biopolymer holds promise to be fabricated in various forms. The aim of the project was to fabricate a trilayered functionally graded GTR membrane by fabricating surface and core layers of non-porous and porous morphologies with complete physiochemical and biological characterisation. Solvent Casting, Freeze gelation (FG) and Electrospinning was performed on CH alone and in combination with Hydroxyapatite (HA). Membranes were characterized with Scanning electron Microscopy, Fourier Transform Infrared Spectroscopy (FTIR), tensile testing, long term degradation and swelling studies were also performed. Cell culturing was performed using human osteosarcoma and progenitor cell line. Sirius red and Alizarin red assays were conducted to assess matrix deposition. Amongst the non-porous membranes fabricated by solvent casting, with Low molecular weight (LMw) CH:HA ratio of 30:70 showed better biocompatibility, and amongst the porous membranes made up of FG, ASa (ascorbic acid) :CH:HA (50:50) showed better stability and biocompatibility after in-*vitro* analysis. Histology of FG membranes conducted after in-*vivo* studies showed ASa:CH:HA to have higher cellular infiltration after 30 days of implantation. Electrospun fibres obtained in both aligned and random orientations were conducive to cellular attachment and mineralized matrix deposition with time. FTIR analysis showed strong co-ordination bond formation in between CH and HA. HA incorporated samples treated with simulated body fluid (SBF) showed an embryonic layer formation of hydroxyl carbonated apatite. Membranes can be combined together in different ways to achieve structural and functionally graded structures. A template was prepared using solvent casting and freeze gelation techniques to achieve functional gradients. Furthermore; CH and HA composite membranes could possibly be used for GTR applications in periodontal lesions and in addition these techniques could be further tuned to achieve desirable characteristics of a GTR membrane for PR and also holds promise to be used in other biomedical applications.

Abbreviations

%	Percentage
^{o}C	Degree Celsius
µm	Micrometre
µCT	Micro computerized tomography
µg	Micrograms
a.u.	Arbitrary units
3D	Three dimensional
ASa	Ascorbic acid
ACa	Acetic acid
AR	Alizarin Red
ATR	Attenuated total reflectance
CH	Chitosan
conc	Concentration
DiH_2O	Distilled water
DD	Degree of deacetylation
Eq	Equation
EtOH	Ethanol
FCS	Foetal calf serum
FG	Freeze gelated
Fgr	Functionally graded
FTIR	Fourier transform infrared spectroscopy
gm or g	Gram
GTR	Guided tissue regeneration
GPa	Gigapascal
HA	Hydroxyapatite
H&E	Hematoxylin and eosin
hrs	Hours
hES-MP	Human embryonic stem cell derived mesenchymal progenitor cell
hPDL	Human periodontal ligament
MSCs	Mesenchymal stem cells
LMw	Low molecular weight
mg	Milligram
mm	Millimeter

MPa Megapascal

MG63's Human osteosarcoma cell line

MMw Medium molecular weight

Mw Molecular weight

min Minutes

MIC Minimum inhibitory concentration

nm Nanometres

NaTPP Sodium tripolyphosphate

Na Sodium

-OH Hydroxyl

PO_4 Phosphate

PAS Photoacoustic sampling

PBS Phosphate buffered saline

PCL Polycaprolactone

PDL Periodontal ligaments

pH Potentiometirc hydrogen ion concentration

PGA Polyglycolic acid

PLA Polylactic acid

PTFE Polytetra fluoroethylene

PU Polyurethane

PVA Polyvinyl alcohol

SEM Scanning electron microscopy

SR Sirius red

TCY Tetracycline hydrochloride

TCP Tri calcium phosphate

TGA Thermogravimetric analysis

UHMWPEO Ultrahigh molecular weight polyethylene oxide

UV-Vis Ultra-violet visible spectroscopy

XRD X-ray diffraction

Publications

Qasim S. B, Delaine-Smith R, Fey T, Rawlinson A, Rehman I.U Freeze gelated porous membranes for periodontal tissue regeneration Acta Biomaterialia, 2015, 23:317-328 doi:10.1016/j.actbio.2015.05.001

Presentations and Published abstracts

1. 23rd Annual British Society of Oral and Dental Research Symposium in Bath Spa, Bath, United Kingdom, "A bioactive functionally graded Guided tissue regeneration membrane" Reference No. 0047: http://www.bsodr.org.uk/meetings/bath-2013/BSODR_Program_Book_30.08.13.pdf 9th to 11th September 2013

2. Presented oral Presentation at University of Sheffield Engineering Symposium 2014 (USES) Periodontal treatments using a novel functionally graded guided tissue regenerative (GTR) membranehttp://eprints.whiterose.ac.uk/85056/, 24th June 2014

3. European Society of Biomaterials Annual Conference in Liverpool 2014, on "Development of a novel Guided tissue regenerative membrane" Abstract code 818, Session Dental biomaterials II, 31st August to 3rd September 2014

4. Poster presentation at Sir Harry Kroto Annual Visit 2014 and oral presentation in 2013

5. Electronic Poster / Oral Presentation 8th Annual conference of European Periodontology (EuroPerio8) Excel Centre, 3rd to 6th June 2015,London. DOI: 10.1111/jcpe.12398

Awards

1. Learned Society of University of Sheffield awards for Travel Grants amount £350(2013), £250 (2014) and £250 (2015)

2. Awarded "Partial support for PhD students abroad" by Higher education commission (HEC) of Pakistan funding for 3rd year of PhD (FEES).

3. Travel Grants by Armours and Brasiers Gauntlet Trust Award for £570.(2015)

Manuscripts in Process

Qasim S. B, Delaine-Smith R, Fey T, Rawlinson A, Rehman I.U Electrospinning chitosan for periodontal tissue regeneration (in preparation)

Qasim S. B, Delaine-Smith R, Rawlinson A, Rehman I.U Chitosan Hydroxyapatite membranes for use as Guided tissue regeneration (in preparation)

Qasim S. B, Rawlinson A, Rehman I.U, Bioactivity potential of Freeze gelated Chitosan hydroxyapatite membranes (in preparation)

Qasim S. B, Rawlinson A, Rehman I.U In-vitro and in-vivo degradation of Porous freeze gelated chitosan hydroxyapatite membranes (in preparation)

TABLE OF CONTENTS

FIGURES

TABLES

1. Chapter. Introduction

1.1. Research Design

The need to understand the concepts of tissue engineering and regenerative medicine in dental biomaterials is becoming more essential as the aging population increases each day. A significant rise has been seen in the amount of surgical and restorative procedures concerning complete or partial oral rehabilitation with dental implants, fixed crowns and bridges. Among the many other clinical procedures adapted for oral rehabilitation is periodontal regeneration. The procedure requires the use of a membrane, gel or powder for guided bone / tissue regeneration (GBR/GTR). The need for using a GTR or GBR agent occurs when an oral condition called periodontitis becomes chronic and progresses to such an extent that the supporting tissues of the teeth become compromised, eventually resulting in tooth loss. Periodontitis affects more than 11 to 15 % of the population worldwide (Preshaw *et al.* 2012). Severe periodontitis was the sixth most prevalent condition in the world between 1990 and 2010. Due to the growing world population there is a predictable increment in the incidence of periodontitis, specially seen with gradual increase in age between the third and fourth decades of life with a peak incidence at around 38 years of age (Kassebaum *et al.* 2014). The majority of treatments provided for the management of periodontitis involve non-surgical root surface debridement and occasionally surgical exposure of tissues to gain access to the sub gingival area. GTR functions to prevent the gingival epithelial cells from migrating down to the root surface and allowing undifferentiated mesenchymal cells in the periodontal ligament migrating to the root surface and differentiating into cells capable of forming new cementum, periodontal ligament and alveolar bone. Although GTR membranes invented earlier were non resorbable, there are now a variety of resorbable membranes available commercially offering the advantage of not having to be removed following complete healing. Currently available regenerative membranes have shown promising results, however there are certain limitations, which hinder complete regeneration (Hughes *et al.* 2010). The search for an ideal membrane continues and it has been suggested that the next generation of GTR membrane lies in functionally graded biomaterials which mimics closely the native extracellular matrix (ECM) (Bottino *et al.* 2012).

1.2. Periodontal Tissues

The word periodontium is derived from a Greek background (perio meaning around and odonto meaning tooth). The periodontium anchors teeth to both the maxilla and mandible, provides nourishment to teeth and preserves their position inside the alveolar socket. It is an

intricate system of tissues supporting and investing the tooth, comprising of gingiva facing the tooth (dentogingival junction), cementum, alveolar bone lining the tooth socket and periodontal ligament (PDL). Additionally the periodontium assures proper function along with distribution of forces evenly by preventing injury to teeth, mandible and maxilla. The gingiva is part of the oral mucosa that surrounds the cervical region of a tooth. When healthy, it is firm, knife edged and pink in colour. The dentogingival junction is comprised of epithelial and connective tissue components. The epithelium is further classified into three functional compartments gingival, sulcular and junctional epithelium (Newman *et al.* 2012). Cementum is the hard avascular mineralized mesenchymal connective tissue that surrounds the root of the tooth. Its primary purpose is to attach and invest principal periodontal ligament fibres. Cementum is classified into two types, cellular and acellular. The periodontal ligament (PDL) occupies the space in between the tooth root and alveolar socket which is housing the tooth. The PDL acts as a shock absorber and fibres are inserted into the cementum of the tooth root on one side and lamina dura of the bone on the other side. Being a dense fibrous network surrounding the teeth they are highly vascular and highly cellular exhibiting a rapid turnover rate. PDL fibres are also responsible for bearing the occlusal forces and in addition the PDL has the tendency to act as sensory receptor necessary for the proper positioning of the jaw during mastication. The alveolar process is part of the mandible containing alveolar sockets (alveoli). The bone lining the socket is called bundle bone, since it is responsible for attaching the periodontal ligament fibre bundle (Nanci and Bosshardt 2006).

1.3. Periodontal disease and treatment options

The accumulation of plaque and tartar for prolonged and untreated time periods results in inflammation of the gingival tissues, commonly known as gingivitis. It is an inflammatory response of gingiva which does not destroy the supporting structures. It is a mild form of periodontal diseases, but if left untreated, can eventually become periodontitis which is more destructive. Gingivitis is a reversible condition if good oral hygiene measures are adopted immediately. This inflammatory condition starts superficially around the gingival tissue and progresses to involve the periodontium. Clinically disease is characterized by the formation of a periodontal pocket between the tooth and gingiva, and with time may lead to tooth mobility as the pocket depth increase, then drifting and eventually tooth loss. The breakdown of the periodontal ligament and formation of a periodontal pocket is an unpredictable event. Pocketing cannot be detected on visual inspection, and examining it with a periodontal probe is essential (Preshaw *et al.* 2012). Consequently, if left untreated, this

process will result in considerable loss of tissue structure and function. Being asymptomatic and not usually painful patients may remain unaware. Chronic stages of the disease can give rise to a periodontal abscess that can compromise patient's general health (Pihlstrom *et al.* 2005). While the progression of periodontal disease usually occurs over time, there is reported evidence of acute exacerbations where rapid periodontal breakdown may also occur, following long intervals of non-progressing quiescent lesions. Periodontal treatments during early stage disease revolve around professional removal of plaque and calculus. When pockets become deeper surgical techniques of debridement may be required for the treatment of pockets that do not resolve following non-surgical treatment. Non-surgical treatment may include scaling, root surface debridement and the advice on plaque removal. In aggressive periodontitis and some cases of refractory disease, systemic antibiotics may also be prescribed as an adjunct to root surface debridement. Success in treatment is usually dependant on patient's commitment to maintain high standards of oral hygiene to reduce bacterial recolonization. If the condition is left untreated bone resorption with increasing pocket depth will occur making the tooth mobile and then eventually leading to tooth loss. If periodontal pockets do not heal after scaling and root surface debridement, surgical treatment methods may be undertaken to gain direct access to the diseased root surface and to remove diseases gingival tissues. Periodontal healing starts by tissue shrinkage, fibrosis and some bone remodelling, but without any appreciable coronal regeneration of the lost tissue present. Surgical options currently available allow the placement of, bone replacement materials, biologically active agents and GTR membranes. GTR materials include both bioresorbable to non-resorbable membranes. Artificial bone substitutes may be made up of a variety of material including hydroxyapatite (HA). Most of the membranes act as a physical barrier to prevent epithelial tissue and connective tissue down growth into the defect in order to encourage regeneration of new PDL, cementum and bone (Ramseier *et al.* 2012).

1.4. Chitosan

Chitosan (CH) has been used in a number of biomedical applications and now its use for tissue repair in regeneration has shown promising results in the biomedical industry (Abbas 2010; Jayakumar *et al.* 2010). Its discovery has revolutionized the field of tissue engineering and regenerative medicine. Properties such as biodegradability, mechanical strength and cell affinity can be tuned by chemical modifications such as cross linking. It can also be used as a delivery system of various bioactive molecules such as growth factors, DNA, siRNA and pharmaceutical combinations of drugs. CH has been found to have an enhanced effect on

tissue engineering process due to the polycationic nature that increases cellular attraction to the polymer (Liu *et al.* 2011).

1.5. Hydroxyapatite

The use of bioceramics both alone and in combination with polymers as a composite material has revolutionized the fields of biomaterials, tissue engineering and regenerative medicine. Some of the typically used bioceramics which are widely researched are hydroxyapatite (HA) Bioglass™ (BG), apatite-wollastonite (A-W) ceramic and glasses. HA [Ca_{10} $(PO_4)_6$ $(OH)_2$] is the main constituent of hard tissues, abundantly present in teeth and bone matrix (Rehman and Bonfield 1997). It is well known for its biocompatibility, ability to encourage osteoconduction and it exhibits bioactive properties, by readily encouraging the formation of a carbonated hydroxyapatite layer and promoting biological fixation (Zakaria *et al.* 2013). A number of techniques have been adapted to synthesize HA such as, sol-gel, hydrothermal, wet precipitation, microwave synthesis and continuous flow method. The size, morphology, shape and other chemical and physical properties of HA can be altered to suit the final application (Zakaria *et al.* 2013).

1.6. Growth factors

Intensive studies on the effect of growth factors on periodontal complex have shown that these bioactive molecules do affect the regeneration potential of the periodontium. The key to success in periodontal regeneration lies in accurate interaction between scaffold materials and other key elements such as blood supply, growth factors and cells. Platelet derived growth factor is the first licensed growth factor to be used in periodontal regenerative applications. It is naturally produced by the body at sites of soft tissue and bone injury (Lynch *et al.* 1991). It is a member of multifunctional polypeptide family that binds to two cell membrane tyrosine kinase receptors; stimulating cell proliferation, migration, extracellular matrix synthesis and anti-apoptosis (Nevins *et al.* 2005). In addition to these, it also initiates the formation of periodontal apparatus, PDL, alveolar bone and cementum (Ramseier *et al.* 2012). Moreover in-*vivo* applications of platelet derived growth factor alone or in combination therapy with others factors or antimicrobial drugs results in partial regeneration of periodontal tissues. Increase in clinical attachment gain and advance alveolar bone repair have been reported (Kaigler *et al.* 2011).

1.7. Drug therapy for periodontal wound healing

A key factor to enhance periodontal regeneration is by controlling and reducing bacterial contamination of the periodontal lesion. Treatment of periodontal infections with antibiotics is very different from the treatment of most bacterial infections (Ana Pejčić *et al.* 2010). The pathogenic flora within the gingival sulcus which later deepens to become a periodontal pocket is different from that of the supra gingival microenvironment as it contains more anaerobes. The use of antibiotics for treating periodontal diseases is sometimes necessary. Lately they have been refined for use as local delivery products aimed specifically at treating isolated periodontal pockets (Walker and Karpinia 2002). The choice of antibiotics may be based on the microbiological analysis of the infected site. Systemic antibiotics available for treating periodontal lesions include tetracycline, doxycycline, metronidazole, penicillin (amoxicillin with or without clavulanic acid), macrolides (azithromycin, erythromycin, sipramycin), clindamycin, ciprofloxacin and different combination of these drugs (Seymour and Heasman 1995; Herrera *et al.* 2002; Buchmann *et al.* 2010). Besides these drugs chlorhexidine has also been used as an effective antimicrobial agent (Cosyn and Sabzevar 2005). Systemically administered antibiotics can reach microorganisms that are inaccessible to instrumentation or even local antibiotics therapy. Controlled and sustained drug release could clearly provide an improvement in the treatment of periodontal infections with GTR procedures, only if a therapeutically effective concentration of an antimicrobial agent could be maintained in the periodontal pocket and around the defect for the desired length of time (Roskos *et al.* 1995).

1.8. Summary

The regeneration of periodontal tissue has been investigated through the use of numerous polymers, ceramics and their composite biomaterials. The use of chitosan and Hydroxyapatite composites has also been explored and the possibilities of successful periodontal regeneration are evident from the past literature. Although these composites templates have proven to be satisfactory for periodontal regeneration, certain specific biofunctional challenges still exist that hinder complete and true periodontal regeneration. These challenges include the complete recreation of the complex hierarchical structure of a cellular cementum and simultaneous regeneration of periodontal tissues and alveolar bone both structurally and functionally. Drawbacks of the existing treatment procedures focus on repair and very little true regeneration tends to occur. Hence, in order to achieve successful regeneration of the most complex tissue of human body a functionally graded approach needs to be developed.

2. Chapter. Literature review

2.1. Periodontium

The periodontium or the periodontal apparatus is part of the oral cavity which provides support to teeth by attaching them to the jaw bone and maintaining functional integrity of the oral mucosa. It is essential to understand basic anatomy of the mucogingival complex to have a better perspective of the pathogenic process and treatment modalities available when dealing with periodontal problems. The structure is made up of four essential components; gingiva, cementum, periodontal ligaments and alveolar bone (Newman 2012).

2.1.1. Gingiva

Gingiva or gums are part of oral mucosa that covers the bone supporting teeth and cervical segment of tooth. It's shape is dependent on the eruption pattern of teeth. The dentogingival complex is present in between tooth and oral mucosa; it is the only form of attachment between hard and soft tissues that is exposed to outer environment. In a healthy individual, gingiva is firm, knife edged and pink in colour. However, its colour is dependent on presence or absence of a pigment called melanin, present in epithelium. The concentration of melanin governs the lightness or darkness of oral mucosa. The keratinization and fibrosity of underlying connective tissue also regulate colour changes in melanin. Gingiva has been divided in two zones, namely marginal and attached gingiva. The part of gums which forms a cuff around tooth which can be easily separated by insertion of a periodontal probe for measuring the depth of periodontal pocket is known as marginal or free gingiva. While on the contrary attached gingival tissue holds firmly to underlying bone and is more apically positioned. Another key landmark is "mucogingival junction", it is this point, where attached gingiva is continuous with alveolar mucosa. Part of gum present in between two teeth is called Interdental gingiva. This Interdental gingiva bridges lingual and facial gingival parts. Most of the debris and food particles accumulate this part and it is a site for bacterial stagnation and initial gingival lesion. Dominant cells that play a vital role in initial healing of gingival lesions include Langerhans cells, Merkels cells and other inflammatory cells which are present in abundance in gingival epithelium. Among all this, there is another essential landmark; arrangement of gingival fibres meant for maintaining integrity of oral mucosa, besides keeping the gingival margin around the neck of the tooth (Newman 2012).

2.1.2. Periodontal ligaments (PDL)

The periodontal ligament is inserted into cementum of tooth root on one side and into the lamina dura of bone on opposite side (Figure 1). There are certain vital functions performed by the PDL, such as neurological control of jaw movements during mastication is aided by feedback from mechanoreceptors located in the PDL, alveolar bone and cementum maintenance and resisting occlusal forces by acting as a shock absorber. Fibres include, sharpy's fibres, alveolar crest fibres, horizontal fibres, apical fibres, inter-radicular fibres and oblique fibres. Most of these fibres are collagen based, but the PDL also contains oxytalan fibres which run parallel to the root surface and occasionally insert into the cementum. They form a meshwork of interconnected fibres rather than a stretch cable like form. Another group of transeptal fibres are able to reconstruct even after destruction of alveolar bone following a periodontal disease. Alveolar crest fibres prevent extrusion of the tooth and resist lateral tooth movement. The width of the PDL varies from 0.15 to 0.38mm. Similar to all other soft fibrous connective tissues, the PDL consist of fibrous stroma in a gel of ground substance made up of cells, blood vessels and nerves (Newman 2012).

2.1.3. Alveolar bone

The most dynamic and diverse tissue present in the human body is bone. It serves as a major structural support system for the whole body. Alveolar bone functions to protect and support teeth (Figure 1). It is divided in two components, namely cortical (compact) bone and cancellous (spongy or trabecullar) bone. Bone remodels with age and there is substantial variation in the morphology of the alveolar bone among individuals. These changes may be in size, shape and thickness of the cortical bone in the same jaw at different locations. Dominant bone cells present for synthesis of bone are called as osteoblasts and osteocytes are responsible for bone maintenance and osteoclasts for bone resorption. Mature osteoblasts are called as osteocytes. There is a constant remodelling phenomenon going on as a result of the mechanical stresses acting (Palumbo 2011). There is a gradual resorption phenomenon in areas of the mouth where teeth are missing, due to the absence of mechanical stimuli. Alveolar bone serves as a calcium and other mineral reservoir in addition to protecting the tooth in its socket (Newman 2012). Extracellular matrix or ECM is a major building block of bone and is composed of a non-mineralized organic component mainly collagen type I fibrils and a mineralized inorganic component of bone which is made up of carbonated apatite. 90% of the total protein in bone is comprised of collagen. The light weight nature of bone is due to the collagen fibres organization being highly ordered. Cancellous bone has about 50-90%

porosity and it makes up 20% of the total bone volume. Cortical bone on the other hand is a highly ordered network of collagen fibres structured into concentric sheets (Mikos *et al.* 2006).

2.1.4. Bone tissue engineering (BTE)

Bone tissue engineering revolves around a clear understanding of the bone ultra-structure, tissue formation and bone mechano-biology. Bone undergoes constant cycles of renewal and resorption, chemical exchange and structural remodeling due to external mechanical demands and internal mediators. There are different key factors involved for successful bone tissue engineering, which include, using a biocompatible scaffold that ideally mimics the natural extracellular matrix and osteogenic cells to lay down bone tissue matrix (Figure 1). The scaffold must allow sufficient vascularization to meet the growing tissue nutrient supply and clearance needs. The use of biocompatible scaffolds in the form of bone replacing substitutes is either played by calcium phosphate ceramic or synthetic polymer ceramic composite scaffolds. Hydroxyapatite (HA) is one such ceramic which has been extensively studied for use in the field of biomaterials and TE (Burg *et al.* 2000; Tetteh *et al.* 2014). Figure 1 shows the important anatomical landmarks of a tooth and its supporting structures. Regeneration may be possible using ideal scaffolds, cell types and signaling molecules as cues for enhancing regeneration of the lost supporting tissue.

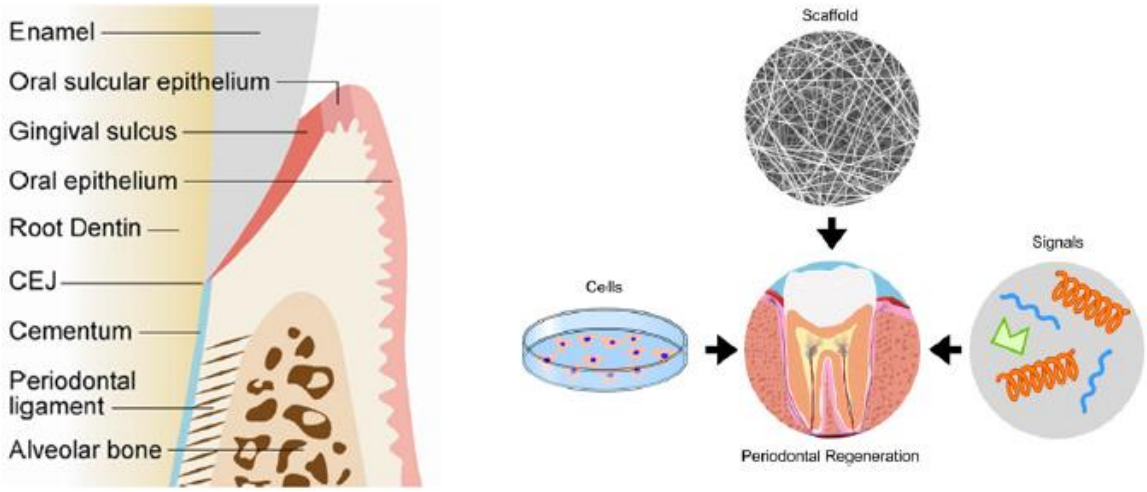

Figure 1: Schematic diagram of a longitudinal section through the periodontal tissues and gingival third of the tooth and the three major components which help guide tissue or bone regeneration in periodontal tissues. Image adapted with kind permission from Elsevier (Bottino *et al* 2012).

2.1.4. Cementum

Cementum is the mineralized connective tissue that covers the root of the teeth in which periodontal fibres are inserted (Figure 1). Similar to the cells in alveolar bone, cells of cementum are called as cementoblasts for synthesis and cementocyte for maintenance and cementoclast for resorption of cementum. It is classified in two parts; acellular and cellular cementum. Except for apical third which is covered by cellular cementum, rest of the entire root is covered by acellular cementum (Palumbo 2011; Newman 2012).

2.2. Periodontal diseases

Periodontal diseases are highly prevalent affecting almost 90% of the population worldwide (Pihlstrom 2005). Any inherited or acquired disorder of the tissue surrounding and supporting the teeth (periodontium) can be defined as a periodontal disease. This disease can be developmental, inflammatory, neoplastic, genetic, traumatic or metabolic origin. However, periodontal disease usually refers to common inflammatory conditions of gingival and periodontal tissues. These inflammatory conditions are caused by pathogenic microflora in the biofilm or dental plaque (Palumbo 2011). Chronic periodontitis exhibits complex interactions between the microbial factors and susceptible hosts. Bacterial agents such as lipolysaccharides and cytokines trigger macrophages to synthesize cytokines such as interleukin-1 (IL-1) and tumour necrosis factor (TNF). These cytokines further activate the fibroblasts present in the periodontal tissue to produce matrix metalloproteinase (MMP's), a plasminogen activator which activates plasmin, which in turn activates other types of latent MMP's. Among susceptible individuals the prolonged and excessive bacterial promotion of MMP's induces enhanced degradation of collagen, which is the primary component of periodontal matrix. MMP's 8, 9 and 13 are responsible for destruction of the periodontium and bone resorption by degrading the collagenous matrix of bone once it is demineralized by osteoclasts (Lee *et al.* 2004).

2.2.1. Gingivitis

Gingivitis is the mildest form of periodontal disease. It is the inflammation of the gingival tissue significantly variable with age. This initial stage of periodontal disease is reversible if simple and effective oral hygiene measures are adapted. These measures are daily plaque removal and regular visits to dental hygienists for scaling or polishing when necessary. If left untreated clinical symptoms will show redness around marginal gingiva initially, followed by bleeding on tooth brushing, later on changes in the contour and colour of gingiva are also features of plaque induced gingivitis (Pihlstrom 2005). Gingival inflammation has also been

correlated as a manifestation of systemic disease and shown to have links with heart disorders as well. Periodontal and cardiovascular diseases (CVD) share quite a few common risk factors such as smoking, gender, age, diabetes and behavioural factors, however, the relative risk of CVD has been quoted as being doubled in patients with periodontal diseases (Kinane and Marshall 2001).

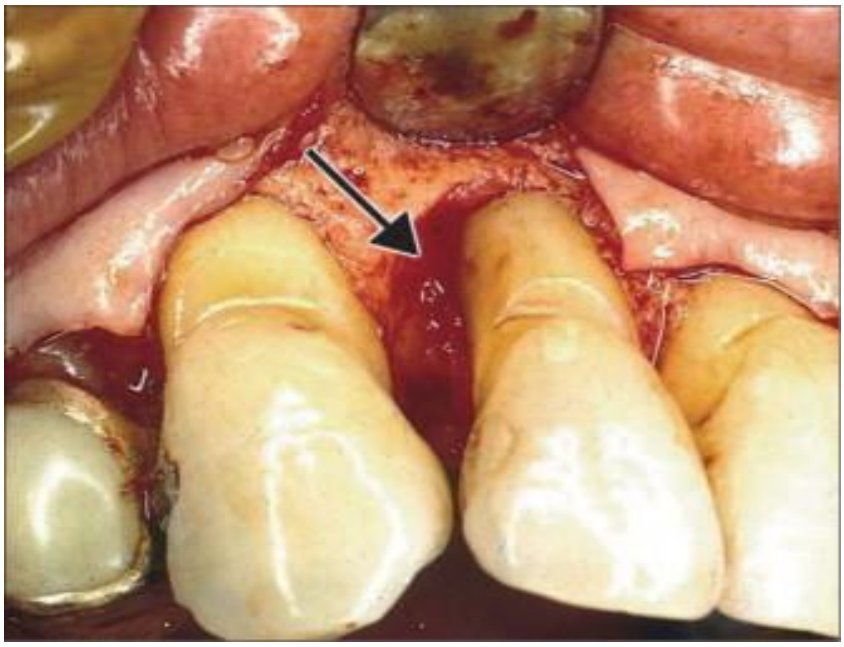

Figure 2: Maxillary Anterior segment, surgically exposed to show the bone loss due to periodontitis, arrow pointing towards the apical root showing excessive bone resorption. Periodontitis. Image adapted with kind permission from Elsevier (Pihlstorm *et al.,* 2005).

A more severe form of periodontal disease is called periodontitis. This results in loss of supporting connective tissue and alveolar bone support resulting in one of the major causes of tooth loss in adults. This eventually leads to formation of deep periodontal pockets that accompanies the loss of bone as depicted in Figure 2. Progression of the disease results in loosening of teeth, occasionally pain, discomfort and impaired mastication. This eventually results in tooth loss. Initially chronic periodontitis may be asymptomatic, until the teeth involved may move out of their normal position, loosens or are lost. Recurrent periodontal abscesses and halitosis are also observed in some cases (Hughes *et al.* 2010). Periodontitis has been classified in different types according to the severity or age group. The most widely accepted classification was proposed at the "International workshop for a classification of periodontal disease and conditions" held in 1999 (Armitage 1999; Dentino *et al.* 2013). Periodontal therapy is largely nonsurgical aimed at controlling the biofilm and other prominent

risk factors. Professional scaling, root surface debridement and personal oral hygiene measures are usually the first line of action in the management of periodontitis. If successful this therapy results in decreased pocket depths and improved clinical periodontal attachment and reduced inflammation. The treatment may be complemented by use of local or systemic antibiotics in certain specific situations. Advanced stages of the disease may also be managed by periodontal surgical procedures, and the use of, grafting materials or Guided Tissue Regeneration (GTR) membrane as an adjunct to encourage the regeneration of tissues lost as a consequence of periodontal disease. A summary of the classification of periodontal diseases and conditions outlined in 1999 is given below.

I. Dental Plaque induced gingival diseases/ Non-plaque induced gingival lesions
II. Chronic periodontitis (localized/ generalized >30% site involvement)
III. Aggressive periodontitis (localized/ generalized >30% site involvement)
IV. Periodontitis as a Manifestation of Systemic Diseases (genetic / hematological)
V. Necrotizing Periodontal diseases (Necrotizing ulcerative gingivitis/periodontitis)
VI. Abscess of the Periodontium (gingival / pericronal / periodontal abscess)
VII. Perio-Endo Lesions (combined periodontic-endodontic lesion)
VIII. Developmental or acquired deformities and conditions

Other classifications of periodontal diseases are,

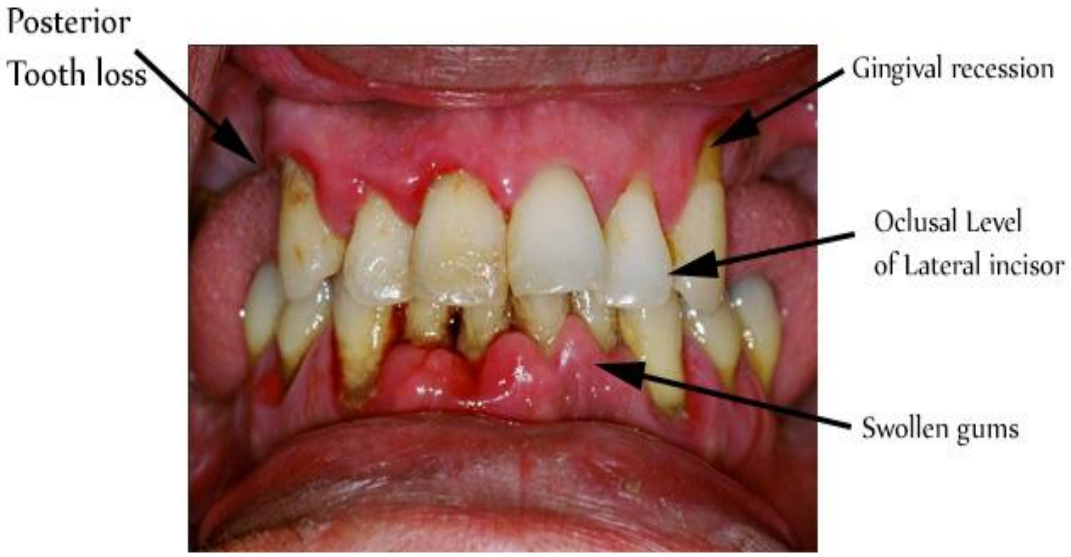

Figure 3: Advanced periodontitis showing poor oral hygiene with gum recessions more visible on maxillary canines and gingival swelling more pronounced on near the mandibular incisors. Image adapted with kind permission from publisher (Aggarwal *et al.* 2014).

2.2.1.1. Chronic and Aggressive periodontitis

In chronic periodontitis, there is no consistent number or pattern of teeth involved. The disease can be localized to a few teeth or can affect the entire dentition. Chronic forms are also usually known to be presented with relatively intense gingival inflammation, whereas the aggressive form was described to exhibit low level of gingival inflammation (redness, swelling) compared with other form of periodontitis. Armitage and Cullinan have reported about the clinical features of chronic and aggressive periodontitis, they mentioned that while most clinicians would agree that aggressive periodontitis exists as clinical entities. The clinical distinction between chronic and aggressive periodontitis is not clear cut (specially generalized) (Armitage and Cullinan 2010).

2.2.1.2. Periodontitis as a manifestation of systemic diseases

Various systemic diseases could manifest in the periodontal tissues. These disorders include herpetic and other viral infections, dermatological conditions such as lichen planus or pemphigoid, haematological diseases such as leukaemia or neutropenia. Diagnosis of these forms of disease is usually based on the clinical as well as pertinent laboratory and biopsy findings. Gingival enlargement could also be associated with various substances including phenytoin, calcium channel blockers and cyclosporins (Pihlstrom *et al.* 2005).

2.2.1.3. Necrotizing Periodontal diseases.

According to the 1999 classification of periodontal diseases, acute necrotizing gingivitis (ANUG) and acute necrotizing periodontitis were classified as the most severe form of periodontal disease. Clinically ANUG has a typical punched out appearance of gingival margins caused by ulceration and necrosis of gingival tissues and intense gingival pain (Atout and Todescan 2013) (Figure 4). It may progress rapidly and is painful at times. Acute inflammation is seen along with exposure to underlying tissue causing severe bleeding which is sensitive a gentle touch. In cases where the disease progresses beyond the mucogingival junction, destruction of alveolar mucosa takes place (Pihlstrom *et al.* 2005).

2.2.1.4. Periodontal Abscess

Trauma, occlusion or blockades of the periodontal pocket orifice are believed to be factors that lead to the formation of a periodontal abscess. Periodontal abscess causes tissue destruction by inflammatory cells and extracellular enzymes, bacterial and tissue breakdown products are also involved. Clinical signs are elevation of the gingiva from the lateral root sides of the effected tooth (Pihlstrom *et al.* 2005).

Figure 4: Generalized punched out papilla and detached midline papillae, Necrotizing ulcerative gingivitis. Image adapted with kind permission from publisher (Atout and Todescan 2013).

2.3. Treatment of Periodontal Diseases

Numerous methods are available for the treatment of periodontal diseases all with common aim of repair and regeneration of the periodontal support to restore the functional integrity of the oral mucosa (Akizuki *et al.* 2005). Whilst the majority of periodontal treatment provided in clinical practice aims to stabilize the periodontal condition using predominantly a non-surgical approach (root surface debridement), there is also much interest in developing techniques to enhance the regeneration of lost periodontal support that generally requires a surgical approach. The regeneration of lost periodontal support is a complex interaction of regenerating lost bone, cementum and periodontal ligament. Consequently attention has been given to difference elements of this process. With respect to the replacement of lost alveolar bone, the two major methods are grafting and the application of growth factors and other proteins (Tan 1993).

2.3.1. Non-Surgical treatment

Non-Surgical treatment involves the provision of advice on plaque control, scaling, root surface debridement using hand instruments, sonic and ultrasonic instrumentation. The aim is to mechanically disintegrate the calculus and remove the plaque biofilm. However, histological studies have failed to show any predictable regeneration of the lost periodontal tissues by this procedure. The use of lasers such as CO_2, neodymium doped yttrium aluminium garnet (Nd:

YAG) or neodymium doped yttrium aluminium perovskite (Nd:YAP) may exert an effect on periodontal regeneration, although clinical and animal studies have shown that there are variations in the results and gain in attachment level tends to vary (Bosshardt and Sculean 2009).

2.3.2. Surgical Treatment

Periodontal therapy is aimed at preventing diseases progression, regenerating the lost periodontal tissues and maintaining optimal therapeutic objectives. A number of different techniques have been used in the past including, subgingival curettage, gingivectomy, flap procedures with or without osseous recontouring. A review on Surgical periodontal therapy conducted by Wang and Greenwell have mentioned that curettage scaling and root planning and modified Widman flap procedure resulted in slightly better attachment level results (Wang and Greenwell 2001).

Gingivectomy: This technique is adapted to excise suprabony pockets if there is sufficient attached gingiva to reduce gingival hyperplasia and for aesthetic crown lengthening in certain situations (Wang and Greenwell 2001).

Open flap debridement: The objective of open flap debridement is to achieve access for root debridement to achieve pocket reduction and to allow maximum flap coverage for devices used for regenerative therapy (Wang and Greenwell 2001).

Modified Widman Flap: This procedure is a type of flap procedure used to eliminate the inflamed pocket wall, provide access for root debridement and preserve the maximal amount of periodontal tissue. It is a conservative procedure and is indicated where aesthetics is primary concern, especially in the maxillary anterior segment (Wang and Greenwell 2001).

Currently the goals of periodontal surgery are to gain access to the root surface, establish favourable gingival contours, and facilitate oral hygiene, lengthening the clinical crown to facilitate adequate restorative procedures and to regain the lost periodontium by using regenerative approaches. The use of periodontal surgical options to enhance periodontal tissue regeneration will increase as a modality of therapy in the future, however the goal of the procedures will be almost totally regenerative (Wang and Greenwell 2001). Combination therapies including surgical options in conjunction with bone grafts or various types of bone substitutes such as transplanted endogenous bone, Bioactive glass and hydroxyapatite have also shown varying degree of success in periodontal regeneration (Gestrelius *et al.* 2000).

2.3.2.1. Osseous Grafting:

The following major types of bone grafts have often employed in such a clinical application (Aichelmann-Reidy and Yukna 1998; Reynolds *et al.* 2003).

2.3.2.2. Autogenous Bone Grafts

These types of grafts are taken from the patient's own body. Cortical bone from the iliac crest, intra oral and extra oral cancellous bones (Mellonig 1992) and iliac crest marrow have been used as auto grafts for periodontal bone regenerative procedures with variable degrees of success in past. Their use is limited in modern periodontal therapy because of the considerable tissue morbidity associated with the surgical procedures and the need for large quantities of material to fill multiple defects.

2.3.2.3. Bone Allografts

Grafts that are taken from another person are known as allografts and the advantage is that they are not associated to tissue morbidity of the host, nor are they limited by the amount of material available. Periodontal treatments have been carried out with three types of bone allografts, namely freeze dried bone allograft (FDBA), under mineralized bone allograft and demineralized bone allografts. Of the three FDBA is most commonly used in clinics. The disadvantage of allografts is that the risk of infection including HIV and Hepatitis transfer persists even when the organ to be transferred is thoroughly sterilized (Mellonig 1992). Bone allografts have been extensively reviewed in the past. The conclusions are controversial, they range from either optimistic to no osteoinductive effect for demineralized FDBA. The popularity of FDBA is greater in United States, compared to European countries (Bosshardt and Sculean 2009).

2.3.2.4. Xenogenic Bone Grafts

These are grafts, taken from different species and then are treated with chemicals or heat to remove all organic bone matrix, and leave an unchanged inorganic form in a non-organic bone matrix. Pigs are currently thought to be the ideal candidates for organ donation, other animals looked into in the past include, cows, baboons or chimpanzees. The advantage of using this includes maintenance of the original bone structure, whether cortical or cancellous, which may assist in the new bone formation (Ramseier *et al.* 2012).

2.3.2.5. Alloplastic Bone Grafts:

These are man-made or synthetic biocompatible grafts which offer the advantage of reduced risk of adverse antigen-antibody reaction as compared to allografts.

A detailed review by Bosshardt & Sculean on "Does periodontal tissue regeneration really work? " highlighted the basic problem with all bone filler materials such as bioactive glass or biphasic calcium phosphate. They mentioned that the biologic rational for regeneration for periodontal tissue is lacking. Bone grafts or bone substitutes do not possess the property to regenerate connective tissue attachment. Their efficacy is proven to be used in combination with barrier membranes for GBR procedures. Furthermore, the available clinical and histological data with regards to periodontal regeneration along with new connective tissue formation does not look promising (Bosshardt and Sculean 2009).

2.4. Root Surface Conditioning

The aim of root surface conditioning is the removal of the smear layer, promoting fibroblast migration, attachment and removing harmful toxins (endotoxins). Ethylene diamine tetra acetic acid (EDTA) gel used for the purpose has shown significant high attachment and reduction in pocket depths over a period of time (Blomlof *et al.* 2000; Sakallıoğlu *et al.* 2004). The biological understanding of root surface demineralization is to enhance blood clot adhesion to exposed collagen fibrils. Stabilization of the clot may have an overall positive effect on periodontal regeneration. MSCs may preferentially attach to blood clot stabilized root interface and prevent epithelia cells from apical migration into the defect (Bosshardt and Sculean 2009).

2.5. Growth Factors

The role of growth factors used for periodontal regeneration has been a topic of interest for researchers recently. Growth factors are polypeptides with a function of regulating proliferation, migration and attachment of cells. The different types of growth factors are transforming growth factors (TGF), fibroblast growth factor (FGF), insulin-like growth factors (IGF), platelet-derived growth factors (PDGF) and bone morphogenic proteins (BMP) (Giannobile 1996; Javed *et al.* 2011). Bone, cementum and wound healing tissues are the sites where these growth factors can be found. These growth factors can be used alone or in combination with each other and the combined effect has been shown to enhance periodontal regeneration (Darby and Morris 2012). Within the large family of growth factors (GF's), PDGF have been extensively investigated a number of times (Javed *et al.* 2011). The use of growth factors for periodontal regeneration have shown promising results alone and combinations with other agents, however the routine use of GF's is still not a reality in clinics (Bosshardt and Sculean 2009).

2.5.1. Platelet Derived Growth Factor

Platelet derived growth factors (PDGF) are polypeptide growth factors and have been shown to increase periodontal regeneration in time and dose dependent studies. They exert their effect by modulating adhesion, proliferation and mitogenesis of PDL cells as shown in numerous studies conducted on beagle dogs, monkeys and human periodontal disease models (Nevins *et al.* 2005; Javed *et al.* 2011). PDGF is a natural protein present abundantly in the bone matrix and has been found to effect cell migration proliferation, synthesis of extracellular matrix and wound repair as well. In a detailed review conducted by Javed *et al.,* on PDGF, it was concluded that PDGF plays a significant role in promoting GBR around dental implants and teeth. It also enhances proliferation of gingival, PDL fibroblasts and cementogenesis is also triggered (Javed *et al.* 2011). Figure 5 shows a series of images showing the effect of using PDGF and bone graft materials in a clinical study conducted by Ramseier and co-workers.

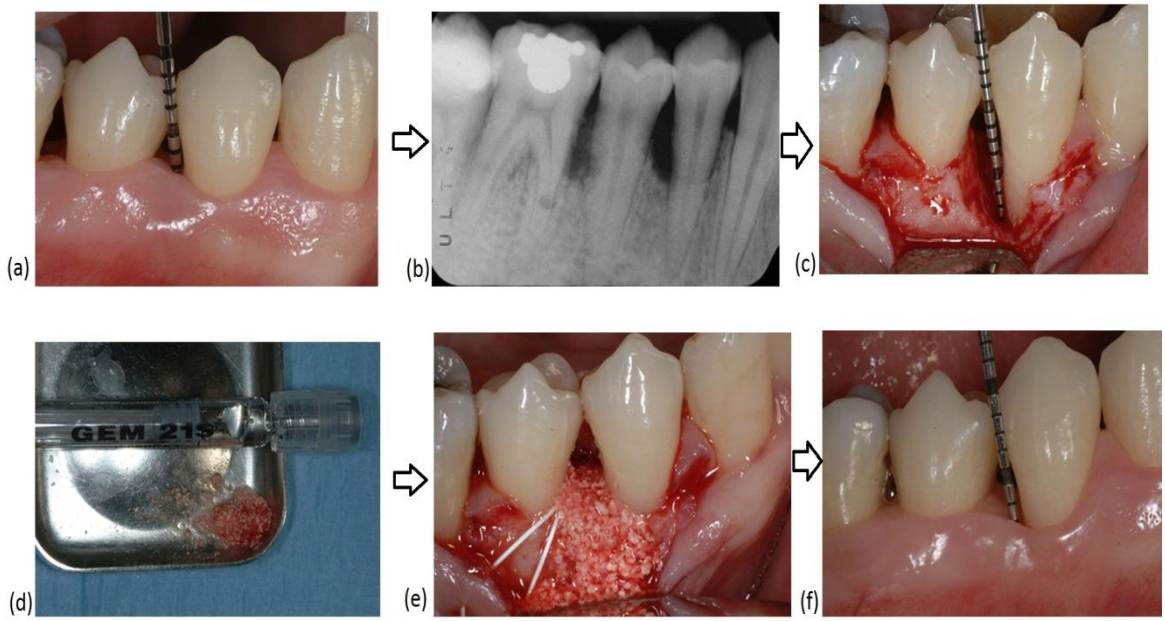

Figure 5: Series of clinical images and a Periapical radiograph showing Periodontal regeneration using platelet derived growth factor and bone graft materials from (a)Periodontal probe being used to measure the pocket depth, (b) Radiograph showing extend of bone resorption, (c) Flap retracted to show bone level. (d) PDGF, (e) Bone graft material adapted to the defect site (f) probing to measure the gain in attachment level. Image adapted with kind permission of publisher (Ramseier *et al.* 2012).

2.5.2. Fibroblast Growth Factor

Fibroblast growth factor (FGF) is a member of heparin binding growth factor family with multiple physiological actions such as stimulation of bone formation as well as new vessel

formation which are of help during the early stages of wound healing and repair(Yun *et al.* 2010; Ramseier *et al.* 2012). In-*vivo* experiments on periodontal regenerative capabilities of FGF have been studied on beagle dogs, and the results indicate that FGF has the capability to assist in regeneration of new cementum and alveolar bone formation. More detailed trials are still needed to establish the use of FGF in periodontal regeneration.

2.5.3. Insulin-Like Growth Factors

Insulin like growth factors (IGF) are released by growth hormones and are known to have a role in remodelling of bone but the exact mechanism of their action is still incompletely understood (Chen *et al.* 2006).

2.6. Enamel Matrix Derivative (EMD)

Among the treatment approaches available for periodontal regeneration (PR) EMD is considered as a serious option for complete regeneration of periodontium. Discovery of EMD has completely revolutionized the field of PR. Periodontal regeneration after EMD application is thought to occur by mimicking the events taking place during normal development of periodontal tissues. EMD is found in large amounts during the secretory stage of crown development. Enamel matrix protein is made up to two families of proteins, that is, amelogenins (90%) and non-amelogenins, like, ameloblastin, enamelin, tuftelin and proteolytic enzymes. Enamel proteins are known to play a significant role in enamel crystal edification, orientation, maturation during crown development and hence serve as a regulator for enamel biomineralization (Grandin *et al.* 2012). Primary acellular cementum is the tissue which provides attachment of ligament fibre bundles to the root surface and is therefore essential for periodontal regeneration (Mian Khalid Iqbal and Bamaas 2001; Yan *et al.* 2012). Recently, the successful use of enamel matrix derivatives (EMD) in periodontal regeneration has supported the role played by cementum in periodontal wound healing. Based upon the idea that enamel matrix proteins from Hertwig's epithelial root sheath initiate the formation of cementum, Hammarstrom *et al* (Hammarström L 1997) showed that EMD can be used to regenerate acellular extrinsic fibre cementum in monkeys. Buccal dehiscence models of monkeys and human periodontal defects have shown to be successfully treated by EMDOGAIN® (Institute Straumann AG, Basel, Switzerland) which is a commercial preparation of EMD; (Gestrelius S 1997; Hammarström L 1997). EMD is a unique and intriguing biological system which should arouse the curiosity of more researchers dealing with protein chemistry, delivery devices, tissue regeneration and tissue engineering substrates (Grandin *et al.* 2012) .

2.7. Bone Morphogenic Proteins

Bone morphogenic proteins (BMP) are responsible for bone and cartilage formation and there are different types of BMP such as BMP 2 and BMP 7. Their osteoinductivity is influenced by several factors such as BMP concentration, carrier properties and influence of local and systemic growth factors and hormones (Wikesjö *et al.* 2009).

2.8. Guided Tissue Regeneration

Guided tissue regeneration is a surgical technique designed to enhance periodontal regeneration (Nyman *et al.* 1987). This special procedure has demonstrated successful regeneration of the periodontium and alveolar bone in the recent years. Figure 6 shows a 3D illustration of how a GTR membrane will be placed in a clinical defect site, by acting as an occlusive membrane and preventing the gingiva to fall into the defect and form a long junctional epithelium. Periodontal defects including Type I and II furcation areas and intra bony pockets have shown to improve with time after using a GTR membrane (Pontoriero *et al.* 1989). Before opting for this last resort treatment option a combination of clinical therapies are performed by the periodontist which involve standard periodontal procedures including scaling, and root surface debridement. However, these therapies are only successful if good home oral hygiene care and professional maintenance is carried out (Pontoriero *et al.* 1988; Karring *et al.* 1993). GTR technique is based on solid biologic principal. The rational as mentioned earlier is to selectively guide cell proliferation and tissue expansion within the tissue compartments using a physical barrier. The procedure of placing a GTR membrane is a technically demanding and surgically sensitive, this makes it a more complex method (Bosshardt and Sculean 2009).

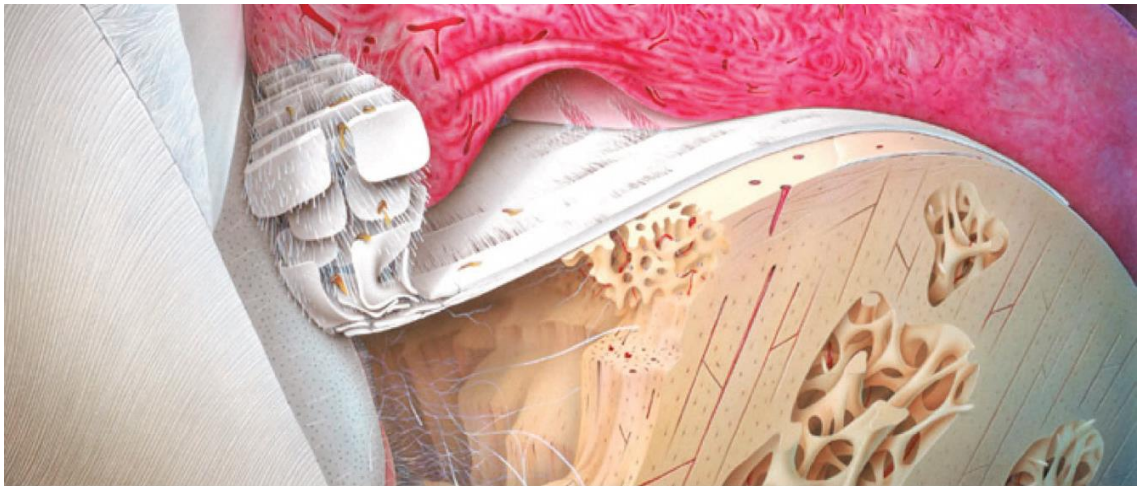

Figure 6: A 3D image of a GORTEX-PTFE GTR membrane covering a defect site. Dentinal tubules and enamel can be seen on the left side of the image, adjacent to the dentinal

tubules is a bony defect (Haversian canals and porous bone in brown colour) covered by a white GTR-PTFE membrane sandwiched on top by the gingiva (pink coloured) adapted with permission from Elsevier, Scantlebury *et al.,* 2012.

2.8.1. Principle of Guided Tissue Regeneration

Guided Tissue regeneration (GTR) works on the principle of acting as a mechanical barrier that prevents epithelial and connective tissue cell migration in order to allow the cells with potential of regeneration such as periodontal ligament cells, bone cells and cementoblasts to repopulate the protected wound area to initiate healing (Nyman *et al.* 1987)(Takata *et al.,* 2001).The essential design criteria outlined for GTR membranes focuses on tissue integration, biocompatibility, cell occlusivity, clinical handling, space maintenance, membrane stability and membrane resorption (Lin *et al.* 2008).

2.8.2. Ideal Properties for use of barrier material in GTR

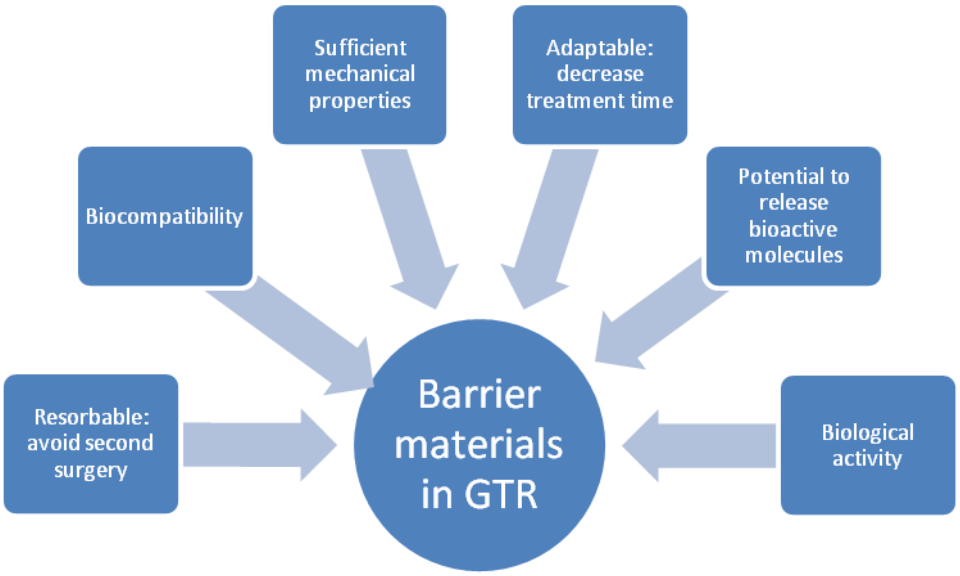

2.8.3. Types of Materials Used In GTR Membrane

Two basic groups of materials are being used in GTR membrane synthesis and they are classified as resorbable and non- resorbable materials with an ever increasing use of resorbable materials as no second surgical procedure is needed for their removal and the chances of complications associated with exposure of the barrier are reduced because of spontaneous resorption of exposed barriers (Windisch *et al.* 1999). They can either be man-made or synthetic materials such as polylactic acid (PLA) or polyglycolic acid (PGA) or natural resorbable materials such as collagen (AlGhamdi and Ciancio 2009; Hughes *et al.* 2010).

2.8.3.1. Non-Resorbable Membranes

The most technologically sophisticated non-resorbable membranes used for GTR are made up of polytetra fluoroethylene. They can be porous (Gore-Tex) or non-porous (Dense non-porous PTFE-a TefGen-FD®). They are biocompatible materials and their application was first reported in the repair of bone lesions (AlGhamdi and Ciancio 2009). Although biocompatibility of these membranes is satisfactory, they have insufficient mechanical strength as they tend to collapse into the created space leading to inadequate regeneration of tooth apparatus and poor prognosis (Gentile *et al.* 2011).

2.8.3.2. Resorbable Membranes

The advantage of these types of membranes is that they do not require a second surgery for their removal as they resorb, resulting in a reduction of overall treatment cost in addition to reduced patient discomfort.

These membranes can either be made from natural materials or synthetic materials which are usually aliphatic thermoplastic polymers. They are classified into two groups based on their origin: natural materials including collagen, chitosan (Honga *et al.* 2007), oxidised cellulose and rubber dam and synthetic materials are PLA, PGA, co-polymer of poly Lactide and glycolide, polycaprolactone (PCL) and composite membrane consisting of PLA / PGA polymer-tricalcium phosphate (TCP) / hydroxyapatite (HA) (Gentile *et al.* 2011).

Numerous studies conducted by various researchers show that clinically there is no difference between resorbable and non-resorbable membranes except for the fact that resorbable membranes do not require second surgery for the removal and hence, they are more popular clinically (Christgau *et al.* 1995; Christgau *et al.* 1997; Garrett *et al.* 1997). There is also increased interest in creating resorbable membranes with various combinations of materials for their application in GTR with adequate biocompatiblity and mechanical properties such as tensile strength and flexibility (Gentile *et al.* 2011).

One such novel membrane has been developed by Nieminen *et al.,(*2006). It consists of poly-l-Lactide (PLLA), poly-d,l-lactide (PDLA), trimethylenecarbonate (TMC) and polyglycolide (PGA) and N-methyl-2-pyrroline (NMP) as a plasticiser. It can be easily shaped into the desired shape and placed to fill the defect due to the presence of NMP which softens the membrane. As the NMP leaches out the membrane stiffens into the required shape (Nieminen *et al.* 2006).

Another novel kind of guided tissue regeneration (GTR) barrier membrane has been fabricated by Hong *et al., (*2007) using a biodegradable natural polymer, chitosan (CH). The membrane has a porous structure consisting of a dense skin layer, a transition region and a

sponge-like porous layer. The key factors that had significant effect on the mechanical properties were porosity, average pore size and absorbed water ratio. In the experiments performed, the porous membrane not only degraded, but maintained the structural integrity for 6 weeks in enzyme solution which is sufficient to meet the demand for GTR. The biocompatibility experiment showed that these asymmetric membranes did not cause adverse tissue reactions indicating excellent biocompatibility and degradability. CH also has a significant effect on the tensile strength and elongation ratio of porous membranes. These were found to be directly proportional to CH concentration as this increases the size of the pores. Evaporation of the solvent also affects the mechanical properties significantly. The longer it lasts, the thicker the dense layer remains resulting in a better tensile strength and elongation ratio (Honga H. 2007).

A three layered composite membrane consisting of nano-carbonated HA/collagen/PLGA composite has been developed by Liao *et al., (*2005) which had a porous surface on one side to facilitate tissue growth and a non-porous opposite surface to inhibit cell adhesion. The fabrication of this membrane was such that one face consisted of 8% nano-carbonated HA/collagen/poly (lactic-co-glycolic acid) (nCHAC/PLGA) porous membrane, the opposite face of pure PLGA non-porous membrane and the middle layer composed of 4% nCHAC /PLGA. This three layered composite membrane exhibited the ultimate tensile strength in the range of 9.7±1.7MPa and an elastic modulus equal to 1.2±0.5 GPa which is above cancellous bone's tensile properties, therefore they could possibly be used for repairing periodontal defects and in other medical applications on account of their properties (Liao *et al.* 2005; Liao *et al.* 2007).

Another group (Kikuchi *et al.,*2002) developed a composite membrane consisting of beta- tri-calcium phosphate (β-TCP) and biodegradable copolymerized poly-L-lactide (CPLA) and tested the mechanical properties of the composite membrane by soaking the composite in physiological strength saline and phosphate buffered saline (PBS). Three-point bending tests were performed which exhibited a rapid decrease in the mechanical strength of the composite from 60 to 30 MPa in the first 4 weeks before reaching a plateau. This rapid decrease was attributed to rapid loss of β-TCP from the surface. It retained sufficient mechanical properties during week 8 to 12 to be used in GBR. In the same study the same composite membrane (250µm thick in dimension) successfully covered the large bone defects in beagle dogs as compared to CPLA alone in which the defect was invaded by soft-tissues, thereby showing the advantage of composite membrane. The drawback associated with this membrane was that it needed a high softening temperature which is not practical in a chair-side surgical setting. This

deficiency was rectified by the same group in (2004) by creating a poly (l-lactide-co-glycolide-co-ε-caprolactone) (PLGC) and TCP composite membrane (Kikuchi *et al.* 2002).

More recently, Bottino *et al.,* (2012 2011) designed a functionally graded electrospun membrane for periodontal regeneration. The graded approach allowed tailoring of the layer properties individually to fabricate a material system that could retain its physical, chemical and mechanical characteristics for enough time for periodontal regeneration to occur. This concept of designing of GTR/GBR membranes by using functionally graded materials (FGM), with graded components and graded structures, where one face of the membrane is porous allowing cell in-growth and the opposite side of the membrane is smooth to, inhibit cell adhesion is a new concept in periodontal therapy. A sequential multi-layered electrospinning technique was used to design this FGM, consisting of a central core layer and two surface layers. Materials used to synthesize this were a neat poly (DL-Lactide-co-e-caprolactone) layer surrounded by two composite layers of protein/ polymer ternary blend. Each layer was designed keeping in mind the surface it would come in contact with, i.e. either bone defect or the epithelial tissue (Bottino *et al.* 2011; Bottino *et al.* 2012)

Further studies and reviews performed by Bottino *et al.,* 2012 have suggested that the success lies in synthesizing a functionally graded e-spun nanomatrix and hydrogel combination. Controlling the mechanical and degradation properties with other biological variables is also a big challenge when synthesizing degradable GTR membranes. Tuning the biological properties and bioactive modification is usually done on “blank state” or by using Bioinert hydrogel matrices of polyethylene glycol or within a biopolymer hydrogel. Growth factors or other agents such as antibiotics can be made soluble or immobilized in the matrix as well (Bottino *et al.* 2011; Bottino *et al.* 2012).

Some of the commercially available GTR membranes are:

Atrisorb®

Atrisorb® is a (DL –lactide polymer) and is composed of 37% of liquid polymer of lactic acid that is dissolved in 63% of N-methyl-2 pyrrolidone (NMP). This is the only membrane that is prepared before the surgery at chairside. Membrane thickness is around 600-700µm. Clinical studies using this material have shown good clinical attachment gains and bone refill in the treatment of class II furcation defects. They also showed favourable tissue response, biocompatibility and safety in animal studies, however, their advantages and long term effectiveness still need to be investigated (Hou *et al.* 2004; Sakallioglu *et al.* 2007).

Mempol®

Mempol® is composed of homopolymer of polydiaoxanon (PDS) which is completely resorbable synthetic polyester. It has been previously used as suture materials and surgical pins (Christgau M. 2002). Use of Mempol membranes have resulted in more frequent recession during the healing phase when compared with other polylactic membranes (Lang *et al.*, 1994).

Guidor®

Guidor® is composed of PLA and a citric acid ester acetyl tributylcitrate and is a double layered membrane with a drawback that it promotes little bone regeneration and shows severe inflammation on resorption of the membrane (Aurer and JorgiÊ-Srdjak 2005).

Gore-Tex Membrane®

Gore-Tex® is made of expanded polytetrafluoroethylene (e-PTFE) and requires a second surgery for membrane removal. The use of a second stage surgery poses a drawback that can affect the integrity of the newly formed periodontal tissues. The material is inert and prevents the tissue in growth. The basic molecule consists of carbon- carbon bond with four attached fluorine atoms which forms a polymer poly (D:L) Lactide dissolved in N-methyl pyrrollidone (NMP)(Gentile *et al.* 2011).

Epi-Guide®

Epi-Guide® is a hydrophilic membrane and is composed of D-, D-L-, L-polylactic acid. The barrier function persists up to 20 weeks and bioresorption occurs in 6 to 12 weeks. Initially it demonstrates a good level of cell-attachment but less than that achieved by Resolute® (Gentile *et al.* 2011).

Resolute®

Resolute® is a barrier membrane which is made up of a porous structure of glycolide polymer fibre and occlusive membrane of Lactide and glycolide co polymer which demonstrates a better cell level attachment than Epi-Guide membrane. The porous and occlusive parts of the membrane works by promoting tissue attachment and inhibiting cell ingrowth within the defect respectively (Takata *et al.* 2001).

Inion GTR™ membrane system

Inion® is a relatively new barrier membrane and is composed of polylactide; polyglycolide and trimethylene carbonate polylactide-co-polymer which undergoes treatment with N-methyl-pyrrollidone (NMP) which acts as a plasticizer. It is claimed by Inion Ltd. that the membrane can be softened prior to application in a biocompatible plasticizing solution so that it can have proper fit needed for filling out the defect. Contact with water stiffens the membrane which helps in keeping the membrane in a desired shape over the wounded area and maintaining the space underneath. It can be used in gingival recessions and in treating class I and class II furcation defects(Gentile *et al.* 2011).

The disadvantages posed to resorbable collagen and synthetic polymer based membranes are lack of space making ability, mechanical stiffness, local biological effects due to the unpredictable rate of resorption process and premature exposure or flap dehiscence that results in postsurgical tissue management problems (Lundgren *et al.,* 1997). It is reported that such exposure in the early phase of healing can lead to bacterial growth and premature degradation of the exposed device which eventually destroys the barrier function, hence, compromising the newly formed periodontal tissues. The current membranes are often used with tenting or supporting materials to avoid space collapse. These membranes may be able to maintain space initially, however, they generally loose strength, collapse into the defect and hence, cause a failed reconstruction (Zellin *et al.,* 1995). Grafting materials when used alone seem to be not as effective when used in combination with a supporting material and barrier membrane (Lundgren *et al.,* 1997).

Degradation of synthetic polymers usually occurs by hydrolysis and this result in an acidic environment which could have a detrimental effect on bone formation (Lang *et al*., 1994). In an animal study conducted on resorption of three collagen based membrane (BioGide®, AlloDerm® porcine derived AlloDerm® human derived) poses a question about the efficacy of these membranes when used as physical barriers beyond one mouth (Owens and Yukna 2001).

2.9. Physiological wound healing in the Periodontium

The main purpose of periodontium is to provide support during mastication and other normal function. Due to the external forces applied on the alveolar bone, it constantly undergoes remodeling, and similarly the periodontal ligament / fibres can also accommodate in functionality by increasing in width. As the forces reduce, the PDL tends to undergo atrophy. The inferior and superior alveolar arteries are the main blood supply to the periodontal tissues. PDL's blood supply is managed by the apical vessel, penetrating vessels from the bone

and anastamosing vessels from gingival tissue. The sequence of healing of a periodontal wound is divided into the following phases, (i) soft tissue inflammation (ii) granulation tissue formation, (iii) Intercellular matrix formation and remodeling. Plasma proteins such as fibrinogen are synthesized rapidly in the bleeding wound and provide a basis of attachment of fibrin clot. Polymorphonuclear leukocytes trigger the inflammatory phase of healing in the soft tissue simultaneously debride the wound by removing the bacterial cells through phagocytosis. While the macrophages continue to invade as the inflammatory phase reaches its later stage. Macrophages through the process of phagocytosis of used leukocytes and erythrocytes additionally release a number of biologically active molecules such as inflammatory cytokines and tissue growth factors. These biologically active factors further recruit inflammatory cells such as fibroblastic and endothelial cells, thus transitioning from the inflammatory phase to granulation tissue formation phase. During granulation tissue formation, fibroblasts help in the formation of new matrix collagen, proteoglycans and fibronectin which eventually result in tissue contraction. Finally the healing phase is reached in which cell rich tissue undergoes maturation. The last stage is the formation of a long junctional epithelium surrounding the dentition. Gingival connective tissue recession and periodontal pocket reduction are also observed during these healing stages (Ramseier *et al.* 2012). The current goal of periodontal research in this area is aimed at the regeneration of periodontal tissues to their original form and function. Events occurring to propel periodontal regeneration are extraordinarily complicated and involve participation from cellular components of the periodontium. Healing components of both the hard and soft tissues need to be coordinated and integrated by a signaling system for new connective tissue fibres to be inserted into the bone and cementum. However, a limited amount of information exists in current literature about the signals that initiate and regulate these interactions in vivo. Consequently, this has driven the need for a better understanding of patho-biology of periodontitis, its systemic association and advances through cell biology, genetics, molecular biology and biomaterials science have intrigued new researchers in regenerative biology focused on tissue engineering therapies (Weinberg and Bral 1998; Adekogbe and Ghanem 2005).

2.10. Tissue engineering periodontal apparatus

The fundamental objective of tissue engineering (TE) is to develop therapies to restore damaged, lost or aging tissues. It is a branch of science that deals with the principles of cell biology, developmental biology and biomaterials science to fabricate new biomaterials to replace damaged or lost tissues. The core requirement for making an engineered tissue

involves taking a suitable cell source, expanding it in culture to get the desired number of cells and then seeding them on a scaffold material, preferably with the same chemical, mechanical and physical properties as the targeted tissue. This environment should then promote organization, development and growth of new tissues. This would eventually lead to implantation of the scaffolds in to the patient. Ultimately the scaffold would degrade away leaving its matrix to amalgamation with the new tissue (Weinberg and Bral 1998; Adekogbe and Ghanem 2005). Broadly speaking, there are five main therapeutic categories for tissue regeneration, conductive, inductive, cell based, gene based and RNA based. In conductive therapeutics the biocompatible scaffolds are a core requirement that guides tissue regeneration by passively promoting growth of progenitor stem cells and vascular elements that reside in the tissue defect. The regenerative capacity is reliant on the availability of bioactive molecules and sufficient progenitor cells present in the defect site for example, HA (Liao *et al.* 2005; Liao *et al.* 2007), β or αTCP (Kikuchi *et al.* 2002). Inductive therapeutics are based on guided regeneration by using a biocompatible scaffold composite with bioactive molecules that engage progenitor stem cells and vascular events from the surroundings of the defect site (Bottino *et al.* 2011; Bottino *et al.* 2012). They are considered to be better than the conductive approach as progenitor cells tend to repopulate the defect site, for example polymers carrying growth factors or HA. The use of Gene based therapies in TE were used initially for soft tissue wounds such as skin. Targeting of signalling molecules or growth factors via protein or genes have opened new horizons in periodontal tissue regeneration (Intini 2010). Chen and co-workers had extensively reviewed different aspects of periodontal regeneration based on the roles and strategies for local delivery of growth factors towards prospects of endogenous regenerative therapies and have concluded that periodontal tissue engineering is a highly complex and programmed biological process that must be robustly controlled by harnessing the intricate events occurring in between biological agents and scaffolds (Chen *et al.,* 2009, Chen *et al.,* 2010). The use of growth factors to enhance cell replication, angiogenesis, matrix biosynthesis and differentiation are a few of the possibilities. Descriptive gene therapies with PDGF-B have shown regeneration in large periodontal defects (Ramseier *et al.* 2012). Stem cells can also be used as a vehicle for delivery of therapeutic agents. In the case of periodontal tissue engineering the ultimate goal is to harness the body's own capability to regenerate functionally active periodontal tissue that physiologically responds to metabolic signals (Adekogbe and Ghanem 2005). Furthermore, for successful Periodontal Tissue regeneration to occur completely, the healing events should occur in an organized and programmed sequence both temporally and spatially, replicating the key events

occurring periodontal development (Lin *et al.* 2008). To enhance regeneration three key elements are required in tissue engineering Figure 7.

1. The presence of appropriate number and type of **Progenitor cells / Stem cells** that will regenerate the new periodontal tissue.
2. Conductive **Scaffolds** to hold the cells in or appropriate extracellular matrix.
3. Adequate level and sequencing of **Signalling molecule**

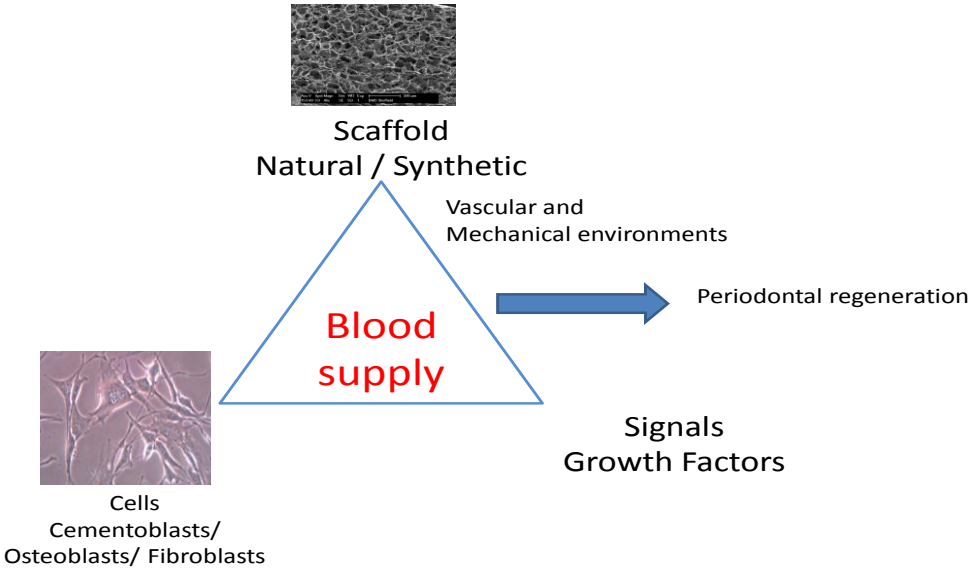

Figure 7: The Tissue Engineering Triangle. Scaffolds (porous and non-porous combination for GTR membrane) cells and growth factors such as BMP, PDGF or IGF combination will lead to periodontal regeneration.

When referring to periodontal regeneration it is defined as the regeneration of tooth supporting structures such as periodontal ligaments (PDL), alveolar bone and cementum. The main goal is to regenerate new acellular cementum with PDL fibres interconnecting the bone and tooth root by preventing the formation of a long junctional epithelium. One way of preventing the down growth of epithelium is by using a guided tissue regenerative membrane. A critical review on periodontal regeneration has stated that currently available modalities of regenerating periodontal tissue can only restore a fraction of the defect and complete regeneration still remains to be achieved (Bosshardt and Sculean 2009). A detailed review by N-H Lin *et al.,* on the use of stem cells in periodontal regeneration has summarized the repair

and regeneration concept. This concept has been represented in the table below (Lin *et al.* 2008).

Table 1: Healing response from conventional periodontal therapies, Table adapted with permission from publisher (Ratner 2004).

Repair	**Control of inflammation** **Long junctional Epithelium** **Connective tissue attachment to the root surface** **New bone separated from the root surface by long functional epithelium** **New bone with root resorption / ankylosis or both**
Regeneration	New functional attachment apparatus with formation of alveolar bone, cementum and periodontal ligaments.

2.11. Role of progenitor / stem cells

Periodontal tissue engineering and regenerative medicine requires an appropriate source of cells to successfully regenerate the complex Periodontium. Due to the complexity in the process of isolating specialized cells and the morbidity involved, stem cells serve as a more convenient alternative (Lin *et al.* 2008). Broadly speaking, the stem cells can be classified into adult stem cells and embryonic stem cells. Due to the ethical issues involved in sourcing embryonic stem cells their use in research is very limited. However adult stem cells are multipotent and further divided into, haemopoetic stem cells or mesenchymal stem cells (MSC's) (Pandit *et al.* 2011).

2.11.1. Periodontal ligament derived cells

In periodontal regeneration the remaining PDL plays a vital role in regenerating new tissue. This ability is attributed to few progenitor cells that maintain their differentiation and proliferative features. It has been shown that these progenitor cells have the capability to differentiate into different lineages, such as osteoblasts, fibroblasts or cementoblasts. They are also capable of preventing epithelial down growth and root resorption. However, the clinical application of PDL derived cells can be demanding due to hurdles of harvesting enough PDL cells from patients. Cell culturing PDL cell to obtain enough numbers of cells is time consuming, possibilities of viral infection in the fetal calf serum can occur and high quality laboratory infrastructure for in vitro culture needs a clean cell processing center (Adekogbe and Ghanem 2005).

2.11.2. Role of Scaffolds

Scaffolds serve as a three dimensional substratum or framework which occupies the space created by the defect and prevents collapse of the tissue space. These serve as a space maintainer, towards which the cells can migrate, attach, proliferate and lay down the matrix to form a functional tissue. In some cases scaffolds also serve as a delivery vehicle for carrying drugs and other bioactive molecules such as growth factors to the defect site. Periodontal scaffolds serve as a barrier to prevent certain cell types from invading the defect and simultaneously allowing certain cell types to repopulate. Biomaterials used for synthesizing scaffolds are broadly classified according to their origin. They could be either be based on materials of natural origin such as proteins (collagen, gelatin, albumin and fibrin), polysaccharides (chitin, cellulose, dextran) or synthetic origin, such as synthetic polyesters, polylactic co-glycolic acid (PLGA), Poly G-Lactic acid, copolymers of PGA and PLA. Over the past few decades the emphasis has been focused on using biodegradable scaffolds. This is mainly due to the fact that non resorbable scaffolds require a second stage surgery to remove the scaffolds, which could eventually harm the newly formed tissue. Avoiding the second surgical stage by using a biodegradable scaffold results in a un interrupted healing and repair (Illueca 2006; Hughes *et al.* 2010; Cho *et al.* 2011).

2.12. Biomaterials for Periodontal Regeneration

A key variable in the selection and design of a scaffolding material is the choice of a specific biomaterial. It has been recently suggested that a combination of materials may be the best way forward to achieve this goal. Biomaterials for periodontal regeneration can be broadly classified in two different types, ceramics and polymers. Biomaterials based on ceramics include calcium phosphate based ceramics such as HA or TCP. Bioactive glass also comes under this heading which is well known for its ability to bond with bone due to the formation of a carbonated apatite layer. A variety of different types of polymers have been used in treating periodontal problems, from naturally occurring polymers like, CH, collagen, cellulose, sodium alginate and natural rubber to synthetic polymers. The synthetic polymers have also been amalgamated with their natural counterparts for different materials (Sun *et al.* 2012). Synthetic polymeric biomaterials range from polymers like polyethylene glycol (PEG), Polypropylene (PP), polyethylene terephthalate (PET), polytetrafluoroethylene (PTFE), polymethyl methacrylic acid (PMMA), Polylactic acid (PLA), Polyglycolic acid (PGA) to combinations of PLA and PGA as well (Shue *et al.* 2012). Some polymers are hydrolytically unstable and show degradation in the body while others could remain unchanged for the

patient's lifetime. Biomaterials used for delivery systems vary from active pharmaceutical agents to growth factors, and even HA is being delivered by the help of different polymers (Sun *et al.* 2012) . The drug characterisation of biomaterials is usually based on their interaction with biological molecules, tissues and cells. Both surface and bulk properties play a pivotal role in regulating the biological response of biomaterials. Certain specific (binding to a cellular receptor) and nonspecific factors (electrostatic repulsion) dictate interaction between a material and cell. Other properties like protein adsorption, surface chemistry and topology also influence the behaviour of biomaterials (Ratner 2004) .

2.13. Biocompatibility of Polymers

The term biocompatibility sets materials used in commerce and technology apart from the materials used in medical application. The commonly used definition for biocompatibility is the ability of the materials to perform and appropriate host response in a specific application (Ratner 2004). Polymers used for biomedical applications may result in damage to various tissues. Therefore a variety of tests are conducted to evaluate the risk of such damage to ensure materials compatibility prior to market launch. Evaluation of biocompatibility is a complex and comprehensive area because a variety of unwanted reactions can occur (Schmalz 2009). Important factors that need to be taken into consideration regarding polymer biocompatibility are listed in the Table 2 shown below (Ramakrishna *et al.* 2001).

Table 2: Factors effecting polymer biocompatibility(Ratner 2004).

COMPONENTS	SPECIFICS		
1st level material properties.	Chemical, biological characteristics, chemical composition (bulk/surface)	Physical Characteristics, Density	Mechanical/Structural characteristics, Elastic modulus, poisons ratio, yield strength, tensile strength, compressive strength,
2nd level material properties	Adhesion	Surface topology, (texture/roughness)	Hardness shear modulus, shear strength, flexural modulus, flexural strength.
Specific functional requirements based on application	Biofunctionality (non-thrombogenic) Bioinert(nontoxic, Bioactive, Biostability,	Form, Geometry, Colour, coefficient of thermal expansion, refractive index. Electrical	Stiffness or rigidity, Fracture toughness, fatigue strength, creep resistance, friction and wear resistance, adhesion strength, impact strength, proof strength, abrasion resistance,

	(hydrolysis, oxidation) (Biodegradation	conductivity, opacity or translucency
Processing and fabrication	Reproducibility, quality, sterilizability, packaging and secondary process ability.	

2.14. Criteria for selection of polymers for clinical use

Gold plates were reported to be used as prosthesis for repairing cleft palate conditions in the late 1588 by Alexander Petronius, described as palatine obturators. Polymers have now taken over the biomedical industry (Lyman 2002)(King and Lyman 1975). Polymer selection for any clinical use is a pivotal step. This selection is dictated by its end application (Shoichet 2010). Depending on the application, polymers can be used alone or in combination as copolymers for successful clinical scenarios. The use of bio stable or biodegradable is governed by the desired longevity of the polymer, its cellular interaction and host response. Certain key characteristics that are looked into more commonly are the mechanical resistance or strength, elasticity and durability of the polymer, its stability and degradability in the clinical function, permeability, response to host cells, surface, interface and bulk properties. Biocompatibility is an essential element of this selection criterion. Successful clinical applications which have used polymers are artificial hip joint prosthesis, articular cartilage, artificial intervertebral disc, tooth implants and dental restorative materials, heart valves, blood bags, IV cannulae, disposable syringes and catheters. Among the most advanced use of polymers is tissue engineering, regenerative medicine and controlled drug delivery applications (Pachence and Kohn 2000;Domb 2011).

2.15. Device Degradation Time/ Bio-erodible Polymers

According to the scientific literature, four different terminologies are used synonymously on materials and or devices and their ultimate fate after transplantation into a living organism. These include biodegradation, bioresorption, bio erosion and bio absorption. Hydrolysis by polymer erosion has been divided into three basic types. First type of polymers are characterized to be water soluble polymer insolubilized by covalent cross-linking that solubilise as either the cross-linking or polymer backbone undergoes hydrolytic cleavage. The second type is initially water soluble, however they are solubilised by hydrolysis, ionization, and protonation of a pendant group. The last type deals with the conversion of water insoluble polymers to water soluble molecules by back bone scission. There are three further sub-classifications.

- Hydrolysis of side groups caused by dissolution
- Dissolution by ionization of pendant group
- Dissolution by protonation of amine functional group.

The release of entrapped drugs from polymers is usually caused by either erosion or the drug dissolves into its surrounding area. Erosion is caused by certain hydrolytically and enzymatically labile bonds present in polymer chains, whereas dissolution is the physical disentanglement of the polymer chain by a swelling solvent. Erosion is referred as a physical change in size, shape or mass of a device which could be an effect of degradation of dissolution. Degradation results in a chemical process causing cleavage of covalent bonds. This degradation can also occur by other means like oxidative or enzymatic mechanisms (Ratner 2004).

2.16. Factors effecting Biodegradation of Polymers

Certain factors that govern the biodegradation of polymers are summarize in Table 3

Table 3: Factors affecting degradation of scaffolds

Polymer Chemistry	Scaffolds Structure	In *Vitro*	In *Vivo*
Composition	Density	Degradative Medium	Implantation site
Structure	Shape	pH	Access to vasculature
Morphology	Mass	Ionic strength	Mechanical Loading
Molecular weight distribution	Porosity	Temperature	Tissue growth
Surface-to-volume ratio	Processing method and condition	Mechanical Loading	Metabolism of Degradation products
Chain motility	Pore structure, Pore size	Type and density of Cultured cells	Enzymes
Configuration	size		

The degradation of polymers have varying methods which range from biological, chemical, mechanical, oxidative, radiative, thermal, enzymatic and microbial degradation. Low molecular weight polymers are degraded by enzymatic action of microbial degradation while macromolecular matrices are very rarely affected. In chemical degradative procedure solvolysis is involved which causes the breaking of carbon bonds (Ratner 2004) (Maganti *et al.* 2011).

2.17. Enzymatically degradable polymers

Degradation of chitosan usually occurs by enzymes like chitonase, lysozyme and papain in-*vitro*. In-*vivo* it usually occurs by hydrolysis through lysozymes on the acetylated residues. The final degradation rate is widely dependant on the degree of deacetylation (DD) and crystallinity of polymer (Shi *et al.* 2006). A study by Azab *et al.,* reported on how the cross linking affects the polymer degradation rate. They used gluteraldehyde as a cross linker to create chitosan gels, and chitosan based gels with low cross linking density showed a faster degradation rate (Azab *et al.* 2006).

2.18. Functionally graded membrane (FGM)

Functional gradation is a characteristic of natural living tissue. A prominent feature of biomaterials is a formation of hierarchical structure. There is a continuous change from one structure or composition to another displaying the complex functionality of various tissues representing non-homogeneity. When each layer of the tissue or organ has one or more specific functions to perform and the tissue or organ has more than a single layer they are said to be functionally graded across the layer. In other ways the organ or tissue is described as functionally graded (Leong *et al.* 2008). Natural bone changes its structure from having a dense stiff external structure (cortical bone) to a porous internal structure (cancellous bone), and illustrates how functional gradation has been employed by biological adaptation (Pompe *et al.* 2003). In order to enhance the compliance of synthetic implants, a functionally a graded interlayer of biopolymers should be a favourable approach. Some other examples where functionally graded approach has been adapted are shoulder and knee joint replacements. This approach has also played a pivotal role for fabrication of scaffold in tissue engineering applications. Studies done on fabricating functionally graded electrospun scaffolds have also shown promising approach (Pompe *et al.* 2003; Bottino *et al.* 2012; Thomas and Vohra 2012).

This approach has also been adapted for fabrication periodontal guided tissue regenerative (GTR) membranes. A diagrammatic representation of a functionally graded GTR membrane is shown in Figure 8. Since GTR membranes are regarded as an interface implant which interfaces gingival connective tissue/epithelium, PDL bone tissue. This interface implant needs to execute a graded structure with compositional and structural gradients that mimic the local functional conditions. GTR membrane when designed with a functionally graded approach by using electrospinning holds promise as in interface implant in periodontal lesions (Leong *et al.* 2008; Bottino *et al.* 2011). Leong *et al.,* 2008 studied the engineering of functionally graded tissue engineering scaffolds. They reported that for a tissue engineered scaffold to be successful it

was important for it to be functionally graded, for facilitation of the cells to regenerate healthy tissue. This approach can have three different perspectives, biological, mechanical and anatomical. From a biological perspective one layer may be have cell types or phenotypes that may be different from other layers, for example a cartilage, where cells are arranged in three different organizations that effect the ECM production. In terms of mechanical considerations the scaffolds mechanical properties should match that of the native tissue structure to avoid stress shielding and give cells the proper mechanical cues, similar to the ones they receive in normal physiological environment (Leong *et al.* 2008). Simultaneous coordination of these properties will give an ideal scaffold for cell proliferation. Sequential electrospinning of the individual layers can be done to achieve a novel functionally graded periodontal membrane (Leong *et al.* 2008).

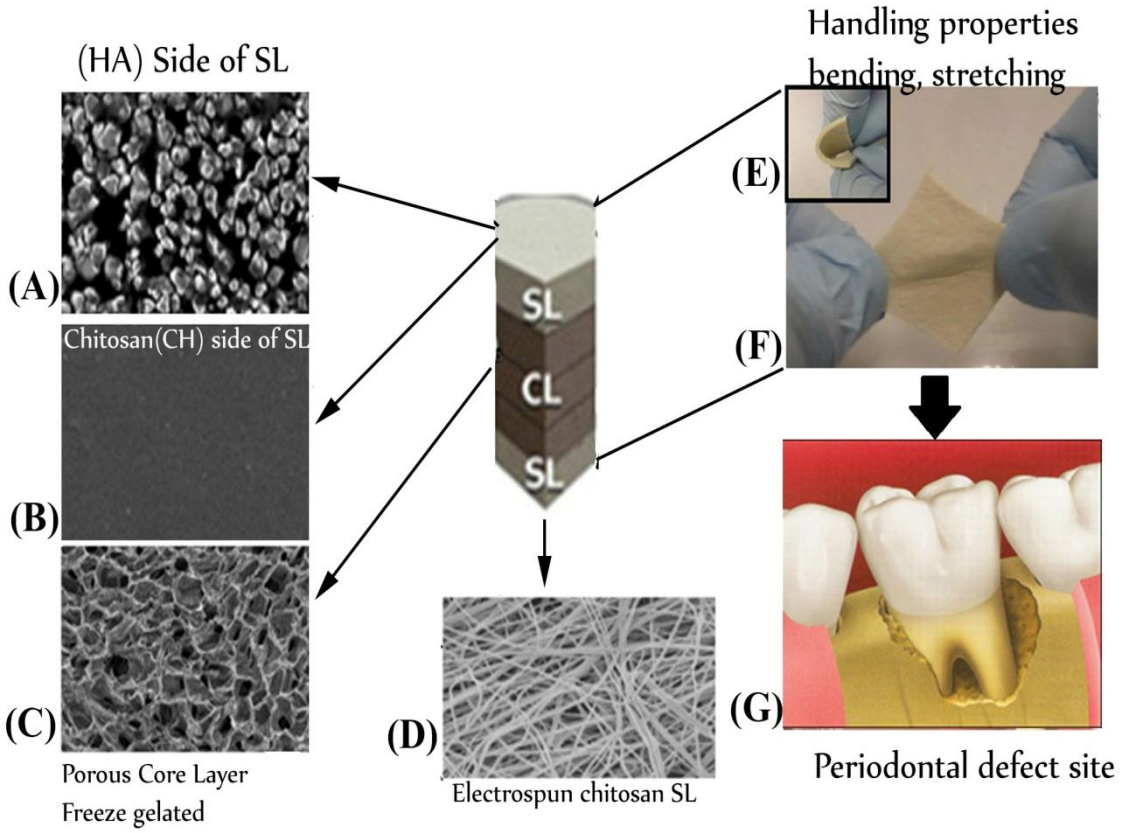

Figure 8: Diagrammatic illustration of Trilayered GTR membrane with Surface (SL), Core (CL) and Surface layer (SL), (A) Solvent casted membrane with HA surface (A) and CH side (B) as surface layer interfacing the Freeze gelated CL (C), and Electropsun mats as SL (D) and (E) a transverse section of the membrane showing layered arrangement, with HA side facing the defect (F) Membrane showing handling and bending properties which can easily be placed at a periodontally compromised segment showing bone destruction (G).

2.19. Chitosan

Chitin is a natural biopolymer that is present in the cell walls of fungi and exoskeleton of crustaceans (shrimps, lobsters and crabs) making it an essential component of exoskeleton. Chitin (Figure 9) was first discovered by the French scientist Barconnot in 1811 and deacetylated chitin was discovered by Roughet in 1859, which is now known as Chitosan (CH) (Figure 9). Chitin is the second most abundant naturally occurring cationic amino polysaccharide in the world (Queen 2006).

2.19.1. Structure of Chitosan

Structurally CH is a linear amino polysaccharide consisting of (β 1-4) linked D-glucosamine residues and randomly located N-acetyl glucosamine groups. This gives CH a three dimensional α-helical configuration which is stabilized by intra-molecular hydrogen bonding. The ratio between these two components gives the measure of deacetylation. Chitin and CH are almost the same polymer but with a different degree of acetylation. The molecular weight tends to vary with the source and method of preparation. It has a range of 300 to 1000kDa (Abbas 2010). That is available commercially range from 50 to 90% (J.-K Francis Suha 2000). The molecular structure of chitin and CH are shown in Figure 9.

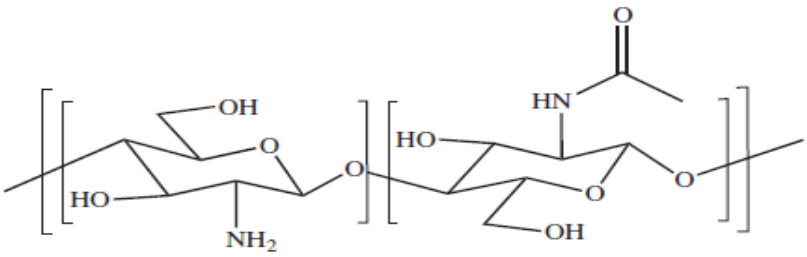

A Chemical structure of chitosan.

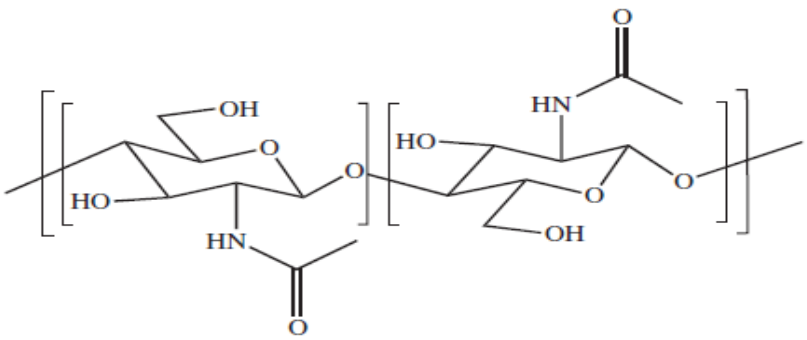

B Chemical structure of chitin.

Figure 9: Chemical Structure of Chitosan (Abbas 2010) Chemical structure of chitosan (A) and chitin (B).

2.19.2. Processing of Chitosan

Processing CH from crustacean shells involves certain steps. These steps can be characterized as : Deproteinization, Demineralisation, Decolouration and Deacetylation. Crustacean shells are reduced in size then the protein is separated from them (Rinaudo 2006).

2.19.3. Properties

The properties of CH can be predicted from the way chitin is processed, since it is the processing conditions that control the amount of deacetylation that occurs. The amount of free amino groups in the polymer chain depends on the degree of deacetylation. These amino groups give CH its positive charge. Along with this amino group, a hydroxyl group gives the polymer functionality which makes CH a highly reactive polysaccharide. A positive charge on CH allows it to establish many electrostatic interactions with negatively charged molecules (Queen 2006). Processing techniques and functional groups formed by deacetylation permit side group attachment; this in turn affects crystallinity which is related to CH's ability to solubilise in aqueous acidic solutions (Hudson 2001).

2.19.4. Chemical Properties

CH is structurally similar to hyaluronic acid and glycosaminoglycan's (GAGS), due to the availability of a highly reactive amino group along the polymer backbone (Nair and Laurencin 2007). Chemically CH exhibits a linear polyamine nature. It has reactive amino and hydroxyl groups. CH can also chelate many transitional metal ions. It forms aldimines and ketimines with aldehydes and ketones at room temperature. The amino group is as the C-2 position of each deacetylated unit. Primary and secondary hydroxyl groups are present at the C-6 and C-3 positions. These reactive groups allow chemical derivatization under certain conditions and allow amalgamation with drugs (Raafat and Sahl 2009). A strong positive charge on CH makes it very effective muco-adhesive and due to this, it can establish strong interactions with negatively charged mucous membranes. Other attributes of CH are its ability to show stimulatory properties on macrophages, and chemo attractive effect on neutrophils (Nair and Laurencin 2007).

2.19.5. Solubility

CH has shown to be soluble in dilute acidic solutions with a pH less than 6.0. CH is considered a strong base due to presence of strong amino groups with a pKa value of 6.3. The pH has a pivotal role in the final charge and properties of CH. A low pH causes these amines to become protonated and change to positively charged. This makes CH a water soluble

polyelectrolyte. Solubility is also highly dependent on the degree and method of deacetylation used. Organic acids such as acetic acid, formic acid, lactic acids can dissolve CH. Furthermore, trifluoroacetic acid (TFA) and hexfluoroisopropanol (HFIP) have also been suggested as solvents for electrospinning CH. However the pH of these acids is around 1.8 to 2.0 (Pillai *et al.* 2009). A pivotal role is played by the concentration of the acid as it imparts functionality. The solubility of CH is a crucial parameter to control as it involves factors like the type of acid used, concentration of the acid, degree of acetylation of CH, amount of CH used and its molecular weight and distribution of acetyl groups along the main chain (Pillai *et al.* 2009).

2.19.6. Biological Property

CH shows excellent biocompatibility being a natural polymer and exhibits biodegradability. Its structure is similar to that of glycosaminoglycans (GAG) of bone extracellular matrix (ECM), and it triggers cellular adhesion, proliferation and osteoinduction (Muzzarelli *et al.,* 1989, Muzzarelli *et al.,* 1984, Muzzarelli 2009). It has the ability to aggressively bind to mammalian and microbial cells, and has shown regenerative effect on connective gingival tissue (Shue *et al.* 2012). Stimulation of osteoblastic activity is also important in bone regeneration applications. Other properties include; haemostatic, fungistatic, spermicidal, antitumor, central nervous system depressant and immune adjuvant. CH exhibits minimal foreign body reaction (Raafat and Sahl 2009). Oral administration of CH in human found to be non-toxic. It is FDA approved for use as a food additive (Nair and Laurencin 2007). According to the 17th rule of medical device directive (MDD), all medical devices containing chitin and or its derivates are classified as class III (Struszczyk *et al.,* 2007).

2.19.7. Antimicrobial Property

CH has also antimicrobial properties. The antimicrobial property arises from 3 different sources; positive charges present in the polymeric chain of CH due to its amino group counteract with negative charges from the remnants of macromolecules like proteins and lipopolysaccharides in the membrane of microbial cells, obstructing with nutrient exchange between the exterior and interior environments of cells. These charges are also responsible for competing with calcium for electronegative sites in the membrane, compromising its integrity and causing the release of intracellular materials eventually causing cell death (Martínez-Camacho *et al.* 2010). In dentistry, CH has shown to have an effective plaque reducing action. It has also shown to have an effect in-vitro against several oral pathogens suspected in plaque formation oral microorganisms like Actino bacillus actinomycetemcomitans, Porphyronomas gingivalis and Streptococcus Mutans (Choi *et al.* 2001; Raafat and Sahl 2009).

2.19.8. Biodegradation of Chitosan

The degradation of polymeric biomaterials used for bone regeneration and tissue engineering is a pivotal factor for successful regeneration of new healthy tissue. The rate of degradation should be ideally tailored to the rate of tissue generation. Biodegradation of the polymer (or the ultimate metabolic fate) is an important aspect to be considered in designing biomaterials with specific application. The degradation, mechanical property and dimensional stability of polymeric implants are directly correlated with the ability to uptake water. The life of an implant device is affected by its ability to uptake and with hold water, which is dependent on the diffusion coefficient of the material. Materials with a high diffusion coefficient bear the tendency to allow water to breach into the matrix allowing water soluble additives to be released more rapidly (Correlo *et al.* 2007). The systemic absorption of hydrophilic polymers such as CH is hugely dependant on the molecular weight for renal clearance. Chitosan like other polymers is sensitive to different types of degradation processes such as, oxidative, hydrolytic, thermo, photo and ultrasonic degradation. Synthesis of CH and its derivative require its exposure to heat, light, water and microorganisms. The process by which CH degrades is dependent on two main factors; namely the DD and the distribution of N-acetyl-glucosamine units. However CH can be degraded by several means, its degradation rate is inversely proportional to the degree of crystallinity. The biodegradation decreases when DD is less than 70%. Enzymatic degradation is mostly responsible for breakdown of CH. Other hydrolytic enzymes such as lysozyme can also be used to naturally degrade CH. Lysozyme commonly exist in the human body fluids and tissues at a concentration level of 4 to 13 mg/ml in serum (Ren *et al.* 2005) and 450 to 1230mg/l in tears and is the main enzyme responsible for degrading CH in human body. The activity of lysozyme tends to decrease with increasing pH or increasing temperature. Degradation behaviour of CH can therefore be triggered (or tuned) with control of the environment. Another factor that affects degradation is conditions surrounding the implanted site (Wei *et al.* 2011).

The DD is a pivotal indicator for predicting the degradation rate of CH. *In vivo* CH degradation product results in the release of amino sugars, which can be easily processed and released through the metabolic system. Hydrolysis and biodegradation of CH due to water and microorganisms is also related to the DD, as the DD increases the rate of degradation decreases. This is due to the high degree of macromolecules packing subsequently decreasing rate of water sorption. This has an effect on the access of microorganisms to the inner regions of the films. A study conducted by Mucha *et al.,* have reported on the basis of spectroscopic studies about the changes in deforming vibration of –C-O-C- groups in the band 1150-1040cm^{-1}

during thermal and photo degradation. A decrease in the absorbance of the wavelength of –C-O-C- bonds is correlated to the scission of chitosan chain into smaller fragments. The scission of CH macromolecules causes formation of free radical that initiate oxidation in some cases (Mucha *et al.* 2002).

Modes of Biodegradation

The biological environment in which a biomaterial is implanted includes different biological agents responsible for degradation of polymeric substances. These agents could be bacteria, fungi or even enzymes. Biodegradation is considered as a relatively rapid process which is affected by moisture, temperature and availability of oxygen. Two different types of microorganisms are responsible for degradation of natural and synthetic polymers, namely, bacteria and fungi (Chandra and Rustgi 1998).

Role of Enzymes

Enzymes are considered to be biological catalysts with a similar action to that of a chemical catalyst. They act by lowering the activation energy thereby inducing or enhancing the reaction rates. The 3-D structure of enzymes contains certain sites on the surface that have a characteristic structure. These active sites act as pockets for substrates to bind to, eventually leading to a chemical reaction. Two most commonly known mechanisms of enzyme activity are biological oxidation or biological hydrolysis (Chandra and Rustgi 1998). Enzymes are known to be responsible for the rate and extent of CH degradation in vitro. Some of the enzymes are chitosanase, lysozyme and papain. In-*vivo* degradation of chitosan through lysozymes takes place by hydrolysis of the acetylated residues. Fast degradation rates of chitosan have been attributed to the deformation of strong hydrogen bonds (Chandra and Rustgi 1998) (Nair and Laurencin 2007).

2.19.9. Cross-linking Chitosan

Agents that stabilise polymers by coupling and bonding functional groups in chains are known as cross linkers. Agents that have been used for cross linking CH in the literature are gluteraldehyde, genipin and di-isocyanate. Chemical modifications in the chemistry of CH are possible due to the presence of reactive groups like amino and hydroxyl groups. Chemical reactions such as acylation, quaternization, sulfation, thiolation and carboxymethylation have the tendency to provide an array of products with antifungal, antiviral, antibacterial, transmucosal and anticoagulation properties. The aforementioned chemical reactions are a

result of esertification or etherification that involves the $–NH_2$ group at the C-2 position and non-specific reactions of –OH groups at C-3 or C-6 positions (Riva *et al.* 2011).

Cross-linking by Aldehydes

Gluteraldehyde is a bi-functional aldehyde, it acts with the formation of imine bonds between amino groups of CH and bi functional gluteraldehyde cross linker. Although this agent is said to have a toxic effect its, cross-linking plays a pivotal role in the physical and swelling properties of CH based gels (Mi *et al.* 2000). The DD governs the extent of cross-linking. It is not dependent on the molecular weight of CH. The degree of cross linking is also governed by the concentration of gluteraldehyde and reaction temperature in CH based microspheres (Chen *et al.* 2011).

Cross-linking by Genipin

Another effectively used cross linking agent is genipin. It's a naturally occurring heterocyclic compound which can be extracted from its parent compound geniposide. Geniposide isolated from fruits of gardenia jasminoides ELLIS. A study performed on evaluating the cytotoxicity of genipin over gluteraldehyde has shown that genipin is about 5,000- 10,000 times less cytotoxic than glutaraldehyde (Sung *et al.* 1999). Cross-linking reactions involving genipin are pH dependant. Acidic and neutral conditions cause genipin to react with CH through a nucleophilic attack by primary amino groups, on the olfenic carbon atoms at C-3 position of deoxyloganin aglycone, followed by opening of the dihydropyran ring and attack by the secondary amine group on the intermediate aldehyde group forming heterocyclic amines. (Mi *et al.* 2000; Chen *et al.* 2011). Strong basic conditions cause genipin to undergo a ring opening polymerization prior to cross linking; these cross-linked bridges consist of polymerized genipin macromers and oligomers. The initiation of this polymerization is caused by extraction of a proton from the hydroxyl groups at the C-1 position of deoxyloganin aglycone, followed by opening of dihydropyran ring to enable and aldol condensation (Mi *et al.* 2002).

Cross-linking by Sodium Tripolyphosphate (NaTPP)

Compared to chemical cross-linking of CH, ionic interactions of CH with other compounds have been suggested to be more advantageous in the literature. CH nano to micro particles and beads have been fabricated using NaTPP ($Na_5P_3O_{10}$), also known as triphosphoric acid, and pentasodium salt. The chemical structure of NaTPP is represented in Figure 10 below.

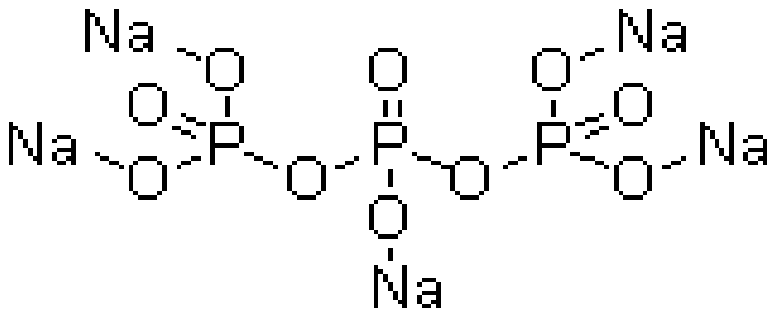

Figure 10: Chemical structure of Sodium Tripolyphosphate

Some authors also report the use of NaTPP to crosslink porous sponges/hydrogels for drug delivery and tissue engineering applications. NaTPP is a nontoxic multivalent anion and has the tendency to cross link by ionic interactions between amide group of CH and anionic NaTPP ions. The charge density and pH of the solution play a pivotal role in the availability of interactive site. A Study conducted by Bhumkar *et al.,* on assessing the effect of pH on cross-linking of CH with NaTPP interactions have reported that at the availability of –OH (hydroxyl) and phosphate ions is dependent on the pH to either be 3 or 9. At pH 3 only phosphoric ions are available and at pH 9 both –OH and phosphate ions compete with each other to interact with amide ($-NH_3^+$) of CH. They state that initially when CH is dissolved in ACa the free $–NH_3$ group gets hydrated (Bhumkar and Pokharkar 2006). The cross-linking density also affects the swelling ratio of scaffolds and varies with the percentage of NaTPP used. The pharmaceutical potential of NaTPP has been extensively explored using CH and different drug interactions and it is known to increase the loading efficiency and prolong the drug release. The electrostatic interactions in between NaTPP and CH in another study by Shen *et al.,* have stated that this type of cross linking leads to decrease in intermolecular spaces and hence results in suspension of the released drug. This causes prolonged disintegration of porous sponges. Concentrations of NaTPP commonly deployed for studying drug release of various complexes vary from 1%, 5% to 10 % wt /v in water. Giri *et al.,* have stated that a maximum drug loading efficiency of 90% was observed when 10% (wt/v) NaTPP was used (Giri *et al.* 2012).

Other Cross-linking Agents

Numerous other bifunctional reagents have been used for cross-linking CH covalently, such as di-isocyanate, epoxy compounds 4 butanediol di-glycidyl ether or ethylene glycol di-glycidyl ether (EDGE) (Chen *et al.* 2011). For applications of making scaffolds by electrospinning CH needs to be cross linked with agents that promote chain entanglements and physical bonds with CH. Synthetic Polymers preferred for this application vary from polyethylene oxide (PEO),

poly vinyl alcohol (PVA), poly lactic acid (PLA), nylon, polycaprolactone, (PCL) and proteins such as collagen, zein and silk have also been blended to get CH based composite nanofibres. Polyethylene is preferred due to its low toxicity and water solubility; it acts as a proton acceptor while CH acts as a proton donor, causing the formation of homogenous polymeric blends (Neto *et al.* 2005).

2.20. Sterilization of Chitosan and Composite scaffolds

Chitosan based biomaterials intended for use in tissue engineering applications need to be sterilized before implanting. A safe method for sterilization should give optimum results without hindering the chemical nature of biomaterials. CH and its composite scaffolds have been assessed for sterilization by various methods in the literature. A few of the commonly used methods for other biomaterials are dry heat, autoclaving, ethylene oxide (EtOX) or *γ*-irradiation (Khor and Lim 2003). A detailed study performed by Lim *et al.,* mentioned about the use and effects of dry heat, saturated steam and *γ*-irradiation on CH based thin film/ membranes. EtOX was not assessed as it is known to effect the chemical structure of CH. Use of dry heat tends to decrease the aqueous solubility of CH and in severe conditions results in insolubility in acidic medium (Khor and Lim 2003). This effect was related to the cross-linking nature of $–NH_2$ groups in CH. A significant effect on mechanical properties is also observed for example a 60% decrease in tensile strength with a 53% reduction in strain at break is reported for CH made scaffolds. When saturated steam was used, CH became water soluble and lost 80% of its tensile strength while retaining only 28% of its strain at break point (Lim *et al.* 1999).

It was reported Lim *et al.,* that, *γ*-irradiation at 2.5Mrad performed under anoxic conditions could possibly be the best means of sterilization of CH products. They reported that although this process cause breakage of the main CH chain, when used at 2.5Mrad, it showed a 58% increase in ultimate tensile strength and overall decrease in the swelling ratio to about 22 to 33% (Lim *et al.* 1998; Khor and Lim 2003). A lot of scope still exists in optimizing the ideal sterilization methodology for CH products when considering scaling up products for commercial use.

2.21. Scaffold fabrication techniques with Chitosan

2.21.1. Solvent Casting

Solvent casting is one of the most commonly used techniques to fabricate thin films or membranes. CH has been used to synthesize thin films by solvent casting to obtain 3D scaffolds with different morphologies and topography. It involves the use of a volatile solvent

to dissolve the polymer; the solution is then casted into a petri dish. To control the thickness and other morphological features of the membranes the evaporation rate can be slowed depending on the application. Other techniques employed with solvent casting / evaporation is particulate leaching, in which a suitable porogen such as salt or sugar is used with a predefined size. If the particle size of the porogen is controlled the pore size can also be harnessed to some extent. These porogen are then dispersed in to the polymer solution which is then casted in a mould for solvent evaporation (Liu *et al.* 2004) .

Solvent casting has been used in combination with particulate leaching to develop scaffolds with controlled porosity, surface area to volume ratio, pore size and crystallinity depending upon a certain application (Maganti *et al.* 2011).

2.21.2. Freeze gelation

Phase separation has been employed to synthesize porous templates for use in tissue engineering and regenerative medicine. Phase separation is achieved in this technique by gradually decreasing the temperature of the polymer solution such that it could freeze. This eventually results in two distinct gradients, a polymer low and or high polymer concentration (Polymer rich and polymer lean phase) (Dutta *et al.* 2004). In this methodology chitosan solution is subjected to temperature such that the solution is frozen. This frozen disc or solution is then immersed in a gelation media at a temperature that is lower than the freezing point of the chitosan solution itself. Ho *et al* and Hsieh *et al.,* have reported in there earlier studies that this methodology is both time and energy efficient, results in less residual solvent and is also convenient for scaling up (Ho *et al.* 2004)(Hsieh *et al.,* 2007). The gelation solution used provides an alkaline environment and is usually a mixture of NaOH and ethanol that is precooled at -20^{o}C, in order to adjust the pH that could assist the gelation of chitosan at a temperature less than the freezing point of the solution. Thus resulting in CH scaffolds that retains it porous morphology without the need of any freeze drying (Ho *et al.* 2004).

By using different solvents and regulating the polymer concentration at various cooling rates, phase separation is achieved. Ho *et al.,* reported the use of freeze gelation technique to synthesize 3-D porous scaffolds using CH Ho *et al.,* reported the use of freeze gelation technique to synthesize 3-D porous scaffolds using chitosan (Ho *et al.* 2004). The freezing process can be carried out in a more controlled manner that allows control over the orientation of ice crystals in a particular direction as they grow (Deville and Nalla 2006; Deville *et al.* 2006). More recently Park *et al.* have used directional freeze-casting with gelatin to

mimic topographies with angular similarities of alveolar crest and natural orientation of periodontal ligaments (Park *et al.* 2014).

2.21.3. Freeze drying

Freeze drying or lyophilisation has also been employed as an efficient method to obtain porous 3 dimensional scaffolds. A polymer solution is prepared with a desired solvent. The solution is then frozen and the solvent is extracted by lyophilisation under high vacuum. Freeze drying usually retains the porous structure. Although freeze drying is a commonly used method to obtain templates with porous features for tissue engineering applications, it is time and energy consuming such that the whole scaffold fabrication process becomes inefficient and economically uncompetitive. Another drawback of this method is the occurrence of a surface skin during the freeze drying stage. If the rate of temperature change is not harnessed well enough, the polymer matrix is not rigid enough to resist the interfacial tension caused by the solvent, hence, porous architecture collapses and dense skin layer forms on the prepared scaffolds (Ho *et al.* 2004). Freeze gelation has been used to synthesize porous scaffolds, and by comparison has shown to be a much more efficient and less time consuming method (Hsieh *et al.,* 2007)..

2.21.4. Electrospinning

2.21.4.1. Introduction to Electrospinning

Electrospinning process was first patented in 1934 by Formhals. They reported the production of polymer filaments using electrostatic forces (Bhardwaj and Kundu 2010). When fibres are spin this way, the process is hence called as Electrospinning. Alternatively this process can also produce nanofibres through an electrically charged jet of polymer solution or melt. This jet is ejected from the tip of the needle, at which the polymer droplet elongates into a conical object known as Taylor cone (Garg *et al.,* 2011). The morphology of the fibres can vary from submicron meters to nano meters (nm). By manipulating the processing parameters fibres of different morphology can be obtained according to the final application. Studies have shown that this procedure is not only used in healthcare, energy production, biotechnology, agriculture, defence and security domains but also has shown success in fabricating scaffolds for tissue engineering application, that have high surface area to volume ratio and mimic natural ECM (Formhals. 1934; Seeram Ramakrishna 2005).

2.21.4.2. Electrospinning Process

The processing is based on spinning technique, by using electrostatic forces to produce fine fibres from polymer solutions or melts and the fibres thus obtained have very thin diameter (ranging from nanometre (nm) to micrometre (µm)) and a much larger surface area usually obtained from conventional spinning techniques (Bhardwaj and Kundu 2010). A DC voltage is used to generate electrospinning within the range of 1 to 30kVs. Currently two kinds of setups are used; vertical or horizontal setup (Figure 11). Three major elements of this technique are a high voltage power supply, a spinneret and a grounded collecting plate like a metal screen or rotating mandrel (Figure 11). The DC voltage source is used to inject a charge of certain polarity into the polymer melt solution which is then accelerated towards the collector of opposite polarity (Liang *et al.* 2007). Polymer solutions are designed by blending polymers and solvents. When the polymer is completely dissolved it is then poured into the capillary tube for electrospinning (Agarwal *et al.* 2008; Khan 2009). The figure below depicts the typical electrospinning setup and the adjacent images show the fibre orientation in random and aligned fashion can be achieved by regulating the parameters such as speed of the collector drum or voltage applied.

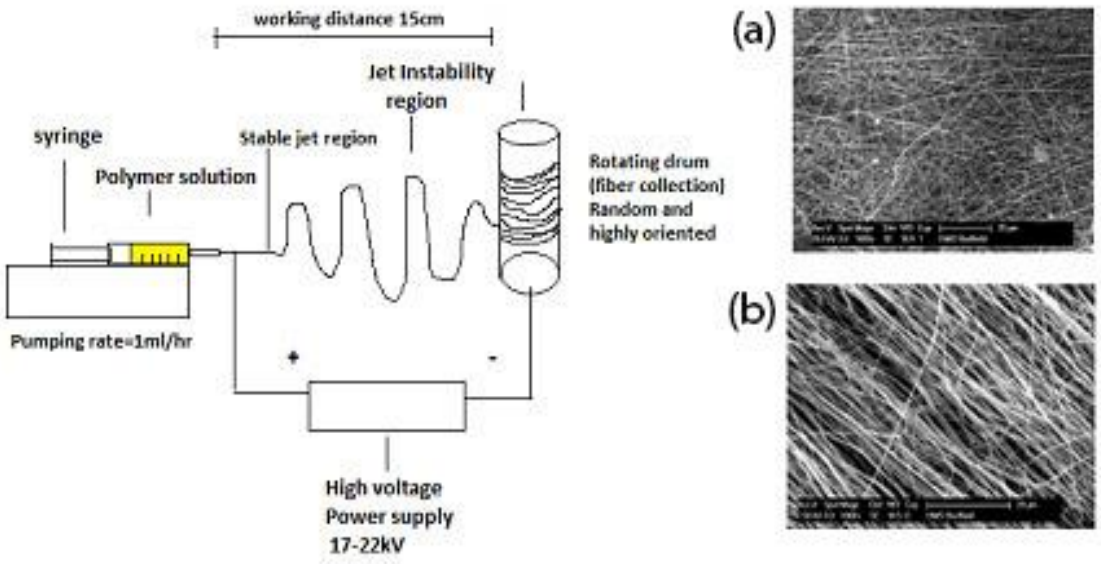

Figure 11: Electrospinning rig showing polymer solution loaded on to a syringe and charged with high voltage to generate fibres and land onto a rotating drum collector (a) Random (b) Highly oriented CH fibres.

A polymer droplet is held by its surface tension at the end of the syringe needle which is subjected to the electric field, an electric charge is activated on the liquid surface due to its electric field. When this field reaches a critical value the repulsive electric forces overcome the

surface tension forces (Bhardwaj and Kundu 2010). Finally a charged jet of polymer solution is ejected from the tip of the Taylor cone consequently an unstable and a rapid whipping of the jet occurs in between the capillary tip and collector as a result solvent evaporates leaving the polymer behind (Huang *et al.* 2003; Dalton *et al.* 2007). Initially the jet is subjected to a linear trajectory, however, the jet later begins to whip in a chaotic fashion at some critical distance (Garg *et al.,* 2011). Figure 11 shows a typical electrospinning setup used for obtaining random and aligned CH fibres.

2.21.3. Effect of processing factors

Processing Parameters

Processing parameters vary with the applied voltage, feed or flow rate of polymer melt, types of different collectors and tip to collector distance. The voltage applied to the polymer solution plays a crucial role; higher voltage increases the electrostatic repulsive force on the fluid jet with increased polymer ejection causing fibres to be formed with larger diameter. However, it has also been reported that greater electrostatic forces cause higher stretching of solution due to greater columbic forces in the jet causing a stronger electric field eventually causing a decrease in the fibre diameter and higher rate of evaporation of solvent from fibres (Haghi and Akbari 2007; Agarwal *et al.* 2008).

The flow rate is also an important parameter to be considered when conducting electrospinning. Slower feed rate will result in fibres with smaller diameters. However, this would eventually increase time of the entire process. Lower feed rate will give enough time for evaporation of the solvent. If the flow rate is increased, this could also inadvertently affect the pores and fibre diameter as well. Some researchers have also mentioned that higher flow conditions result in the formation of beaded fibres due to unavailability of drying time before reaching the collector (Zuo *et al.* 2005).

While electrospinning the collector also serves as a critical component of the electrospinning assembly, acting as a conductive substrate were nano fibres can be collected. Aluminium foils are commonly preferred agents to be used as a collector, however, due to the problems in transferring collected fibres other available options include conductive paper, conductive cloth, wire mesh, parallel or guided bar, rotating wheel or rotating rods are also opted as collectors. To keep a controlled fibre diameter and morphology the tip to collector distance is also of paramount importance. Bead formation is another common consequence if this

parameter is not tailored. This distance is important as it favours the evaporation of solvent from the nanofibres (Agarwal *et al.* 2008).

Solution Parameters

The concentration of the polymer solution should be adequate enough to deliver a polymer fibre. Low concentration solutions result in a mixture of beads and fibres, as concentration of solution increases, fibres acquire a more spindle like structure and show uniformity with fibres having increased diameters because of higher viscosity resistance or there is obstruction in the formation of fibres due to the inability to maintain solution flow at needle tip eventually resulting in larger fibres (Sukigara *et al.* 2003) (Haghi and Akbari 2007).

The molecular weight can also have a serious effect on conductivity, dielectric constant, surface tension, viscosity, electrical and rheological properties. Preferably high molecular weight solutions are selected as they give desirable viscosity for fibre generation. Molecular weight also gives an idea of the number of entanglements of polymer chains in a solution. Solution viscosity plays a key role in determining the fibre morphology and size and an optimal viscosity is a needed to achieve fibre formation (Bhardwaj and Kundu 2010). At high viscosity there is hindrance in ejection of polymer melt and at low viscosity there is no continuous fibre formation. Highly viscous polymer solutions show longer stress relaxation times which restricts the fracturing of ejected jets subsequently fibres obtained at high viscosity also exhibit larger and more uniform fibre diameter. The polymer solution viscosity has been correlated to the concentration of the solution, hence, viscosity, molecular weight and polymer concentration are interrelated with each other. Surface tension of the solvent helps obtaining nanofibres with no beads. Different solvents can be used for the same polymer but they all contribute to different surface tensions (Bhardwaj and Kundu 2010). Higher surface tension of polymer solutions obstructs electrospinning because of fluctuation of the jets and generation of sprayed droplets. Another factor determining the outcome of the fibres is surface charge density or conductivity. An increase in the electrical conductivity of the solution affects the fibre morphology by making the diameter smaller, whereas, the low conductivity of solvent causes insufficient elongation of the jet by electrical force to produce uniform fibres that exhibit some visible bead formation. Polymers are mostly conductive and charged ions in the polymer solution are highly substantial in jet formation (Agarwal *et al.* 2008).

Polymers used for Electrospinning

A wide variety of polymers are used for electrospinning. They range from synthetic and natural polymers to blend of synthetic and natural polymers together. More than 200

types of polymers have been electrospun from; PGA, poly Lactide co-glycolide (PLGA), PCL, polyurethane (PU), PLA, polystyrene (PS) and poly vinyl alcohol (PVA). Natural polymers preferred for electrospinning are silk, gelatin, hyaluronic acid, cellulose, collagen, and CH. Copolymer solutions or combinations of natural and synthetic polymers are used to manage the properties of the fibres depending on the application. This method offers tailoring the properties like thermal stability, mechanical strength and barrier properties. Other properties like cell affinity, morphology, structure, pore size, pore distribution and degradability can also be manipulated by copolymer electrospinning (Bhardwaj and Kundu 2010).

Electrospinning of Chitosan

Generating nano or micro fibres by electrospinning of CH is a time consuming and laborious task. The most common solvent used currently for dissolving CH is trifluoro acetic acid (TFA) or combinations of dilute acetic acid and copolymerization with polyethylene oxide (PEO) (Muzzarelli 2011). Using TFA relies on empirical knowledge, since varying viscosity, temperature, electrical potential, geometry of collector and other parameters can affect the final morphology of nano fibres. Alternative approaches adapted involve neutralization with alkaline compounds or even cross-linking (gluteraldehyde and genipin). However, their neutralization causes unwanted contraction leading to partial or complete loss of features (Muzzarelli 2011).

CH is usually soluble in most organic acids. Its protonation changes it into a polyelectrolyte in acidic solutions. Due to this unique property, CH is unable to produce continuous fibres, because of the formation of continuous formation of droplets. It has been reported, that it is the repulsive forces between ionic groups within polymer backbone of CH that are generated due to application of high electric field while electrospinning inhibit the formation of continuous fibres (McKee *et al.* 2005; Jayakumar *et al.* 2010). Electrospinning CH is a challenging task due to the difficulties in achieving the ideal viscosity. Its inherent rigid chemical nature, high crystallinity and tendency to hydrogen bond leads to poor solubility in organic solvents (Lee *et al*. 2009). Being a cationic polymer, polyelectrolyte nature it undergoes a polyelectrolyte effect when in aqueous solution, its polymer coils are stretched to large extent due to the existence of charged groups. If the solution is free of added electrolytes the polymer coil shrinks and the concentration of the polymer increases. Solutions with a high concentration of CH are not injectable and those with low amount of polymer will eventually result in a low output rate. The use of toxic organic solvents denatures the properties and

structure of CH (Ohkawa *et al.* 2004). Figure 12 shows how the fibres repel when two needles were used for electrospinning, a typical phenomenon when electrospinning CH.

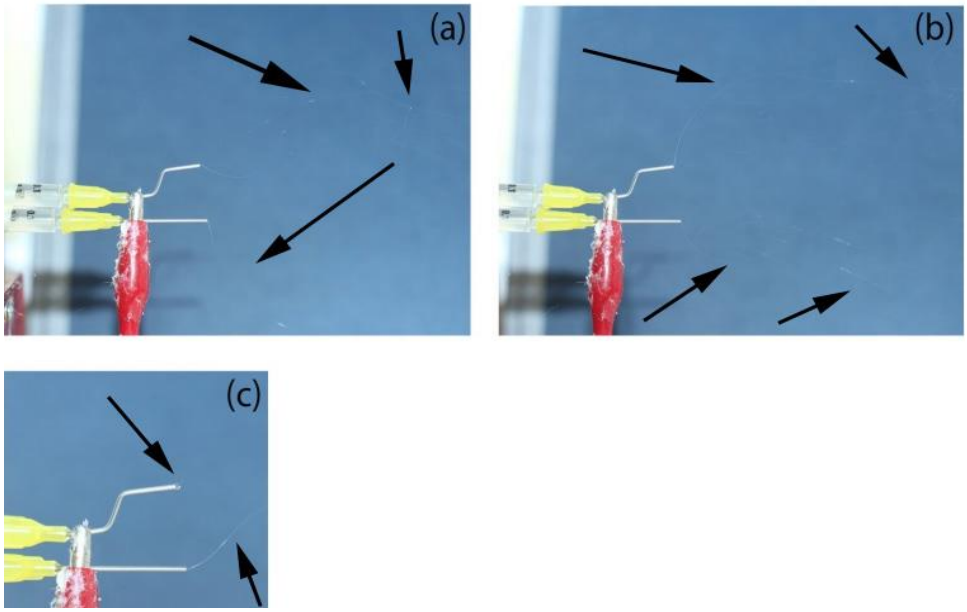

Figure 12: Electrospinning Chitosan, Dual needle setup, showing how fibres repel and showing an unstable whipping fibre (A, B), Taylor cone formation is seen in (C), black arrows showing the fibre direction.

The formation of amide bonds between CH and organic solvents has been studied by various researchers. The use of lactic acid for the formation of lactamidated CH in the form of thin films, which after purification with chloroform and methanol were tested on fibroblasts for their biocompatibility was conducted by Yao *et al.,* (Yao *et al.,* 2003). Similar studies were performed by using acetic acid and propionic acid, with respect to regeneration of chitin from CH *via* amide bond formation by Que and Toffey *et al.,* (Qu *et al.* 1999; Toffey and Glasser 1999). SEM imaging of CH fibres have shown that as the total concentration of polymer increases the fibre diameter decreased. PEO and CH solutions show phase separation with time passage, as a result blended solutions can be electrospun within 24 hours of blending. Adding sodium chloride (NaCl) further stabilizes these solutions for a longer time before and during electrospinning. Pure CH fibres with a deacetylation degree of 80% cannot be spin in aqueous acetic acid solutions. Electric field generated is insufficient to overcome the combined effect of surface tension and solutions viscosity (Klossner *et al.* 2008; Muzzarelli 2011).

2.22. Bioactivity of Polymers

The basic theme of bioactivity revolves around the fact that any biomaterial implanted within the body should actively encourage cells in the surrounding vicinity to elicit a response

within physiological environment (Hench and Polak 2002). The mechanism is triggered by a combination of ion exchange involving hydrogen, bicarbonate and sodium ions, similar to that of bonding between bone and bioactive glass ceramic. An increase in surface energy results in the formation of anchorage sites for heterogeneous nucleation hence crystallisation occurs which mimics the inorganic phase of bone (Hench 1998). This organized nucleation invites resident osteoblasts to colonize the hospitable surface and subsequently differentiate and organize via proliferation, in effect further reinforcing strong osseointegration bonding at the host and implant surface. Furthermore, molecular interactions may come in certain specific forms. Growth of vascular tissue into a cell seeded biodegradable macro porous foam based constructs is also an illustration of bioactivity of the scaffolds that serve to promote vascularisation followed by cellular differentiation and matrix synthesis that eventually leads to re organization of extra cellular environment. The concept of bioactivity may also involve the release of micro spherical particles such as ionic dissolution products promoting the cells to release certain growth factors for achieving cellular network self-assembly among other responses, therefore it is clear that the two processes of osteoproduction and osteoconduction in case of bioactive glass occur simultaneously at the bone glass interface, enabling release of critical amounts of soluble ionic species such as P, Na, Ca and Si in the immediate surroundings of cellular environment (Jones and Hench 2001; Hench and Polak 2002).

2.23. Hydroxyapatite

Bone is a pivotal component of our body as it supports and protects internal organs. When damage to the bone is small it can heal, however severe injuries with bone loss require external sources or substitutes to repair bone such as allografts or autographs. Broadly bioceramics used in healing and repair are characterized into three different types, as shown in the Table 4.

Table 4: Ceramic types used for repair of bone (table presented with kind permission of Sage Publications) Kamitakahara *et al.,* 2008.

Type	Example
Bioinert ceramics	Sintered alumina (Al_2O_3) ceramics, Calcium aluminates Sintered zirconia (ZrO_2) ceramic, Porous alumina oxides
Bioactive ceramics	Bioglass(Na_2O-CaO-SiO_2-P_2O_5 glass) Sintered hydroxyapatite [Ca_{10} (PO_4)$_6$ (OH)$_2$] ceramics

Bioresorbable ceramics	Sintered β-Tricalcium phosphate (β-TCP)

The "bioinert" ceramics are almost inert and form a thin non-adherent fibrous layer at the bone ceramic interface. The bioactive ceramics bond directly to the bone, this ability to bond is termed as osteoconductivity or bioactivity (Saravanan *et al.* 2011). Hench *et al.,* in 1970's reported that Bioglass ® had the ability to bond to living tissues without the formation of a fibrous tissue layer (Thein-Han and Kitiyanant 2007). The third type of ceramic undergoes natural resorption with time to be replaced with bone. It is a widely accepted fact that the osteoconductive property of bone is imparted by calcium phosphates (CaP) ceramics. Due to the varying chemical compositions and properties different types of CaP ceramic have been employed for bone regeneration research both in-*vivo* and in-*vitro*. Some of the more commonly researched are HA, β-Tricalcium phosphate (β-TCP), multiphasic Bioglass™, bicalcium phosphate (BCP) and octacalcium phosphate (OCP)(Hench 1998).

One of the most widely researched and studied materials for healing and repairing bone is HA [$Ca_{10}(PO_4)_6(OH)_2$] (Ratner 2004). Being a natural inorganic component of bone and teeth it's a calcium phosphate based ceramic. HA has a high elastic modulus, however; it tends to be brittle and is not easily moulded. Levit *et al.,* have been the pioneers in applying this bioceramic in biomedical application (Levitt 1969; Ratner 2004). It is now widely used for fabricating biodegradable and stable scaffolds for various tissue engineering applications such as a coating on hip implants or dental implants. Due to its slow decaying nature unlike its other crystalline phase (β-TCP) it is more osteoconductive (Lommer *et al.* 2012). Apatite refers to a broad group of structures comprised of different components. In general the apatite formula is $Ca_{10}(PO_4)_6\ X_2$, here X is typically denoted to be F, or fluoroapatite (FAp) or (OHAp) hydroxyapatite, or chloroapatite (ClAp). In HA the hydroxyl ions can be substituted for carbonate ions to become carbonated apatite. The unit cell of hydroxyapatite is made up of two types of calcium ion sites and six phosphate ions per unit cell (Zhang *et al.* 2003). The basic apatite, non-stoichiometric structure is hexagonal and with a space group of $P6_3/m$. The approximate lattice parameters are a= 9.37Å and *c*= 6.88Å. Its unit cell comprises, $Ca\ (1)_4\ Ca(2)_6\ (PO_4)_6(OH)_2$. The close relationship between Ca/P ratios is very pivotal. Lower Ca/P ratios increase the solubility and acidity of mixtures (Kong *et al.* 2005).

In the recent years the use of β-TCP has been growing. The α and β phases of TCP have exceptional resorbability. The compressive and tensile strength of β-TCP is equal to that of cancellous bone, although in *vivo* it is replaced by bone, less new bone is laid down than β-TCP

is resorbed. It is reported that it might take more than one year to replace the natural bone. TCP has been reported to repair marginal periodontal defects however, the resorption rate is still controversial. Two different hypotheses have been put forward. A process which is dependent on interstitial fluid is related to the dissolution by biological fluids due to the absence of osteoclasts around the implant. Other theory based on cellular responses or cell mediated bioresorption due to the presence of osteoclasts (Silva *et al.* 2004).

BCP is a combination of HA and β-TCP in varying amounts. BCP resorption in vivo results in the release of calcium and phosphate ions into the microenvironment, and hence these ions could be utilised for new bone formation. Octa calcium phosphate (OCP) is another promising resorbable bone substitute. It is advocated to be biological precursor of HA. OCP has shown to promote osteoblast attachment and differentiation in vivo, however, its brittleness limits its use. (Silva *et al.* 2004) With respect to the bioresorption process of HA, this class of calcium phosphate undergoes a combinations of steps (Pighinelli and Kucharska 2013). Physical factors effecting resorption are abrasion, fracture, disintegration, shape, porosity, surface area, crystallinity, and grain size. Chemical factors involve dissolution, local increase of Ca and P on the surface, composition of the material. Other factors are reduction of pH caused by cellular activity, ultimately leading to increased rate of degradation due to dissolution. Biological consideration effecting resorption are pH involving cellular involvement, diseases on infections, extent or degree of bone contact, type of bone, sex, age, hormonal and genetic causes (Pighinelli and Kucharska 2013).

2.23.1. Bioactivity and biocompatibility of hydroxyapatite

Since the discovery of Bioglass® in 1960's by Professor Hench, it has been used to repair and reconstruct bone defects in orthopedics and maxillo facial reconstruction. After 40 years of research on bioactive Bioglass® no other Bioglass composition has been found to have better properties than the original Bioglass® 45S5 composition. Most of the periodontal defects have been repaired by a particulate Bioglass® composition of 45S5 which is commercially known as Perioglass® (U.S. Biomaterials Corp). Bioactive glass coatings have the potential to not only bond to the host bone but also trigger bone growth away from the bone-implant interface, hence imparting bioactivity. This mechanism is attributed to the formation of hydroxycarbonate apatite layer on the surface of glass as a result of initial dissolution of glass. Dissolution products are usually calcium ions and soluble silica that trigger osteoblast to deposit bone matrix and minerals. Bioactive glass being biodegradable tends to have a significant effect on the bioactive coating as well, which degrades resulting in instability of the

implanted devices. Hydroxyapatite has similar issues of slow resorbability even though it bears bioactive properties. Bioactivity is broadly divided in two different types (Murphy *et al.* 2010). The level of bioactivity of a material has been correlated to the time taken for more than 50% of the interface to bond to bone. This is known as the bioactivity index or I_B (Hench 1998; Jones and Hench 2001).

1. Class A bioactivity is rapid bone bonding, also bonds to soft connective tissues, produce bone throughout the particle array, process known as osteoproduction. This class also exhibits osteoconduction ability which is the process of bond migration along a biocompatible surface e.g. 45S5, have a bioactivity index higher than 8.

2. Class B bioactive materials (e.g. hydroxyapatite) exhibits slow bone bonding ability, slow incomplete proliferation of bone throughout the particle array. This class exhibits only osteoconductivity and have a I_B value less than 8 but greater than 0 (Jones and Hench 2001; Macchetta *et al.* 2009).

Tissue compatibility or biocompatibility has been described as the ability of a material to perform with an appropriate host response when applied as intended. However, a biocompatible material may not be completely “inert” in fact the appropriateness of the host response is decisive. This is usually assessed by experts who compare new biomaterials with that already present in the market. The biocompatibility of materials is mainly determined by its release of substances through solubility or corrosion. The byproducts of solubility and corrosion may damage cells or in certain cases stimulate cellular synthesis of certain proteins to induce inflammation (Schmalz 2009).

2.24. Chitosan as a GTR membrane for periodontal regeneration

Chitosan is a very versatile polymer derived from chitin which is the second most abundant naturally occurring polysaccharide in nature. It is well acknowledged for it biocompatibility, antimicrobial bio adhesive and degradation properties. Antimicrobial ability to inhibit both gram positive and negative bacteria makes it an ideal biomaterial for tissue engineering applications. Studies based on using CH gel to heal periodontal diseases have shown to decrease the gingival inflammation markers. (Silva *et al.* 2004) Regeneration of hard tissue for tissue engineering applications using hydroxyapatite (HA) as a bioceramic is a common approach. Incorporating HA into the polymer back bone or surface grafting it has been known to accelerate apatite layer formations on biomedical implant surfaces (Sabokbar *et al.* 2001). Studies based on using HA nanocrystal in combination with CH have shown

regenerative capability of the composite in periodontal defect. Fraga *et al.,* studied CH HA composite membranes coated with hydroxycarbonate apatite for guided bone regeneration and found favourable results in vivo (Fraga *et al.* 2011). Another study by Hunter *et al.,* used a CH HA and gelatin composite membrane for GTR and showed successful regeneration of periodontal apparatus (Hunter and Ma 2013). Certain parameter that govern an ideal scaffolds are, net surface charge distribution, pore interconnectivity, optimal porosity size for a particular application, elastic behaviour and material texture (Loh and Choong 2013). The diversity of CH has been illustrated in Figure 13, which depicts the possibilities that CH can change its form with respect to pH to be able to forge itself into particles, films, fibres, membranes, sponges, hydrogels or porous templates for use in tissue engineering are limitless. The potential use of CH for fabricating a trilayered functionally graded membrane specifically for use in periodontal tissue regeneration could be possible considering the diverse properties this biopolymer possess.

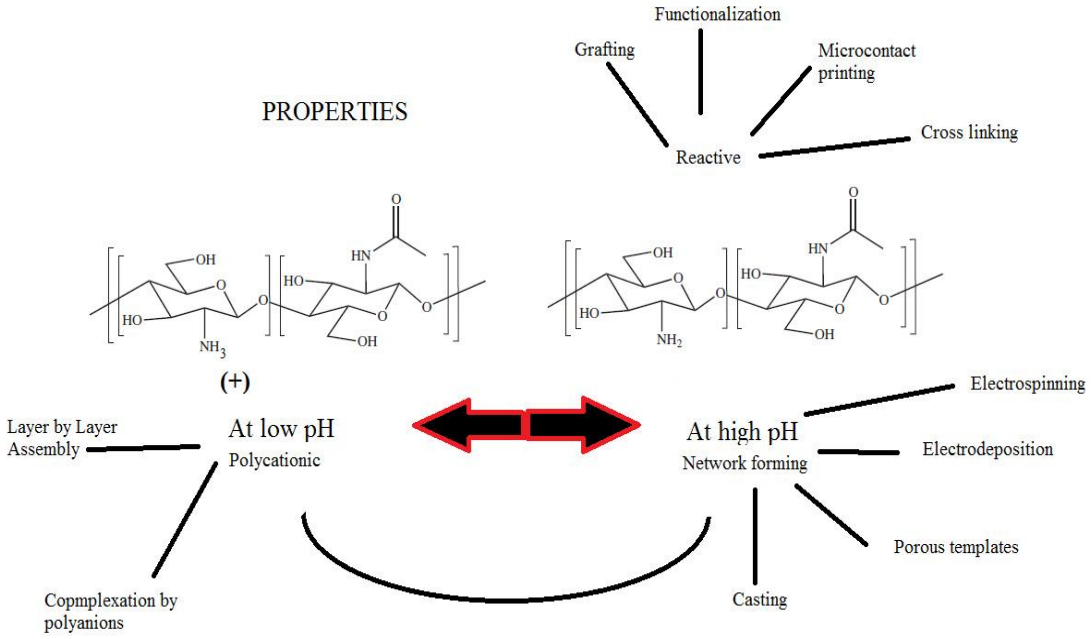

Figure 13: Schematic illustration of Chitosan versatility, At low pH (< 6) CH amines are protonated, exhibiting polycationic nature. At high pH (>6.5) CH amines are deprotonated and reactive, also interpolymer associations possible at high pH encouraging fibre, gel formation (Yi *et al.* 2005).

2.25. Drug Delivery in Periodontal Therapy

It is a well-established fact that periodontal inflammation is caused by bacterial deposits in supra and sub-gingival location. It has also been established that systemic

antibiotics can enhance the effects of mechanical periodontal therapy (van Winkelhoff and Winkel 2009) in some cases. Drug delivery in periodontal therapy may play a role in reviving the natural tissue conditions and reducing the bacterial count of microorganism occupying the defect site. Antibiotics have a prolong history of being used as adjunct to the treatment of aggressive and chronic Periodontitis (Hirsch *et al.* 2012). Systemic delivery of antibiotics leads to therapeutic concentrations at the site of infection, however, it is for a short time span resulting in the need for repeated doses for longer time periods. Local drug delivery is suggested as an alternative to overcome the limitations pertaining to systemic delivery. Another solution to this is controlled drug release which can provide therapeutically effective concentration of the drug which can be maintained for desired time period. Studies have shown that even greater improvement could be appreciated if drug delivery could be coupled with appropriate growth factors (Roskos *et al.* 1995). Drugs which have been used in periodontitis include doxycycline Hyclate, metronidazole, tetracycline, amoxicillin, azithromycin and chlorhexidine gluconate (Jain *et al.* 2008).

Combinations of drugs have also been extensively studied e.g. systemic amoxicillin and metronidazole, with both drugs being taken as an adjunct to root surface debridement (Herrera *et al.* 2002; van Winkelhoff and Winkel 2009). Systemic reviews have shown that amoxicillin-and metronidazole has shown the best clinical outcomes (Herrera *et al.* 2002). More recently there is added interest in using azithromycin. Azithromycin could have a triple role in treatment and resolution of periodontal diseases, suppressing perio-donto-pathogens, anti-inflammatory activity and healing through the persistence of low levels in macrophages (Hirsch *et al.* 2012). In another review by Muniz and co-workers, they reported that the use of azithromycin as an adjunct to conventional treatment to chronic and aggressive periodontitis generally improves clinical and microbiological findings compared to the conventional treatment alone (Muniz *et al.* 2013). A primary goal of treating periodontitis is the suppression or eradication of specific pathogens which cause a shift in the bacterial strains towards those related to a normal physiological flora (Gates 1999). In order for the drug to be effective, the perio odontopathogens should be susceptible to the drug, they should not induce resistance to the drug and the bacteria should be exposed to effective inhibitory concentrations of the drug for adequate time. Controlled drug delivery (CDD) has advanced with time from non resorbable drug carrying membranes to bioerodible polymers based membranes, fibres, micro and nano particulate systems, films, gels, (Aichelmann-Reidy and Yukna 1998) spheres, capsules and even microelectronic chips to deliver biopharmaceuticals by different delivery routes (Langer and Peppas 1981; Balmayor *et al.* 2011).

2.25.1. Role of Tetracycline (TCY) in Periodontal therapy

Tetracycline (TCY) antibiotic therapy was introduced to clinical practice in the late 1940's. It has been used since then both systemically and locally for treating chronic Periodontitis. It has a potent action against Gram negative and Gram positive species, especially against specific periodontal pathogens which is Aggregatibacter Actinobacillus actinomycetemcomitans with anti-collagenase property to reduce tissue destruction and bone resorption. TCY has been useful in treating aggressive periodontitis in which the prime pathogen Aggregatibacter actinomycetemcomitans is susceptible to the drug. However, in current clinical practice the drugs of choice are azithromycin and or a combination of amoxicillin and metronidazole.

TCY fibres have been used in periodontal treatment successfully; they are able to maintain a gingival crevicular fluid (GCF) concentration of 1590 µg/ml over a range of 10 days compared to when administered systemically the GCF concentration reaches 4-8 µg/ml. This concentration is known to be considerably higher than the minimum inhibitory concentration (MIC) for periodontal pathogens. TCY has also used in sub gingival irrigation, the usual concentration being 2cc of 5% TCY hydrochloride (50mg/ml) applied after scaling and root surface debridement (Vishakha Patil 2013).

2.25.2. Pharmacokinetics

Within 30 minutes of oral administration of TCY, detectable serum levels are achieved with peak concentration attained within 1 to 3 hours. The half-life of tetracycline hydrochloride is about 8 hours. Other members of TCY group have higher half-lives, such as minocycline and doxycycline hyclate have 16 to 18 hours, this allows a low initial dosage and less frequent dosing as compared to TCY. In a fasting state, TCY adsorption is about 75 % from the upper duodenum and stomach. Multivalent cations chelate TCY and inhibit its absorption. Once absorption occurs the drug is widely distributed to body tissues and fluids. One of the drawbacks of administering TCY during pregnancy or during fetal development is permanent discolouration and inadequate calcification of permanent teeth (Weinberg and Bral 1998).

2.25.3. Mechanism of Action

Tetracyclines are closely related to bacteriostatic antibiotics that cover a broad spectrum of activity against Gram positive and Gram negative species. Bacteriostatic action occurs by inhibition of microbial protein synthesis. The drug accumulates intracellularly or gain access to inside of bacterial cell wall through energy dependant transport systems. The rate of

drug uptake and intracellular drug level is reliant on the drug entry through the outer cell membrane and the subsequent rates of uptake and efflux at the inner membrane. Once the drug enters through the cell membrane, it could either, be transported out again, bind to cellular constituents or chemically modified hence preventing efflux. If the drug remains within the cell membrane it can bind to 30S ribosomal unit thereby preventing the binding of aminoacyl transfer RNA to the "A" receptor site on 30S messenger RNA-ribosome complex. Hence protein synthesis is suppressed by inhibition of chain elongation (Weinberg and Bral 1998).

2.25.4. Spectrum of Antimicrobial activity

Absorption of TCY when administered orally from GI tract is fairly rapid, although this absorption is reduced if it is taken with milk or substances having magnesium, iron, aluminium or calcium. These metallic ions tend to chelate with TCY. This chelated agent formed with TCY and ions is not absorbed. The daily recommended dosage is 250mg Q.I.D. The gingival fluid concentration achieved is 4-8 µg/ml, and its plasma concentration is 1.9-2.5µg/ml (Vishakha Patil 2013).

TCY are well known to exhibit an anti-collagenase property, which is related to the source of enzyme and type of TCY used. Interstitial collagenases are proteinase type enzymes, which degrade connective tissue. These enzymes are derived from either fibroblasts, epithelial cells, macrophages (MMP-1) or neutrophils (MMP-8). TCY are most active against neutrophil derived collagenase and least active against fibroblast type collagenase. This ability of TCY to inhibit collagenase is related to its tendency to bind with calcium and zinc ions. It is reported that oxygen radicals such as hydroxyl groups (-OH) activate latent collagenase (Golub *et al.* 1991; Vishakha Patil 2013).

TCY ability to inhibit neutrophil collagenase (MMP-8) affects other proteolytic events, because MMP-8 and neutrophil derived reactive oxygen species such as H_2O_2 or hydroxyl radicals can degrade and inactivate alpha-1 protienase inhibitor (Golub *et al.* 1991; Vishakha Patil 2013).

TCY's are known to exhibit bone anti-collagenase and anti-proteolytic activity as mentioned earlier, which helps inhibit bone resorption as well. Bone resorption induced by parathyroid hormone is also inhibited by TCY. It also restrains osteoblast collagenase and to some extent affects osteoclasts as well (Vishakha Patil 2013).

Anti-inflammatory properties include the ability to suppress polymorphonuclear activity, by scavenging action of reactive oxygen metabolites (Vishakha Patil 2013).

Other properties of TCY involve enhancement in fibroblast attachment in when dentine is pre-treated with tetracycline to enhance fibroblast adhesion and colonization (Vishakha Patil 2013).

Although the bacteriostatic doses of TCY (100 to 200mg/day) are linked with antibiotic resistance, the literature suggests that doxycycline at sub antimicrobial doses (20mg b.i.d) improves the condition of periodontium without these problems. Studies have also suggested that at sub antimicrobial dose, doxycycline has the ability to decrease GCF collagenases activities (Golub *et al.* 1992) (Slots and Rams 1990; Crout *et al.* 1996; Lee *et al.* 2004; Bostanci and Belibasakis 2012).

2.25.5. Pharmacokinetics & Mechanism of action of Tetracycline Hyclate

The main action is by binding to 30s ribosome and inhibits coupling of this component to amino acyl transfer RNA (tRNA) to the acceptor site of 50s ribosomal unit. Thus protein synthesis is suppressed by inhibition of protein elongation. It has also been suggested that the mechanism by which TCY inhibit collagenase is by chelation of calcium. Under most conditions inhibition of bacteria occurred when the antibiotic concentration was less than the Ca^{2+} concentration. Therefore, it is more likely that TCY's bind essentially to the Zn^{2+} in the collagenase. The binding of doxycycline to Zn^{2+} is stronger than the binding of tetracycline's to Zn^{2+}(Lee *et al.* 2004),(Rashi Chaturvedi 2008). Osseous regeneration is also potentiated in periodontal defects when administered locally due to its anti collagenolytic effect, which enhances osteoblastic activity and reduces bone resorption (Lee *et al.* 2004).

2.26. Aims and Objectives

The main aim of the work in the thesis was to synthesize functionally graded bioactive spatially designed guided tissue regenerative (GTR) membrane for treating periodontal diseases.

In order to achieve this aim the project was broken down into the following list of objectives

1. **Fabricating composite membranes using a biodegradable polymer to serve as a surface layer**
    a. Fabricating thin films of different polymer to ceramic ratios using the solvent casting method to find the best possible combination
    b. Characterisation for physiochemical, mechanical properties and biocompatibility

c. Performing bioactivity studies and assessing the degradation characteristics

2. **Fabricating bioactive and biodegradable porous scaffolds using a natural polymer with controlled porosity to serve as a core layer**

    a. Fabricating porous membranes as core layers

    b. Construction of polymer ceramic composites

    c. Characterisation of physiochemical, mechanical properties and biocompatibility

    d. Degradation studies and assessing the bioactivity

3. **Fabricating electrospun scaffolds to serve as the second surface layer**

    a. Fabricating fibrous scaffolds with random or highly aligned fibre orientation of

    b. Characterisation of physiochemical, mechanical properties and biocompatibility

4. **Combining the surface and core layers together to form a trilayered functionally graded spatially designed constructs**

    a. Combining membranes made using solvent casting, freeze gelation and electrospinning to create trilayered membrane.

    b. Physiochemical characterisation of the prepared membrane.

3. Chapter. Materials and Methods

3.1. Introduction

This chapter describes in detail the materials and methodology used to fabricate the membranes/ thin films, freeze gelated membranes and electrospun mats. Detailed characterisation of the prepared membrane was also conducted to assess the physical properties by optical imaging and Scanning electron microscopy (SEM), chemical properties by Fourier transform infrared (FTIR) and Raman Spectroscopy, mechanical testing of wet and dry specimens in tensile condition and biological characterisation was performed to assess cellular viability, proliferation and mineralised matrix deposition over a period of time. Histology on the cultured scaffolds was also conducted to visualize cellular attachment.

In-*vitro* degradation of each scaffold was conducted by assessing the changes in pH profile, weight analysis, chemical alterations were studied by FTIR and UV-Vis Spectroscopy. Freeze gelated membranes were also cross-linked (Sodium tripolyphosphate) and loaded with drug (Tetracycline Hydrochloride). In order to study the bulk and surface uptake of drug they were characterized with FTIR Spectroscopy and percentage recovery was calculated using dissolution studies.

All glass wares used in the experiment were washed carefully with neutral detergents in warm water and rinsed with deionised water followed by drying in an oven at 100°C. In all reactions stirring and heating was carried out using Stuart US152 magnetic stirrer/ heater. Continuous stirring was carried out with magnetic stirrers covered by polyethylene. Table 5 enlist the essential materials used during the project.

3.2. Materials

Core materials used in this study were chitosan and hydroxyapatite for preparing the surface and main layers of the functionally graded membranes. All other solvents and acids used in this study are listed in Table 5, refer to the next page.

3.2.1. Chitosan

Detailed chitosan chemistry has been mentioned earlier in the Literature review sections. Medium (190-310kDa) and Low Molecular weight (50-190 kDa) chitosan was used as supplied by Sigma-Aldrich® (UK).

3.2.2. Hydroxyapatite

Medical grade Hydroxyapatite (HA) was obtained from Plasma Biotal Limited (Plasma Science Group) Whitecross Road Industrial Estate Derbyshire SK17 8PY (UK) CAPTAL®S, Hydroxylapatite (sintered powder) Batch No P220 S, (XRD Ident No 3703). Particle size of the HA used varied from 0.5±2 to 12±1 µm evaluated by Particle size analyzer (Malvern Mastersizer 3000® Hydro EV wet dispersion unit, UK).

3.2.3. Phosphate buffered Saline (PBS)

PBS Buffer tablets were acquired from Oxoid Ltd, (Dulbecco A, Basingstoke, Hampshire.UK) 100 ml of distilled water was used per tablet. To obtain a final concentration of 100 mM, 5 tablets were dissolved in 500 ml of distilled water which was sterilized in autoclave for 10 minutes at 115°C. Prepared PBS was stored at room temperature (RT) (20 ± 2°C) (Qasim *et al* 2015).

Table 5. Main chemicals used in the study are enlisted below with the details of Grade, Molecular weight and Supplier.

Reactants	Grade	Mw*	Supplier
Chitosan	Medium Mol .Wt	190-310kDa	Sigma Aldrich® Lot No. SLBH2747V
Chitosan	Low Mol.Wt	50-190kDa	Sigma Aldrich® 448869 Lot No. MKBL7900V MKBK4182V
Glacial Acetic Acid >99.8% $C_2H_4O_2$ (2.5L-33209)	Reagent Grade	60.05g/mol	Sigma Aldrich® Lot No. SZBB2210V
Ethanol	AnalaR NORMAPUR	46.06g/mol	VWR® Prolabo® Batch No. 12K270517
Sodium Hydroxide (pellets) Product No. 28244.295		40.0g/mol	VWR® Prolabo® Batch No. 11F200024
Ultrahigh molecular weight poly ethylene oxide (UHMWPEO) $(-CH_2CH_2O-)In$	AnalaR Grade	5000,kDa	Alfa Aesar (A15536) Lot :F22W030
Ascorbic acid ($C_6H_8O_6$)		176.12g/mol	Sigma Aldrich® A92902 Lot No. STBC8330V
Dimethyl sulphoxide (DMSO) C_2H_6OS	Laboratory Reagent Grade	78.13 g/mol	Fisher Scientific Lot 1214398

Glycerol $C_3H_8O_3$		92.09g/mol	Fisher Scientific
Lysozyme from chicken egg white	N/A	14.3kDa	Sigma Aldrich® 69271 Lot No. BCBG4804V
Tetracycline Hydrochloride $C_{22}H_{24}N_2O_8.HCl$		480.91g/mol	Alfa Aesar B21408 Lot No. 10176525
Sodium Tripolyphosphate $Na_5P_3O_{10}$	85% pure Tech	367.85	Fisher Scientific Arcos Organics™ Code 218670250

3.3. Neat chitosan membrane/ film casting

Thin films were prepared by making a solution of a 2 wt % of MMw and LMw chitosan (CH) in 0.2 M acetic acid (ACa). Firstly, distilled water was measured and poured in a beaker and CH was weighed and added to this distal water. This mixture was heated to 50°C for 1 hour (hr) under magnetic stirring (Stuart US152, SC162, BioCote® Hot Plate Stirrer). After an hour of stirring, ACa was added drop wise with a micropipette and then the heating was switched off and the solution was left stirring at room temperature (RT) (20 ± 2°C). After 2 hours of stirring glycerol was added at 0.25 ml/gm of chitosan drop wise using a micropipette. The breaker was covered with an aluminium foil during this process. Low molecular chitosan took 5 hrs to dissolve while Medium molecular weight chitosan was left stirring for 12 hrs at RT. The solutions were then carefully transferred into glass vials and centrifuged at 45000 rpm for 5 mins. This was done to settle the undissolved bits of chitosan into the bottom of the vial. The clean solution was then carefully poured in a polytetra fluoroethylene (PTFE) petri dish and left at RT for drying. Roughly a 30 ml of solution was poured in a 9cm (diameter) petri dish. A schematic illustration in shown in Table 6 of the steps adapted to fabricate neat chitosan membranes/ thin films. Neat films have been referred as LMw 100:0 and MMw 100:0 in text below.

3.4. Composite Chitosan hydroxyapatite membrane/ film casting

Composite solutions of chitosan and hydroxyapatite were prepared in different ratios. CH:HA ratio of 70:30, 50:50 and 30:70 were prepared. The steps to composite solutions were similar till the addition of Acetic acid in neat LMw and MMw solution (Table 6). After 1 hr of ACa addition Hydroxyapatite was added in above mentioned ratios in the neat LMw and MMw solution by dropping the powder as the solution was kept stirring to have even distribution of HA throughout the solution. After 2 hrs of HA addition glycerol was added at 0.25 ml/gm and the solution was left stirring at RT. For LMw CH HA solutions, the mixture showed homogenous

distribution within 5 hrs of HA addition. MMw CH HA solutions were left stirring for 12 hrs. The solutions (30 ml) were then casted in a plastic petri dish (9cm diameter) and left in a fume hood with the lid on for 48hrs at RT. The lids were taken off after 48 hrs and the solvent was allowed to evaporate. Table 6 shows a schematic illustration of steps taken to prepare composite solutions for membrane / thin film casting. All membranes were dried for 3 days at RT before characterisation. Neutralization of the membranes was performed by 1M Sodium Hydroxide (NaOH) / 50% Ethanol solution in deionised (Di) water for 1 hr, and given 15 mins washed with phosphate buffered saline (PBS

Table 6: A schematic table showing step by step guide to prepare neat CH membranes and composite CH HA membranes in different ratios.

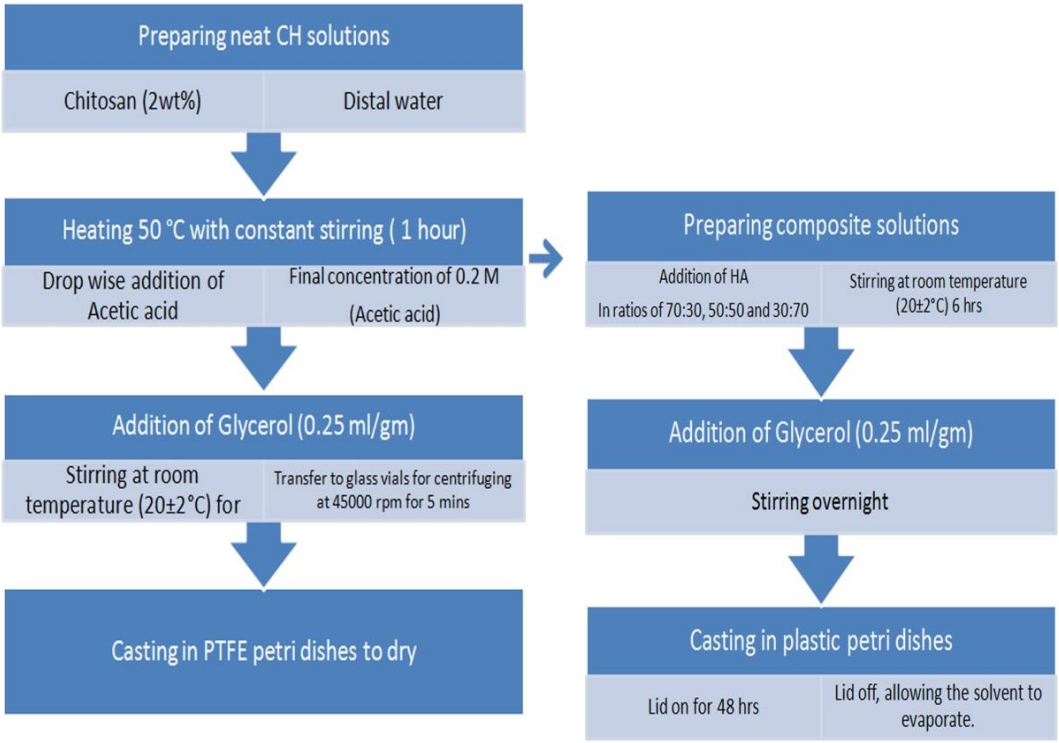

3.5. Freeze Gelation

Chitosan (75–85% deacetylated) was dissolved in 0.2 M L-ascorbic acid (ASa) (powder dispersed evenly) (99.9%) or 0.2 M acetic acid (added drop wise using a micropipette) (ACa) (Fisher Scientific, UK) to create 3% w/v solutions with or without HA. This solution was kept stirring for 6 hrs before adding HA. HA was incorporated in a ratio of 50:50, and was added to the neat CH solutions by gently spreading the HA powder and waiting for it to evenly disperse. These solutions were then stirred for 12 hrs at RT and then casted into a plastic petri dish before storing at 4 °C for 2-3 hrs and then at −20 ^{o}C for 12 hrs.

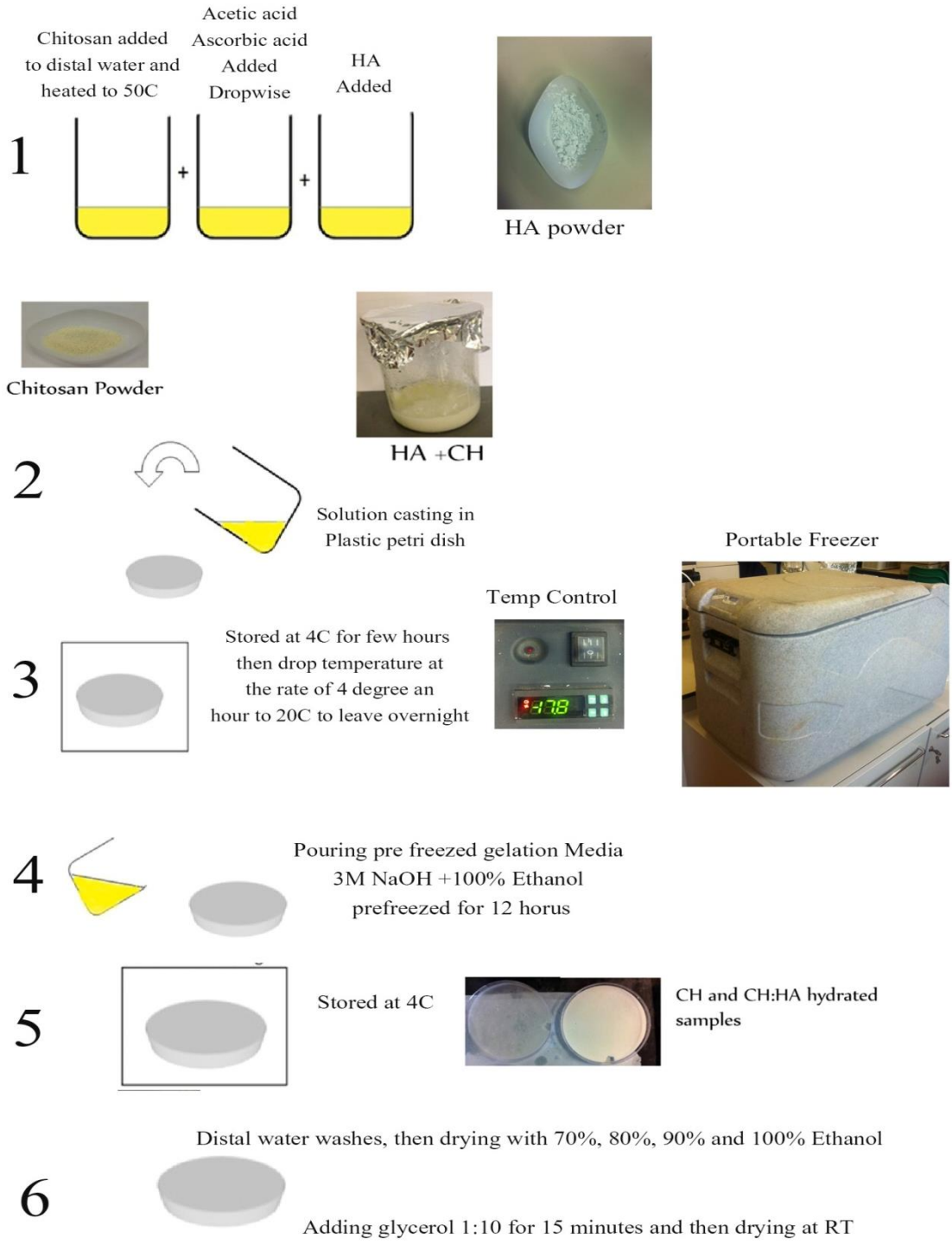

Figure 14: Diagrammatic illustration representing the freeze gelation process step by step from melting the polymer, addition of HA (1), casting in the petri dish (2), Freezing in different cycles (3), pouring the pre-freezed non-solvent (4), Storing the frozen membrane in non-solvent overnight (5), Washing out the membrane with PBS and ethanol washes to dry out (6).

The temperature was gradually brought down by decreasing 4°C after every hour until -20°C was reached by adjusting an electronic thermostat in a portable freezer (Euroengel Heavy duty 32 litre Compressor Fridge/ Freezer T0032, Italy). After 12 hrs the frozen polymer discs were carefully removed by slightly compressing the edges of the plastic petri dishes. A solution (gelation media) of Sodium hydroxide (NaOH) 3 M in 100% ethanol in a ratio of 1:1 (v/v) was pre-cooled to −20 °C was used to submerge frozen discs for 12 hrs. Such that the gelation media was poured into the plastic petri dishes and the frozen disc were placed on top. Some more gelation media (non-solvent) was then poured on top of these frozen membranes as well. Membranes were then washed with PBS (Oxoid PBS Tablets, used with distilled water to obtain a 100 mM solution, UK) to elude the remaining neutralizing solution and specimens were dried using a series of ethanol washes (70%, 80%, 90%, 95% and 100%) for 15 min each. and then plasticized with a combination for 1:10 of Glycerol ($C_3H_8O_3$) and distilled water. The freeze gelation scaffold was left in the plasticizer solution for 15 mins and then dried in air to obtain a porous scaffold. Specimens were also prepared with 0.2 M Ascorbic acid (ASa) as a solvent following the same protocol. In total four different membranes were fabricated denoted as ASa-CH, ASa-CH:HA, ACa-CH and ACa-CH:HA. Figure 14 illustrates how the freeze gelation procedure is conducted and table 7 enlists the different combinations used for freeze gelation.

Table 7. Types of Chitosan: Hydroxyapatite combinations used for freeze gelation

	Chitosan	Hydroxyapatite
3wt % Medium Mol wt	100	0
CH in 0.2M Acetic acid	50	50
3wt % Medium Mol wt	100	0
CH 0.2MAscorbic acid	50	50

3.6. Electrospinning Chitosan

Electrospinning Chitosan solution was made with a ratio of 4.5 wt% of Low molecular weight CH in combination with Polyethylene oxide (PEO) in a ratio of 95:5. They were mixed in a combination of 3wt% ACa with Dimethyl sulfoxide (DMSO) in a ratio of 10:1. Low molecular weight Chitosan was weighed and mixed in distilled water, heated to 60°C for 30 mins. After 30 mins Acetic acid was added drop wise and the solution was allowed to mix for another 15 mins. PEO was then added to rest of the solution and after 30 mins DMSO was added and the solution was left stirring for 24 hrs. The solution was centrifuged before electrospinning at 45000 rpm for 5 mins. Each prepared electrospinning solution was utilized within 24 hrs of

preparation. The solution were loaded in two 1 ml syringes with a needle gauge of 4.699 mm and placed onto an automated syringe pump (New Era Syringe infusion pumps NE-300, World precision instrument, USA) and dispensed at a constant rate 1 ml /hr. Preferred voltage was 17.8 kV-22 kV. Distance of needle tip from the collector was 15 cm (6cm diameter). Collector was rotating at 160 rpm for random fibres and 2500 rpm for aligned fibres. Fibres were collected on an aluminium foil which was wrapped around a rotating collector. Scaffolds were taken off from the collector and placed in vacuum for 24 hrs at room temperature (RT) (20 ± 2°C) to remove any remaining solvent. They were then stored in a sealed plastic bag at RT.

3.7. Neutralization Protocols

Neutralization of membranes/ thin films and electrospun mats was performed in a combination of ethanol (CH_3CH_2OH) and NaOH. Industrial methylated spirit (IMS) was used at 70% dilution with distilled water for washes. To optimize the neutralization media for the membranes four different solutions were used to find out the effect of concentration of ethanol and NaOH. 0.1M NaOH, 1M NaOH, 1M NaOH with 50% Ethanol and 0.1M NaOH with 50% ethanol were made up and membranes were immersed in such way that at each interval their physical nature was noted. The effect of addition of glycerol in the membrane was also kept as a variable. It was noted that after consecutive washes with each type of the solution made up, membranes showed stability with 1M NaOH and 50% ethanol. No curls or wrinkles were observed at the end of the washings. All distilled water washes were performed for 15 mins at each time point.

Neutralization is known to play a significant role in degradation profile. Neutralizing the scaffolds results in deprotonation of the CH polymer, hence; this process reduces the overall charge to the polymer and renders it less soluble in aqueous solutions. This can contribute to slower degradation (Sangsanoh *et al.* 2007).

Table 8 to 10 enlists the results obtained after neutralizing the membranes with different types of combinations of NaOH and Ethanol

Table 8: Table below shows the effect of 0.1M NaOH on CH:HA membranes with and without addition of glycerol after consecutive washes and sterilization

0.1M NaOH						
	After 30 minutes	**First DiH_2O wash**	**Second Di H_2OWash**	**Third Di H_2Owash**	**70% IMS after 30 minutes**	**Di H_20**
CH:HA 70:30+ Glycerol	Curled up, rolled	Still curled up/ rolled	Still curled up	Curled edges, wrinkled	Getting stable	Wrinkled
CH:HA	Curled up	Curled up	Curled	Still curled	Relaxed	Curled
CH+ Glycerol	Slightly curled	Curled edges	Curled edges	Curled	Still Curled	Curled

Table 9: Table below shows the effect of 1M NaOH on CH:HA membranes with and without addition of glycerol after consecutive washes and sterilization

1M NaOH						
	After 30 minutes	**First DiH_2O Wash**	**Second Di H_2O Wash**	**Third Di H_2O Wash**	**70% IMS after 30 minutes**	**Di H_20**
CH:HA 70:30+ Glycerol	Slightly swelled	Flattened out, swelled	Flattened, still swelled	Flattened, Still Swell	Curled	Swelled again
CH:HA	Stable	Stable	Stable	Stable	Curled	Swelled
CH+ Glycerol	Slightly swelled	Still stable / swelled	Still stable, Swollen	Swollen	Stabilizing	Stable, flat

Table 10: Table below shows the effect of 0.1M NaOH +50% Ethanol on CH:HA membranes with and without addition of glycerol after consecutive washes and sterilization

0.1M NaOH + 50% Ethanol						
	After 30 minutes	**First DiH_2Owash**	**Second Di H_2OWash**	**Third Di H_2Owash**	**70% IMS after 30 minutes**	**Di H_20**
CH:HA 70:30+ Glycerol	Swelled up	Flattened, swelled	Flattened, swelled	Flattened, swelled	Curled up again	Swelled up
CH:HA	Curled up	Curled up	Still curled	Curled up	Curled up	Swelled up
CH+ Glycerol	Wrinkled edges	Curled up, wrinkled edges	Curled/ wrinkled	Wrinkled up / curled	Curled up	Curled up, Swelled

Table 11: Table below shows the effect of 1M NaOH +50% Ethanol on CH:HA membranes with and without addition of glycerol after consecutive washes and sterilization

	1M NaOH + 50% Ethanol					
	After 30 minutes	**First DiH_2Owash**	**Second Di H_2OWash**	**Third Di H_2Owash**	**70% IMS after 30 minutes**	**Di H_20**
CH:HA 70:30+ Glycerol	Slightly swelled/ stable	Flat, firm, stable	Stable/ similar feat-	Stabilizing,	Slightly curled	Stabilizing
CH:HA	Curled up	Slightly curled	Similar features	Flattened, stabilizing	Stable , Rigid	Stable, rigid, firm,
CH+ Glycerol	Stable and firm	Stable, firm, flat	Stable/ firm/ flat	Stable,	Stable, firm rigid	Stable, firm handling

3.8. Characterisations

3.8.1. Introduction

Complete characterisation of biomaterials is an important aspect of science and engineering. Characterisation of a material is described as those features of structure and composition of a material that are significant for a particular preparation, study of properties and sufficient reproduction of a certain material (Lyman 2002).

The physiochemical properties of biomaterials exert a heavy influence over their cellular interaction and play a vital role in materials ultimate in-*vivo* performance (Kumar 2013). Bulk, surface and interface properties of biomaterials intended to be used for tissue engineering and regenerative application must be adequately characterized, as this gives a base line information upon which the performance of a biomedical implant can be correlated (Lyman 2002). More importantly the surface which is just a few atomic layers thick acts as an interface between the biomaterial and biological environment, it plays a critical role in biological and chemical response in-*vitro* and in-*vivo*. Physical properties involve the inherent internal structure or micro architectural geometry such as shape or size of particles, density, surface area, porosity, pore orientation, percentage porosity and pore morphology. Microstructural characterisation has been possible by using different types of microscopy like, electron, optical and confocal microscopy techniques (Kumar 2013). Chemical characterisation revolves around the determination of the chemical nature, composition and distribution of elements within a biomaterial. Over the past few decades advancements in science and engineering have led to the development and innovation of various tools for image and

material analysis. Among these techniques, FTIR and Raman Spectroscopy have evolved remarkably over the last decade or so and are play very instrumental role in chemical characterisation, as the key aspect of advancements have relied on enhancing the speed of data collection for mapping and imaging biomaterials or other soft and hard tissues for generating chemical maps at cellular level (Rehman *et al.* 2013).

The design of a biomaterial also always involves some aspects of mechanical characterisation. This begins with fabricating standardized test specimens, which are pivotal in obtaining reproducible and precise measurements of materials property. The time dependant behaviour of biomaterials can influence stress strain relationship and thus affect the mechanical properties (Roeder 2013). Another aspect of characterisation is heavily reliant on the investigating the cell biomaterial interaction. Advanced tools that give better insight and understanding of cellular interaction with a medical implant are also critical in characterisation of in-*vitro* and in-*vivo* nature (Thasneem and Sharma 2013). In this project we have employed various characterisation techniques to evaluate the biomaterial fabricated. A detailed list of the characterisation techniques performed during this project is enlisted below.

1. Chemical
    I. Fourier transform infrared (FTIR) spectroscopy
    II. UV-Vis Spectroscopy (UV-Vis)
    III. Raman Spectroscopy

2. Physical
    I. Scanning electron microscopy (SEM)
    II. Swelling ratio
    III. Weight loss analysis (in-*vitro* degradation)
    IV. pH measurements
    V. Mechanical testing
    VI. Micro Computerized tomography (µCT)

3. Biological
    I. Bioactivity (Simulated body fluid immersion)
    II. Biocompatibility (cellular compatibility)

3.8.2. Chemical Characterisations

Spectroscopic techniques have been employed to chemically characterize the fabricated material. While studying inorganic and organic structures in chemistry spectroscopic analysis plays a pivotal role to study the surface texture, surface energy and composition of biomaterials (Kumirska *et al.* 2010).

3.8.3. Fourier Transform Infrared (FTIR) Spectroscopy

FTIR is a routine technique widely applied for characterisation of biomaterials (Figure 15a). Various alternative techniques such as Attenuated Total Reflectance (ATR) (Figure 15b), Diffuse Reflectance (DRIFT) and Photoacoustic sampling (PAS) (MTech, USA) (Figure 15C) can be employed for analysing surface and bulk profiles of specimens (Rehman *et al.* 2013). In this study, FTIR spectra were obtained using a Nicolet 8700 and Thermo Scientific iS50R FTIR spectrophotometer along with a Photoacoustic sampling (PAS) cell. Spectra were obtained in the mid infrared region (4000-400cm^{-1}) at 8cm^{-1} resolution, accumulating 64 numbers of scans. The sample chamber of the PAS cell was purged with dry helium gas (BOC, Worlsley, Manchester UK). A background scan was obtained before each set of tests using a carbon black specimen. OMNIC™ software (version 9) was used to visualize the spectral data collected.

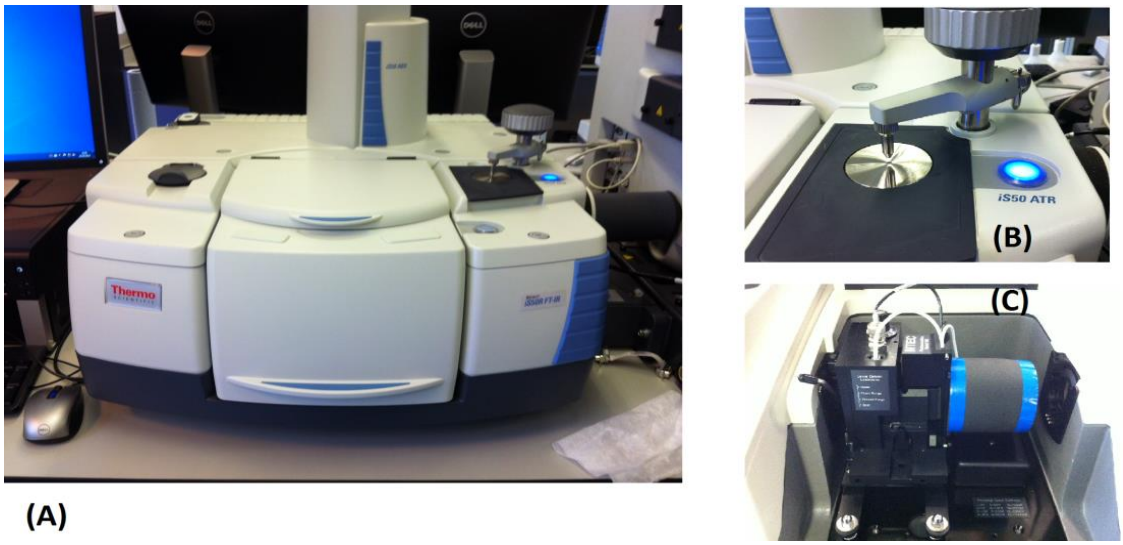

Figure 15: (A) FTIR spectroscopy unit by Thermo Scientific, (B) ATR accessory with diamond crystal (C) PAS accessory for bulk analysis.

3.8.4. Raman Spectroscopy

Raman spectroscopy has been used as a tool for biomaterials characterisation for many years. It is a vibrational spectroscopic technique recognized as a significant analytical method in biomedical applications. It allows detailed investigation of functional groups, molecular conformations and bonding types. It has the ability to analyse wet samples to mimic

Figure 16: Raman Spectroscopy unit used for mapping trilayered template (Thermo Scientific DXRi).

physiological conditions (Rehman I U *et al.* 2013). In the current study Raman DXRi (Thermo Scientific, Madison WI, USA) (Figure 16) was used for mapping of the trilayered template. For intensity mapping the trilayered membrane, Raman Spectroscopy was used equipped with a 532nm (diode pumped solid state laser) laser, laser power of 10mW at 8 number of exposures, (number of background exposures 32). The microscope was equipped with a X10 objective. Exposure time was set 0.02 seconds. In total 1660 spectra were collected in 5.27 mins. Acquired spectral data was processed and analysed by OMIC XRi™, OMIC Atlus™ and TQ Analyst™ software suit (Thermo Scientific, Madison, WI, USA).

3.8.5. UV-Visible-Spectroscopy (UV-Vis)

Ultra violet visible spectrophotometry was performed on LAMBDA 950 UV Vis spectrophotometer PerkinElmer by taking blank background and PBS was used as a reference. Analysis was performed between ranges of 500 to 200nm. A common use of UV Vis is to detect concentrations of specimens dissolved in solvents in which solvent is used as a blank (Kumirska *et al.* 2010). In this study UV Vis was used for degradation studies and drug release analysis. Two Quartz cuvette were purchased from Thor Labs, UK for UV-Vis studies of chitosan. Data of the UV-Vis was processed by Vision pro™ software by Thermo Scientific.

3.9. Physical Characterisation

Physical properties of CH and HA plays a critical role in defining the final properties of resulting composite scaffold which ultimately helps in identifying the final clinical application. Therefore

it is very important to evaluate the physical properties of biomaterials fully. Surface and interface properties such as texture and morphological features need to be assessed keeping in mind the final application (Lyman 2002).

3.9.1. Scanning Electron microscopy (SEM)

The surface morphology of all CH-based membranes, were characterized by scanning electron microscopy, (spot size: 3.0, voltage range 5- 10kV) SEM (For SEM observations, a Philips X-L 20 microscope was used (Figure 17). The samples were mounted on aluminium stubs with double sided carbon adhesive dots (Agar Scientific, UK) and were sputter coated under vacuum with carbon using Speedivac carbon coating unit (Model 12E6/1598)

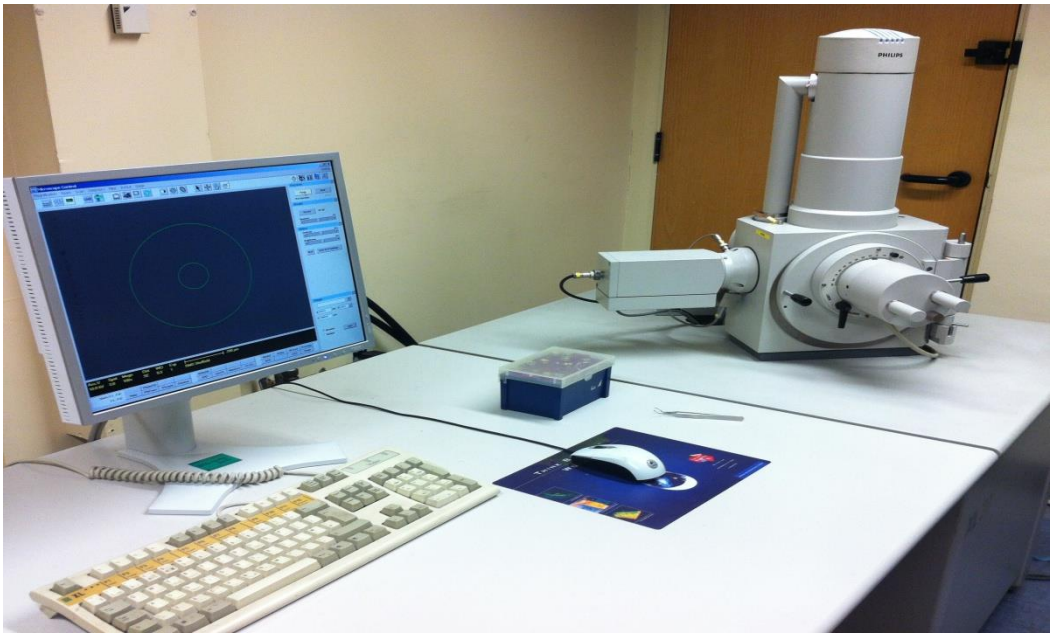

Figure 17: Scanning electron Microscopy unit used for imaging samples. (Philips X-L 20).

Images obtained from SEM were scaled using Image J software (NIH, USA) Pore sizes of freeze gelated membranes and diameters of the fibres were measured using the same software. The directionality histograms were obtained with ImageJ2 (Fiji) (NIH, USA) software using directionality plug-in for generating orientation graphs.

3.9.2. Mechanical Testing

The mechanical properties of CH HA composite membranes / thin films freeze gelated membranes and electrospun fibres were fully evaluated in both dry and hydrated state. All samples were tested in tension on a BOSE ELF 3200 (BOSE Electroforce Tense Instruments, MN) using a 22.2 N load cell and strained at a rate of 0.1 mm/sec to failure with a maximum strain distance of 6 mm. All measurements were performed on WinTest 4.1 software. From the

obtained stress-strain curves, the point at which the samples snapped was used to calculate the Ultimate Tensile Strength (UTS). The initial linear gradient of stress versus strain plot was taken as the Young's Modulus of Elasticity (*E*). The specimens were rectangular discs with 5mm x 20mm x T, where T is the thickness of the scaffolds in dry and wet condition.

3.9.3. Micro Computerized tomography (µCT)

µCT is a non-destructive technique that uses X-ray and computed tomography to produce very high resolution images. It has been extensively used to study porous scaffolds for tissue engineering applications. The technique can deliver parameters such as porosity percentage, pore morphology and interconnectivity. In this study µCT was performed at Erlangen University in collaboration with Dr Tobias Fey (Germany) on Freeze gelated (FG) CH and CH:HA membranes. The equipment details and scanning specifications are given below.

Skyscan 1172, Skyscan B.V., Koentich, Belgien. Source Type: Hamamatsu 80/100Camera: Hamamatsu C9300 11Mp camera, Voltage 80kV and Current100 µAExposure time per slice (ms)= 655, Rotation Step (deg)=0.250, Frame Averaging=OFF (4), Random Movement=ON (10), Use 360 Rotation=YES, Reconstruction with Nrecon 1.6.9.3, Skyscan B.V., Koentich, Belgien, Analysis with CTAn 1.13.2.0 (Skyscan B.V., Koentich, Belgien) , Visualisation with Amira 5.6, (FEI Visualization Sciences Group, Berlin)

3.9.4. Swelling Analysis

Neutralized sample discs (13 mm Ø) were dried and weighed before storing in PBS at 37° C to allow any swelling to occur. At set time intervals, samples were removed from PBS and any excess water was removed by placing the sample between sheets of tissue paper before weighing samples. Time intervals used were 0, 15, 30 mins and 1, 24, 48 hrs for electrospun fibres and upto 168 hrs for thin films and FG membranes. The swelling ratio was calculated using the following formula (Xianmiao *et al.* 2009).

Equation 1 : Swell Ratio % ***(Q)*** **= (Ww – Wd)/Wd x 100**

Where dry weight is given as W_d and wet weight is given as W_w

3.9.5. In vitro-degradation studies of thin film, FG membranes and fibres

Samples were neutralized, weighed and noted as W_o. They were then immersed in degradation media containing PBS, lysozyme egg hen (Sigma Aldrich, UK) at a concentration of 5mg/ml. Samples were incubated at 37 ^{0}C for 1 hr, 7, 14, 21 28, 36 and 54 days. Degradation media was renewed after every 2 to 3 days. At each time point specimens were washed with distilled

water for 3 times and then dried out thoroughly before weighing them again and the dry weight was noted as W_t. Dimensions of the specimen used for degradation were kept constant at 13 mm diameter for all three scaffolds cut out with a cork borer (#8).

Degradation was calculated by finding out the percentage weight loss or the percentage weight remaining. Freeze gelated membrane degradation was evaluated by calculating the % eight loss. By using the following equation

Equation 2 : Weight loss % = $(W_o - W_t) / W_o \times 100$

Solvent casted membranes / thin films of CH HA and electrospun fibre degradation were calculated by evaluating the percentage weight remaining. By using the following equation

Equation 3 : Weight remaining % = $100 - (W_o - W_t) / W_o \times 100$ (Thein-Han and Kitiyanant 2007)

pH Measurement

pH measurements of the supernatant were performed on Mettler Toledo S20 Seven Easy pH meter at each time point by first calibrating the pH meter in standard solutions and then immersing the bulb until the reading stabilized at RT (20 ± 2°C).

3.9.6. Bioactivity analysis

Bioactive materials are usually referred to as materials that simulate beneficial response with regards to bonding to host tissue such as bone. Bioactivity is regarded as their ability to form this bond. This is a complex sequential phenomenon which can be summarized into three short steps of ion leaching initially, limited dissolution of ceramic surface and finally precipitation of bone like apatite. The in-*vivo* conditions can be reproduced in-*vitro* by simulated body fluid (Kokubo and Takadama 2006; Jones 2013).

Synthesis of Simulated Body Fluid (SBF)

Simulated body fluid (SBF) is a solution that has an ion concentration almost similar to that of human blood plasma. The protocol adapted to synthesize SBF was a modified version of the work performed by Kokubo *et al.,* (Kokubo and Takadama 2006). Reagents used for preparation of SBF were of analytical grade and supplied by Sigma Aldrich®. UK, listed in the Table 12.

Initially, approximately 700 ml of distilled water was poured into a 1 liter plastic container placed on a hot plate with a suspended temperature probe and pH electrode set at 37°C ± 1.5°C. The reagents were measured accurately and added in a sequence to this till Na_2SO_4

(number 8). All reagents were added after each preceding reagent had completely dissolved. At this stage the pH of the solution was 2.0 ±1.0 at 35.6°C ±1.5°C, just prior to adding the Tris-buffer in minute amounts to raise the pH gradually. At first the pH was brought upto 7.3, and then gradually increased to 7.45. At this stage the pH was again adjusted to 7.42 by adding 1M HCl, gradually using a 10 ml syringe. The addition of Tris-buffer and HCl was repeated until all the weighed Tris-buffer was consumed. At this stage, the pH was carefully maintained within the range of 7.45 to 7.42 at 37°C. The final SBF solution was set at 7.40 and made up to 1000 ml with distilled water and allowed to cool at RT (20 ± 2°C) before being transferred to sterile polystyrene bottle with a screw lid and stored in refrigerator at 5°C. Some SBF was also stored to examine the precipitates.

Table 12. Chemical reagents and amounts used for synthesizing SBF for Bioactivity assay (Kokubo and Takadama 2006).

Order	Compounds	Chemical	Quantity (g/ ml)
1.	Sodium Chloride	NaCl	8.035
2.	Sodium Bicarbonate	$NaHCO_3$	0.355
3.	Potassium Chloride	KCL	0.225
4.	Potassium Hydrogen Phosphate Trihydrate	$(K_2HPO_4.\ 3H_2O)$	0.231
5.	Magnesium Chloride Hexahydrate	$MgCl_2.6H_2O$	0.311
6.	Hydrochloric acid 1.0M(mol/l)- HCl	HCl	39ml
7.	Calcium Fluoride	$CaCl_2$	0.292
8.	Sodium sulphate anhydrous	$Na_2\ SO_4$	0.072
9.	Tris-hydroxymethyl aminomethane	$(HOCH_2)_3CNH_2$Tris	6.118

3.9.7. Preparing Samples for Bioactivity

Samples for assessing bioactivity over an experimental period of 21 days were prepared by using a cork borer for thin film/ membranes and porous freeze gelated scaffolds to obtain samples of 13 mm in diameter (cork-borer # 8) Samples were neutralized and then soaked in SBF for predetermined time points. Samples were fully immersed in SBF and stored in an incubator (Sanyo MCO 175 incubator) set at 37°C and 0.2% CO_2 injection rate. All samples were subjected to same parameters throughout the course of the experiment.

In order for the specimens to receive constant supply of SBF, the media was changed after every 2 to 3 days. At each time point samples were removed from SBF and rinsed with distilled water and dried overnight in an oven at 40°C, followed by characterisation by weight analysis

and FTIR spectroscopy. OMNIC™ (version 9) TQ Analyst® software was used to calculate peak area measurements from the spectral data collected.

3.10. Biological characterisation

3.10.1. Scaffold Preparation

A combination of Low and Medium molecular weight CH and HA membranes were utilized. Membranes were casted by the method mentioned in 3.4. Prior to cell seeding the thin films and fibres, they were placed in a 12 well plate and neutralized with 1M NaOH in a ratio of 1:1 with 50% Ethanol for 2 to 3 hours and then placed in DiH_2O overnight. At the time of cell seeding, the scaffolds were put in 70% IMS for 1 hour and given Phosphate buffered saline rinses for 15 minutes each. Electrospun fibres were prepared in a similar manner. The FG membranes were sterilized with ethanol for 1h, washed twice with PBS for 15mins, and then coated with either culture medium for 1hr prior to seeding MG63's or gelatin for 1hr prior to seeding hES-MPs. Cell free membranes were included as controls.

3.10.2. Cell Culturing conditions

All cell culturing procedures were performed inside a standard class II laminar flow hood (Walker safety Cabinets, UK.) T-75 flasks were used to expand cells using either DMEM[Dulbecco's modified Eagle's Medium] (Biosera UK) or α-MEM [Minimum Essential medium] (Gibco, Paisley, UK) for expansion of cells, which were stored in a humidified incubator maintained at 37°C with 5% CO_2. Media was changed regularly after every 2 to 3 days along with periodic observations of cell morphology and density, until the cells reached confluence they were then passaged. Before passaging cells, media was removed and flasks were washed with PBS twice. 2.5ml of EDTA-trypsin (Sigma Aldrich®, USA) (Ethylene Diamine tetra acetic acid) [Trypsin 0.05%/0.02% EDTA w/v stored in -20°C] was then added to the flask, which was incubated for 5-10 mins to detach cells and incubated at 37°C for 5 to 15 mins. The detached cells were diluted with fresh media to halt the trypsin-EDTA reaction and this suspension was centrifuged for 5 mins at 1000 rpm (revolutions per minute) to obtain a cell pellet in universal tubes. Supernatant of this suspension was poured away and the cell pellet was resuspended in a known volume of media. A haemocytometer was used to perform cell counts. Cells to be utilised for future experiments were freezed using a solution of 10% DMSO and 90% FCS (Fetal calf serum, Sigma Aldrich®, UK). They were stored in -80°C for 24 hrs before moving them to liquid nitrogen.

3.10.3. Cell counting

Cell counting was performed on a modified Neubaur hematocytometer (Weber Scientific International, UK) was used for counting cells. Four 1 mm^2 squares [1 $x10^4$ ml volume] were counted and an average was calculated to acquire total cell number using the formula given here.

$$\frac{\text{Mean number of cells/1mm}^2 \text{ dilution factor /}}{\text{Volume counted, 1 x10}^4 \text{ ml}} = \text{cell/ml}$$

3.10.4. Human Osteosarcoma Cell line (MG63's)

Mature osteoblasts, human osteosarcoma cell line were used (Donated by Dr A. Scutt of University of Sheffield). They were expanded in DMEM supplemented with 10% FCS, 2mM of L-Glutamine and 100 µg/ml of penicillin / streptomycin (Sigma Aldrich®, UK) was used for cell expansion as a basal media in a humidified atmosphere with 5% CO_2 at 37°C. MG63's were used in between passage number of 60 to 70. Confluent cells (90%) were trypsinised and cell density was adjusted to 194 x 10^4 cells / ml. Sterile thin films / membranes, freeze gelated and electrospun mats were transferred to 12 well plates and a metal ring was placed on top of the scaffold to ensure placement in the centre of the ring.

3.10.5. Progenitor cell line

Human Embryonic stem cell-derived mesenchymal progenitor (hES-MP's, obtained at 2.5 from Cellartis, Gothenburg, Sweden). α-MEM supplemented with 10 % FCS, 2mM L-Glutamine, 100 µg/ml penicillin/streptomycin (Sigma Aldrich®, USA) and 20 nM of FGF (Fibroblast Growth Factor, Gibco, Invitrogen, recombinant human FGFb, Lot No, 1049396B, stored at -20°C) was used for cell expansion as a basal media in a humidified atmosphere with 5% CO_2 at 37°C. hES-MP's were used between passage of 3 to 7.

3.11. Cell seeding

Cell seeding was performed using a metal ring for all three types of scaffolds, membranes, freeze gelated and electrospun fibres. A steel ring was placed on top of the scaffolds such that the centre of the metal ring was fully covering each sample. 500 µl of media was poured inside the steel ring and 500 µl was poured around the ring such that the samples were fully immersed in media. Then the cell suspension after cell count was poured into the centre of the steel ring. After 24hrs in incubation rings were removed and replaced with fresh media which

was then changed after every 2 to 3 days. Membranes were seeded with a seeding density of 25000 cells per sample. FG membranes and fibres were seeded at 250,000 cells per sample.

3.11.1. Alamar Blue™

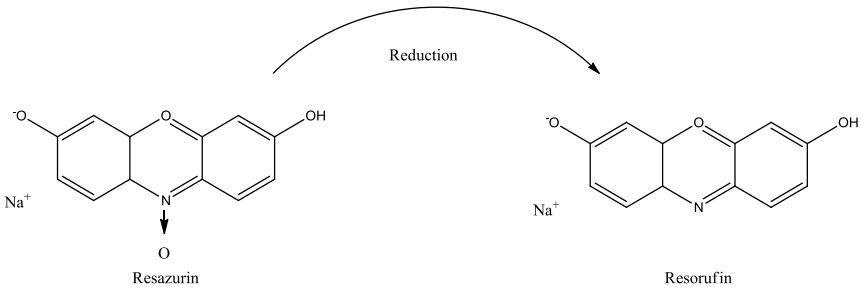

Figure 18. Reduction of Resazurin by mitochondrial dehydrogenase (O'Brien *et al.* 2000).

Alamar Blue™ (AB) assay is a colorimetric growth indicator based on detection of metabolic activity. The redox indicator in the solution changes colour from blue to red in response to chemical reduction of Alamar blue into purple by the mitochondrial dehydrogenase activity in cell nuclei. The chemical reaction of this reduction process is shown in Figure 18. The changes in the colour which indicate the number of cells or cell viability was then measured using a plate reader (O'Brien *et al.* 2000).

3.11.2. Making Alamar Blue™ Medium

Stock solution of AB was prepared by dissolving Resazurin sodium salt (Lot No MKBN4870V, Sigma Aldrich®, USA, Mw 251.17) in distilled water to obtain a concentration of 1mM. This solution was filter sterilised and stored at 4°C. AB medium was prepared by making a mixture of 90% normal culture medium and 10% AB stock solution. Just before performing the assay, warmed culture medium and AB stock solution were added in a vial covered in aluminium foil in ratio of 9:1.

3.11.3. Alamar Blue™ Protocol

At day 1 of the AB assay, media was carefully removed from well plates containing the membranes / thin films, freeze gelated scaffolds and electrospun fibres. They were then rinsed with PBS for 15 mins (3x) and then transferred to a 24 well plate. The lights of the fume hood were switched off before pouring the AB medium to prevent its reaction with light. Approximately 0.5 ml of AB medium was poured onto the scaffolds and the well plates were wrapped in an aluminium foil, to be placed in an incubator for 4 hrs at 37°C.

3.11.4. Measurement

Reduction of Resazurin can be detected by absorbance or fluorescence. After 4 hrs of incubation at 37°C the well plates were removed and at least 2 aliquots of 200 µl were pipetted from each sample into a 96 well plate. Fluorescence was measured at 570 nm using a fluorescence plate reader (Bio-TEK, North Star Scientific Ltd, Leeds, UK) Based on the metabolic activity the system incorporates an oxidation-reduction (REDOX) indicator that both fluoresces and changes colour in response to chemical reduction of the growth medium resulting from cell growth (Qasim *et al* 2015). Reduction related to growth causes the REDOX indicator to change from oxidized (blue) form to reduced (red) form. After the measurements were taken, samples were gently washed with PBS, fresh media was added and the samples were stored in the incubator for next reading (Qasim *et al* 2015).

3.11.5. MTT assay

MTT (5 diphenyl tetrazolium bromide) assay is a commonly used assay to measure cell viability and proliferation. A yellow MTT solution is reduced by active mitochondria existing in the living cell to form a dark blue or purple insoluble salt. This insoluble salt is conveniently visualized which, is indicative of living cells and it could be quantified by measuring the absorption of the dissolved salt supernatant on an absorbance plate reader at 540 nm. This absorbance is directly correlated to the number of living cells. MTT assay was performed on CH:HA membranes on the bottom surface to evaluate the effect of gelatin on cellular attachment. Culturing for MTT assay was performed by MG63 cell line.

3.12. Histological sectioning

Histological samples were prepared from the cross section of unseeded and cell-seeded FG membranes. Samples were fixed with 3.7% formaldehyde and washed 3 times for 15 mins each with PBS. These samples were then embedded in paraffin wax using a Leica Tissue processor and 5 µm sections were prepared with a Leica Microtome. Slides were then immersed in Xylene for 3 mins and then in 100% and 70% ethanol (EtOH). They were left in distilled water for 1 min before immersing them again in haematoxylin (Thermo Fisher Scientific Ltd) (1 x 1). Followed by washing with water to remove excess stain and then immersed in eosin (VWR International) (1 x 3). The slides were then immersed in distilled water and 70% (EtOH). Left for 1 min in 100% (EtOH) and then dunked in xylene. All slides were then fixed with using a DPX Mounting medium (Fisher Scientific. UK) samples were observed

with a Leica optical microscope using Kohler illumination at 4X, 10X and 20 X objective magnification and scaled at 100 µm.

Histological sectioning of electrospun fibres were taken as complete transverse-sections across the centre of electrospun scaffolds. Samples were fixed with 3.7% formaldehyde, soaked in 1% sucrose solution for 30 mins prior to embedding in OCT™ (Tissue-Tek®, Sakura, freezing medium) compound media. Samples were cryo-sectioned (Leica CM1860UV Ag protect) at 7 µm and mounted on glass slides (Thermo Scientific, Menzel- Glaser, Saarbruckener, Germany) and stained with Haematoxylin (Harris) and Eosin (Sigma Aldrich, UK). Stained sections were imaged with a light microscope (Leica, Motic) with 4X, 10X and 20X objective. Software used to take images was Motic tek. Images were saved scaled on Image J (NIH, USA) software.

3.13. Analysis of collagen deposition by Picro-Sirius red

To qualitatively identify collagen on scaffolds or tissue sections deposited by cells, Picro-sirius red staining method is used. A strong red staining complex is formed if collagen is present, which can be easily destained for quantitative analysis. Sirius red is a strong anionic dye whereby the sulphonic groups of the dye bind with amino acids like, lysine, hydroxyproline and guanidine group of arginine of collagen molecule. This bound dye then later aligns itself parallel to the long axis of collagen molecule. The dye can be used as a fluorescent marker of collagen(Delaine-Smith 2013).

Media was removed from the cells and the scaffolds were washed with PBS up to 3 times for 15 minutes each to ensure complete removal of media. Samples were then fixed using 3.7% formaldehyde for 30 mins, which was then removed and washed three times with PBS again. Direct red dye was added to saturated picric acid (1mg/ml) and then 1ml of this was added to each sample such that the samples were fully immersed. Samples were left for 18 hrs on an automatic tray to shake gently at RT (20 ± 2°C). Excess and the unbound dye was removed with DiH_2O until no more colouring was eluted and the samples were left in air to dry. Light microscopy was used to visualize the bound dye.

3.14. Analysis of Calcium Deposition by Alizarin Red

Alizarin red is a dye that has the ability to bind Ca^{2+} ions to form strong red complex and is commonly used as an indicator of cells and tissues depositing calcium. Samples are fixed in a similar manner described for collagen staining at each time point, and washed with distilled water to remove any non-cell produced calcium ions. Alizarin red dye (Sigma Aldrich®) powder

was added to distilled water (10 mg/ml) and the pH was adjusted to 4.1 using NH_4OH before pouring it on the samples and subjecting it to mild shaking for 15 mins at RT (20 ± 2°C) . Excess dye was then washed away using distilled water and the samples were left to air dry in a fume hood before quantitatively assessing the calcium deposited. Samples were destained with a known volume of 5% perchloric acid, under mild shaking for fifteen minutes; this caused the clear 5% perchloric acid to turn in a clear dark yellow solution. Absorption was measured at 405 nm using a 96 well plate reader. Calcium and collagen deposition were analysed on separated samples (Delaine-Smith 2013).

3.15. Nuclei and F-actin labelling

To visualise cellular attachment and morphology on the membrane/thin films cell nucleus and actin filaments were stained with labels (DAPI and Phallodin TRITC) and imaged under fluorescent microscopy. After 7 days of seeding MG63 cells on the top and bottom surface of LMw 50:50 CH:HA membrane. Samples were fixed with 3.7% formaldehyde in PBS for 30 mins. Washed with PBS, followed by permeabilization with 0.1% Triton X-100 for 10 mins, followed by wash with PBS (thrice). A final solution of 1ug/mL Phalloidin TRITC (from 1 mg/mL in 100% DMSO) and 0.1 µg/ml of DAPI (4', 6-diamidino-2-phenylindole dihydrochloride) was made in PBS. Samples were incubated for 25 mins and kept in dark. Finally scaffolds were washes with PBS (thrice) and kept in PBS for imaging. Fluorescent images were taken with the help of a epifluorescent microscopy (AXON Image Xpress 5000A.USA) magnification of 10X, Phalloidin was excited λat ex= 540-545 nm and emission taken at λem = 570-530nm and DAPI was excited at λex 360 and emission at λem = 420- 460. Images were analysed using fluorescent image analyser.

3.16. In-*vivo* study

In-*vivo* studies were performed to assess the cellular and degradation response of FG membranes after implantation. Experiments were conducted at the Medical institute of Sumy State University. They were approved by the Commission on Biomedical Ethics of Sumy State University (#16/12 on 15/12/2014). 48 chinchilla rabbits, aged 8-9 months, were involved in the experiment. Animals were housed at 22±2 ^{0}C on a 12 hr light/dark cycle and received food and water. Keeping of the animals and experiments were carried in accordance with the Directive 2010/63/EU of the European Parliament and of the Council of 22 September 2010 on the Protection of Animals Used for Scientific Purposes and The General Ethical Principles for Experiments on Animals, which were accepted by the First Bioethics National Congress (Kyiv, 2001).

All animals were divided into four groups according the materials that were used for implantation

1. group 1 –Chitosan in acetic acid (ACa-CH)
2. group 2 –Chitosan in acetic acid with 50:50 Hydroxyapatite (ACa-CH:HA)
3. group 3–Chitosan in ascorbic acid (ASa-CH)
4. group 4 –Chitosan in ascorbic acid with 50:50 Hydroxyapatite (ASa-CH:HA)

3.16.1. Operation design

After administration of general anesthesia (Ketamine 7 mg / kg and thiopental 10 mg / kg) and peripheral vein catheterization, left thigh was shaved to prepare the implantation site. The surgical site was treated with C-4 solution and then a longitudinal incision was made on lateral surface of the thigh and muscles were separated to gain access to the bone. A round bone defect was made upto the bone marrow using a 10mm drill. The defect was filled by grafts that had similar dimensions in diameter and did not need fixation. All grafts were sterilized in 96% ethanol for 1 hr. After the operation the wound was sutured and as a prophylaxis of postoperative bacterial complications animals were given antibiotic (ceftriaxone, 50 mg per 1 kg) for 1 week.

The operation was done in 2 days:

1. 08/01/2015 – 24 grafts were implanted: 12 – ACa-CH, and 6 – ACa-CH:HA
2. 09/01/2015 – 24 grafts were implanted: 12 – ASa-CH, and 6 – ASa-CH:HA

The animals were killed at 7 and 30 days after the operation (narcosis overdose - ketamine, 70 mg/kg).

3.16.2. Histology

After the animals were sacrificed, grafts were removed with some surrounding bone to prevent any damage to the graft. All samples were fixed in 10 % formaldehyde for 24 hrs and decalcificated in 4.5% of acetic acid for 48 hrs. Then the samples were dried in alcohols of elevated concentrations and set into paraffin wax. 12 - 15 µm thick sections were prepared and stained with hematoxylin and eosin. The specimens were analyzed using a light microscope. SEO Image Lab Bio software was used to analyse the histological slides (Sumy, Ukraine, license number 27335). 10 histological slides were made from each sample (5 from deep zone and 5 – from superficial). Each slide was divided into 6 zones that were captured using the light microscope “OLYMPUS”. The squares of the empty pores were measured, as well as fibrous tissue and osteoid that filled pores in each from 6 zones.

3.17. Cross-linking freeze gelated scaffolds

Scaffolds were completely dried in an oven maintained at 30°C overnight. The dry weight was calculated and samples were immersed in a 5 and 10 % (wt/v) solution of Sodium Tripolyphosphate (NaTPP) (Arcos Organics, New Jersey, USA) made up in DiH_2O. After 24 hrs of immersion samples were dried in an oven at 30°C overnight. Dry weight was noted and samples were submerged in a 100 mg/ml solution of tetracycline dissolved in methanol (Sigma Aldrich, 2.5L 34885 Germany). After 24 hrs the scaffolds were taken out dried again for 2 hrs subsequently weighed to calculate the loading efficiency.

Chemical Characterisation

FTIR spectroscopy was used to study the chemical interactions of cross-linking agent and drug interactions with polymer. Samples were analyzed using both Attenuated total reflectance (ATR) and Photoacoustic sampling accessory (PAS) for characterizing the surface and bulk polymeric interactions. Spectral acquisition was carried out according to the **procedure described in section 3.3.3, page 96**

3.18. Drug Entrapment efficiency

Drug entrapment or loading efficiency was calculated by weighing the scaffolds before and after drug loading in dry state. Each sample was dried by storing in a desiccator with silica gel for 24 hrs followed by drying in an oven at 40°C. Drug entrapment efficiency was calculated by the following formula

$$\text{Drug Entrapment Efficiency} = \frac{\text{Weight of sample after cross linking}}{\text{Weight of samples after drug loading}} \times 100$$

3.18.1. Dissolution Studies

Drug release analysis was carried out using a USP type II paddle dissolution test apparatus (Model VDA-1D) by Veego Instruments Corporation (India). PBS at a pH of 7.2 was used as a dissolution medium. pH was monitored by using a Metler Toledo pH meter (Leicester. UK). Fresh 500 ml of PBS was used for each sample. Temperature was maintained constant at 37°C throughout the testing and the paddle speed was fixed at 100 rpm. 5ml of sample was withdrawn at each time point and replaced with 5 ml of fresh PBS which was preheated to maintain and mimic normal body conditions. Testing was carried out for 180 mins and samples were withdrawn after every 5 mins. The drug dissolution unit used is shown below in Figure 19

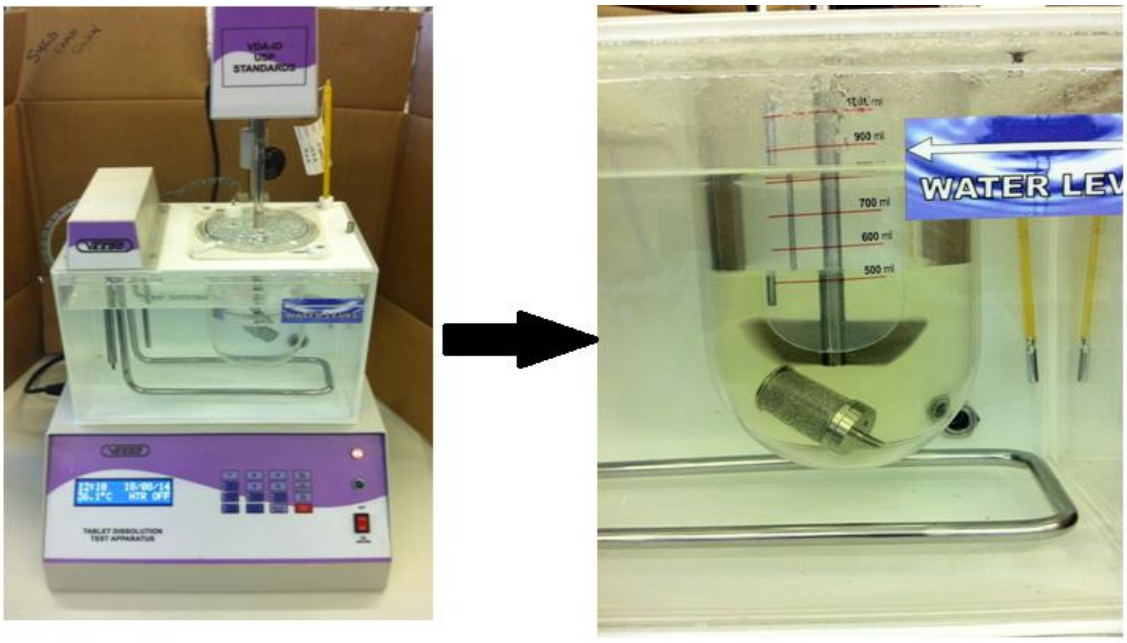

Figure 19. Drug dissolution setup (VEGO) Adjacent image in focus, Scaffolds places in a porous basket to prevent floating and yellow colour is indicative of Tetracycline release

3.18.2. Calibration Curve

Tetracycline was dissolved in Methanol and a stock solution was prepared at a concentration of 100 µg/ml of drug. Dilutions were performed in methanol to obtain concentration of 2, 4, 8, 10, 15, 20, 30 and 40 µg/ml. Absorbance peak at 270 nm was used to plot the calibration curve using the Beer's-Lambert Law and calculate the molar absorptivity constant by using the formula

$$A = E\,l\,c \quad \text{OR} \quad A = A^{1}/_{1}\ 1\%\ b\ c$$

Where

"A" is the Absorbance at a specific wavelength,

"E" or "$A^{1}/_{1}$ 1%" is the molar absorptivity constant,

"l" or "b" is the path length through the sample (1cm)

"c" is the concentration of tetracycline hydrochloride

By calculating the concentration at a specific absorbance and fixed path length the % recovery of the drug from freeze gelated chitosan scaffolds was calculated by.

% recovery = c / initial weight of drug in film x100

3.19. Statistical Analysis

Unless stated otherwise, all experiments were conducted at least three times in triplicate. All presented data refer to mean ± standard deviation (SD). In order to check for any statistically significant differences, a one-way ANOVA was performed followed by Tukey's post hoc test. Results with *p*-values of $\leqslant 0.05$ (*) were considered statistically significant.

All data were analysed using Graphpad Prism version 6.0 software

4. Chapter. Results

This chapter is divided into four sections, Section I is related to the Thin films/ membranes (Surface layer) and their complete characterisation, Section II is about freeze gelated porous scaffolds (Core layer) and complete characterisation of this mid layer, ending with drug delivery studies. Section III is about electrospinning CH and complete characterisation of aligned and random mats. Section IV presents results pertaining to functionally graded templates. Each section of this chapter contains a brief introduction and then description of the results.

SECTION I

4.1. Introduction

Thin films/membranes were synthesized to serve as a surface layer component of the functionally graded guided tissue regenerative membrane. The aim was to develop a Trilayered membrane with a relatively inert surface facing soft tissue and bioactive surface facing the defect to promote bone regeneration. Presented in the results are the optical images of Medium molecular weight (MMw) and Low molecular weight (LMw) CH:HA membranes, Scanning electron microscopy of as prepared membranes and CH flakes, chemical characterisation with FTIR-PAS of top and bottom surfaces, Swelling ratios, Weight loss studies by analyzing pH change, Weight remaining, UV-Vis spectroscopy and FTIR-PAS. Biocompatibility studies for cell viability (MG63 and hES-MP) and matrix deposition by Sirius red and Alizarin red assay.

4.1.1. Optical Images of membranes

Optical images of prepared membranes of LMw and MMw CH and CH:HA are shown in Figures 20 and 21. Neat CH membranes were of a transparent nature with a slight yellowish tint due to CH. Change in the colour of the bottom surface could be clearly appreciated as the amount of HA varies in ratios of CH: HA 70:30, 50:50 and 30:70. It was observed that the top surface gets lighter in shade. Bottom surface of 30:70 CH:HA is completely white. This could be seen for membranes made with LMw CH as well. A neat LMw CH membrane exhibits a much lighter tint as compared to MMw. The Top surface of LMw CH:HA membranes were much lighter in colour and bottom surface showed white HA. On visual examination the top surface was smooth and shiny due the presence of CH and the bottom surface was slightly rougher due to HA dominance.

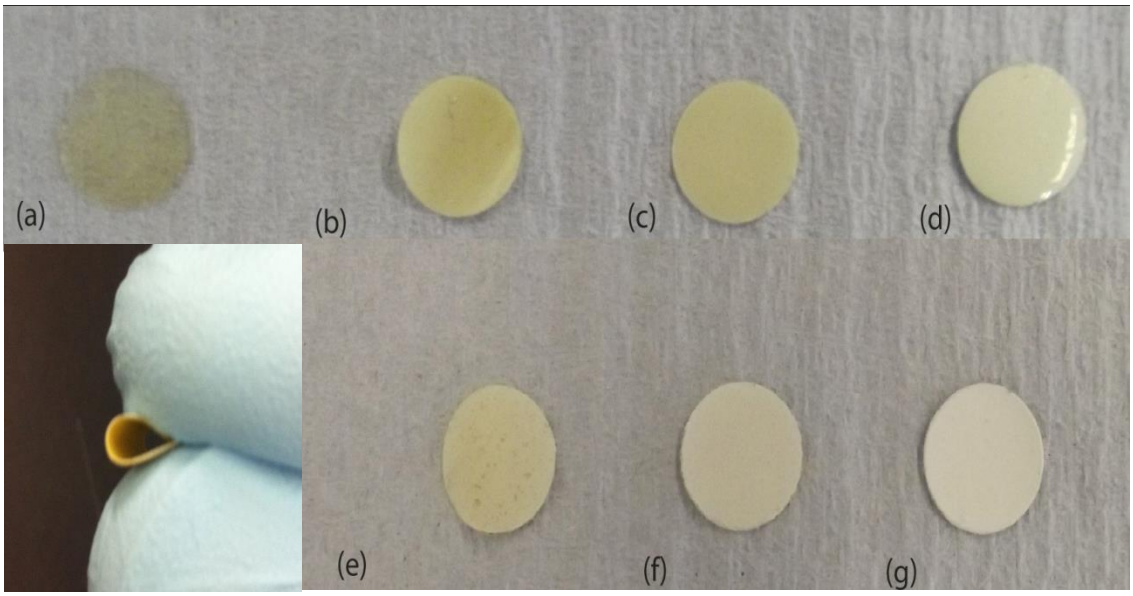

Figure 20: Macroscopic view of as fabricated MMw CH: HA membranes (a) MMw 100:0. (b) Top surface MMw 70:30 (c) Top surface MMw 50:50,(d)Top surface MMw 30:70 (e) Bottom surface LMw 70:30 (f) Bottom surface MMw 50:50(g)Bottom Surface MMw 30:70. Images taken with a DSLR S5600 with Macro lens (Nikon), inset image shows the handling properties of the as prepared membrane while bending.

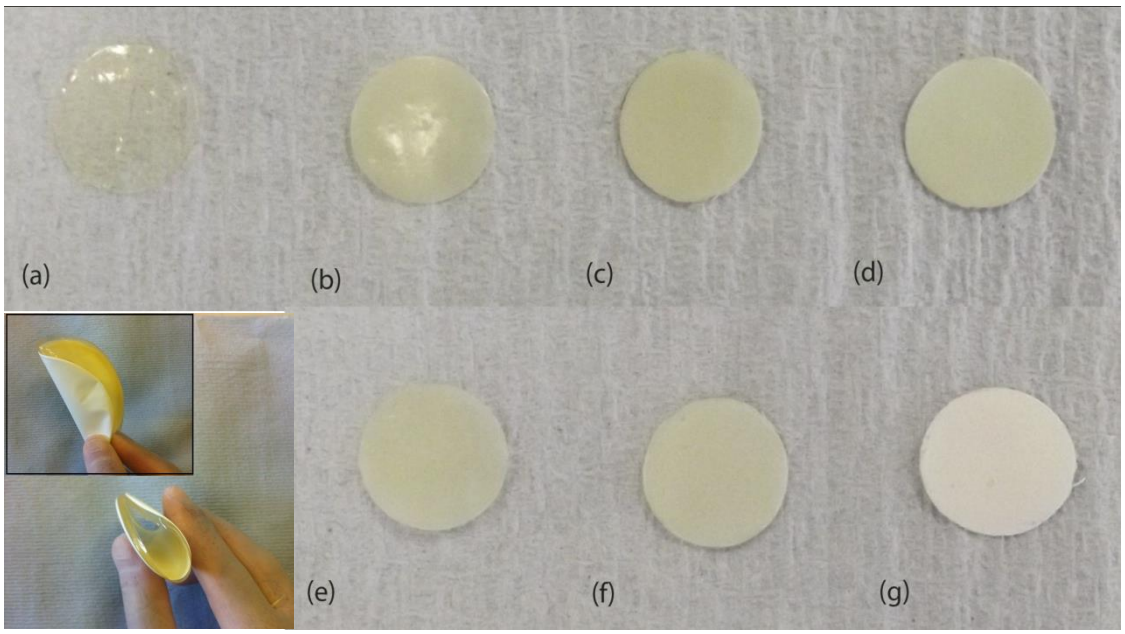

Figure 21: Macroscopic view of as fabricated LMw CH:HA membranes (a) LMw 100:0. (b) Top surface LMw 70:30 (c) Top surface LMw 50:50, (d)Top surface LMw 30:70 (e) Bottom surface LMw 70:30 (f) Bottom surface LMw 50:50 (g) Bottom Surface LMw 30:70. Images taken with a DSLR S5600 with Macro lens (Nikon). Inset image shows handling properties while bending and the colour difference between CH and HA is more evident.

4.1.2. Scanning electron microscopy (SEM) of Membranes / Thin Films

SEM micrographs of MMw and LMw CH flakes are shown in Figure 22 (a and b). It can be seen that CH flakes are smaller and finer in size for LMw as compared to the MMw which show a much larger over all flake size. Composite of LMw and MMw CH and CH:HA membranes are shown in Figures 23 and 24. Top and bottom surfaces of LMw and MMw CH membranes with varying ratios to HA were imaged to investigate the difference in morphologies obtained for each combination. Ratios imaged were 70:30, 50:50 and 30:70 CH:HA. When HA content was increased to 70%, bottom surface showed pure particles tightly packed together, high segregation of CH from HA was seen as the top surface showed very few HA particles. As the ratio of HA increases the bottom surface shows more compact HA particles in both LMw and MMw. Top surface is dominated mainly by CH except in LMw 30:70 in which presence of some larger particles are also visible. When compared with MMw 30:70 the top and bottom surfaces have clear distinction. The ratio of HA tends to vary on the bottom surface as HA particles appear to be surrounded with CH in 70:30 ratio but tends to fade away in 30:70 ratio. Bottom surface of MMw 50:50 shows HA particles being surrounded with CH.

Figure 22: SEM micrographs of (a) Medium (b) Low molecular weight Chitosan flakes all scaled at 500µm.

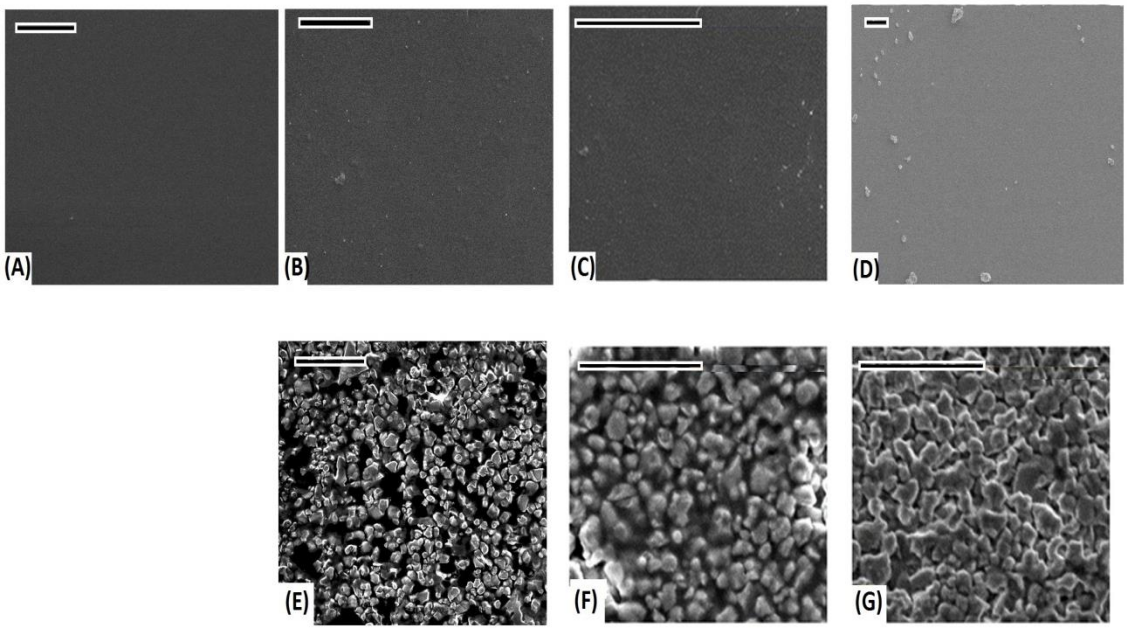

Figure 23: SEM performed on (a) Low mol wt CH 100:0 (b) Top surface of LMw 70:30 HA, (c)Top surface of LMw 50:50 HA, (d) Top surface LMw 30:70 HA, (e) Bottom Surface LMw 70:30HA (f) Bottom Surface of LMw 50:50 HA (g) Bottom Surface LMw 30:70HA. All images scaled at 20µm.

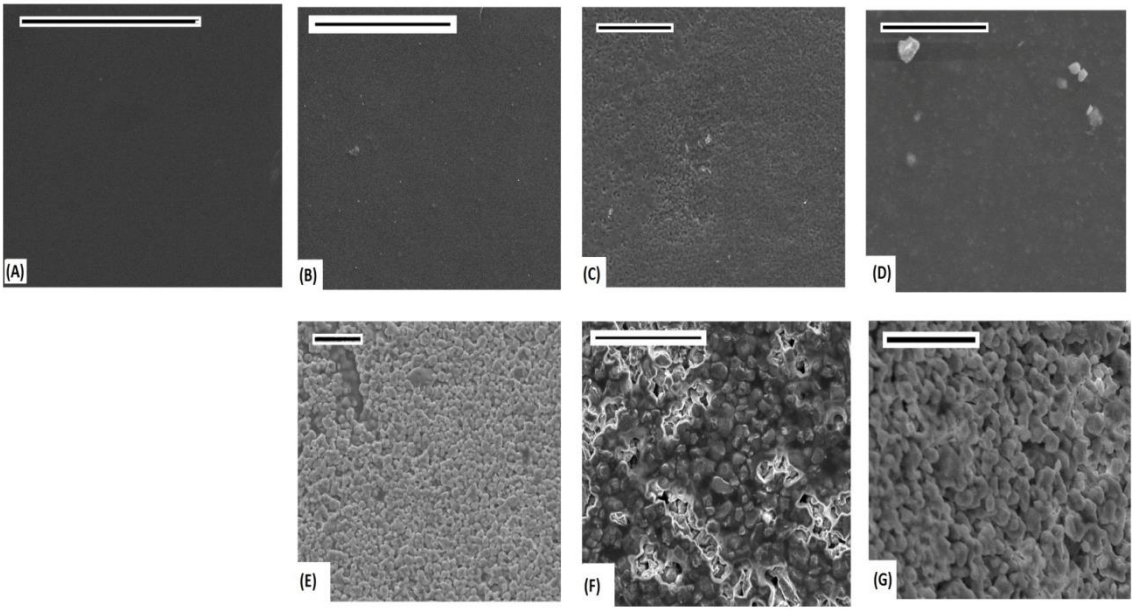

Figure 24: SEM performed on (a) Medium mol wt CH 100:0 (b) Top surface of MMw 70:30 HA, (c)Top surface of MMw 50:50 HA, (d) Top surface MMw 30:70 HA, (e)Bottom Surface MMw 70:30HA (f) Bottom Surface of MMw 50:50 HA(g) Bottom Surface MMw 30:70. All images scaled at 20µm.

4.1.3. Fourier Transform Infrared (FTIR) Spectroscopy

FTIR spectra were obtained in accordance with the procedure described in Chapter 3, Section 3.8.1, to identify important chemical interactions between the polymer and HA using PAS accessory.

The Figure 25 shows neat Low (Blue) and Medium (red) molecular weight CH with a neat Hydroxyapatite (HA) (purple) Spectra. A virgin CH exhibits a broad band around 3100 to 3500cm^{-1} , and another one at 1550cm^{-1} which are commonly attributed to N-H and O-H stretching of the primary amino group (due to hydrogen bonds with O-H group) and N-H stretching vibrations of secondary amides (Amide II). Carbonyl (C=O-NHR) groups show stretching peaks at 1653.6cm^{-1}(Amide I). C-H stretching is also seen at 2800cm^{-1}. Glycosidic bonds due to glucosamine segment of CH are present at 1150 and 1040cm^{-1}(C-O-C). The commercially available HA shows a typical hydroxyl (–OH) stretch at 3569cm^{-1} which is attributed to HA functional group and phosphate (PO_4^{3-}) ν_3 peaks are present at 1096, 1085 and 1056cm^{-1} and ν_4 bands appear at 660 and 520 cm^{-1} and ν_1 band is observed at 961 cm^{-1} ν_2 band is observed at 472 and 436 cm^{-1}. A more detailed description is provided in Table 13 which includes important peaks, their assignments and reference from literature.

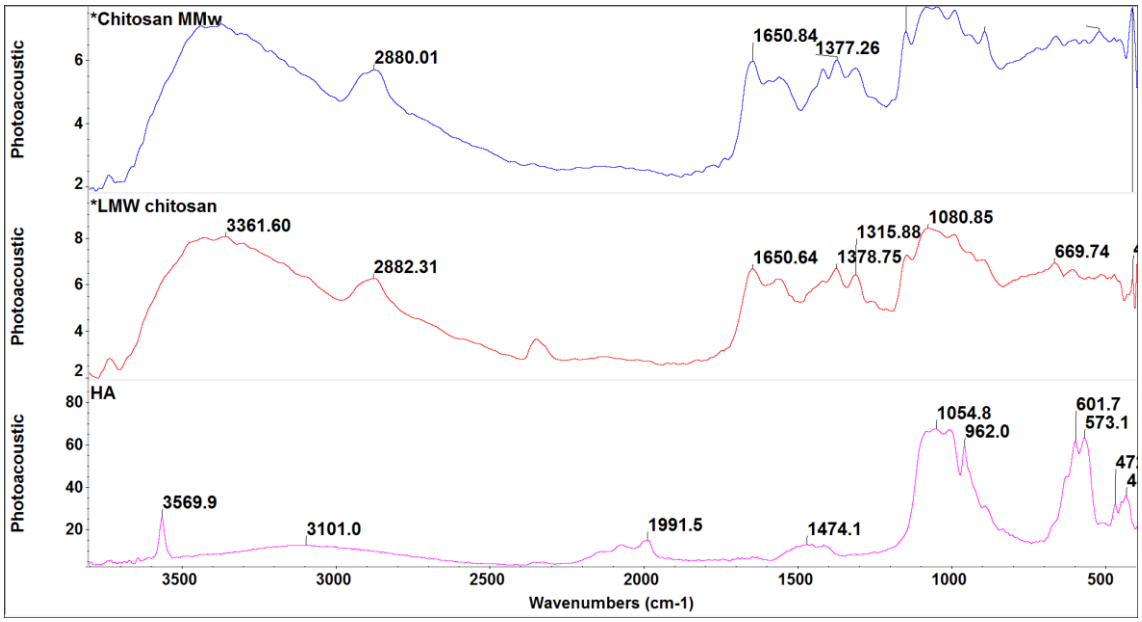

Figure 25: FTIR-PAS Spectra of, MMw CH, LMw CH and HA.

Spectra from the top surface of LMw CH combinations with HA are shown in Figure 26 with ratios of 100%, 70%, 50% and 30% CH to 30%, 50% and 70% HA. Top surface spectral

data of LMw and MMw shows more CH content as they resemble the neat CH spectra. Although some HA peaks can be seen interacting on the top surface spectra of both LMw and MMw in spectral data. In samples with ratios of higher HA content. Figure 27 shows the bottom surface of the LMw CH:HA films. The bands in between 1550 to 1700 cm^{-1} are attributed to mode superposition of the HA -OH group and the CH Amide I and Amide II groups. The HA functional group peak of -OH is more prominent in the specimens with higher amounts of HA. As the intensity of HA increases, peak at 3568cm^{-1} can be seen increasing in intensity as well. The different modes of phosphate groups are also more pronounced in bottom surface spectra. A significant broadening of the band at 1050cm^{-1} is depicting the presence of polymer and its interaction with the phosphate groups. Figure 28 (top surface) and 29 (bottom surface) show the spectral information obtained using MMw CH is similar to LMw CH: HA. MMw 70:30 bottom surface shows more CH dominance in the spectral data. Other combinations of MMw 50:50 and 30:70 bottom surface show more peaks pertaining to HA. Phosphate modes and hydroxyl modes are more pronounced in the other two ratios. Collectively clear differences can be appreciated in the top and bottom surface spectral profiles in both molecular weights and all there combinations with HA.

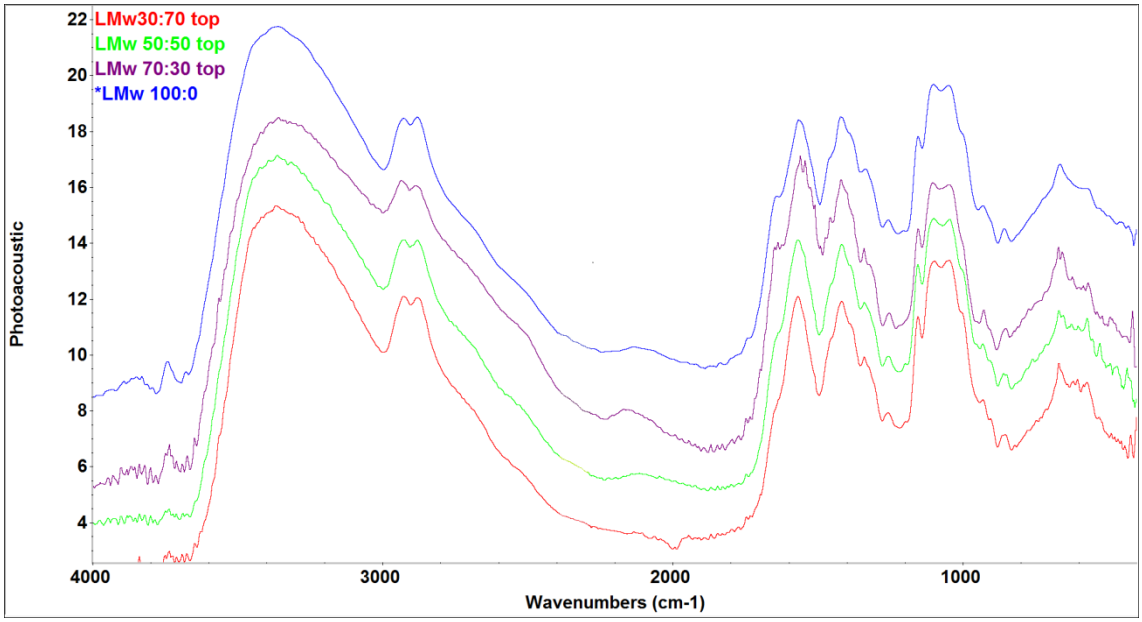

Figure 26: Top surface of LMw CH:HA membranes, 100:0, 70:30 , 50:50, 30:70, acquired using PAS accessory of FTIR.

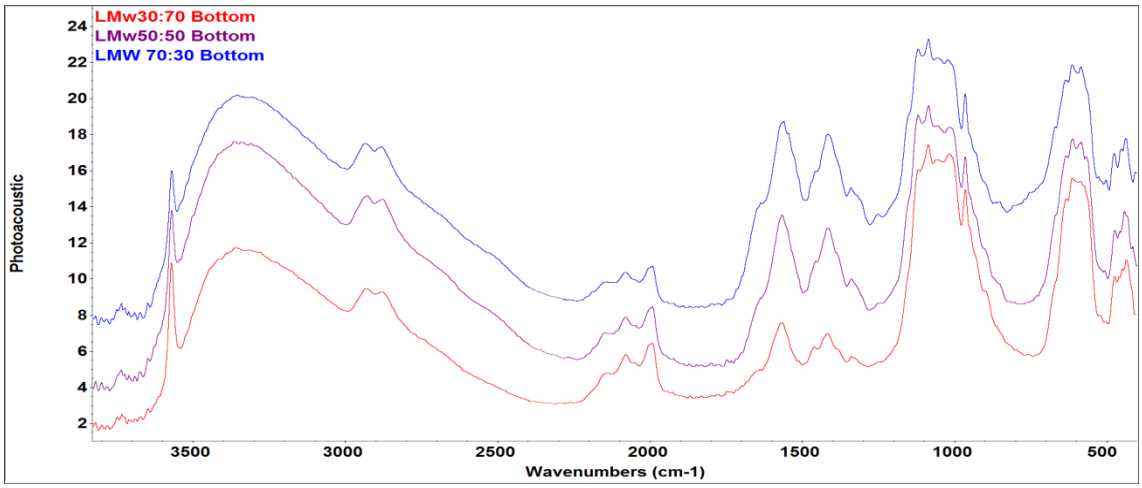

Figure 27: FTIR- PAS spectra of bottom surface of LMw CH:HA membranes 70:30 , 50:50, 30:70.

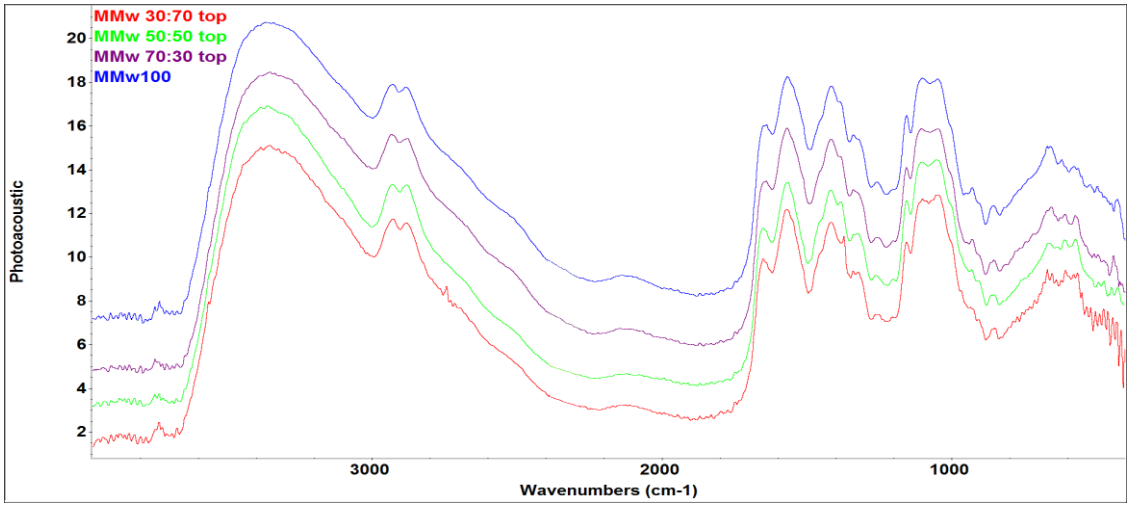

Figure 28: FTIR-PAS of top surface of MMw CH:HA combinations MMw 100:0, 70:30, 50:50 and 30:70 CH:HA.

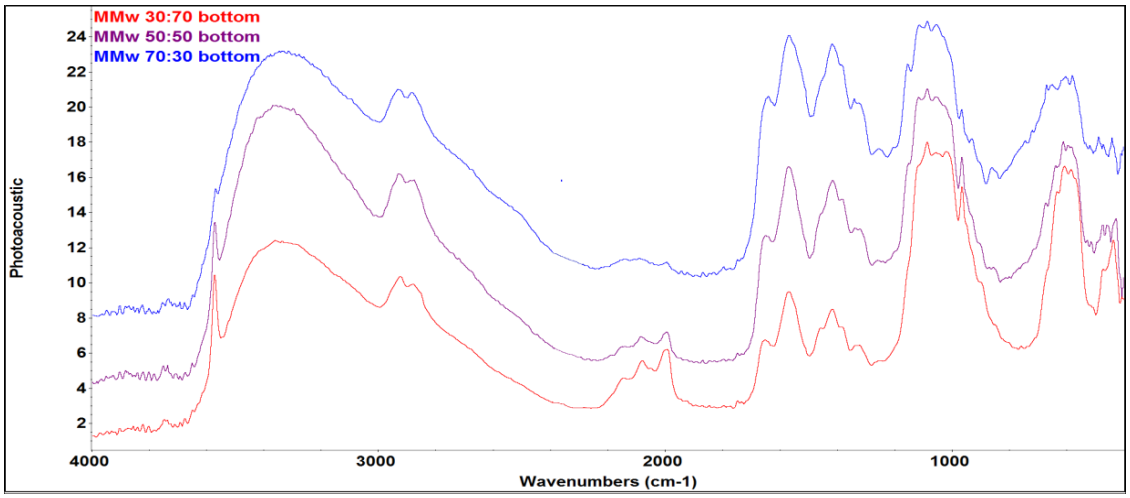

Figure 29: FTIR-PAS of bottom surface of Medium mol weight Chitosan and HA combinations 70:30, 50:50 and 30:70 CH:HA.

Table 13: Bands and Peak identification in neat Chitosan, neat HA and composite CH:HA scaffolds (thin films, and freeze gelated membranes).

PEAKS (cm^{-1})	EXPLANATIONS	REFERENCE
Chitosan peaks (Low and Medium mol wt)		
3354	-NH group Stretching Vibration	Thein-Han *et al.,* 2009
3450	-OH group	
2872-2920	CH_2 symmetric and asymmetric stretching vibration	Manganti *et al.,* 2011
1655	C=O in amide group (Amide I)	Xianmiao *et al.,* 2009
1560	-NH bending vibration in amide group	Mucha *et al.,* 2002
1590	$-NH_2$ bending in Amine group	Wang *et al.,* 2005
1430	CH_3 bending deformation (pyranose ring) (C-H)	Thein-Han *et al.,* 2009
1320-1380	CH_3 in amide group, CH bending, CH stretching	Manganti *et al.,* 2011
1252-1255	Free primary amine at C2 position of glucosamine	Thein-Han *et al.,* 2009
1150-1040	Glycosidic linkages(symmetric and asymmetric stretching vibration(C-O-C)	Manganti *et al.,* 2011, Xianmiao *et al.,* 2009
895	Assigned to polysaccharide structure	Thein-Han *et al.,* 2009
599	Bending vibration of Amide group	N.Manganti *et al.,* 2011
Neat Hydroxyapatite peaks		
3500	Hydroxyl Stretch (-OH) on lattice sites of HA crystal	Rehman *et al.,* 1997, Manganti *et al.,* 2011, Thein-Han *et al.,* 2009
1190,1085	Phosphate (PO_4^{3-}) ν_3	Rehman *et al.,* 1997, Walters and LeGeros *et al.*,1990
960	Phosphate (PO_4^{3-}) ν_1	
660-520	Phosphate (PO_4^{3-}) ν_4 Bending deformation	
472-460	Phosphate (PO_4^{3-}) ν_2	
Composite scaffolds (CH:HA)		
3560	-NH group Stretching Vibration	Thein-Han *et al.,* 2009

3308-3362	-OH group	Thein-Han *et al.,* 2009
2880-2927	CH_2 symmetric and asymmetric stretching vibration	Manganti *et al.,* 2011
1652-1654	Symmetric stretching vibration of (C=O) amide I	Manganti *et al.,* 2011, Xianmiao *et al.,* 2009
1542-1547	$-NH_2$ bending in Amine group	Thein-Han *et al.,* 2009
1419	Bending vibration(C-H)	
1378	CH_3 in amide group, CH bending, CH stretching	Manganti *et al.,* 2011
1150	Glycosidic linkages(symmetric and asymmetric stretching vibration(C-O-C)	Manganti *et al.,* 2011
1080		
1057		
963	Phosphate (PO_4^{3-}) ν_1	Rehman *et al.,* 1997
898	Assigned to polysaccharide structure	Thein-Han *et al.,* 2009
601-629,571-578	Phosphate (PO_4^{3-}) ν_4 Bending deformation	Rehman *et al.,* 1997

4.1.4. Mechanical testing

Mechanical testing performed on dry and wet membranes / thin films as prepared by LMw and MMw CH and CH HA composites were performed in tension and their obtained values are tabulated (Table 14 and 15). Each membrane was cut into thin films of 20 mm in Length, 5 mm in Diameter. Hydrated samples were first neutralized and then tested in tension. The samples became very weak on handling during moist conditions. Values show that neat CH membranes had higher *E* and MMw CH membranes during dry conditions had a higher Young's modulus. Addition of HA lowers the elastic modulus. As seen by the decrease in the Elastic modulus values with increasing ratio. Surprisingly LMw 70:30 in moist conditions had a higher E than neat LMw CH. Similarly in Dry state it also showed higher E values when compared with neat CH. Overall LMw CH and CH HA membranes have higher modulus than MMw in wet conditions, whereas MMw CH and CH HA in dry state had higher values. Strain values in most conditions were higher as compared to dry conditions. UTS values were also higher for neat CH and showed a drop with HA combinations. Examples of stress strain (curves) relationship of dry CH:HA membranes are represented in Figure 30.

Table 14: Tensile properties of LMw and MMw membranes conducted in wet/moist conditions. To calculate the Ultimate tensile strength (MPa), Young's Modulus (*E*) or Elastic Modulus (MPa) and Strain (%), Values shown are mean ± SD where n=6.

Wet Membranes	UTS (MPa)	*E* (MPa)	Strain (%)
LMw 100:0	1.75±0.16	10.76±3.21	0.32±0.16
LMw 70:30	2.00±0.49	20.84±2.41	0.12±0.03
LMw 50:50	3.01±0.60	18.51±1.72	0.36±0.12
LMw 30:70	1.51±0.29	13.12±5.09	0.25±0.06
MMw 100:0	2.02±0.24	7.70±0.98	0.27±0.01
MMw 70:30	6.85±0.23	6.85±0.23	0.47±0.04
MMw 50:50	1.81±0.26	5.55±0.23	0.42±0.10
MMw 30:70	1.17±0.32	4.19±0.27	0.35±0.09

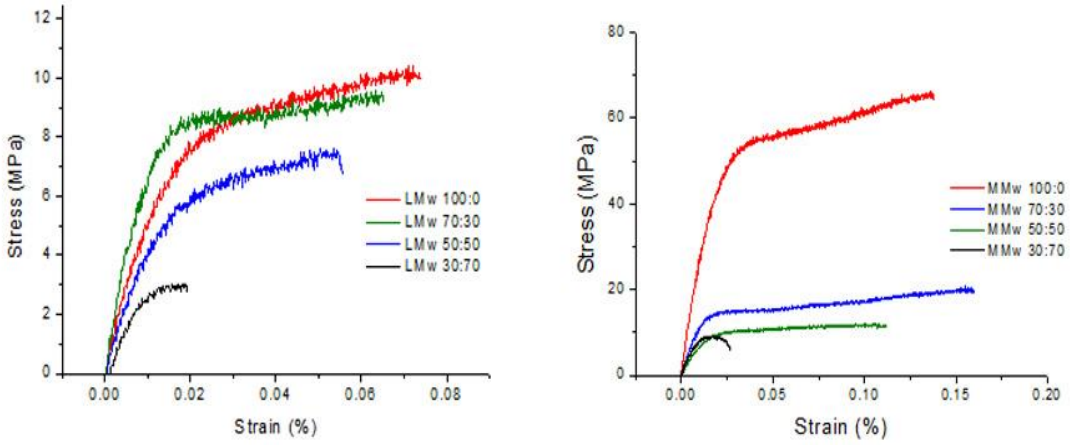

Figure 30: Examples of Stress Strain relationship of LMw and MMw CH and CH: HA membranes when tested under Dry condition for tensile properties.

Table 15: Tensile properties of LMw and MMw membranes conducted in Dry conditions. To calculate the Ultimate tensile strength (MPa), Young's Modulus (*E*) or Elastic Modulus (MPa) and Strain (%), Values shown are mean ± SD where n=6.

Dry Membranes	UTS (MPa)	*E* (MPa)	Strain (%)
LMw 100:0	10.50±0.69	460.37±111.2	0.06±0.01
LMw 70:30	8.73±0.58	554.98±61.7	0.07±0.03
LMw 50:50	8.03±2.18	387.76±87.0	0.06±0.01
LMw 30:70	2.95±0.05	291.36±6.43	0.02±0.00
MMw 100:0	30.60±29.8	1066.7±829.3	0.12±0.09
MMw 70:30	16.90±2.57	955.9±26.1	0.13±0.04
MMw 50:50	10.42±1.41	589.54±37.37	0.07±0.05
MMw 30:70	9.07±2.86	680.37±129.68	0.04±0.02

4.1.5. Swelling Ratio

The swelling ratio or water uptake/ retention ability of the LMw and MMw CH: HA films are shown in Figures 31. The films were seen to reach a swelling equilibrium after 0.25 hrs. The swelling data shows that LMw CH:HA membranes swell less; compared to the MMw membranes. Neat LMw shows an initial swelling ratio of 45% in 0.25hrs and MMw

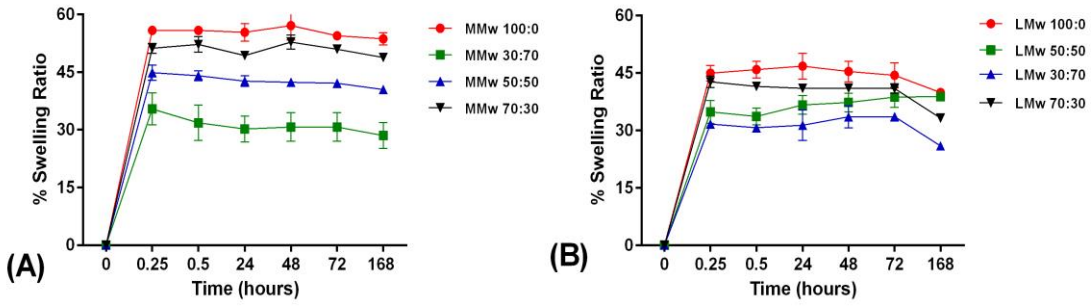

Figure 31: Swelling ratio shown in percentage of MMw and LMw CH and CH:HA membranes assessed for 168 hours, Values shown are mean ± SD (n=3). Samples reach equilibrium in 15 minutes of immersion in DiH_2O.

shows 57%. Over the 168 hour regime the ratio shows a plateau is reached after the initial 0.25 hrs. As the amount of HA increases swelling tends to decrease. The difference in the swelling percentages of MMw CH and CH:HA ratios are higher than the LMw ratios. Least

swelling percentage is observed with 30:70 CH:HA ratios where an overall 30% swelling can be seen after 15 mins of immersion in distilled water.

4.2. In-*vitro* degradation

4.2.1. Weight profile analysis

Percentage weight remaining studies of CH:HA membranes / thin films prepared with LMw and MMw were performed for upto 48 days and the trend can be seen in Figure 32 below. At the end of 48 days LMw 100:0, had 60 % of its weight remaining. The LMw CH HA membranes showed a stable profile up to day 21. In between 28th and 48th days, the % weight remaining falls for LMw 50:50, 30:70 and 70:30. An overall 25 to 30% weight remains after the experimental period. MMw 100:0 showed stability with an overall % weight remaining of

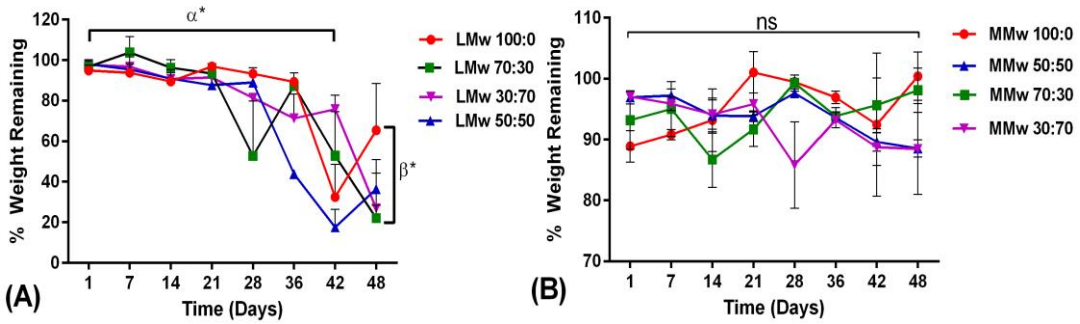

Figure 32: Weight loss profile of LMw (a) and MMw (b) CH and CH:HA membranes /thin films conducted over a 48 day experimental period, Values shown are mean ± SD (n=3). The values are shown as mean ± SD (n=3), α* denotes statistically significant difference between D1 and D42, for different groups *p*≤0.05, β* denotes significant difference between LMw 100:0 and LMw 70:30 at D48, ns denoted no significant different between D1 and D48 for MMw 100:0 and MMw 70:30.

100%. MMw 70:30 showed a stable profile as compared to MMw 50:50 and 30:70 which had an overall 87% weight remaining at 48th day of degradation. Overall MMw membranes when compared to LMw showed a more stable profile.

4.2.2. pH analysis

pH measurements were performed from the degraded supernatant till 28 days and the trend can be seen in Figure 33. The pH profile over the degradation period of LMw and MMw CH HA membranes shows a dissimilar trend. pH of the lysozyme solution taken at day 0

was 6.7. There is an initial rise in the pH value at day 4 (6.7 ±2 to 7.2 ±2). There onwards slight fluctuations are observed and towards the end of day 28, the pH of MMw CH HA membranes reached 7.4±2. Neat LMw CH show a steep rise at day 11 to pH 8 and rises to 8.5 for day 21 and 25. Fluctuation in the pH profile of LMw CH HA membranes are also observed and day 28 an overall pH values of 7.5 ±2 is observed.

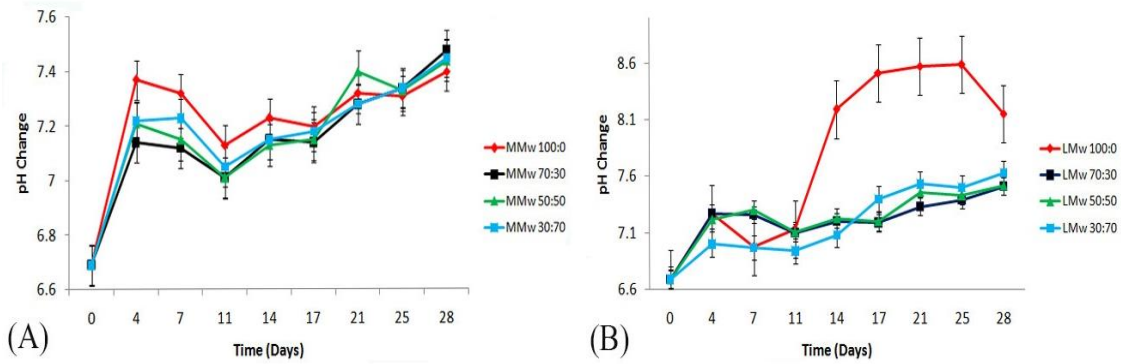

Figure 33: pH change of (a) MMw and (b) LMw CH and CH:HA ratios calculated over 28 day time period (n=3).

4.2.3. UV-Vis spectroscopy

Spectral information collected by UV-Vis spectroscopy of the degraded lysozyme solution over a range of 300 to 200nm of the degraded media for MMw and LMw CH HA membranes is shown in Figures 34 and 36.

Degraded supernatant was analysed by UV-Vis spectrometry to study whether carboxylic or aldehyde groups formed after hydrolytic scission of β-1,4 glycosidic bonds of CH. Spectra were obtained in a 1.0 cm quartz cell at different time points for all LMw and MMw CH and CH:HA ratios. Two absorption bands were observed in all samples at 220 and 280nm, respectively. The peaks tend to vary in absorption as they were taken at Day 4, 11 and 21. Figures 35 and 37 depict the intensity variation for each sample at each time point for the two bands observed in the graphs. The intensity graphs show a gradual increment in absorbance for MMw membranes for both peaks at 220 and 280, whereas fluctuations were observed in the intensity for LMw samples.

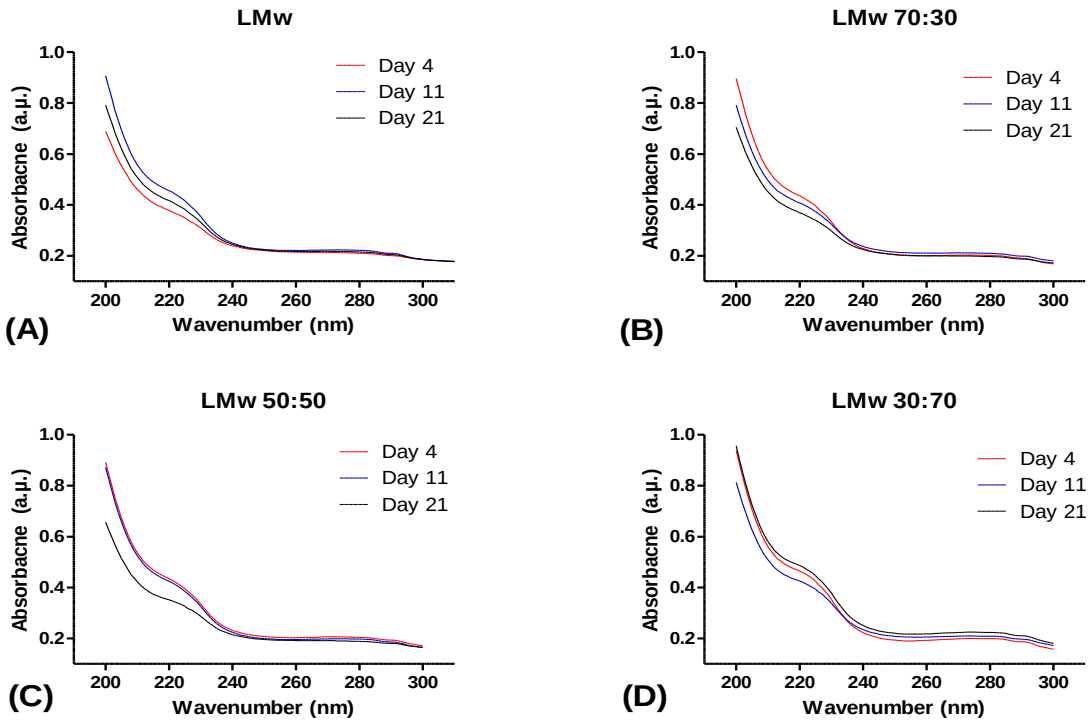

Figure 34: UV-Vis spectrometry performed on degradation supernatant of neat LMw CH and CH:HA combinations, 100:0. 70:30. 50:50 and 30:70.

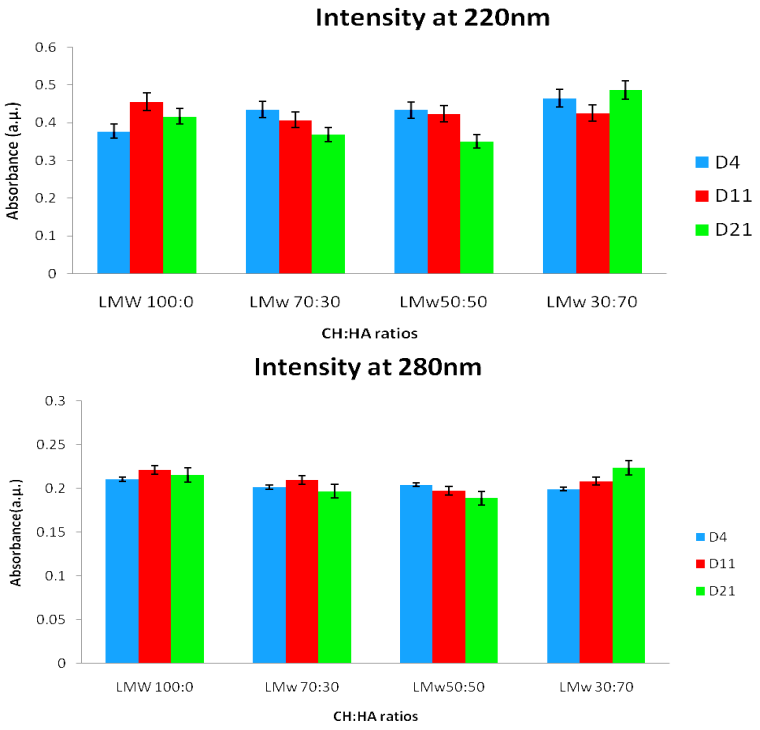

Figure 35: Absorbance intensity plotted for peaks at 220 and 280 nm at Day 4, 11 and 21 of degradation for LMw CH and CH:HA ratios.

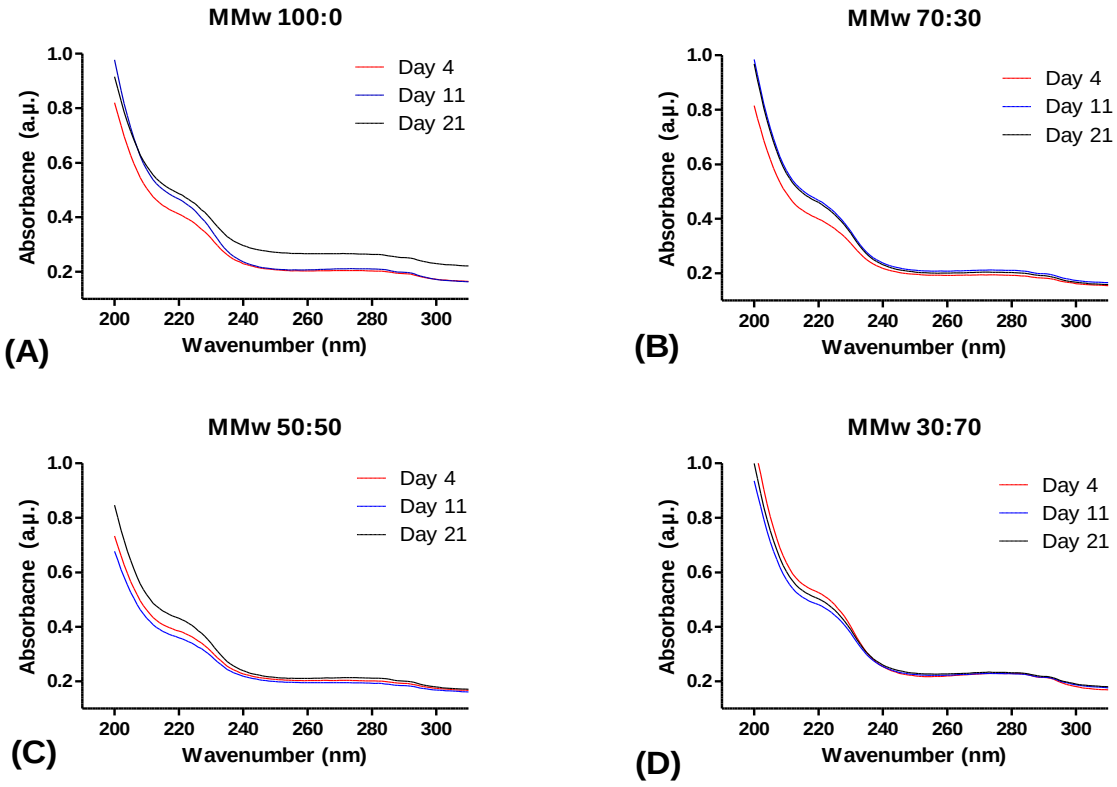

Figure 36: UV-Vis spectroscopy performed on degradation supernatant of neat MMw CH and CH:HA combinations, 100:0. 70:30. 50:50 and 30:70.

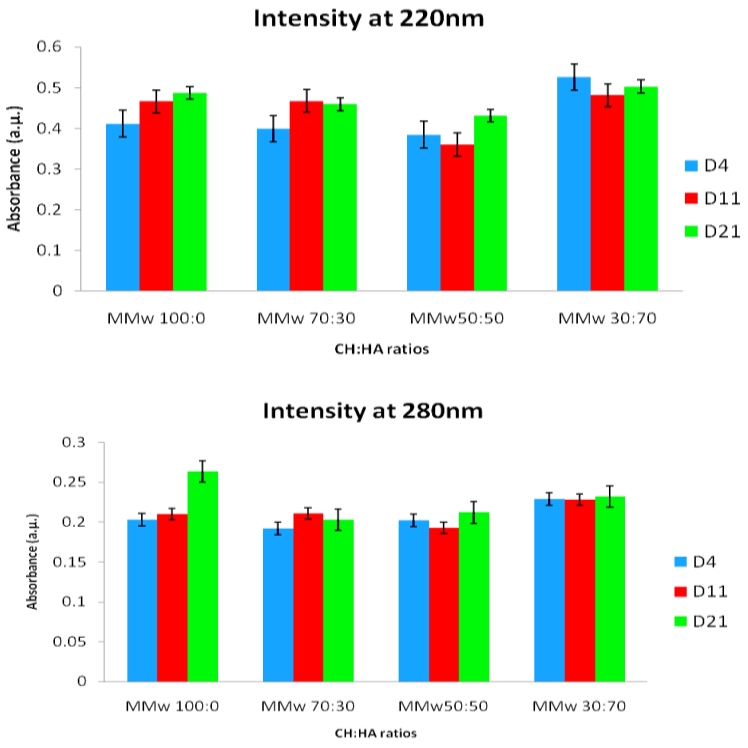

Figure 37: Absorbance intensity plotted for peaks at 220 and 280nm at Day 4, 11 and 21 of degradation for MMw CH and CH:HA ratios.

4.2.4. FTIR Sepctroscopy

FTIR-PAS spectroscopy performed using PAS as an accessory on MMw and LMw CH and CH:HA ratios on the top and bottom surface of the degraded membranes is shown in Figures 38 - 46, 39 (i and ii) (MMw 70:30). Spectral data collection of top and bottom surface of each membrane for each time point was the aim of the analysis. Although at some time points the membranes curled up making the characterisation process of CH side difficult. Hence; only HA side was used to acquire the spectral information. This behaviour of membrane was particularly noticed for LMw CH:HA ratios. Chemical shifts in peaks within the membranes at each time point and relative shifts in absorbance were taken into account. Spectra collected for neat CH MMw and LMw (Figure 38-43) membrane collected from day 0 to 28 shows subtle changes it the peaks. Particularly the glycosidic region, amide II bands and CH stretching vibrations show a decrease in intensity. FTIR-PAS of bottom surface of MMw membranes with HA incorporation show changes in intensity of CH_3 bending and CH stretching vibration at 1420 and 1380cm^{-1}.

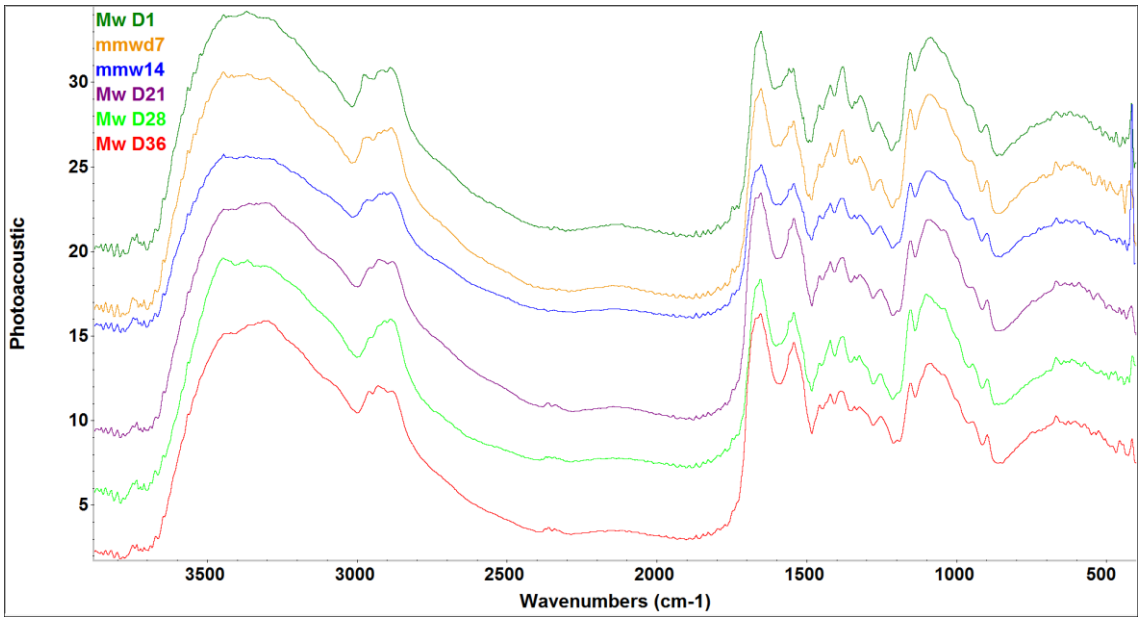

Figure 38: FTIR-PAS spectroscopy of neat MMw CH membrane at Day 1, 7, 14, 21, 28 and 36.

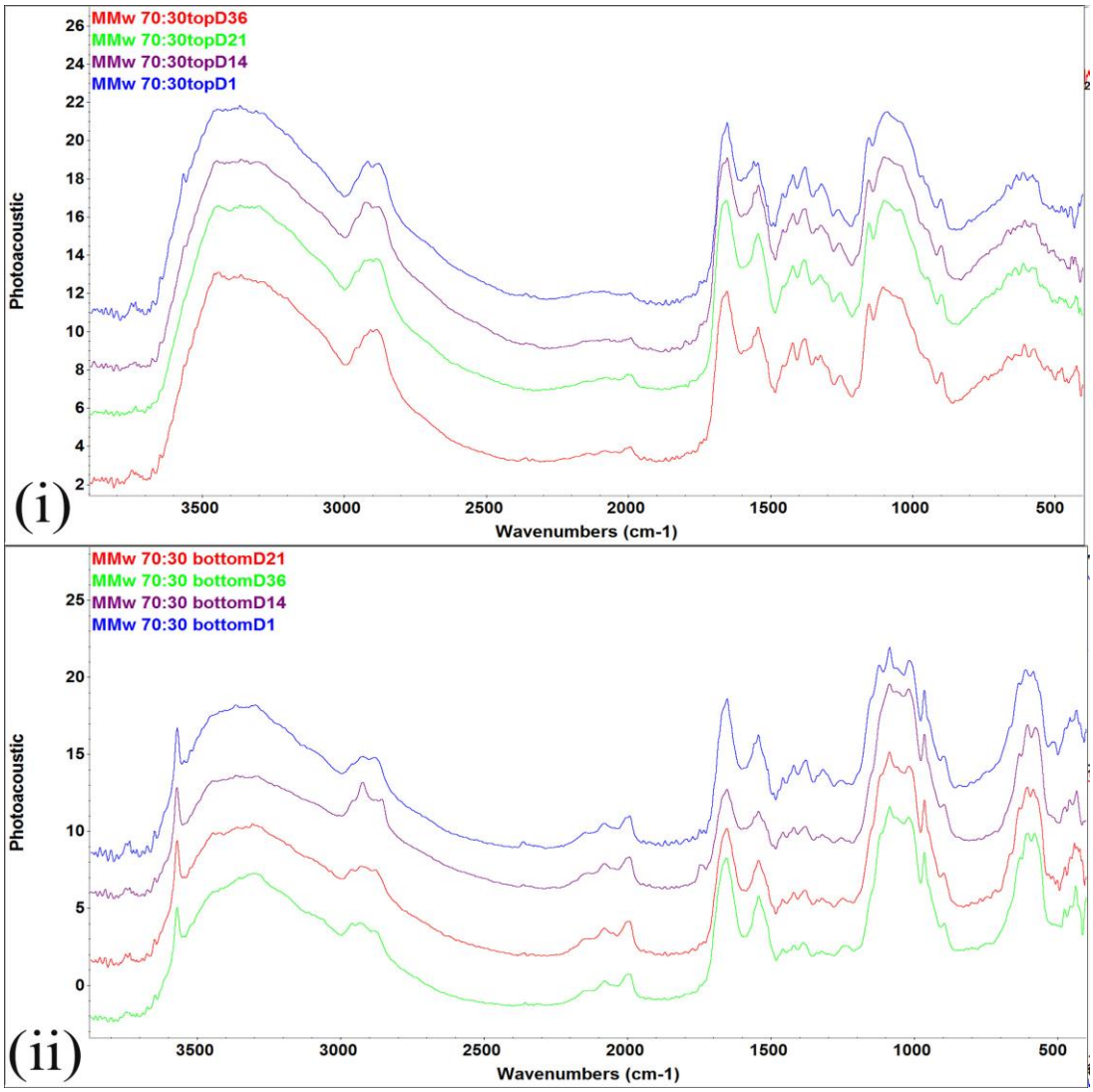

Figure 39: (i) Top surface Day 1, 14, 21, and 36 (ii) Bottom surface of MMw CH:HA 70:30 degradation rate of thin film shown over a period of Day 1, 14, 21 and 36 of immersion in lysozyme solution.

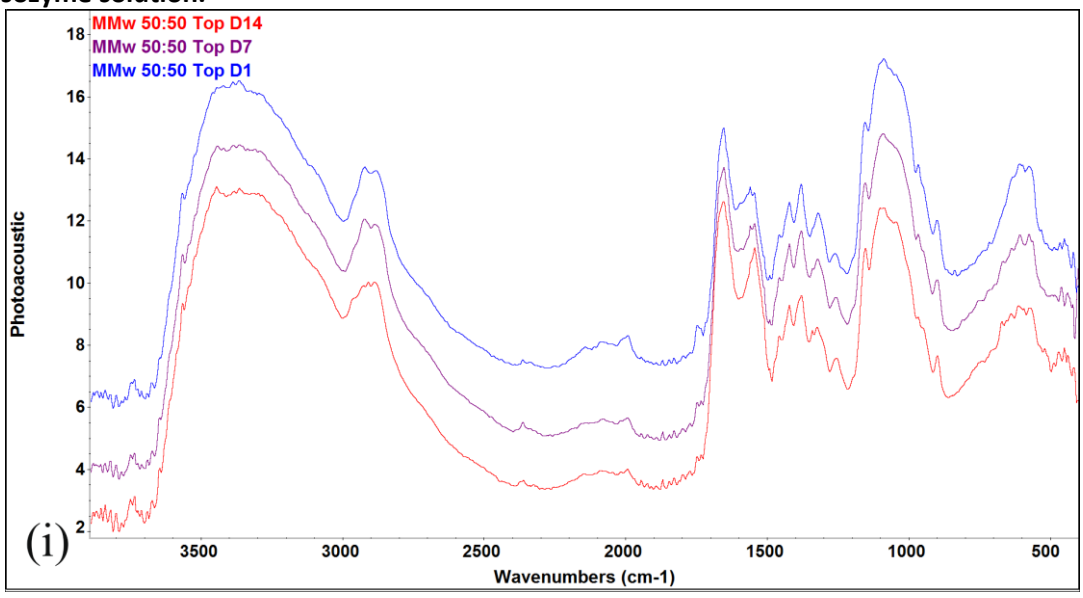

Figure 40: (i) Top surface Day 1, 7 and 14 of MMw CH:HA 50:50.

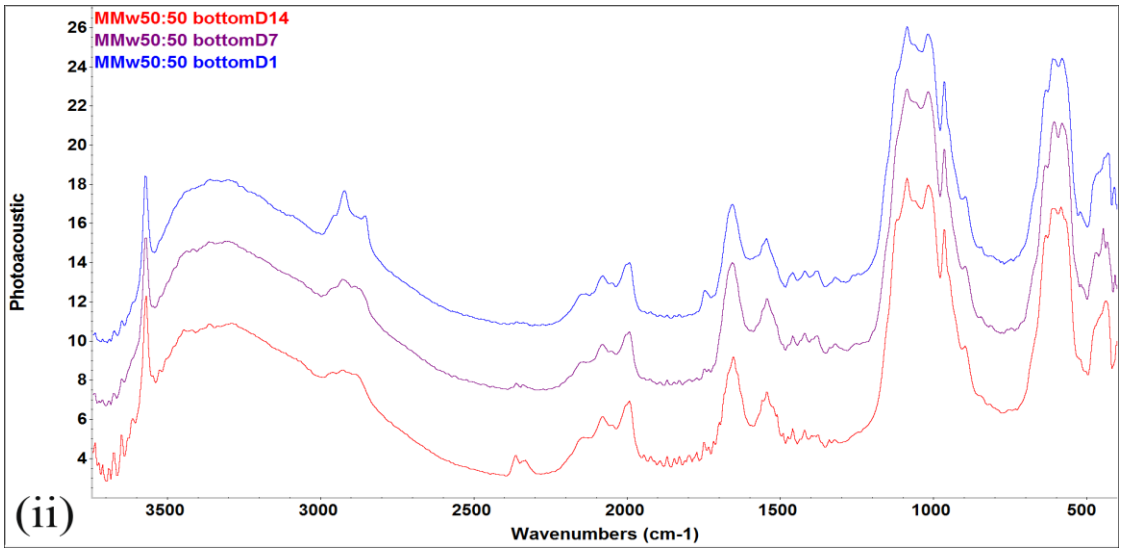

Figure 41: (ii) Bottom surface of MMw CH:HA 50:50 degradation rate of thin film shown over a period of Day 1, 7 and 14 of immersion in lysozyme solution.

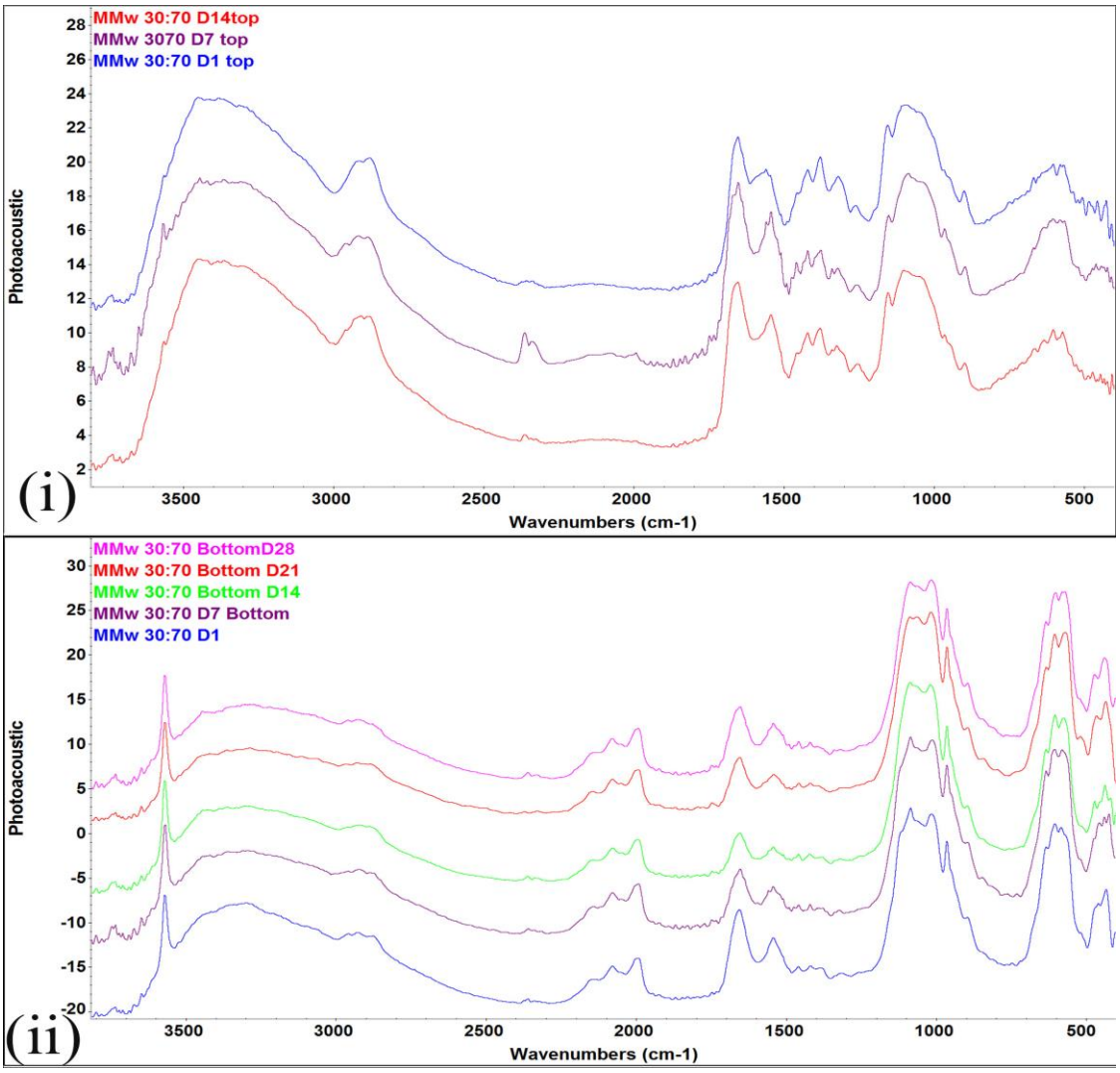

Figure 42: (i) Top surface Day 1, 7 and 14 (ii) Bottom surface of MMw CH:HA 30:70 degradation rate of thin film shown over a period of Day 1, 7, 14, 21 and 28 of immersion in lysozyme solution.

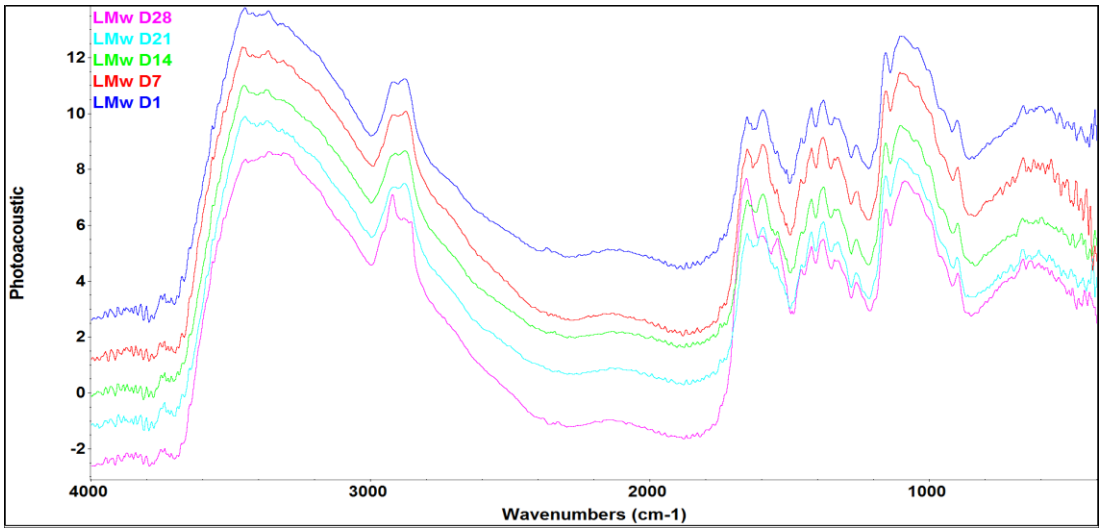

Figure 43: FTIR-PAS of LMw 100:0 degradation profile conducted at Day 1, 7, 14, 21 and 28.

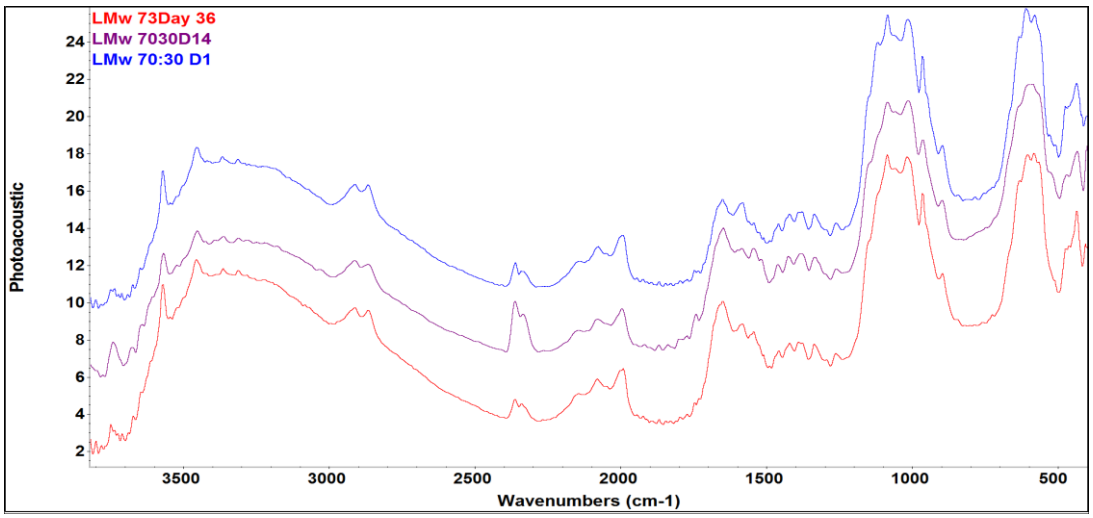

Figure 44: FTIR-PAS of LMw 70:30 degradation profiles conducted at Day 1, 14, and 36 after immersion in lysozyme solution

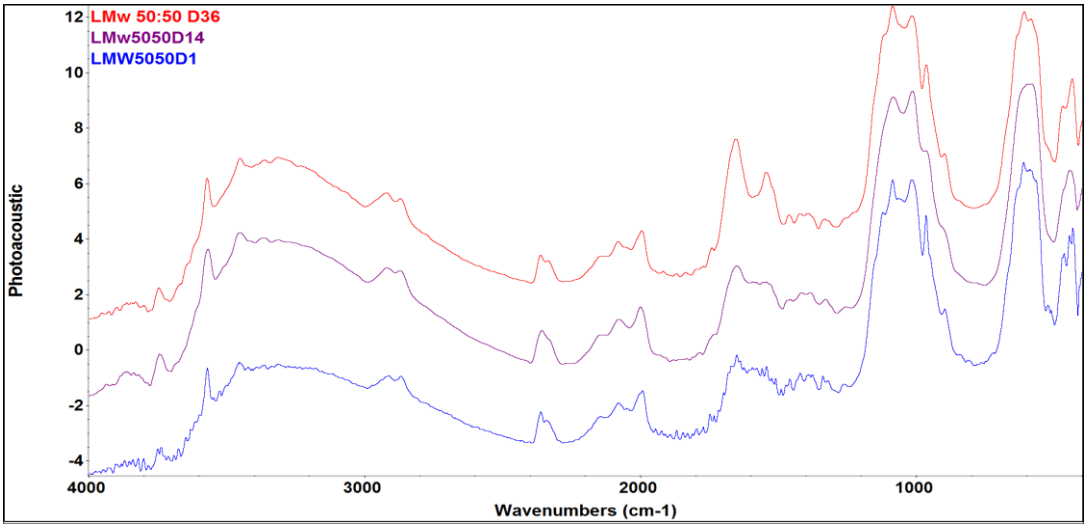

Figure 45: FTIR-PAS of LMw 50:50 degradation profiles conducted at Day 1, 14, and 36 after immersion in lysozyme solution

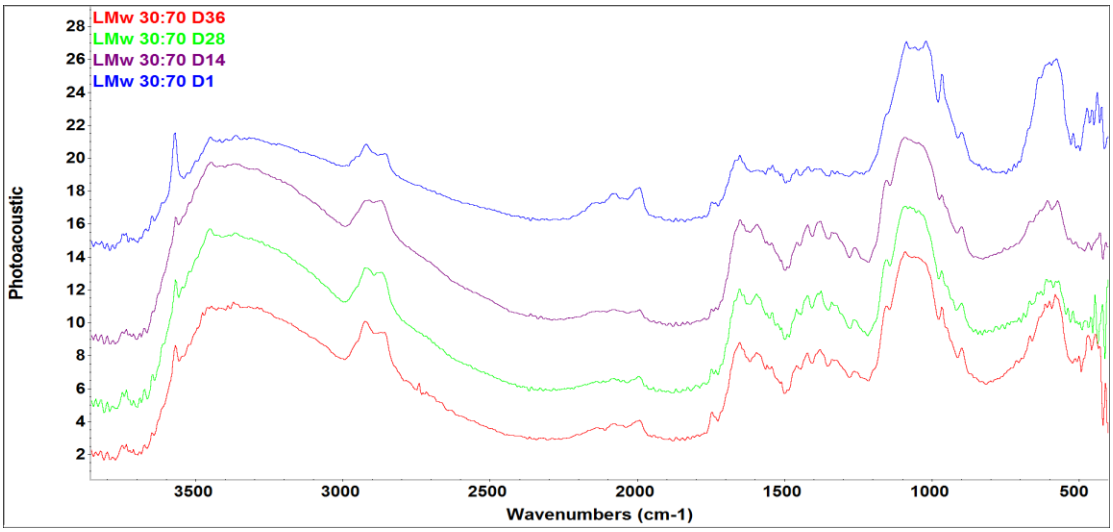

Figure 46: FTIR-PAS of LMw 30:70 degradation profiles conducted at Day 1, 14, 28 and 36 after immersion in lysozyme solution

4.3. Optical Images

Optical images of the LMw and MMw membranes taken at each time point from Day 1 to Day 48 are shown in Figure 47. It can be observed that the LMw membranes with HA tend to curl

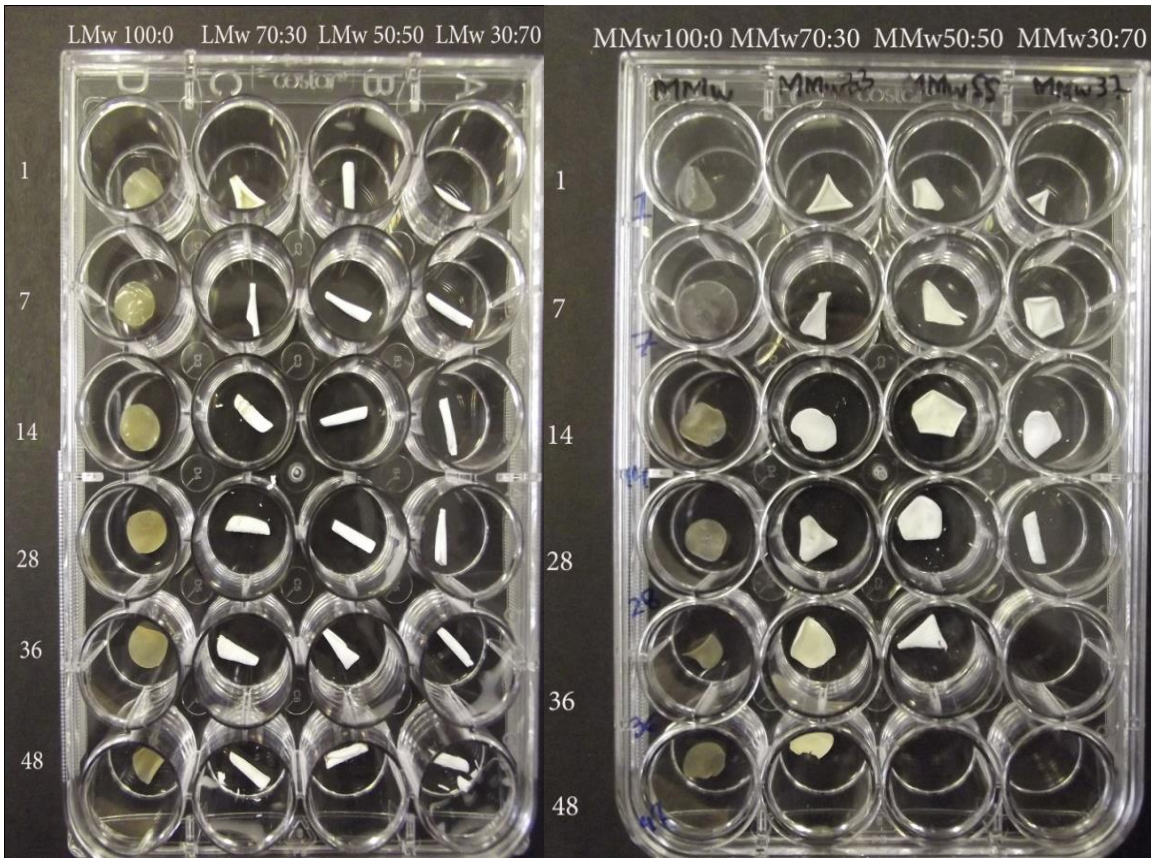

Figure 47: Optical Images of LMw and MMw CH and CH:HA ratios after degradation study at Day 1, 7, 14, 28, 36 and 48.Samples were selected out of three at each time point.

up, which as mentioned previously cause difficulties in spectral data collection. When compared to MMw CH and CH:HA membranes, some of the ratios (MMw 50:50 and 30:70) lost their integrity around day 28 and 36.

4.4. Biocompatibility

Biocompatibility studies performed after culturing MG63 and hES-MP cell line on the bottom surface of LMw CH:HA and MMw CH:HA 50:50 and 30:70 are shown in Figure 48 (a and b). Day 1 values show that initial attachment was achieved for all ratios. A gradual increment was observed for LMw 30:70 which were statistically significant from day 1 to 7. When LMw 100:0 was compared with MMw 50:50 an overall statistically significant difference was observed. At day 7 of culturing hES-MP's on the bottom surface of LMw and MMw membranes, viability values for HA incorporated specimens were higher as compared to virgin LMw. When the same ratios were seeded with MG63's and gradual increment was seen for all specimens but higher values were observed for LMw 30:70 and MMw 50:50. Day 1 values

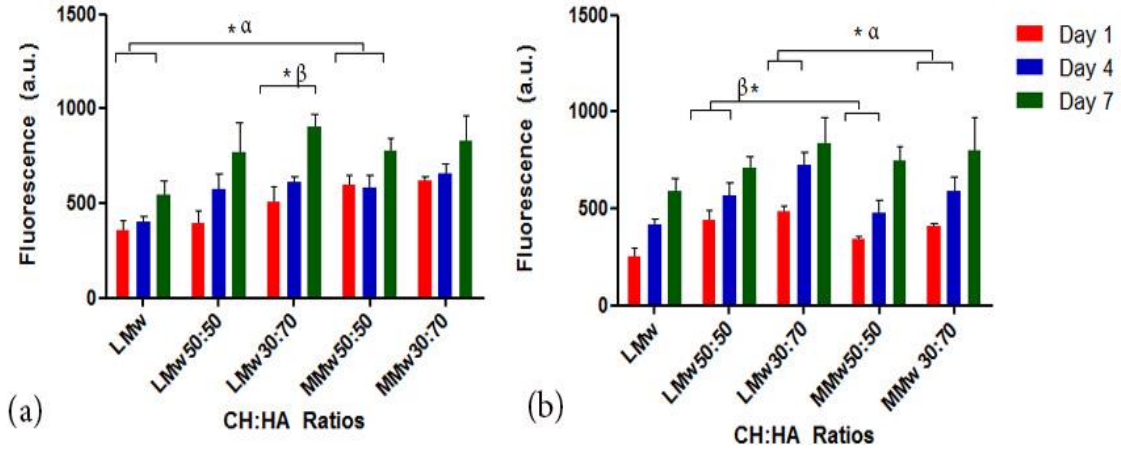

Figure 48: Cell Culturing performed with (a) hES-MP and (b) MG63 seeding and assessing with Alamar blue at day 1, 4 and 7 for viability. Values shown are taken from mean ± SD where n=3. (48a) α* denotes statistically significant difference between LMw 100:0 and MMw 50:50, with in the same group $p \leq 0.05$, β* denotes significant difference between D1 and D7 for LMw 30:70, (48b) α* denotes statistically significant difference between LMw 30:70 and MMw 30:70 for D1 and D4. β* denotes significant difference between LMw 50:50 and MMw 50:50 for D1 and D4.

were suggestive that cells were able to undergo attachment. Statistically significant difference was seen for LMw 50:50 compared to MMw 50:50 for Day 1 and 4. When LMw 30:70 was compared with MMw 30:70 for day 1 and 7 values, statistically significant difference was also seen in this case. To assess the effect of gelatin on the cellular attachment and proliferation,

MG63 were cultured on the bottom surface of membranes with and without gelatin incorporated in them Figure 49 (a and b). LMw 50:50 and 70:30 show higher attachment at the end of Day 7. Higher viability values were seen in samples treated with gelatin compared to without gelatin. Figure 50 shows DAPI (Blue stain for nucleus) and FITC (red stain for cytoskeleton) staining of MG63's after 7 day culturing on the bottom and top surface of LMw 50:50 membranes. Images show that a higher attachment on the bottom surface as compared to the top surface was seen.

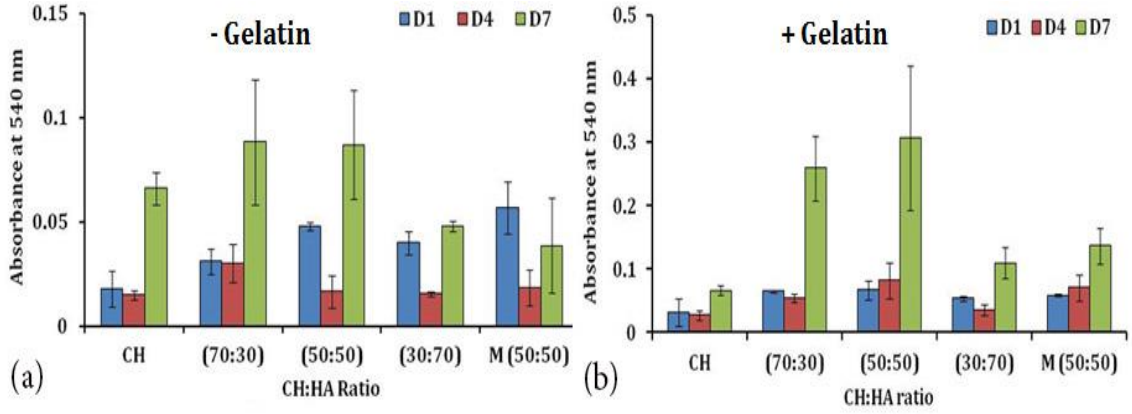

Figure 49: MG63 Cultured on CH:HA LMw and MMw 50:50 membranes to assess the effect of gelatin addition on cell viability over a period of Day 1, 4 and 7 by Alamar blue, (a) without Gelatin (b) with Gelatin.

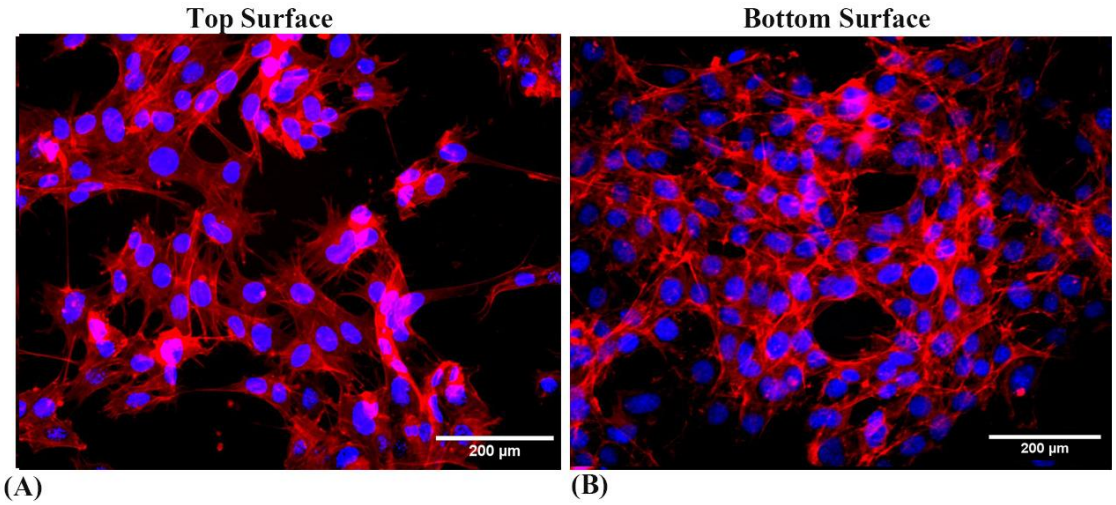

Figure 50: Nuclei and F-actin stained on the LMw 50:50 membranes after seeding with MG63 at day 7. Images showing top and bottom surface to cell attachment of MG63 on the membrane surface, both images scaled at 200µm.

4.4.1. Extracellular Matrix production

Sirius red and Alizarin red staining performed to assess collagen and calcium deposition on the bottom surface of membranes is shown in Figure 51 (a and b). Higher collagen deposition is noted for MMw 30:70 when compared with LMw, 50:50, 30:70 and MMw 50:50 at day 28. Statistically significant difference was observed when day 14 values were compared with Day 21. Between LMw 50:50 and 30:70 statistically significant difference was noted when Day 21 and 28 values were compared. Neat LMw and LMw 50:50 membranes shows a static trend for from day 14 to 28 when read for total collagen deposited.

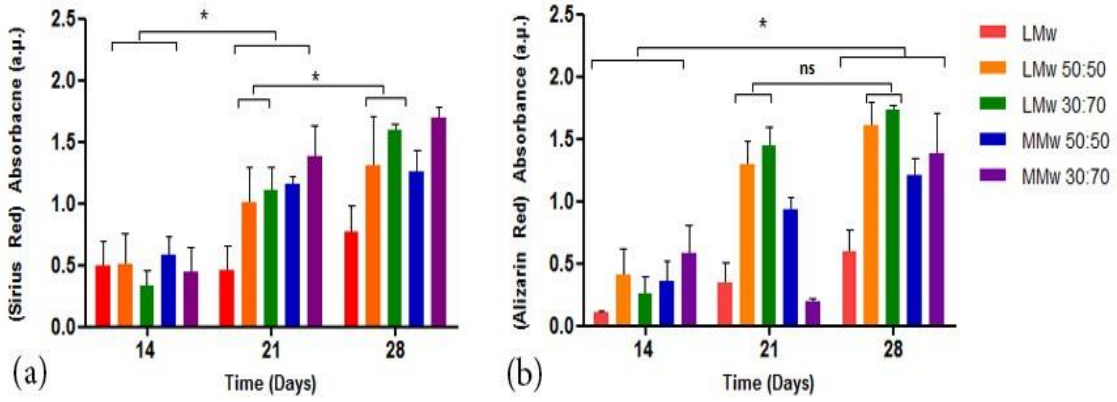

Figure 51: (a) Collagen and (b) Calcium deposition at Day 7, 14 and 21 of culturing with hESMP's of CH and CH:HA membranes. Values shown are mean ± SD (n=6). (51a) * denoted statistically significant difference between D14 and D21 values between LMw 50:50, 30:70 and MMw 50:50, 30:70

For calcium deposition LMw 50:50 membranes showed higher deposition at day 28 when compared to LMw 30:70 and MMw 30:70. Total calcium deposition assessed by Alizarin red assay showed that statistically significant difference was observed between day 14 and 28 values. No significant difference was seen when day 21 and 28 values for LMw 50:50 and 30:70 were compared with each other. The neat LMw 100:0 shows a gradual increment but is negligible when compared with HA incorporated samples. Overall hES-MPs culturing performed on the bottom surface of CH:HA ratios showed gradual increment for collagen and calcium deposition.

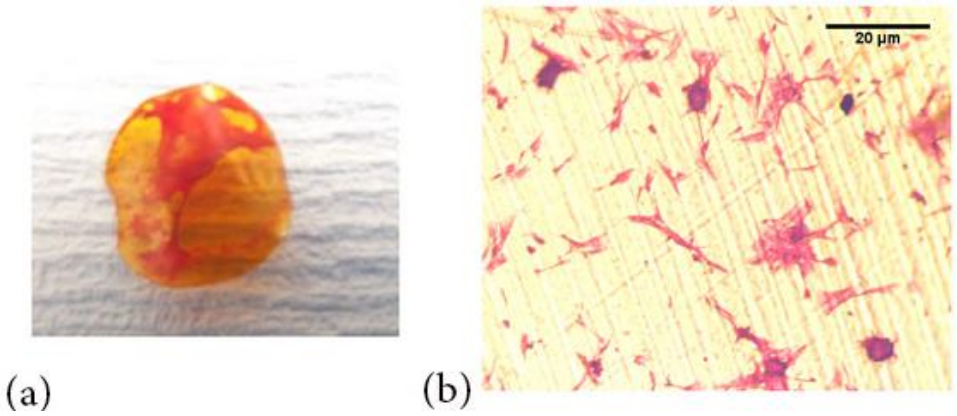

Figure 52: Sirius Red stained on neat LMw CH membrane (a) Optical Image (b) image taken at 40X magnification of the stained collagen, Scaled at 20µm.

4.5. Bioacitivty

It is a well-established fact that HA has the tendency to promote the formation of a bone like apatite layer at its surface when treated with SBF (Fathi *et al.* 2008). The in-*vitro* bioactivity studies based on morphological and structural changes were performed to determine if the HA incorporated CH membranes were able to promote the formation of a carbonated apatite layer on the bottom surface (HA enriched) of the membranes. The specimens were immersed in SBF media and assessed at 0, 1, 4 , 7 and 21 days for changes in pH values, percentage of weight change and FTIR spectroscopy using PAS for bulk analysis of the specimens on the HA side only. FTIR spectra were quantitatively analysed by measuring peak area ratio using TQ analyst available in OMNIC™ software (version 9.02).

4.5.1. pH Analysis

pH readings of the MMw and LMw CH and CH HA membranes were assessed at each time point after immersion of SBF medium (Figure 53 and 54). These figures show results obtained from normalized values. A means plot of all the reading for each time point at the end of predetermined days were recorded. A gradual increment was observed from Day 0 to day 21. At Day 0, baseline pH values of SBF were recorded around 7.4 ±0.45 at 37°C after storing in an incubator. The values showed a slight increment from day 4 to 7. At day 14 samples with HA show a pH of 7.7 and virgin MMw at the same day is 7.6. After day 21 all specimens showed a pH value of 7.6. LMw CH and CH HA membranes showed a similar profile with pH value of 7.4 at day 0 and a gradual increase over time was observed. At starting point (day 0) pH was 7.4, which similar to what were seen in MMw, at.

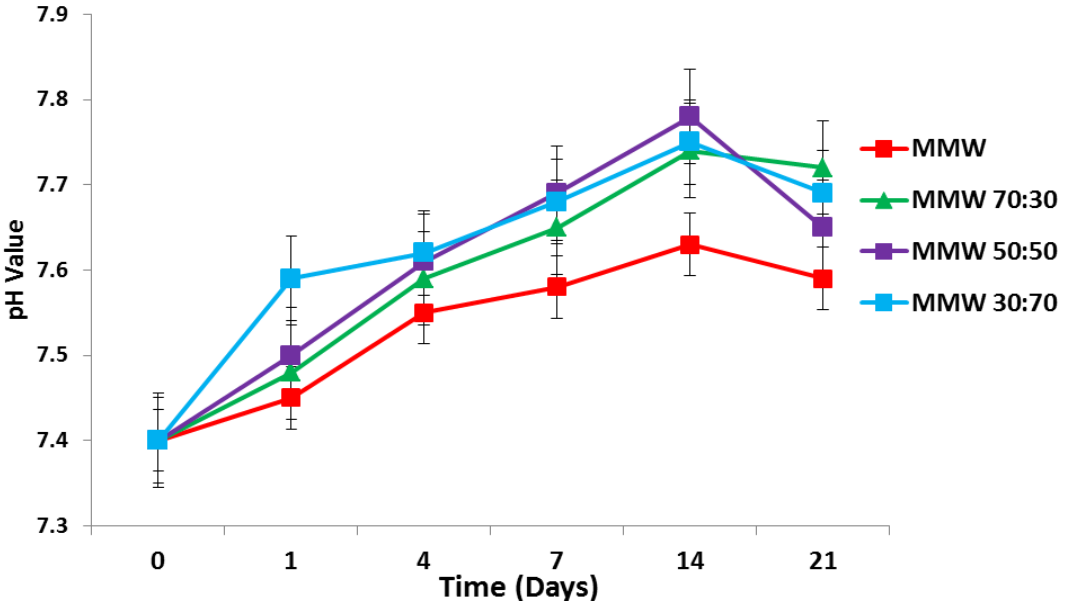

Figure 53: pH Change at each time point after immersion in SBF solution of MMw CH and CHHA membranes over a period of 21 days.

From Day 1 to 7 an increase in pH is seen from 7.4 to 7.5. LMw 30:70 and MMw 30:70 show a higher pH profile initially with a pH of 7.55 on day 1 (LMw 30:70) and 7.6 for MMw 30:70. LMw 30:70 at the end of 21 days showed a pH value of 7.7.

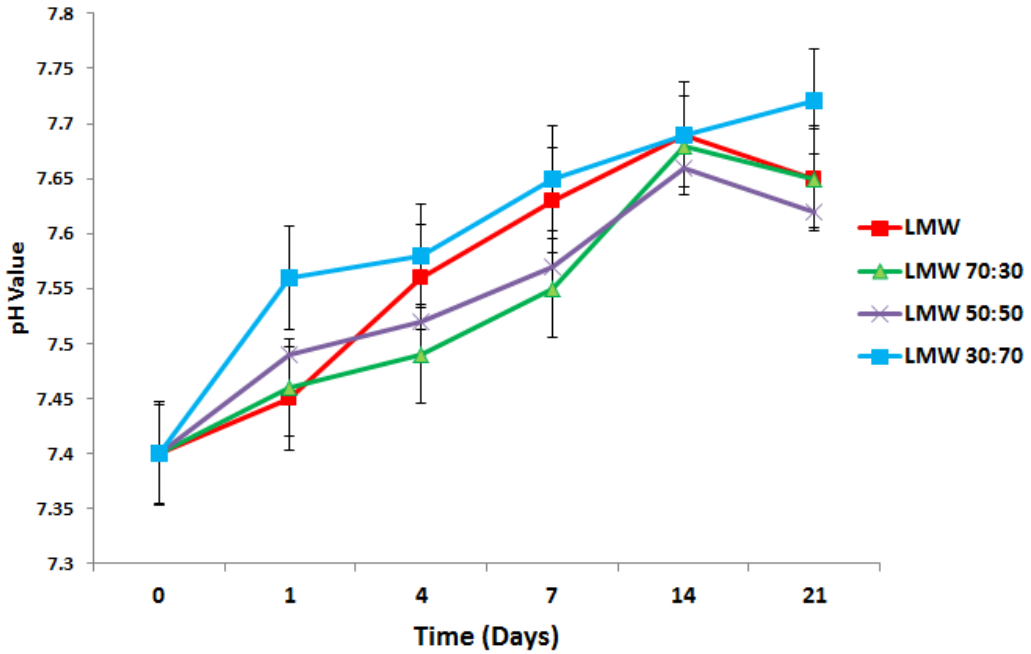

Figure 54: pH Change at each time point after immersion in SBF solution of LMw CH and CHHA membranes over a period of 21 days.

4.5.2. Weight Analysis

Weight profile of LMw and MMw CH and CH HA membranes after immersion in SBF over the experimental period was performed till day 21 (Figure 55 and 56). The net change in mass was calculated on successive days was recorded. This was achieved by expressing the initial mass of each dry membrane before immersion as a percentage of change in weight profile of the final weight after immersion followed by complete drying of the membrane on successive day of the immersion protocol. Virgin MMw CH membrane shows a -30% weight loss after 21 days. A gradual decrease was observed from the starting point.

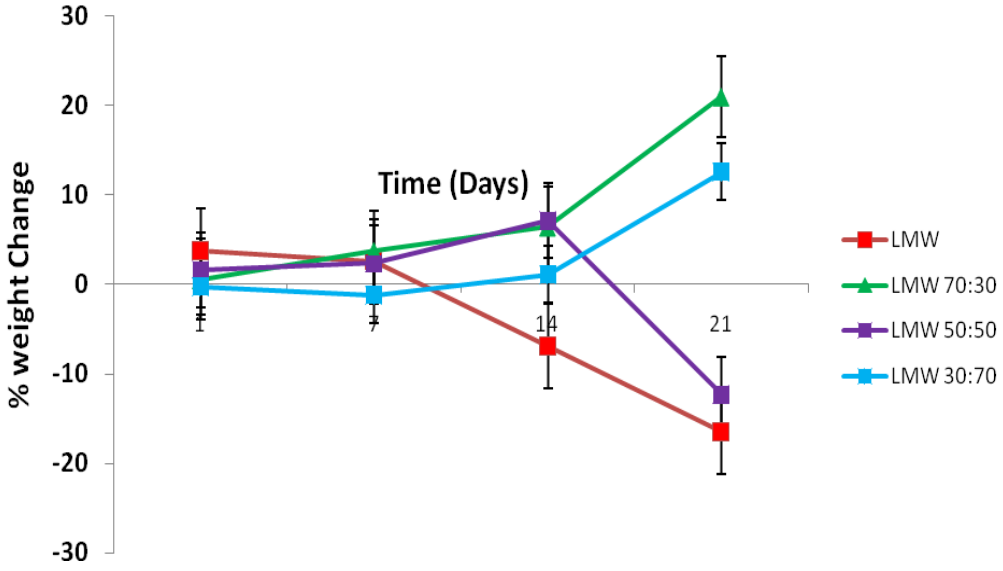

Figure 55: % Weight change of LMw CH and CH:HA samples after immersion in SBF solution.

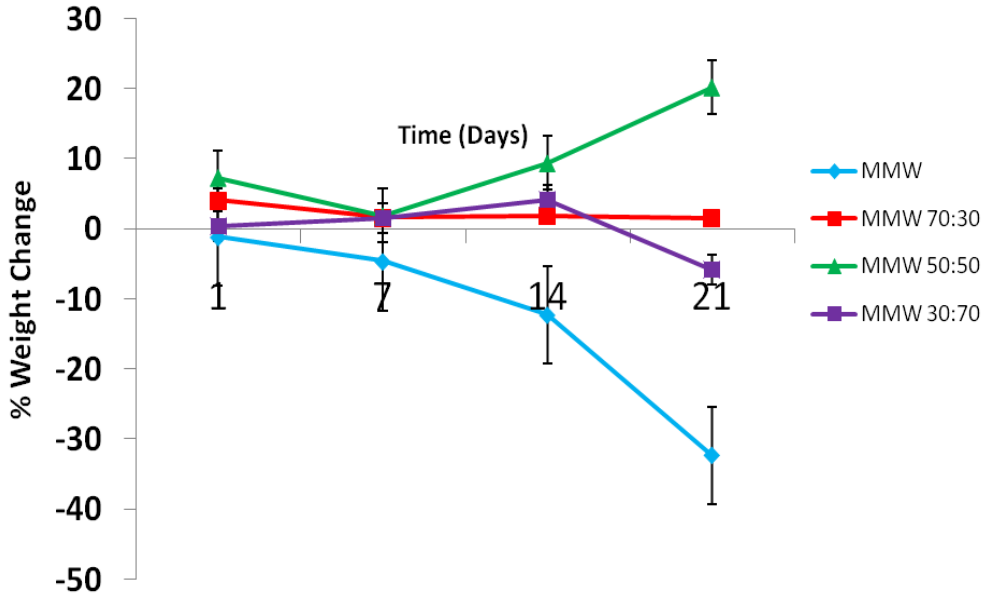

Figure 56: % Weight change of MMw CH and CH:HA samples after immersion in SBF solution.

MMw CH HA samples showed a different trend with MMw 50:50 showing an increment in weight over time and MMw 70:30 and 30:70 follow a steady profile till day 14. MMw 30:70 shows a slight drop in % weight change after 21 days. LMw CH and CH HA membranes showed a different profile with neat LMw CH and LMw 50:50 showing a -20% weight loss. Whereas, LMw 30:70 and 70:30 showed a net increment in weight profile after 14 days of immersion in SBF, an overall rise of 10 to 20% was noted for these specimens at the end of the 21 days of experimental period.

4.5.3. FTIR-PAS Spectroscopy

FTIR Spectroscopy was conducted using PAS as the sampling accessory at consecutive time points on the bottom surface, which was HA enriched. The comparative spectral data collected for MMw 70:30, 50:50 and 30:70 at Day 1, 4, 7, 14 and 21 are given in Figures 57, 58 and 59. The spectral profile of the bottom surface of the membranes showed visible changes in peak positions and intensities at each time point. Alterations of the spectra were noted in –NH and –OH stretching vibration in the region of 2800 to 3300cm^{-1}. The finger print region showed subtle changes in amide I and II regions at 1650 and 1545 cm^{-1}, CH_3 symmetrical deformation mode at 1420 and 1318cm^{-1} and glycosidic linkages at 1150. The presence of apatite layers also changed the characteristic patterns of peaks occurring around 566 and 603cm^{-1} due to bending of phosphate group of HA. Figure 60, 61 and 62 shows LMw 70:30, 50:50 and 30:70 CH:HA membrane data of FTIR-PAS spectral information collected on consecutive days after immersion in SBF media.

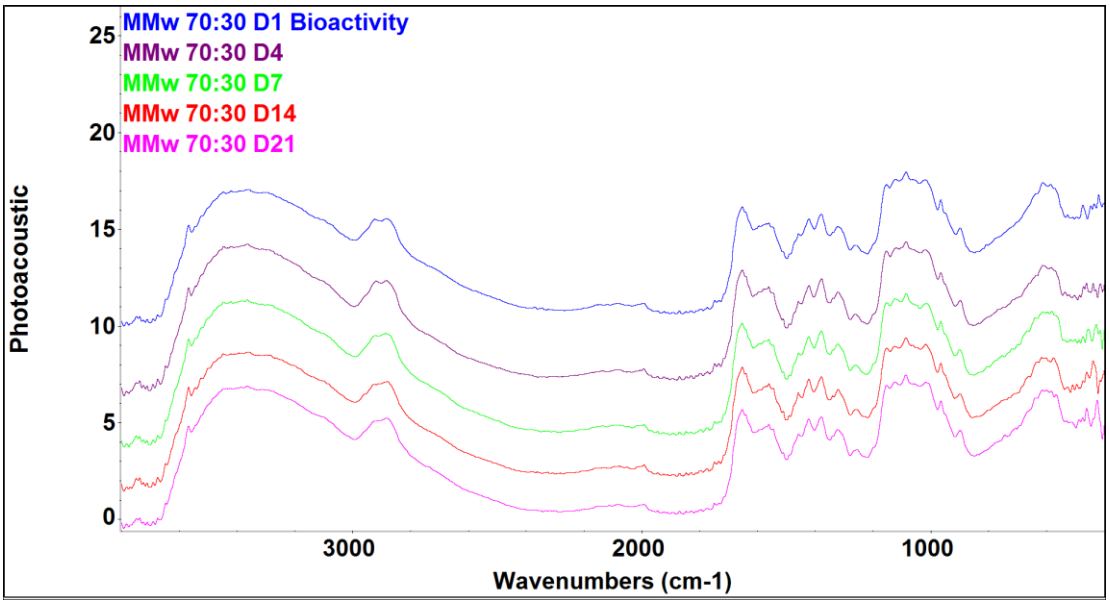

Figure 57: FTIR-PAS of MMw 70:30 CH HA membrane of the bottom surface. Spectral data collected after immersion in SBF solution at Day 1, 4, 7, 14 and 21.

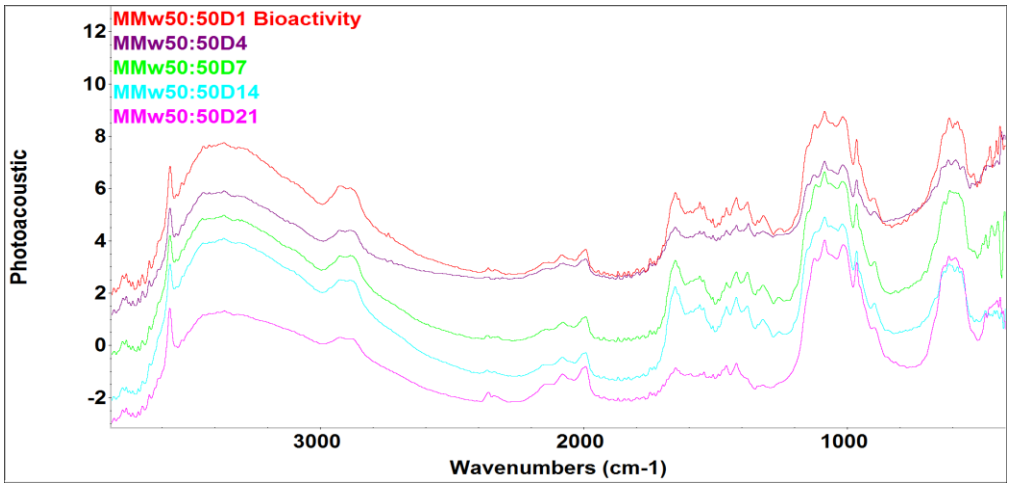

Figure 58: FTIR-PAS spectra of MMw 50:50 CH HA membrane of the bottom surface. Spectral data collected after immersion in SBF solution at Day 1, 4, 7, 14 and 21.

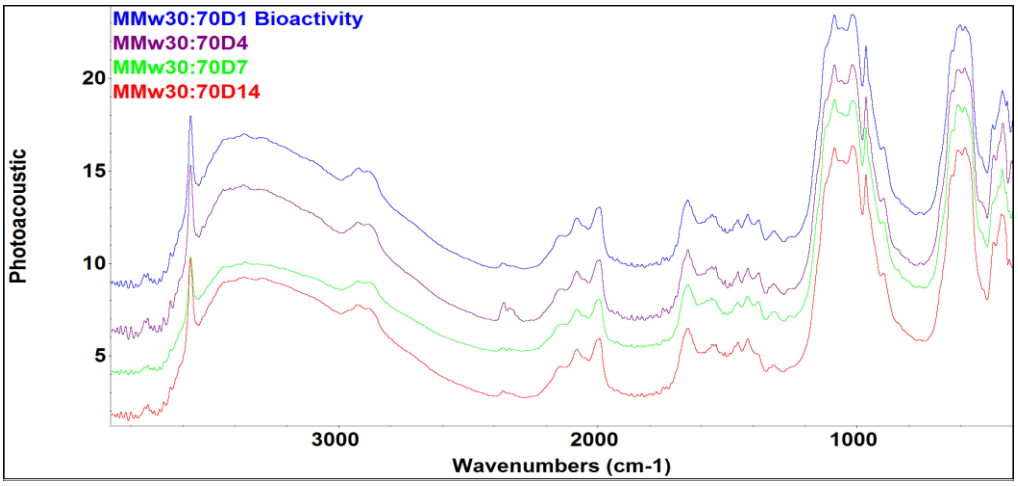

Figure 59: FTIR-PAS of MMw 30:70 CH HA membrane of the bottom surface. Spectral data collected after immersion in SBF solution at Day 1, 4, 7 and 14.

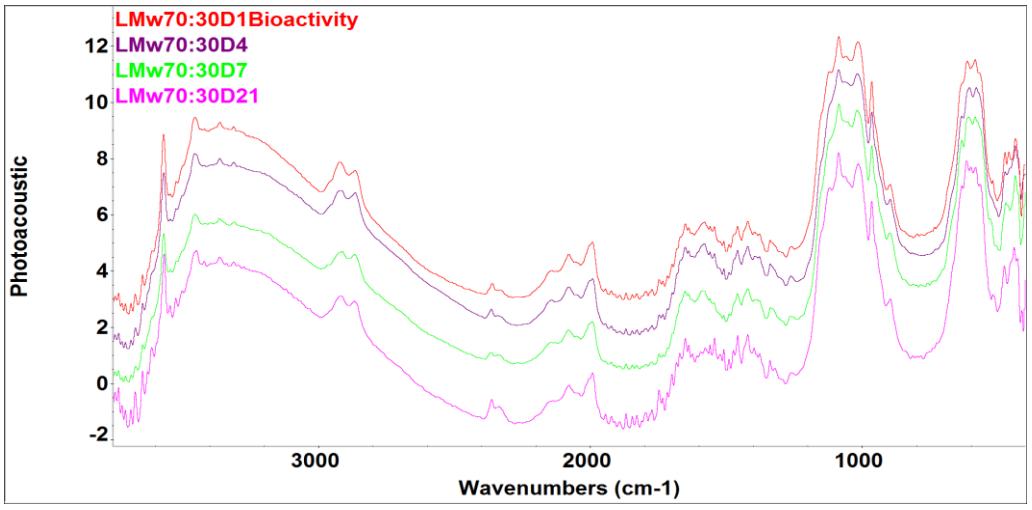

Figure 60: FTIR-PAS of LMw 70:30 CH HA membrane of the bottom surface. Spectral data collected after immersion in SBF solution at Day 1, 4, 7 and 21.

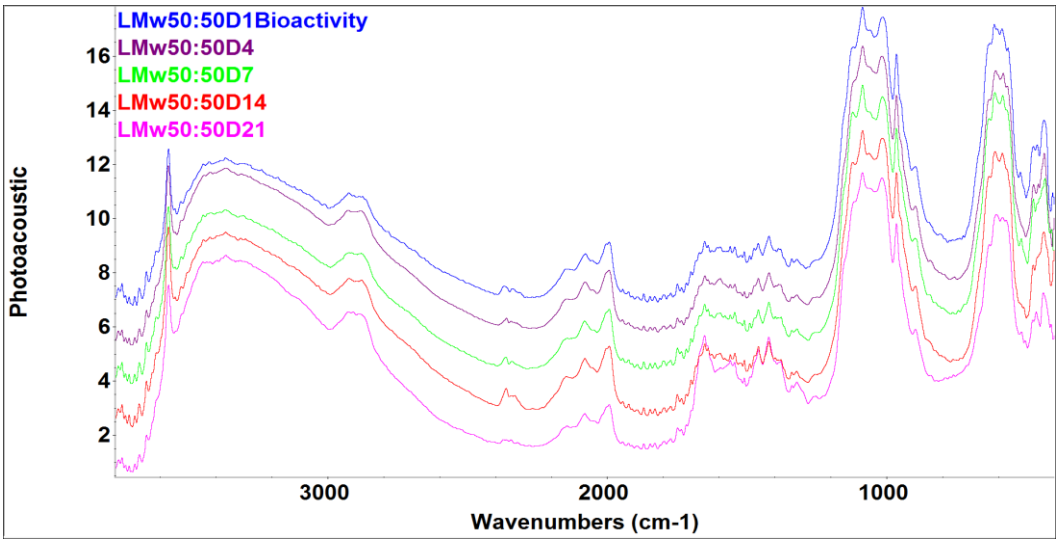

Figure 61: FTIR-PAS of LMw 50:50 CH HA membrane of the bottom surface. Spectral data collected after immersion in SBF solution at Day 1, 4, 7, 14 and 21.

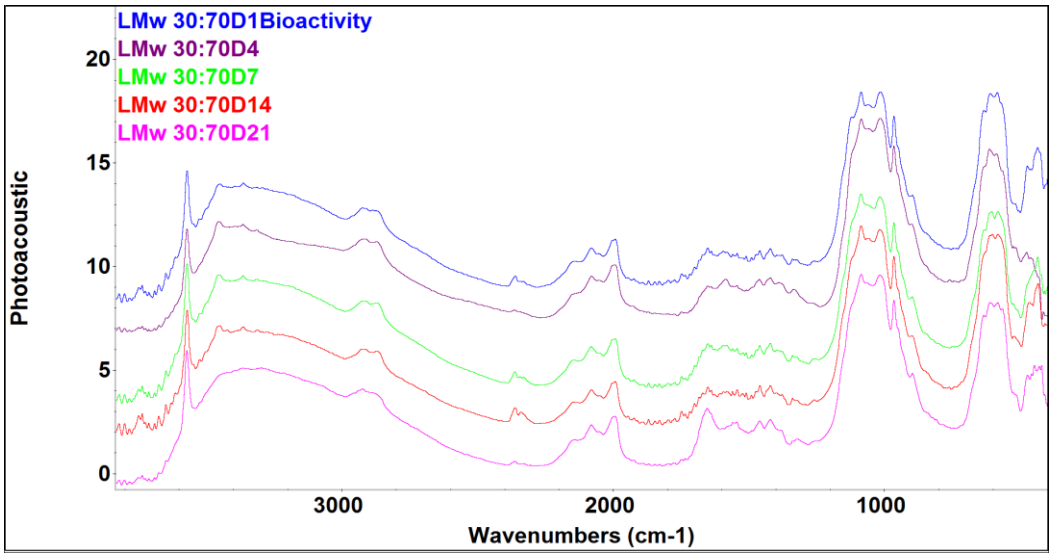

Figure 62: FTIR-PAS of LMw 30:70 CH HA membrane of the bottom surface. Spectral data collected after immersion in SBF solution at Day 1, 4, 7, 14 and 21.

4.5.4. Peak Area analysis

Peak area analysis was performed using OMNIC™ TQ analyst software® for peaks at 3650cm^{-1} and 960cm^{-1} pertaining to –OH and PO groups respectively at each time points and from the spectral information of the bottom surface of the LMw and MMw CH and CH HA membranes (Table 16 and 17). Time points at which the peak area was measured were Day (D) 1, 4, 7, 14 and 21. Calculations of MMw CH HA membranes show that the values at D1 (22, 90, 99) are higher than those obtained at day 4 (19, 84, 80) except for LMw 70:30 (74), 50:50 (86). A drop in the peak area was observed at D7 for these specimens and LMw 30:70 had a more delayed decrease at D14.

Table 16: Peak Area analysis by TQ analyst Software at different time points (days) of -OH peaks at 3650cm^{-1}.

3650cm^{-1}	D1	D4	D7	D14	D21
MMw 70:30	21.94	18.89	21.23	23.46	22.48
MMw 50:50	89.86	83.83	45.36	50.63	64.27
MMw 30:70	99.59	80.21	65.87	96.79	na
LMw 70:30	62.71	73.56	60.71	na	na
LMw 50:50	57.2	86.35	59.4	57.65	53.76
LMw 30:70	89.19	78.70	96.51	71.16	125.24

For peak area calculations of phosphate peak at 962cm^{-1}, the values are higher for D 1 than at D4 for MMw membranes. LMw memrbanes showed the peak area rise from D1 to D7 for LMw 70:30. LMw 30:70 showed a steady profile till D 7. Spectral information from LMw 70:30 specimens for D14 and D21 was not obtained and hence no peak area was calculated.

Table 17: Peak Area analysis by TQ analyst Software at different time points (days) of PO peaks at 960cm^{-1}.

960cm^{-1}	D1	D4	D7	D14	D21
MMw 70:30	6.57	4.96	5.60	5.68	6.75
MMw 50:50	10.80	8.84	13.63	12.02	16.33
MMw 30:70	24.48	20.74	24.10	24.17	na
LMw 70:30	17.73	19.16	20.06	Na	Na
LMw 50:50	18.15	22.83	16.49	19.4	17.03
LMw 30:70	20.90	20.85	20.50	18.22	26.23

SECTION II

4.6. Freeze gelated membranes

4.6.1. Introduction

This section describes the synthesis and characterisation of the core layer. This layer is an essential element of a functionally graded structure for periodontal tissue engineering constructs. The aim off this core layer of functionally graded membrane was to serve as a

porous interface to mimic extracellular matrix and allow cell attachment, proliferation and matrix deposition.

4.6.2. Optical images and handling of scaffolds

It was very important to evaluate the physical handling of the membranes in a clinical environment. Therefore, it was passed on to a dental surgeon to analyse its handling properties (Qasim et al., 2015). Figure 63 shows representative images of FG CH and CH:HA membranes being stretched and inset images depict their ability to withstand bending forces. These parameters are of utmost importance while handling and inserting during surgical procedures. Thickness of the membranes can be controlled by controlling the amount of similar concentration of the solution poured into the same size of petri dishes. In this study, ACa-CH (3% w/v) solution was prepared and an amount of 30 ml was poured into 9 cm diameter petri dish to obtain a 0.57 mm thick membranes. Membranes could also be easily cut with a scalpel or scissors to obtain the desired shape. These images in figure 63 show that all membranes had good handling characteristics and are resilient and flexible.

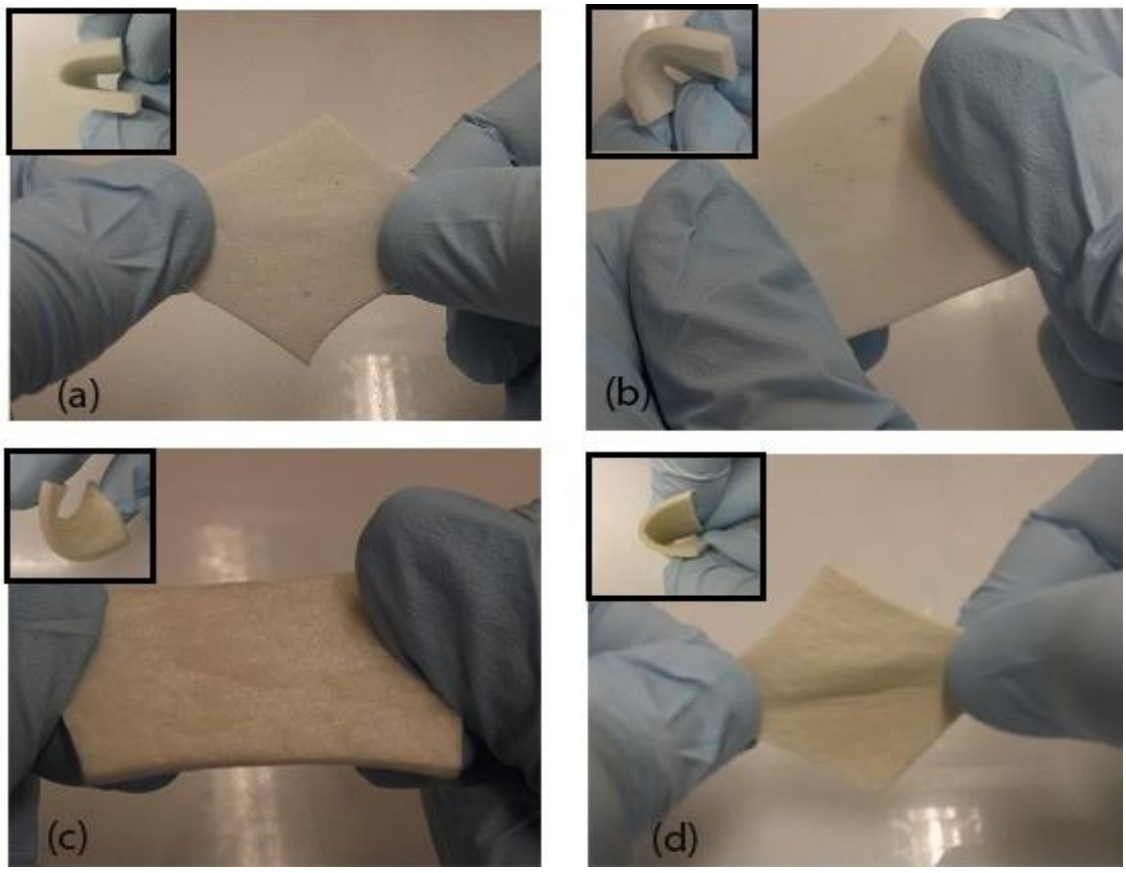

Figure 63: Optical images taken with Nikon DSLR D5600 camera using macro lens, (a) ACa-CH (b) ACa-CH:HA, (c) ASa-CH, (d) ASa-CH:HA, all images depicting handling characteristic and INSET image showing bending ability.

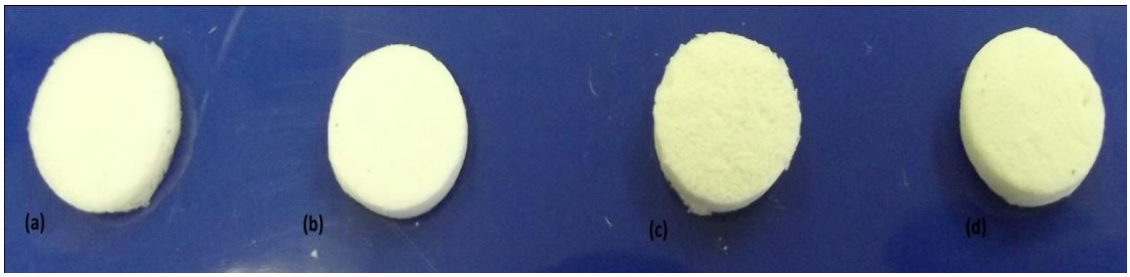

Figure 64: Optical images of FG membranes cut using a cork borer (a) ACa-CH (b) ACa-CH:HA, (c) ASa-CH, (d) ASa-CH:HA membranes. Images show the samples shape used for FTIR, swelling, Degradation, Cell culture and bioactivity studies. 13mm in diameter specimens

4.6.3. SEM of Freeze Gelated Scaffolds

SEM images of freeze gelated specimens are shown in Figure 65. The Top surface and cross section of the specimens prepared with 3 wt % MMw CH in acetic acid (ACa) are shown in Figure 64 (a, b, e and f). The Same weight percentage of polymer was dissolved in 0.2M Ascorbic acid (ASa) and surface / cross sectional features are shown in figure 65 (c, d, g and h) (Page 140). Specimens prepared with ASa showed a much more even porous structure compared to the freeze gelated scaffolds made by ACa. The porosities can be observed in cross sectional image. Figure 66 shows a frequency plot against pore size in nm and the graph shows variations in the pore size measured using Image J software (NIH, USA). The pore distribution was spread over a range of 40µm to 250µm (Figure 66). Results from the µCT data are shown in Figure 67 shows the cell size (pore size) and inter strut size ranging from 15µm to 100µm. ACa-CH possessed 85% porosity as compared to that of ASa-CH having 79%. Samples containing HA had a porosity of 78%, which was relatively lower to ACa-CH and similar to that of ASa-CH. This may be due to the incorporation of HA particles within the network structure of chitosan resulting into closing of pores, hence, lowering the porosity.

Figure 68 show freeze gelated membranes made by using LMw CH. The image depicts top surface and cross sectional view of the scaffold. In cross sectional view a layered structure is visible with no defined pores. Consecutive layers of CH have been gelated and lack porous features seen in low molecular weight membranes.

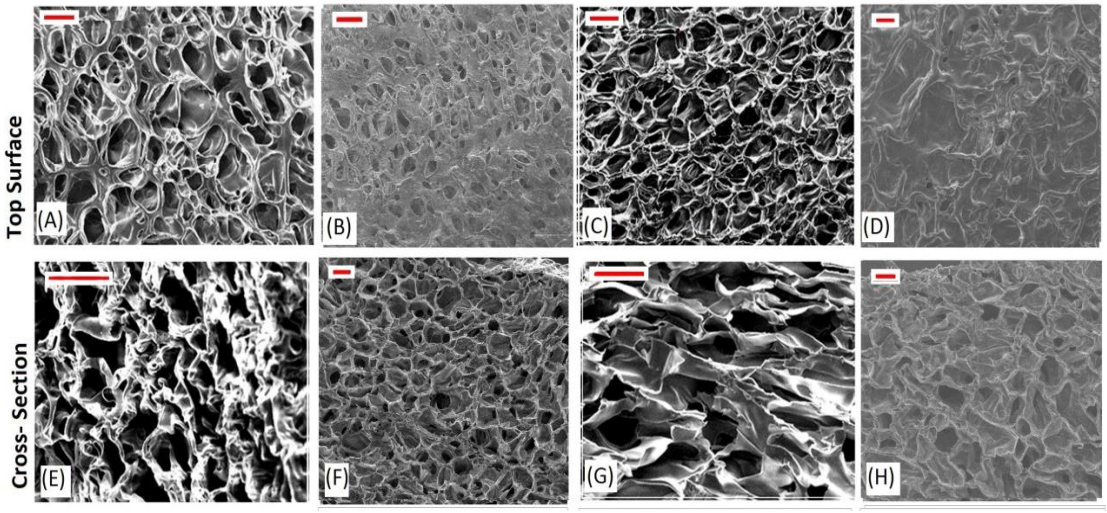

Figure 65: SEM micrographs of porous freeze gelated chitosan (a) Top surface of ACa-CH (b) Top Surface of ACa-CH:HA (c) Top surface of ASa-CH (d) Top Surface of ASa–CH:HA (e) Cross sectional image of ACa-CH (f) Cross sectional image of ACa-CH:HA (g) Cross sectional image of ACa-CH:HA (g) Cross sectional image of ASa-CH (h) Cross sectional image of ASa–CH:HA. (Scale bar = 100µm).

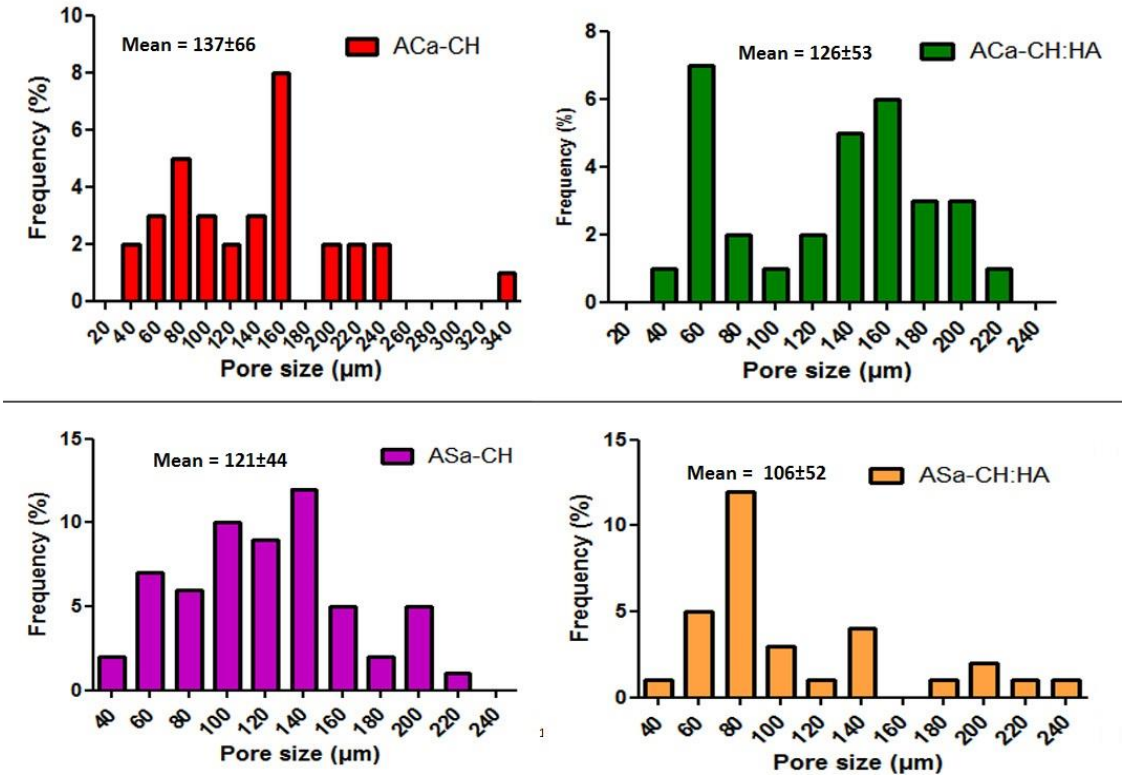

Figure 66: A histogram of the pore diameters (n=100).Average pore diameter of CH scaffolds collected from cross sections of scaffolds using SEM images and measured using Image J software.

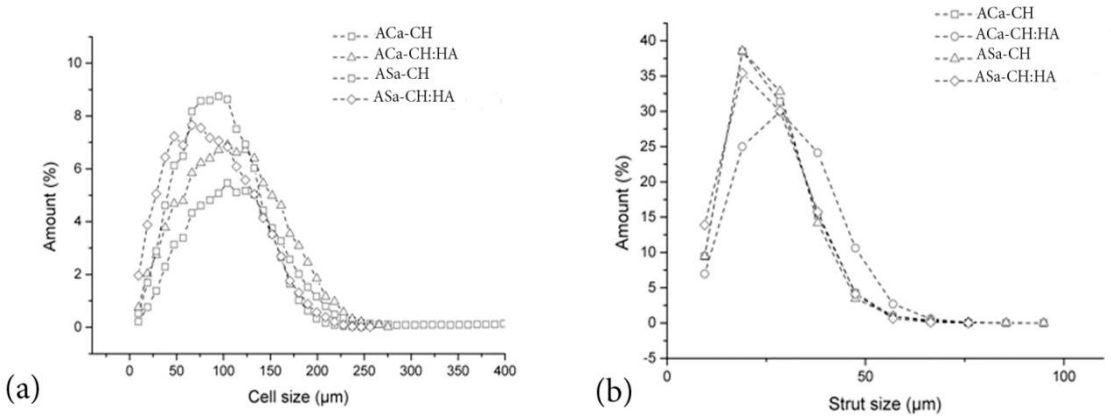

Figure 67: µCT analysis (a) Graphs depicting percentage porosity plotted against size (µm) and (b) inter strut thickness obtained by µCT analysis , Porosity percentage calculated as ACa-CH 85.50%, ACa-CH:HA 77.75%, ASa-CH 78.51%, ASa-CH:HA 78.27%.

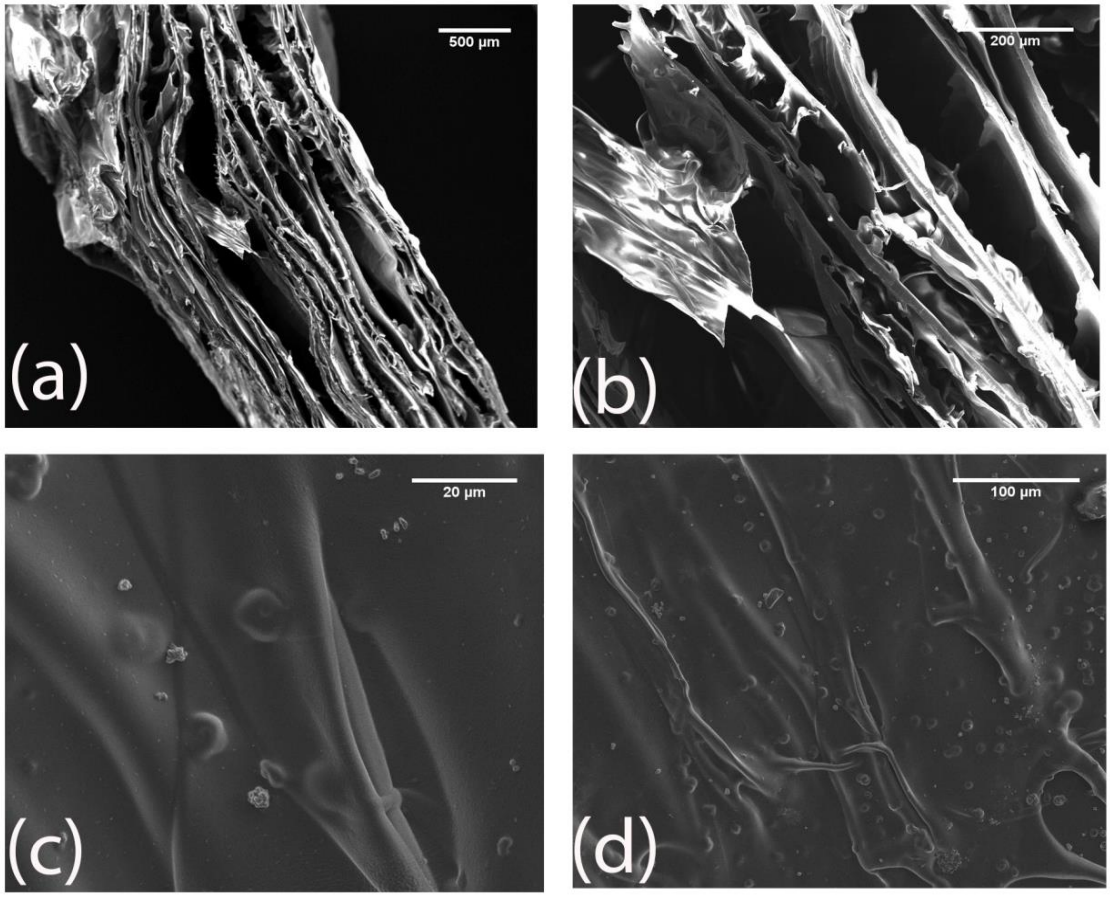

Figure 68: SEM micrographs of Freeze gelated scaffolds fabricated with LMw CH 3% (wt/v).

4.6.4. FTIR-PAS spectroscopy of Freeze Gelated Scaffolds

FTIR spectroscopy coupled with a photo-acoustic sampling (PAS) cell was utilized to obtain chemical structural properties. FTIR-PAS is an excellent technique for obtaining

chemical structural properties from the bulk material. The FTIR spectra of FG CH and CH : HA in ratio of 50% are shown in Figure 71. Spectral peak identification is made on Figure 70 depicting neat CH and HA peaks. Identification of spectral peaks of CH, HA and composite peaks is given in Table 13 (Page 119-120). Figure 69 shows FTIR spectra of ASa, spectral peaks from 3524 to 3214cm^{-1} were attributed to, –OH stretching vibration of lactone C=O forming intramolecular hydrogen bonding occurs at 1754cm^{-1} and that of lactone forming intramolecular hydrogen bonding occurs at 1673cm^{-1}.

Typical spectral bands of N-H and OH stretching vibrations are present within the range of 3600 to 3300cm^{-1}. Spectral band at 2880 cm^{-1} is attributed to C-H stretching. Amide I stretching vibration is observed at 1654cm^{-1} denoted to C=O, Secondary amide II (-NH_2) bending vibration is confirmed from 1542-1547cm^{-1}. Moreover, C-H stretching or rock and bending modes were noticed at 1419cm^{-1} and 1378cm^{-1}, pyranose ν_3 C-O-C (glycosidic linkages) and C-O stretching modes were detected at 1150cm^{-1} and 1084cm^{-1}. HA incorporated membranes presented in Figures 70 bottom spectra) and presence of HA was confirmed by the hydroxyl peak (-OH) centred at 3568cm^{-1}, characteristic peaks of ν_1 (PO_4^{3-}) at 962cm^{-1}, and ν_4 (PO_4^{3-}) asymmetric bending stretch at 571cm^{-} .

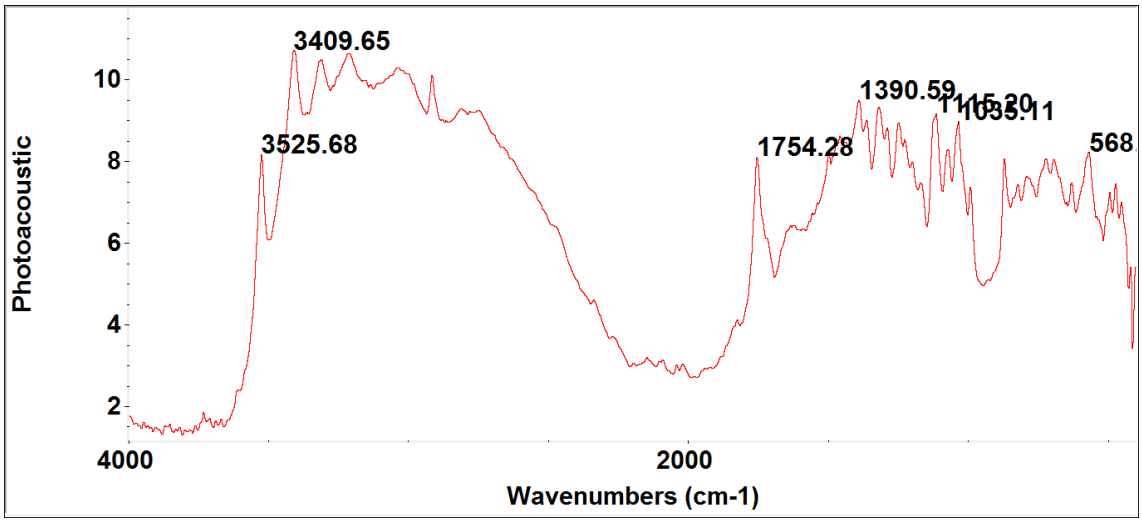

Figure 69: FTIR-PAS spectra of neat Ascorbic acid crystals 99% as obtained.

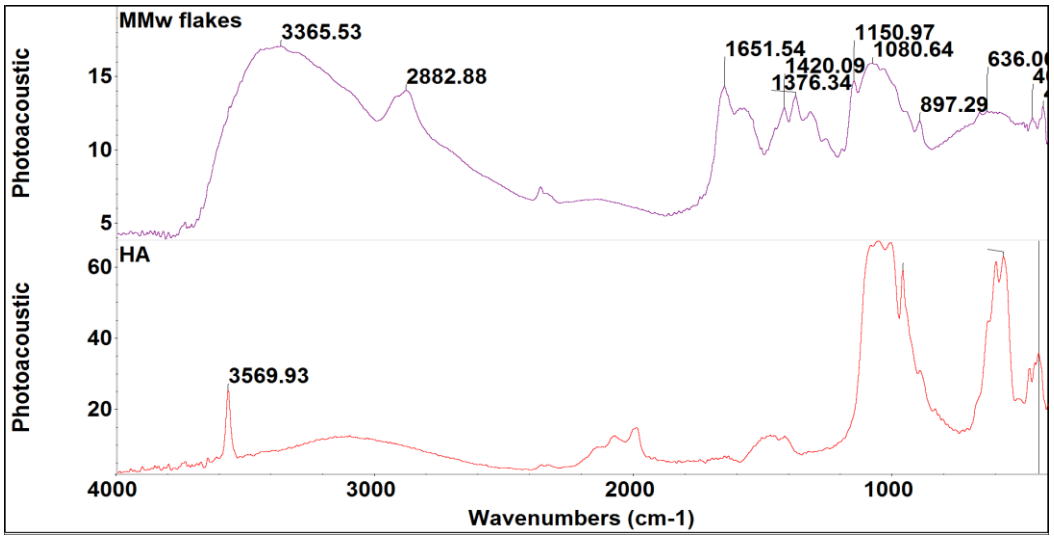

Figure 70: FTIR spectra or (a) Neat medium mol weight chitosan, (b) Neat hydroxyapatite with peak identification.

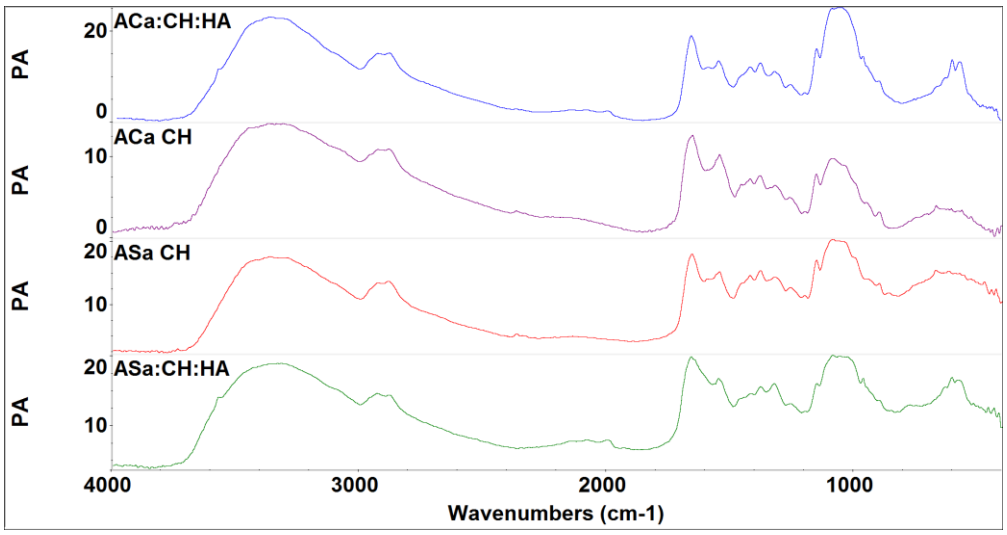

Figure 71: FTIR spectra of ACa:CH, ASa:CH, ACa:CH:HA, ASa:CH:HA. Molecular fingerprint region of HA composite scaffold show the presence of phosphates bands of HA integrated with CH.

4.6.5. Mechanical testing

Dry and wet FG membranes were analyzed for their Ultimate Tensile Strength (UTS), Young's modulus of elasticity (*E*) and Strain (%) at UTS (Table 18). *E* and UTS values were higher for all dry membranes as compared to specimens in wet conditions. UTS of dry ACa-CH:HA was higher than neat ACa-CH membranes, whereas, *E* values of dry ACa-CH:HA were lower than neat ACa-CH FG membranes, however, this trend was revised under wet conditions. Dry ASa-CH had a lower *E* as compared to ASa-CH:HA. Interestingly, under wet conditions ASa-CH:HA membranes had a lower UTS than neat ASa-CH, although there was no

significant different in the *E* values of these membranes. Examples of stress strain curves of dry and wet FG membranes are shown in Figure 72 a and b.

Table 18: Mechanical properties of dry and wet CH freeze gelated scaffolds.

Wet Scaffolds	UTS (MPa)	*E* (MPa)	Strain (%)
ACa-CH	0.04±0.03	0.07±0.01	0.38±0.04
ACa-CH:HA	0.06±0.02	0.12±0.03	0.64±0.04
ASa-CH	0.06±0.03	0.10±0.03	0.68±0.04
ASa-CH:HA	0.03±0.01	0.11±0.02	0.35±0.05
Dry Scaffolds	**UTS (MPa)**	**E (MPa)**	**Strain (%)**
ACa-CH	0.11±0.05	0.28±0.12	0.46±0.09
ACa-CH:HA	0.13±0.05	0.26±0.09	0.59±0.09
ASa-CH	0.15±0.08	0.20±0.07	0.75±0.19
ASa-CH:HA	0.13±0.03	0.29±0.04	0.50±0.10

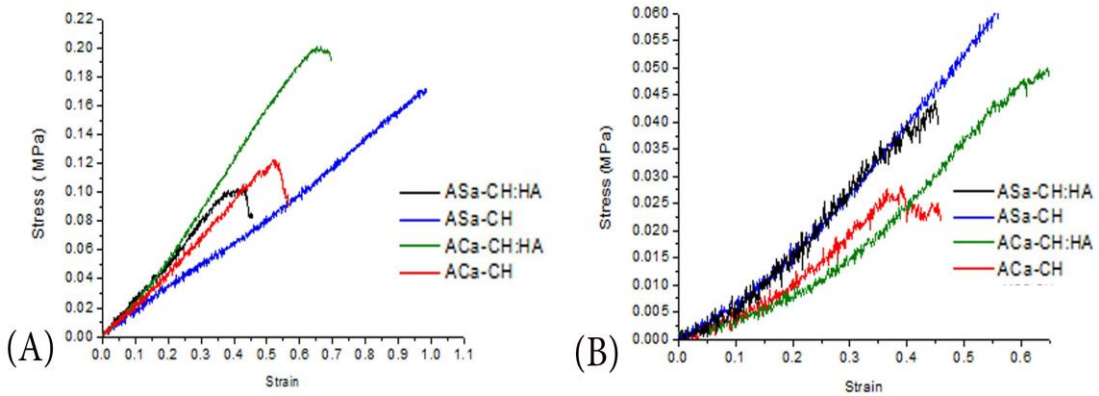

Figure 72: Examples of stress/strain curves for (a) Dry and (b) Wet samples, ACa-CH and ACa-CH:HA, ASa-CH and ASa-CH:HA. Scaffolds were cut into 20 mm by 5 mm strips and stretched at 0.1 mm / sec to failure.

4.6.6. Swelling analysis

The swelling ratio of CH and CH:HA FG membranes for both solvent systems are shown in Figure 73. Equilibrium is reached within 15 mins of swelling for most of the FG CH membranes. ACa-CH and ASa-CH showed the highest swelling ratio (up to 80%) when compared with ASa-CH:HA and ACa-CH:HA (up to 60-65%). The swelling profile remained constant over the 48 hr time period. ACa-CH:HA membranes showed the least amount of swelling (up to 60%) over the experimental period. Representative images depicting the

swelling ability of ACa-CH:HA and ASa-CH membranes are shown in Figure 73 (adjacent image) for both dry and hydrated specimens. Note that membranes incorporating HA showed less swelling as compared to ASa-CH membrane

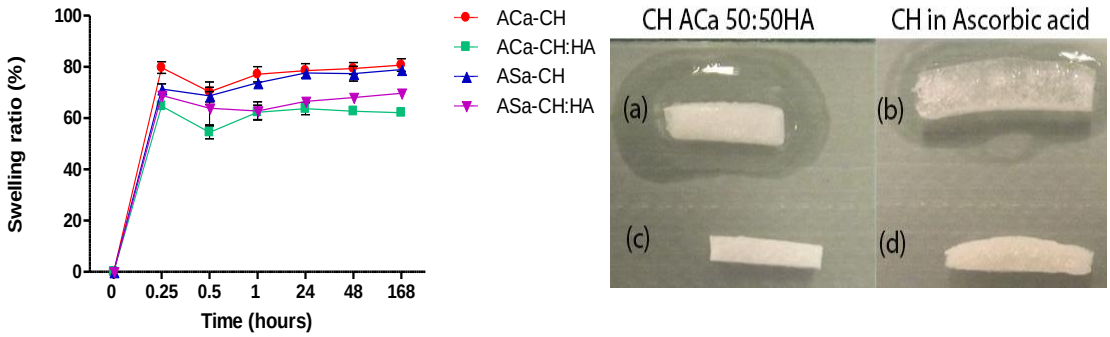

Figure 73: Swelling ratio of CH freeze gelated scaffolds over 168 hours plotted against percentage swelling. Adjacent image show examples of wet (a, b, fully swollen) (top) and dry membranes(c, d) observed from the cross section.

4.7. In-*vitro* Degradation analysis

4.7.1. Weight loss analysis

The weight loss (%) profiles of FG membranes immersed in lysozyme solution for a period of 28 days are shown in Figure 74. ASa-CH and ACa-CH showed similar degradation profiles across the 28 days showing a weight loss of ~50% at day 4 and ~60% at day 28. The

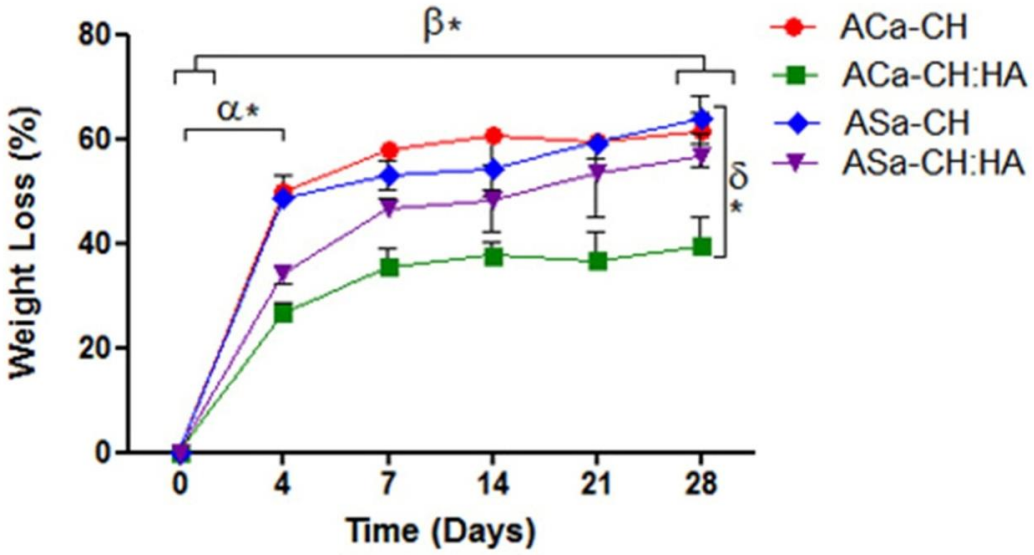

Figure 74: Weight loss (%) of Freeze gelated ACa-CH, ACa-CH:HA, ASa-CH and ASa-CH:HA conducted over a 28 day time scale. (α*) Statistically significant difference was noted in between

time points from D0 to D4, (β•) statistically significant difference was observed from time point D0 to D28. Within groups at D28 ACa-CH:HA and ACa-CH showed significant difference (δ•). Each value represents mean ± SD (*n* = 3).

addition of HA to the membranes resulted in a reduction in weight loss for membranes produced from both solvents, however, this was more significant for ACa-CH:HA which showed the least amount of weight loss at 30% to 40% between day 7 and 28. Statistically significant difference ($p \leq 0.05$) (α*) was observed between day 0 and 4. From day 0 and 28 significant different was also noted (β*). Within groups ACa-CH and ACa-CH:HA showed statistically significant ($p \leq 0.05$) difference at day 28. No significant difference was observed in between ASa-CH:HA and ASa-CH at 28th day of experimental period.

4.7.2. pH Analysis

pH change with degradation was monitored over the 54 day time point shown in Figure 75. All scaffolds follow a trend of gradual increase over time. pH value of lysozyme solution is 6.9 at Day 0 and increases to 8.4 pH at day 48. ASa-CH samples show a spike at day 21 to pH 7.5 which showed an increasing trend till day 48. Change in the pH values was more prominent from Day 21 to 48.

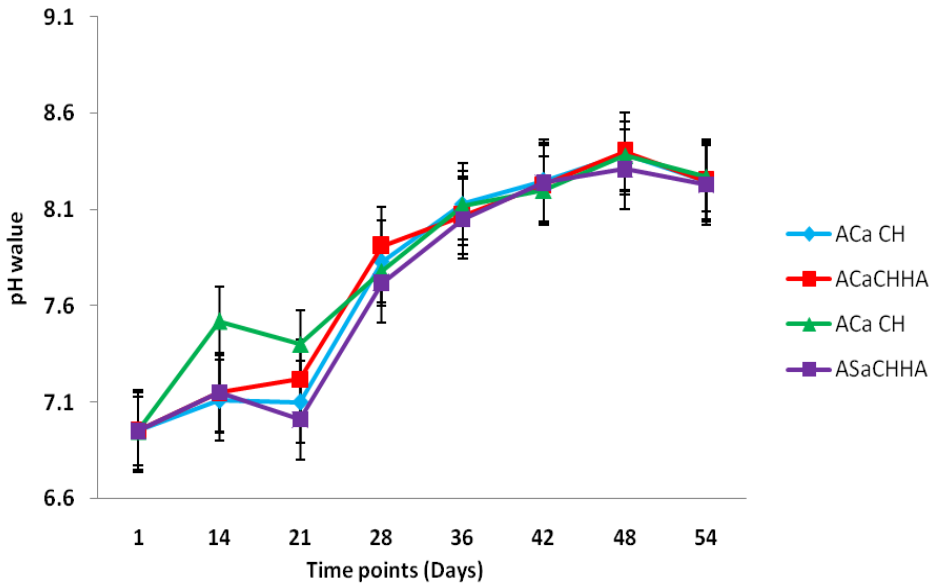

Figure 75: pH changes for freeze gelated scaffolds monitored over 54 days.

4.7.3. Optical images of degraded freeze gelated scaffold

Optical images of the scaffolds taken at different time points to see visual changes in structure are presented in Figure 76. From Day 1 to day 54, neat ACa-CH showed rapid breakdown in the size of the specimen as compared to other scaffolds. This is visible at day

14. At day 21 rest of the specimens also showed signs of cracks. Neat ASa-CH showed stability after being subjected to lysozyme media over the 54 day time period. ACa-CH:HA also showed stability till day 14 which is similar to images of ASa-CH:HA scaffolds.

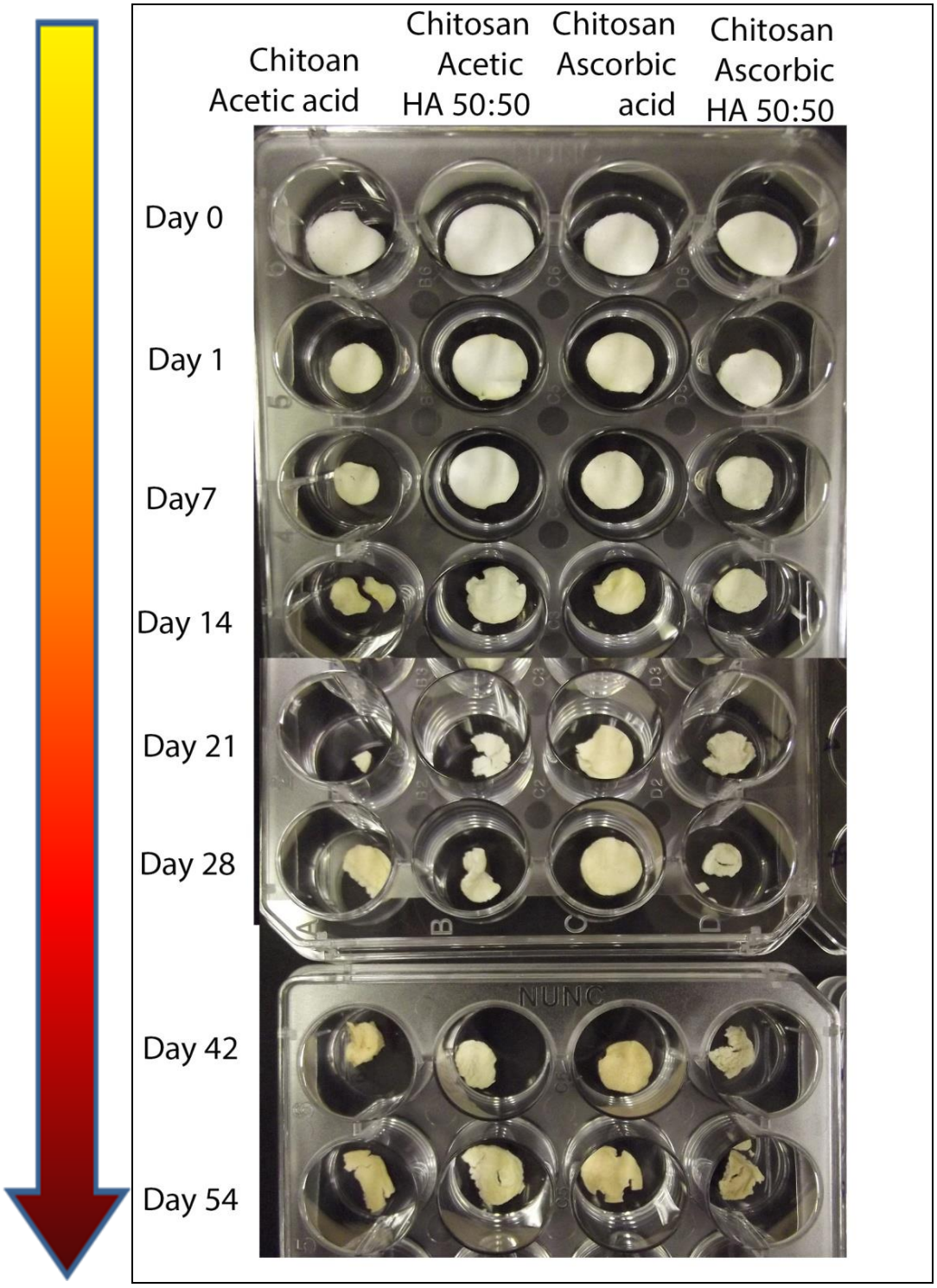

Figure 76: Optical Images taken from a Nikon Camera of scaffolds at different time points after drying and subjected to degradation media till 54 days.

4.7.4. FTIR-PAS spectral data of Freeze gelated degraded scaffolds

Comparative FTIR spectra of degraded samples in lysozyme solution were collected using PAS accessory at 1, 7, 14, 21, 28 and 36 days of immersion in degradation media depending on the availability of the specimen (Figure 77, 78, 79 and 80). Figure 77 and 79 of ACa-CH and ASa-CH show similar trends in spectral information. The finger print region of the degraded specimens show peak shifts and broadening of glycosidic region (C-O-C) at 1150cm^{-1} with simultaneous reduction in intensity of peaks at 1419 and 1378cm^{-1} which are attributed to CH_3 amide, CH bending and stretching modes. Broadening of the peak at Amide I (1652cm^{-1}) region can also be observed from day 1 to 28. A typical CH exhibits strong bands of O-H and N-H stretching vibration at 3440cm^{-1} and minuscule changes in the bands corresponding to symmetric and asymmetric vibrations of CH_2 group at 2900cm^{-1} and 2800 cm^{-1} which are also observed in these samples with time. Deforming vibrations pertaining to $-NH_3$, in the region of 1150 and 1040cm^{-1}, also showed decreased intensity. Peaks at 1655 and 3450cm^{-1} predict the degree of deacetylation, which can also be observed by the reduction of these peaks. It is envisaged that the scission is due to hydrolytic degradation rather than oxidation. For HA incorporated specimens Figure 78 and 80 changes in the phosphate bands of HA can be observed, which is evident from spectral data in the fingerprint region, where the changes were observed in the phosphate (PO_4^{3-}) vibrational bands, particularly in ν_4 (601-572cm^{-1}) region, as the intensity of this doublet band goes down. With time intervals accompanying glycosidic bonds (1087-1075cm^{-1}) depict bond breakage and main chain scission of CH as well.

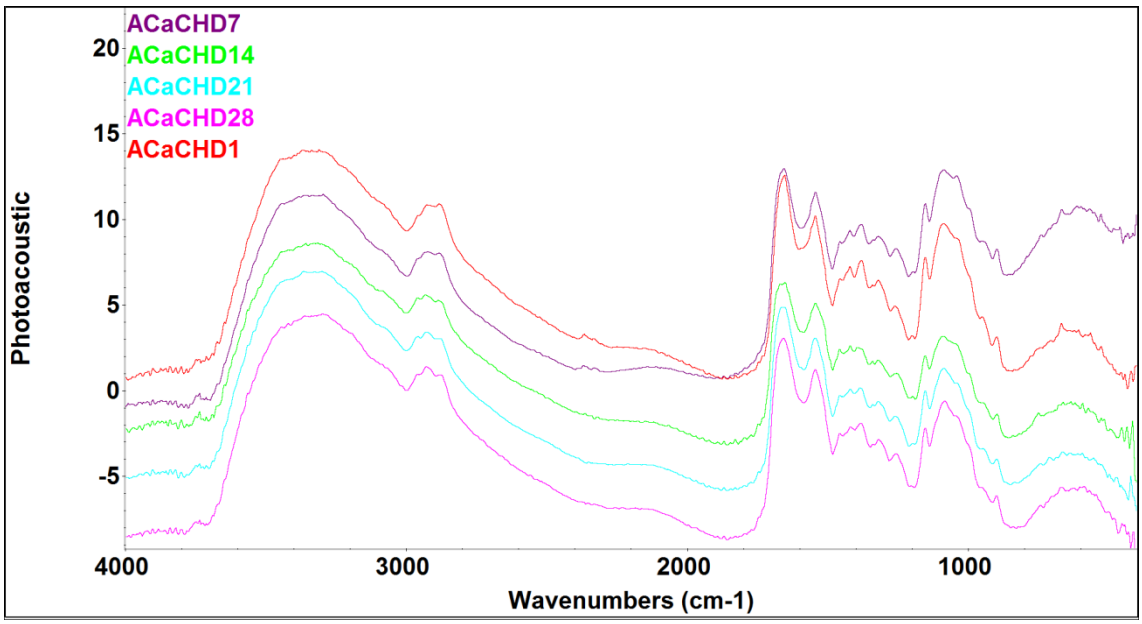

Figure 77: FTIR-PAS spectral data of ACa-CH membrane over a period of Day, 1, 7, 14, 21 and 28.

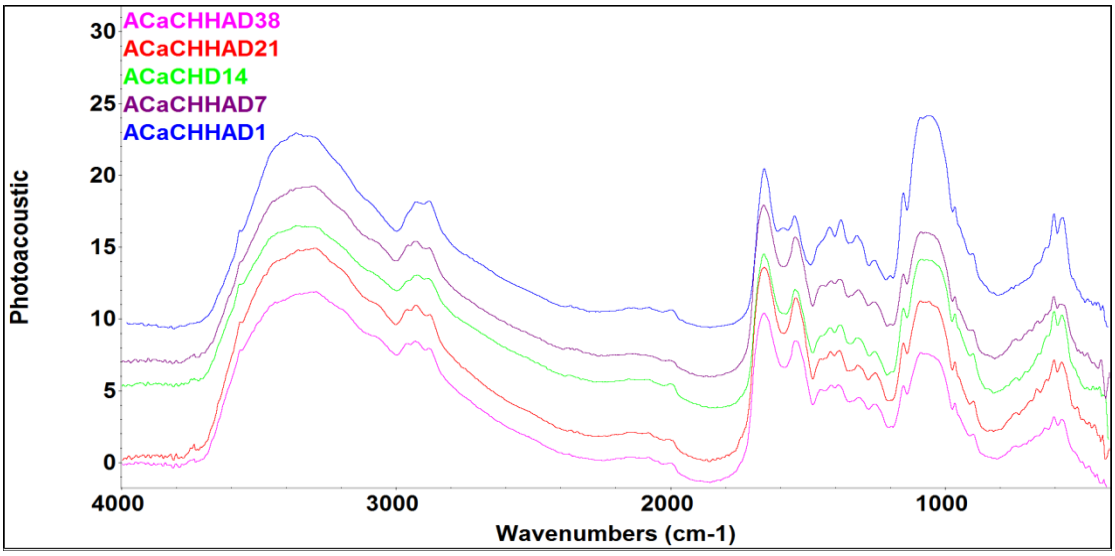

Figure 78: FTIR-PAS spectral data of ACa-CH:HA membrane over a period of Day, 1, 7, 14, 21, and 38.

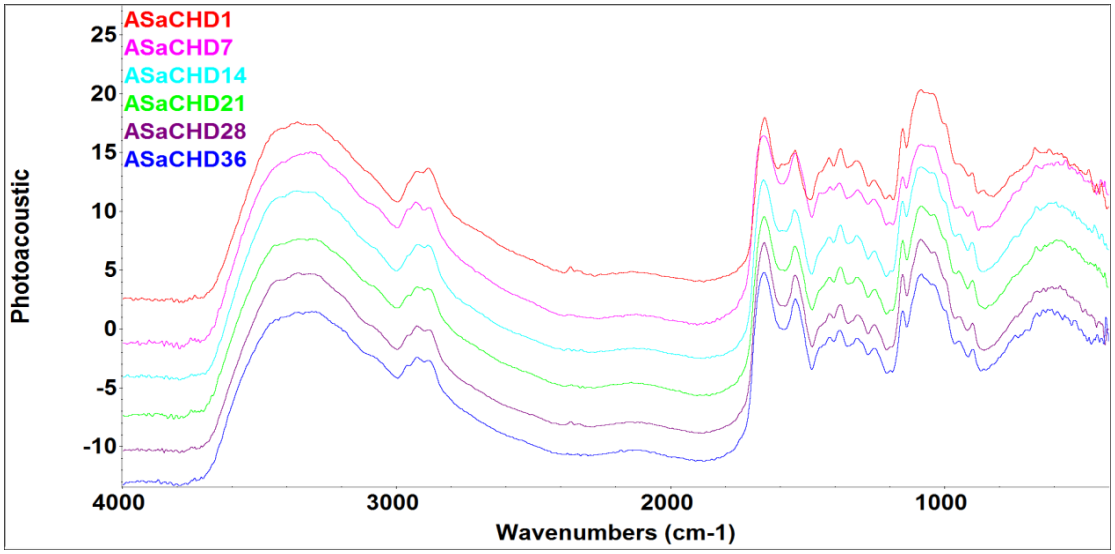

Figure 79: FTIR-PAS spectral data of ASa-CH membrane over a period of Day, 1, 7, 14, 21, 28 and 36.

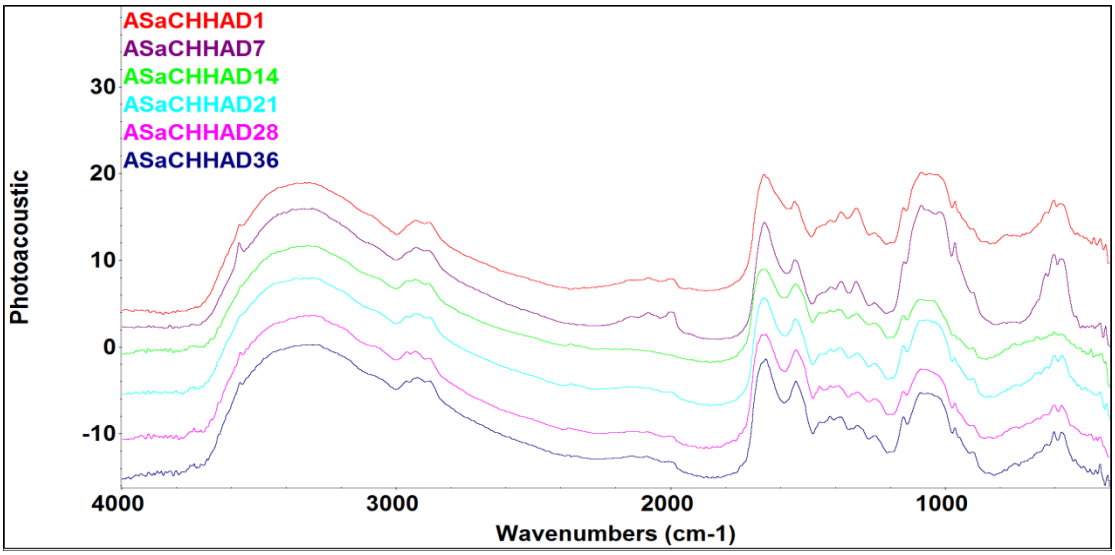

Figure 80: FTIR-PAS spectral data of ASa-CH:HA membrane over a period of Day, 1, 7, 14, 21, 28 and 36.

4.7.5. UV-Vis Spectroscopy

UV-Vis spectroscopy performed on the degraded media of FG membranes is shown in Figure 81. Samples were analysed on day 4, 11 and 21. Depending on the availability of the certain specimens, such as ASa-CH were analysed from day 1, 4, 7, 11 and 21 and ASa-CH:HA were analysed for day 1 and 11 only. UV-Vis spectral data of degradation media gives rise to two absorption bands at 230 and 280 nm respectively. ACa-CH:HA sample showed a progressive increase in band intensity with time as compared to ACa-CH, in which the band at D 21 showed an higher overall absorbance. Peaks at 230 could be due to the n-σ * transition attributed to the amino group and π-π* transition denoted to carbonyl or carboxyl groups. The degradation phenomenon is related to the peaks increasing in intensity over time, which is indicative of a decrease in molecular weight and formation of carbon- oxygen double bonds forming after chitosan chain scission and hydrogen abstraction followed by ring opening (Ulanski and Rosiak 1992).

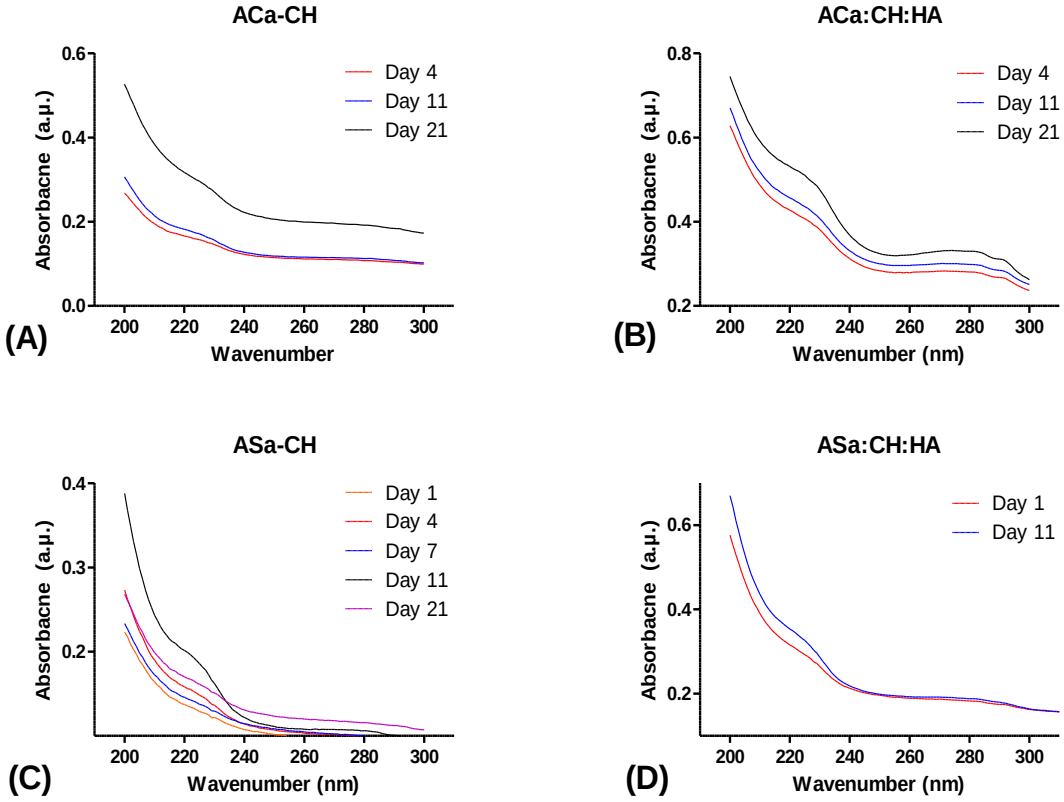

Figure 81: UV-Vis Spectral data of Degraded media of Freeze gelated scaffolds (a) ACa-CH, (b) ACa-CH:HA, (c) ASa-CH , (d) ASa-CH:HA, Samples were analysed in a quartz cell depending on the availability of degraded solution obtained at different time points.

4.8. Biocompatibility assay

Alamar blue analysis of FG CH:HA membranes seeded with MG63 or hES-MP cells is represented in Figure 82 (a and b). An increase in cell viability was seen in all of the membranes from day 1 to 7 (statistically significant) for both cell types, except for ACa-CH (Figure 82a) cultured with MG63 from day 4 to 7, which showed a non-significant increase. This indicates that the cells were able to attach and proliferate on CH and CH:HA membranes over the course of the culture period. Cell viability was similar at day 1 for all membranes, suggesting that cell attachment was also similar across all membranes. At day 7 of culture, MG63 seeded ACa-CH:HA membranes showed the highest viability (although not statistically significant) when compared with other groups. For membranes cultured with hES-MPs (Figure 82b), ASa-CH:HA and ACa-CH showed the highest viability at day 7 but this was not statistically significant when compared between groups.

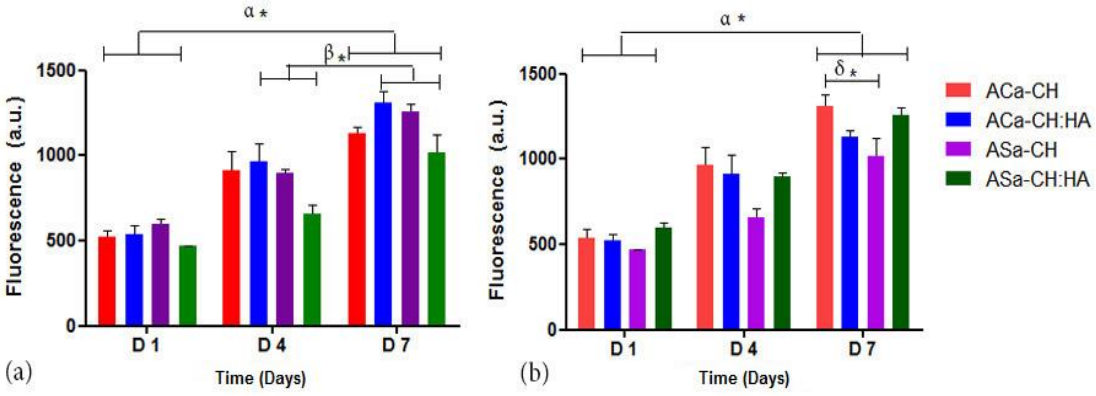

Figure 82: Metabolic Activity using Alamar Blue of CH FG membranes with (a) MG63s and (b) hE-SMP's over a period of day 1, 4, and 7. The values are shown as mean ± SD (n=6). α* denotes significant difference between D1 and D7 ($p \leq 0.05$). β* denotes significant difference between groups on D4 and D7(MG63), δ* denotes significant different between ACa-CH and ASa-CH groups at D7 (hESMPs).

To analyze the ability of CH-based FG membranes to facilitate osteogenic mineralised-matrix deposition by hES-MPs, quantification of total secreted collagen and calcium was performed at days 14, 21 and 28 of culture. Collagen deposition increased on all membranes from day 14-28 (Figure 83a). Collagen production on ASa-CH:HA was highest at all time points with highest absorbance value noted on day 28 (statistically significant) compared with all other groups. Calcium depositon (Figure 83b) increased in all membranes from days 14 to 28 with the greatest increases seen in both HA composites (significant compared with CH membranes). At day 28 Alizarin absorbance was highest for ASa-CH:HA although this was not significant when compared with ACa-CH:HA. ACa–CH:HA showed a more gradual increment in calcium deposition from days 14-28, whereas, ASa-CH:HA peaked at day 21.

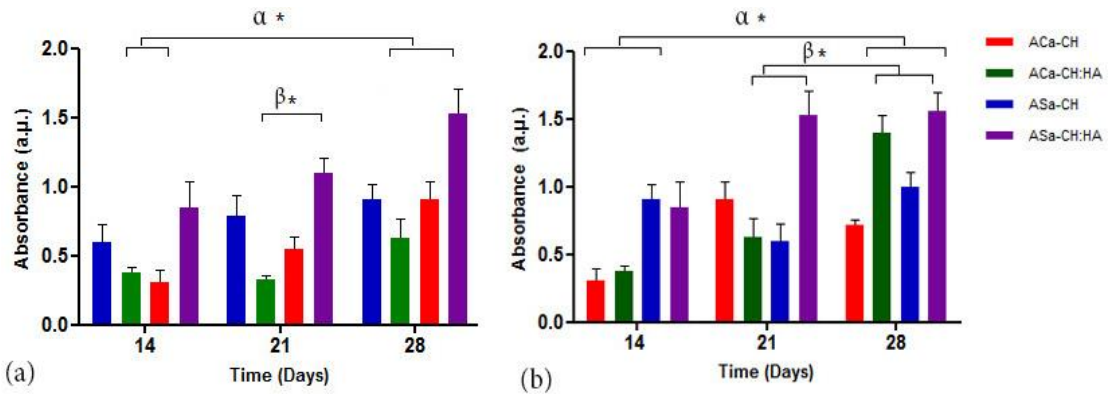

Figure 83: (a) Collagen deposition assessed at day 14, 21 and 28 day of seeding with hESMPs, (b) Calcium deposition on FG CH membranes on Day 14, 21 and 28 of seeding with hES-MP. The values are shown as mean ± SD (n=6), α* denotes statistically significant difference between D14 and D28, between same groups $p \leq 0.05$, (83a) β* denotes significant difference between ASa-CH:HA and ACa-CH:HA at D14, (8b) β* in denotes significant difference between ASa-CH:HA and ASa-CH at D14 and D28.

4.8.1. H&E staining

H&E staining of FG control scaffold and CH/CH:HA membranes seeded with hES-MPs are shown in Figure 84. Cells can be seen within the pores of all membranes. HA-composites appeared to show clumps of cells dispersed throughout the membrane pores, whereas neat CH membranes appeared to show individual cells. ASa-CH:HA membranes (figure 8e) contained clumps of cells that were much larger than ACa-CH:HA cell clumps. ASa-CH membranes showed a layer of cells at the surface with fewer cells located beneath the surface in the pores compared with other membranes.

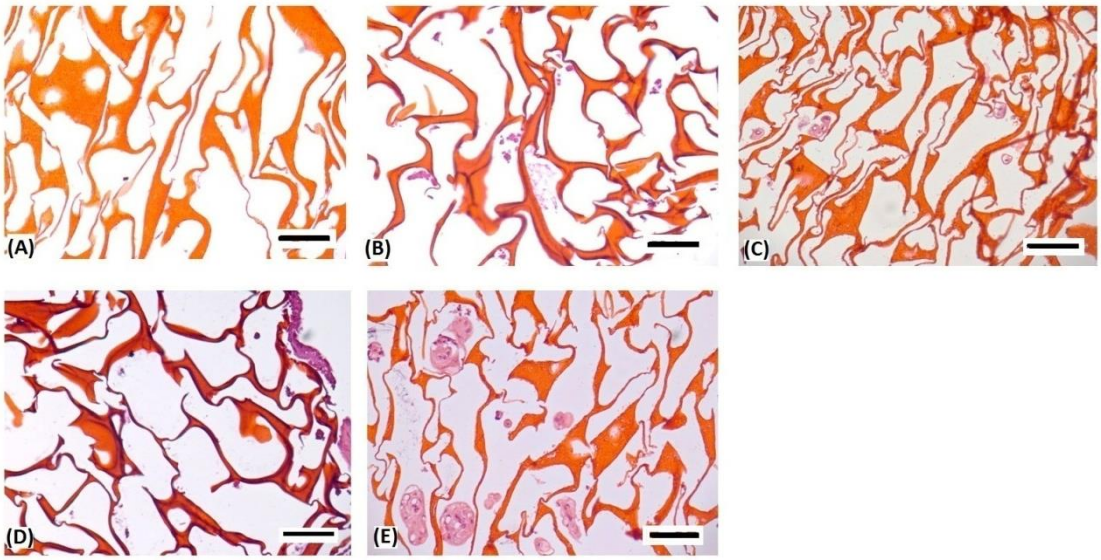

Figure 84: Cross sectioned H&E staining performed on Freeze gelated scaffolds seeded with hES-MPs (a) Control Specimen, (B) ACa:CH, (C) ACa:CH:HA , (D) ASa:CH, (E) ASa:CH:HA. Images scaled at 100 µm at 20 X magnification.

ACa-CH:HA membranes also showed cells dispersed within the construct indicating that the cells penetrated through the depth of the membrane. H&E images suggest interconnectivity of the pores within the CH-based constructs due to linking of pores and good cell penetration.

4.8.2. Histological sections after in-*vivo* implantation

4.8.2.1. First time point (7 days)

All animals were alive and grafts were placed inside the implantation site. No macroscopic reaction was observed at the implantation site.

Microscopic images show differences between CH and CH:HA samples. In pure CH FG membranes two zones can be distinguished, superficial zone, the part of implant in contact with bone and bone marrow, and 2) deep zone (Figure 85 and 86). Images obtained from the deep zone were void of cells. The superficial zone was filled with cellular infiltration. Pores that were located near bone were filled with newly formed bone tissue (Figure 85).

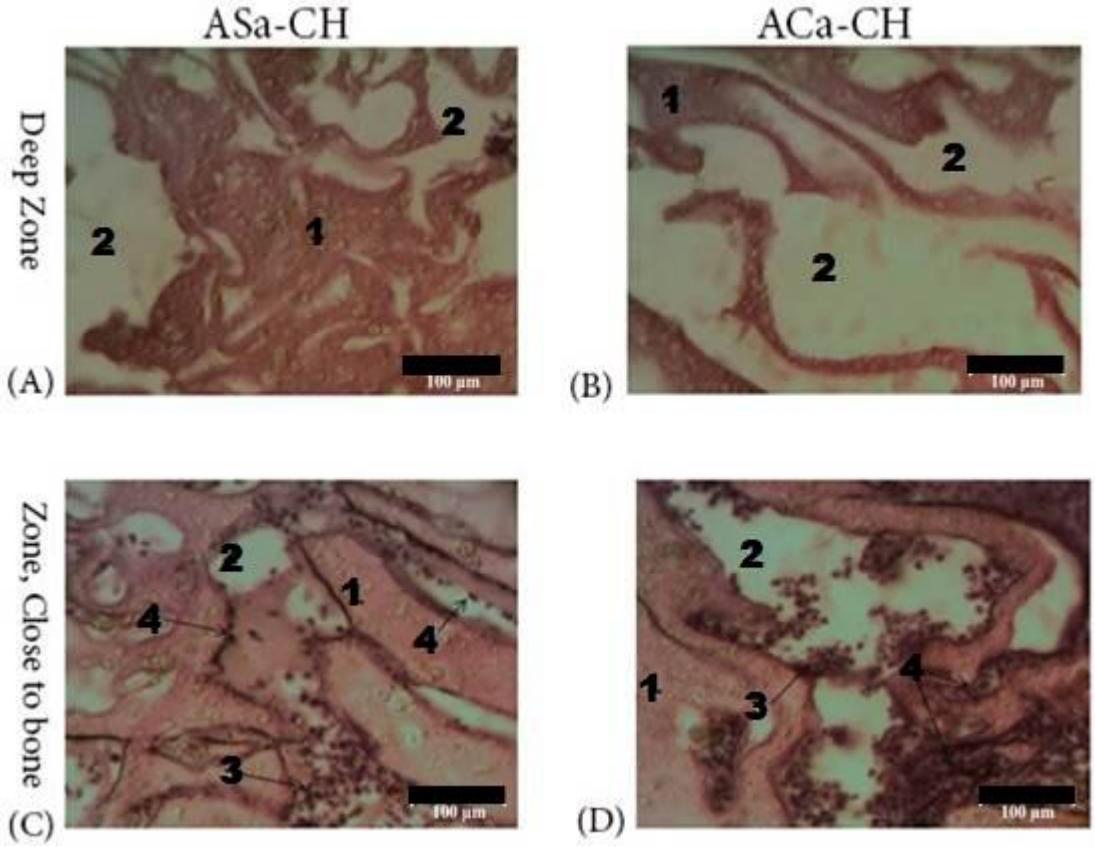

Figure 85: H & E staining was performed on deep zones (a) ASa-CH (b) ACa-CH, Zone close to bone are shown as (C) ASa-CH and (d) ACa-CH, Zones closer to bone show more cellular infiltration within the pores and ACa-CH show more cells than ASa-CH, Images were taken at 7 days after bone implantation, magnification 300x: 1 – CH; 2 – empty pore; 3 – leukocyte; 4 – fibroblast. Images scaled at 100µm

HA loaded samples showed higher number of cellular infiltration as compared to neat CH membranes (Figure 86). Observation of the zone close to bone in HA loaded samples revealed less empty pores. Cellular infiltration of ASa-CH:HA samples was higher as compared to ACa-CH:HA.

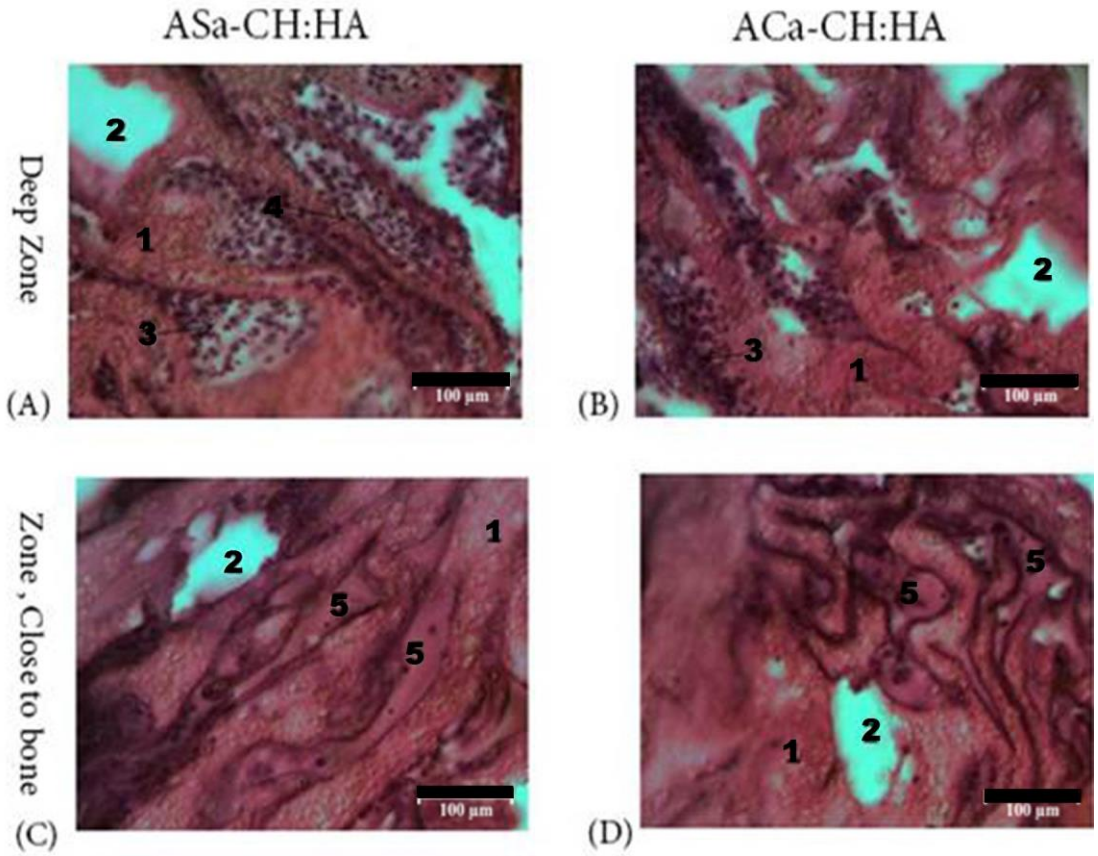

Figure 86: H & E staining was performed on deep zones (a) ASa-CH (b) ACa-CH, Zone close to bone are shown as (C) ASa-CH:HA and (d) ACa-CH:HA, Zones closer to bone show more cellular infiltration within the pores and ACa-CH:HA show more cell number than ASa-CH:HA. Images taken at 7 days after bone implantation, magnification 300x: 1 – CH; 2 – empty pore; 3 – leukocyte; 4 – fibroblast. Images scaled at 100µm.

HA seem to have a significant effect to increase cellular infiltration with the first 7 days of implantation. Layers of cells can be visually seen accumulating in a layer by layer manner with in the porosities of FG membranes in Figure 86a and 86b. Larger and somewhat empty pores can be appreciated in Figure 85a and 85b, on neat CH samples as compared to CH HA membranes. Although, deeper zone facing the bone does have cellular accumulation in figure 86c and 86d.

4.8.2.2. Second time point (30 days)

During the course of the study one animal died (from group 3 ASa-CH) on 9th day, after the operation. There was no apparent reason for the death of the animal, as all other main organs (liver, heat, kidney, spleen and intestine) had normal structure. There were no signs of any inflammatory reaction at the implant site. The sample recovered from the dead animal was not deemed suitable for investigation.

On visual inspection some evidence of periosteal reaction was noted after the bone removal from all specimens. This was noted as a small elevation of bone over the implantation site. No colour difference was seen at this site hence, this was taken to be indicative of new bone formation on implant site. No difference was seen in between neat FG CH and HA loaded specimens at this stage.

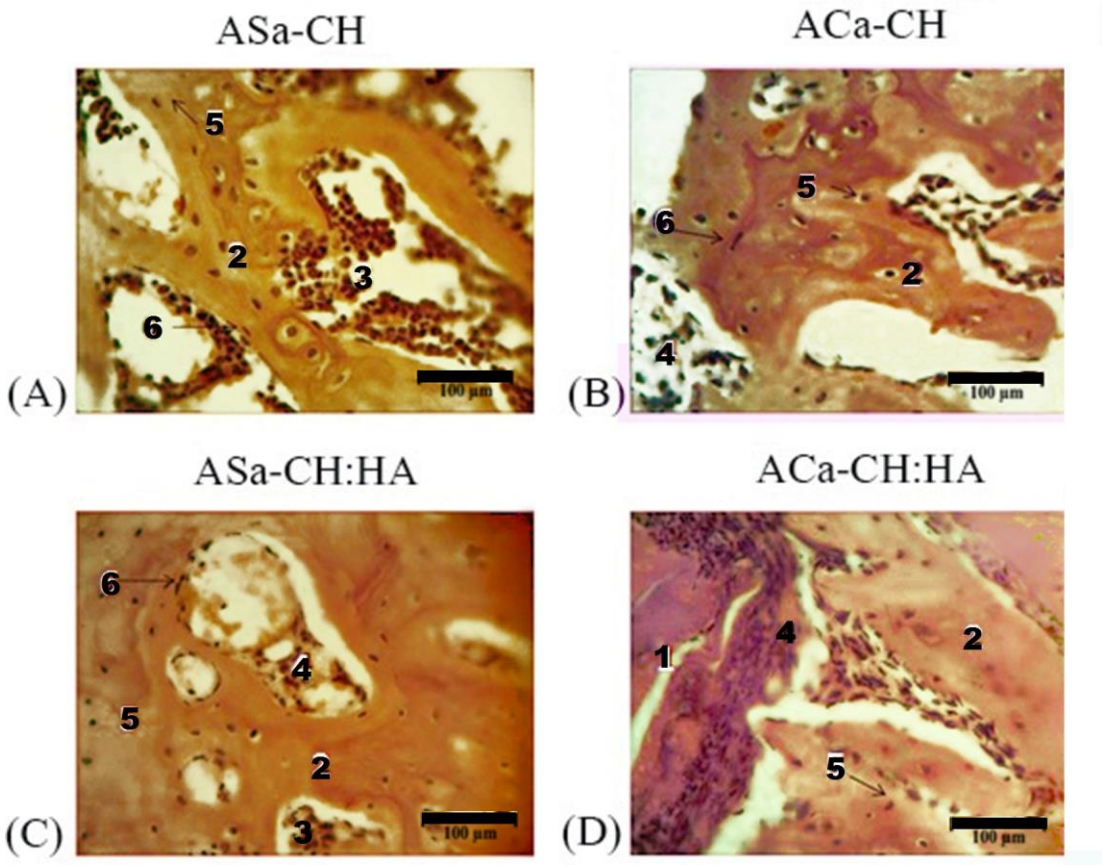

Figure 87: H & E staining was performed on CH FG membranes at day 30 after bone implantation, magnification 300x: 1 – remnant of CH scaffold, 2 – bone trabecula, 3 – bone marrow, 4 – fibrous tissue, 5 – osteocyte, 6 – osteoblast. Images scaled at 100µm

Histological images taken on the 30th day showed significant bone in-growth when compared with first time-point on 7th of implantation. Neat CH FG membranes completely degraded till

30th day after the operation and no signs of remnants of the specimen were observed. Bone defect are filled with usually three types of tissues – bone, fibrous and bone marrow. Bone tissue occupied the most peripheral part of the defect and forms trabecular network. Osteoblasts lie on the trabecular surface while osteocytes in lacunae (can be observed on the inside of trabeculae). Thickness of the trabecular part decreased from the peripheral to central zone of the defect. Inter-trabecular spaces fill with bone marrow cells that migrate from the non-injured parts of the bone. In central part of the defect fibrous tissue observed were tightly connected with new bone tissue and probably get replaced in at a later stage. Also, fibrous tissue can be found within inter-trabecular spaces, especially in central zone of defect.

HA incorporated FG scaffolds did not degrade completely. In the central zone of defect their remnants can be seen, in both ACa-CH:HA and ASa-CH:HA. When compared with the neat CH FG scaffolds, zone of defect was filled mostly by bone tissue and bone marrow cells. Some images were also suggestive of fibrous tissue. Bone trabeculae have similar thickness in peripheral and central zones of defect. It is suggested that HA can stimulate bone in-growth in all part of defect. As in previous groups, trabeculae covers with osteoblast, that has higher density.

4.9. Bioactivity studies

Bioactive studies were carried out in SBF according to the protocol described by Kokoubu *et al.,* (2006). Samples were assessed for their change in weight, regular monitoring of the change in pH was also performed and FTIR was conducted in conjunction with PAS unit to analyse the bulk chemical and structural alterations after immersion in SBF on the FG scaffolds.

4.9.1. pH Analysis

Changes in the pH value of the SBF were monitored whilst the FG scaffolds were immersed in SBF. pH value of SBF Day 0 was 7.4 and in order to mimic natural conditions SBF was changed after every 2 to 3 days to have optimum ionic concentration levels. A generalized trend was observed for all the specimens (Figure 88). At Day 21 pH value showed an increment from 7.4 to 7.8 with time. ACa CH had a pH 7.9.

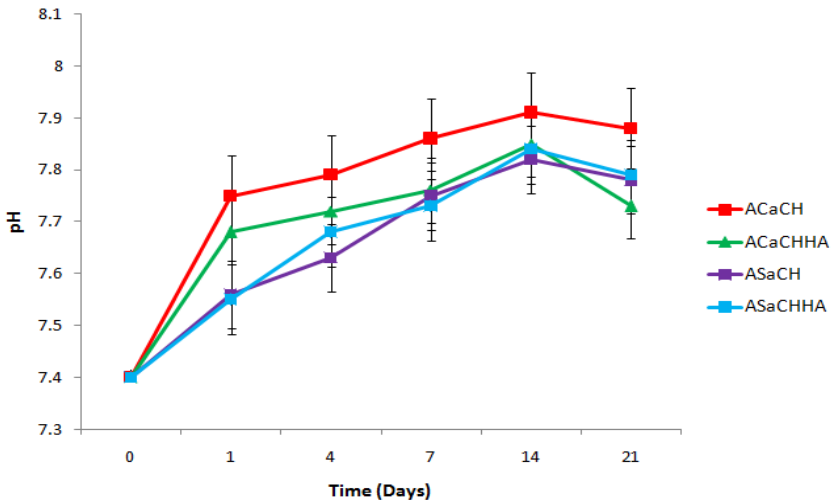

Figure 88: pH analysis of Freeze gelated scaffolds in SBF over the 28 day time period.

4.9.2. Weight analysis

Weight assessment of FG membranes over a period of 21 day is given in Figure 89. It was observed that at day 1 of SBF immersion, there was a steady drop in all specimens. Membranes with HA incorporation showed more stability and a linear drop was observed and correlated to weight gain of the dried specimens. Some specimens of neat ASa and ACa were not able to reach the full length of the experimental period due to contamination of the samples and hence were excluded from the experiment beyond 7 days. The weight gain might be indicative of a formation of the carbonated apatite layers on HA scaffolds although the weight change in neat CH membranes could be due to the some left over water with in the main chain of the polymer.

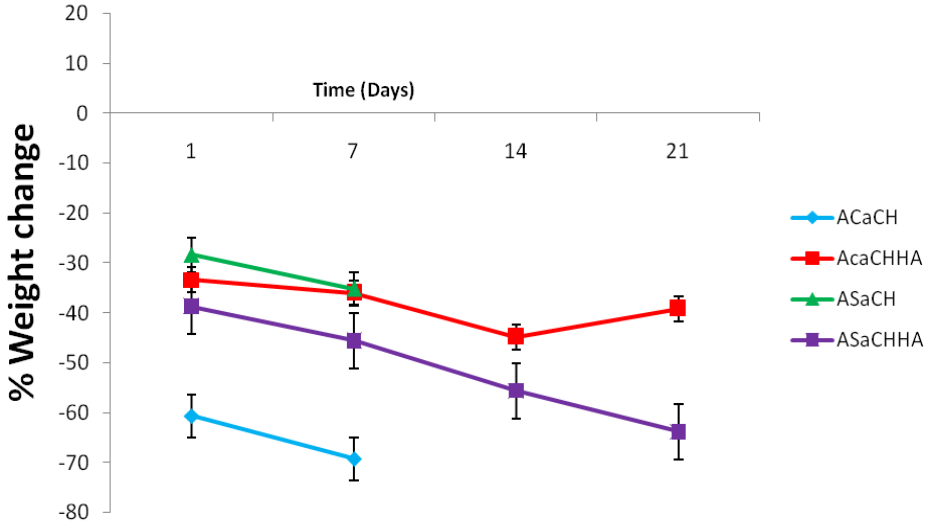

Figure 89: % Weight profile of freeze gelated membranes over a period of 20 days.

4.9.3. FTIR-PAS Spectroscopy

The comparative FTIR spectra of ACa-CH:HA at 1, 4, 7, 14 and 21 days and ASa-CH:HA at day 1, 4 and 7 of immersion in SBF are given in Figure 90 and 91. The peak shifts, intensity drops and variations in relative absorbance with respect to the peak were taken in to account to assess surface changes after immersion in SBF. PAS gives bulk information of sample CH with a strong broad band at 3400 cm^{-1} and prominent CH band, Amide II bands and glycosidic bands in the molecular finger print regions (1150, 1030 cm^{-1}). ASa-CH:HA samples after the day 7 of immersion in SBF could not be used for bulk profile analysis due to the specimens being disintegrated into a powdery form and being mixed with the SBF media.

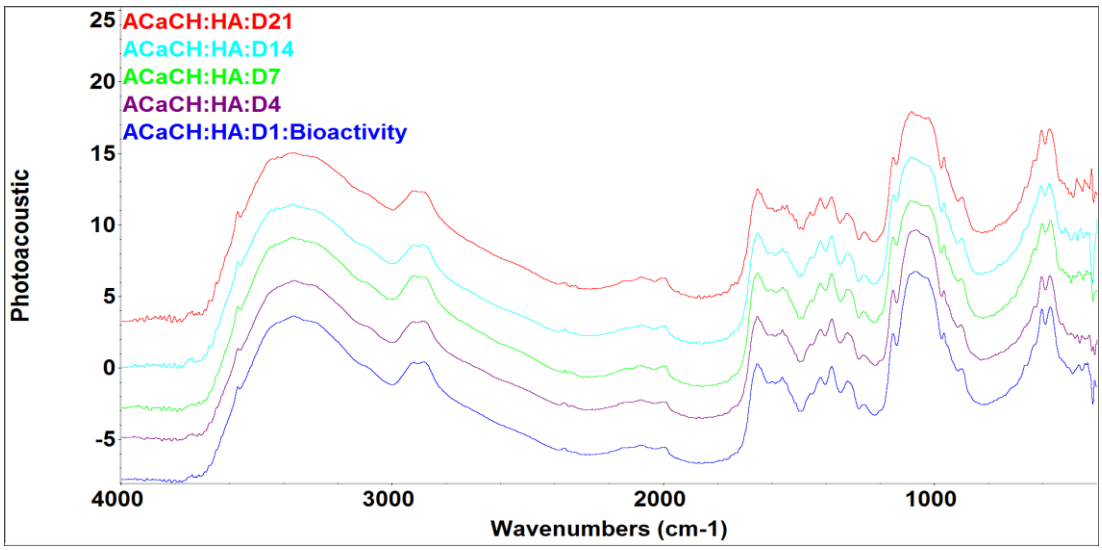

Figure 90: FTIR-ATR spectra of SBF treated ACa-CH:HA at Days 1, 4, 7, 14, and 21.

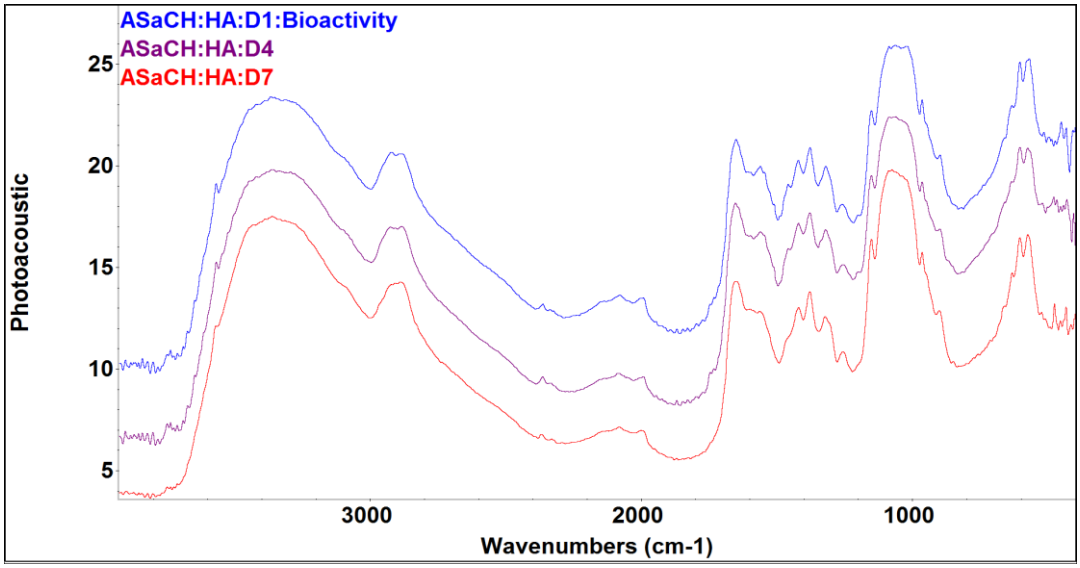

Figure 91: FTIR-ATR spectra of SBF treated ASa-CH:HA at Days, 1, 4 and 7.

4.9.4. Peak area analysis

Peak area calculations were conducted at each time point from D1 to D 21 respectively using TQ Analyst. This analysis was performed on HA incorporated specimens. For Aca-CH:HA the values decreased from D1 (22.13) to D14 (14.58) with a rise at D21. Whereas, for ASa-CH:HA after a drop at D4 the values rise back to the ones obtained for D1.

For peak area calculations at 960cm^{-1} for Aca-CH:HA samples values decrease at D7 only and rise back to 9.13 to match that at D1. ASa-CH:HA show a decrease at D4 and rise back up on D4 again to 7.44.

Table 19: Peak area analysis by TQ Analyst software at different time points (days) of (-OH) Hydroxyl peak at 3650cm^{-1}.

3650cm^{-1}	D1	D4	D7	D14	D21
ACaCHHA	22.13	20.56	18.02	14.58	21.59
ASaCHHA	15.77	10.69	14.92	Na	Na

Table 20: Peak Area analysis by TQ analyst Software at different time points (days) of PO peaks at 960cm^{-1}

960cm^{-1}	D1	D4	D7	D14	D21
ACaCHHA	9.48	9.2	6.89	7.56	9.13
ASaCHHA	6.28	4.79	7.44	Na	Na

4.10. Drug loading and release studies

Drug release studies were performed on FG CH scaffolds after cross linking with Sodium tripolyphosphate (NaTPP) at various concentrations. Presented here are: 1) the Scanning electron micrographs of all scaffolds after cross linking and drug loading 2) FTR in ATR and PAS mode of drug loaded and cross linked scaffolds 3) Results of the swelling ratio conducted after cross-linking 4) Calibration curve of tetracycline and 5) drug release studies over a period of 180 mins and loading entrapment efficiency of drug on each scaffold.

4.10.1. Scanning election microscopy

Scanning electron microscopy images of drug (tetracycline hydrochloride) loaded and cross-linked scaffolds are shown in Figure 92. It can be observed that top surface and cross sectional images show the porous nature of the scaffold even after cross linking and drug loading. Particles of TCY can be seen surrounding the pores. The cross sectional images depict that the pores were more compact and compressed together. Top surface micrographs of HA and Drug loaded scaffolds showed no pores emerging on it as compared to neat CH in ACa and ASa had porosities visible on this side of the constructs.

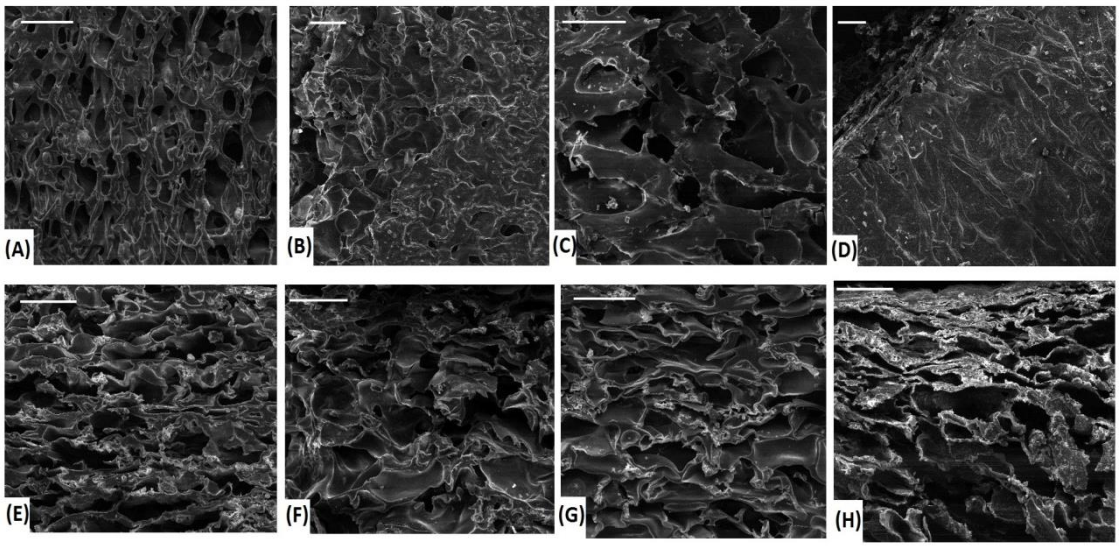

Figure 92. SEM micrographs of drug loaded and cross-linked porous freeze gelated chitosan (a) Top surface of ACa-CH (b) Top Surface of ACa-CH:HA (c) Top surface of ASa-CH (d) Top Surface of ASa–CH:HA (e) Cross sectional image of ACa-CH (f) Cross sectional image of ACa-CH:HA (g) Cross sectional image of ACa-CH:HA (g) Cross sectional image of ASa-CH (h) Cross sectional image of ASa–CH:H. All images scaled at 200µm.

4.10.2. FTIR- ATR/ PAS Spectroscopy after cross-linking and drug uptake

FTIR spectra data of TCY, CH, sodium tripolyphosphate (NaTPP) and HA are shown in Figure 93, obtained by using ATR as an accessory. Peak numbers have been identified and their chemical nature is listed in Table 21 (Page 166). The non-cross-linked FTIR-ATR spectra of freeze gelated scaffolds is shown in Figure 94 and shows typical peaks of Neat CH and HA incorporated spectra show typical PO_4^{3-} peaks depicting surface interaction of HA with CH and possible hydrogen bone interaction. The 5% NaTPP cross-linked scaffold spectra data shown in Figure 94 show peak shifts and new peak formation, which may be due to some surface interaction of NaTPP with CH and CH:HA specimens. Significant change is observed for ACa-CH and ASa-CH:HA with a sharp peak at 3527cm^{-1} and reduction in the Amide II peak at 1577cm^{-1}.

The emergence of the peak at 1209cm^{-1} is due to the phosphate linkages of NaTPP. Figure 94 shows 10% NaTPP used to crosslink FG scaffolds and more prominent phosphate peaks such as 1090 cm^{-1}, 1208, 1120 and 876cm^{-1} can be observed. Furthermore peaks at 1150cm^{-1} and 877 cm^{-1} are attributed to symmetric and asymmetric stretching of phosphate linkages. It can be envisaged that the terminal PO_4 groups of NaTPP seemed to link with NH_3 moieties of CH.

Surface interactions of TCY and cross-linked CH are shown in Figure 97, and prominent peaks of the drug are observed. Presence of peak at 1643cm^{-1} is attributed to C=O, 1450 and 1390cm^{-1} δ(-OH). Furthermore, peaks at 1450, 1103, 1172, 1223, 1450 and 1576 cm^{-1} are attributed to drug having surface interactions with CH. To study bulk changes in chemical structures of drug loaded CH scaffolds, PAS accessory was adapted and spectral data was obtained with neat, cross linked and drug loaded specimens. In Figure 98 neat ACa-CH shows decrease in intensity of amide II band at 1577cm^{-1}. Appearance of peaks at 1208cm^{-1} 1094 cm^{-1} is indicative of PO_4^3 linkages of NaTPP with -NH_3 of CH, furthermore, C-O-C peak broadens after cross linking. FTIR-PAS of drug loaded specimens show clear indication that the drug was present within the bulk of scaffolds and peaks at 1649, 1456, 1179, 1114 and 1044 cm^{-1} are all coinciding with the peaks identified after spectroscopic analysis of TCY. Photoacoustic of cross linked scaffolds show the amide II peak reducing in intensity indicating the ability of phosphate ions to interact with the amide group of CH. More visible interactions are seen in spectroscopy data obtained by PAS when compared with ATR spectra. The hydroxyl functional group of hydroxyapatite has a small shoulder appearing in the region of 3600cm^{-1}, this shoulder is observed in all spectra of neat, cross linked and drug loaded CH in ASa with 50:50 HA. Whereas; CH in ACa with 50:50 HA PAS spectral data shows this hydroxyl group in neat and cross linked scaffolds only.

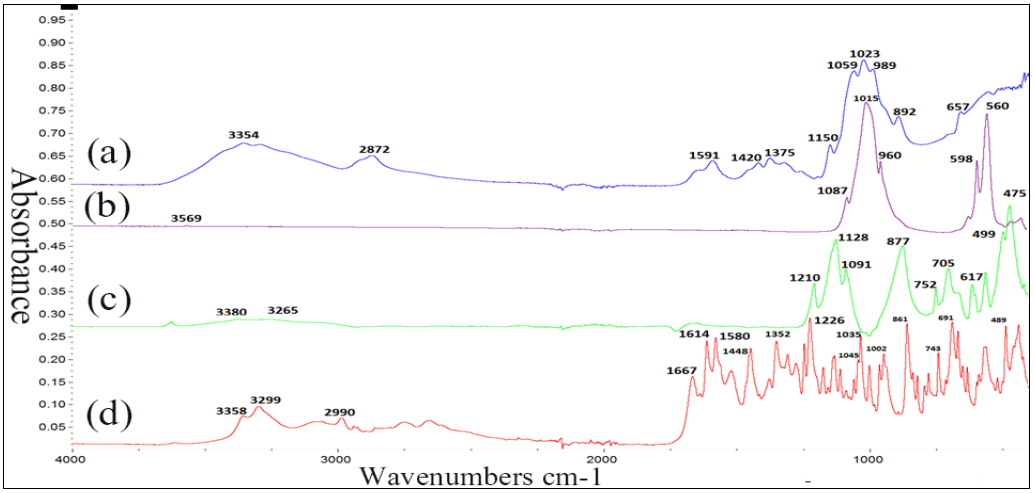

Figure 93: FTIR _ATR spectra of (a), Chitosan Medium Mol. wt, (b) Hydroxyapatite, (c) Sodium Tripolyphosphate (NaTPP), (d) Tetracycline Hydrochloride.

Table 21: FTIR peak identification and references of Tetracycline Hydrochloride and Sodium Tripolyphosphate.

Wave numbers (cm^{-1})	Peak Identification	Reference
1643	V(C=O)	Gunasekaran *et al.*, 1996 (Qualitative Analysis on the infra red bands of tetracycline and ampicillin)
1650-1600	V(C=C) aromatic ring	
1450 -1390	δ(-OH)	
1200-1270	δ (C-C), δ(N-H), v(C-C). v (C-N)	
1003	C-O stretching , C-H in plane bending	
1039	C-O, C-N, C-H	
1113	C-C and C-N stretching (S)	
1140	C-C STRETCHING (s)	
1177	C-N stretching, C-C stretching	Ghadim *et al.*, 2013(Ghadim *et al.* 2013)
1229	C-C stretching, C-N stretching	
1357	vs (C-O stretching, Symmetric CH_3 bending, terminal gem dimethyl bending	
1456	Unsymmetrical CH_3 bending, ring C-C stretching	Madhumati *et al.*, 2014(Madhumathi and Kumar 2014)
1580,1618,1670	Ring C-C stretching , C=O stretching	
2665	C-H stretching of Methyl group	
2755	C-H stretching of Methyl group	
2860	Symmetrical stretching of Methyl group	
3364	Associated Hydroxyl absorption	
NaTPP Spectra band numbers and Peak Identification with Reference		
3419	-NH and –OH groups Inter or intra molecular hydrogen bonding within	Bhumkar *et al.*, 2006 (AAPS PharmSciTech)
3200	-NH and –OH groups	
1656	Amide I	Bhumkar *et al.*, 2006
1321	Amide III	
1150	P=O of TPP attributed to linkages between phosphate and ammonium ions	
1089-1152, 1090	Aliphatic amines	
1650	N-H	
1060-1300	Phosphate linkages between NH_3^+ of CH and PO_4 of NATPP	F.Pati *et al.*, 2011 (Carbohydrate research)
1140-1280 (1280 due to restricted rotation)	Symmetric and asymmetric stretching of phosphate linkages	
640	Triplet broad band phosphate PO_4	

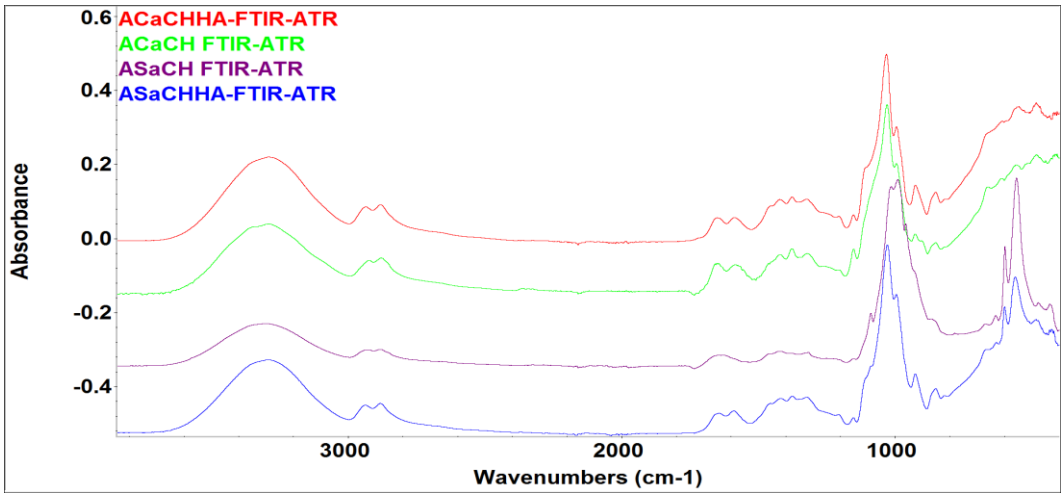

Figure 94: Non Cross-linked FTIR-ATR spectra of Freeze gelated Chitosan ACa-CH, ASa-CH, ASa-CH:HA and ACa-CH:HA.

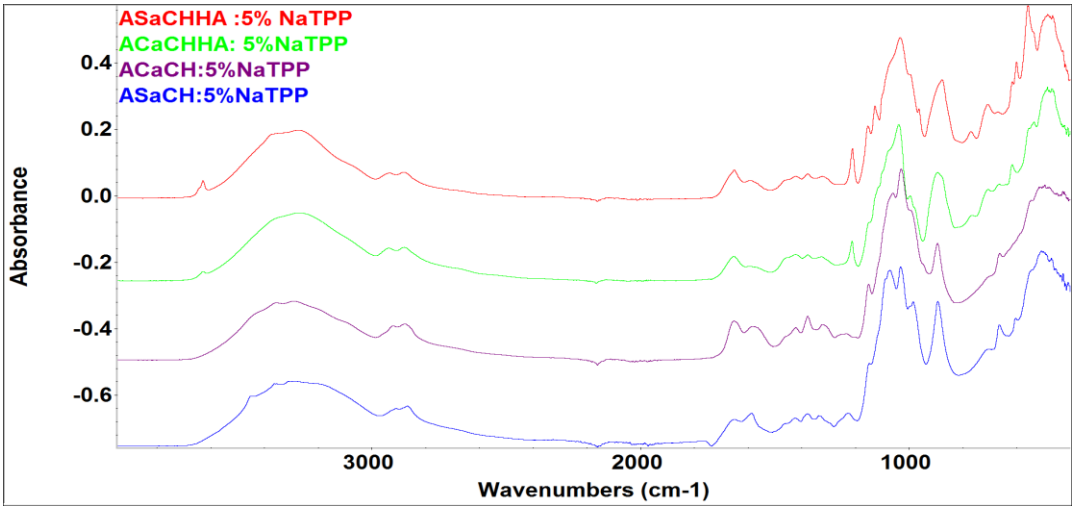

Figure 95: Cross-linked at 5% (wt/v) of NaTPP FTIR-ATR spectra of Freeze gelated Chitosan ACa-CH, ASa-CH, ACa-CH:HA and ASa-CH:HA

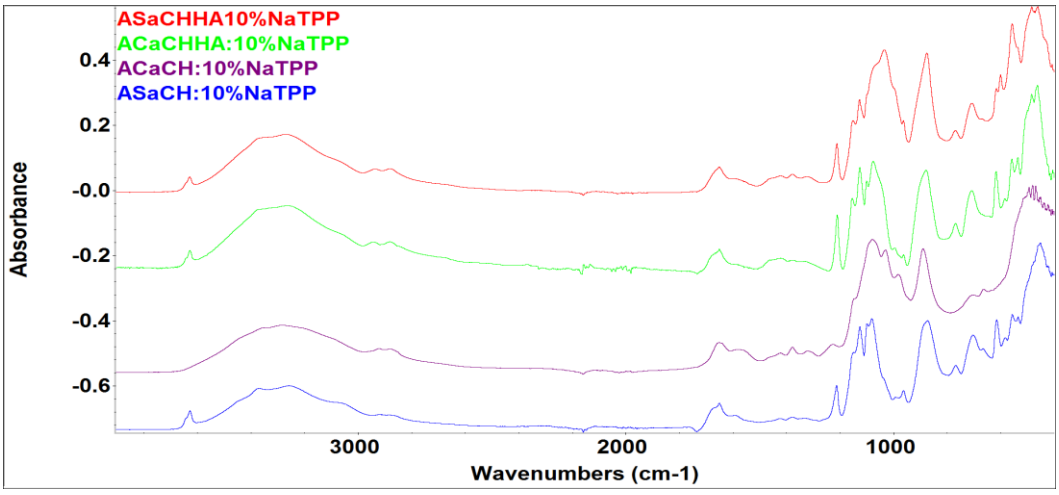

Figure 96: Cross-linked at 10 % (wt/v) of NaTPP FTIR-ATR spectra of Freeze gelated Chitosan ACa-CH, ASa-CH , ACa-CH:HA and ASa-CH:HA.

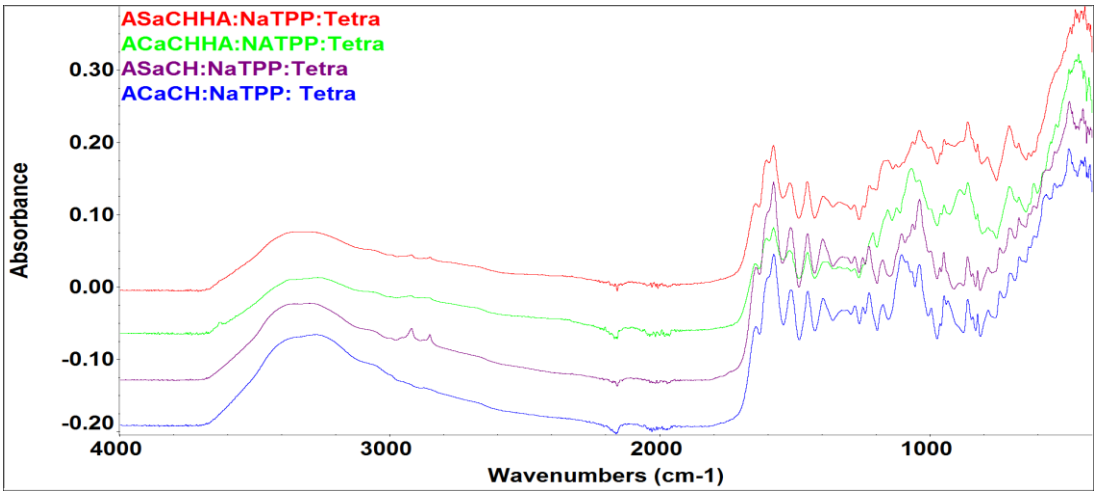

Figure 97: Cross-linked at 5% (wt/v) of NaTPP and Drug (tetracycline Loaded) loaded FTIR-ATR spectra of Freeze gelated Chitosan ACa-CH, ASa-CH, ACa-CH:HA and ASa-CH:HA.

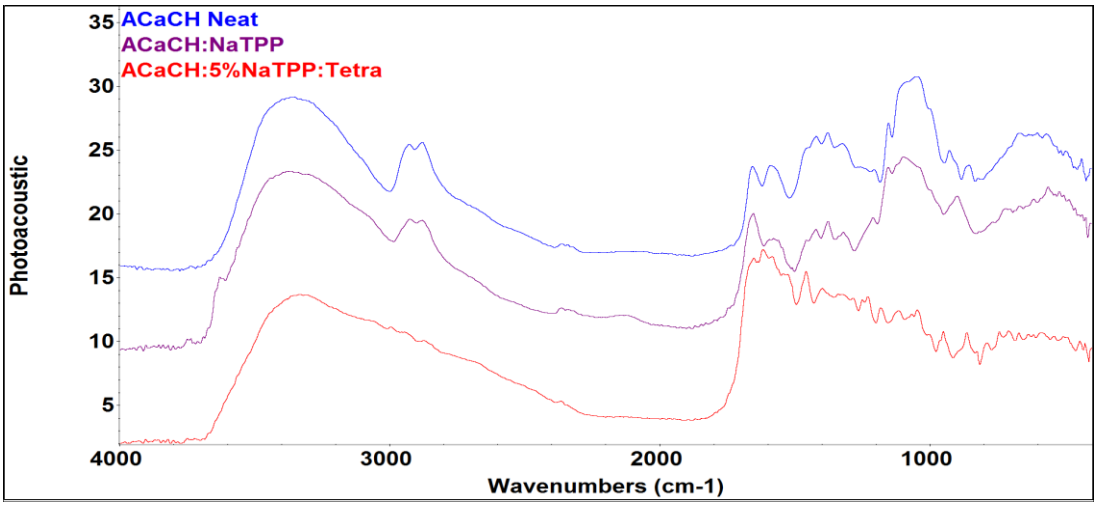

Figure 98: FTIR-PAS of ACa:CH, ACa:CH:5% NaTPP and ACa:CH:NaTPP:TCY.

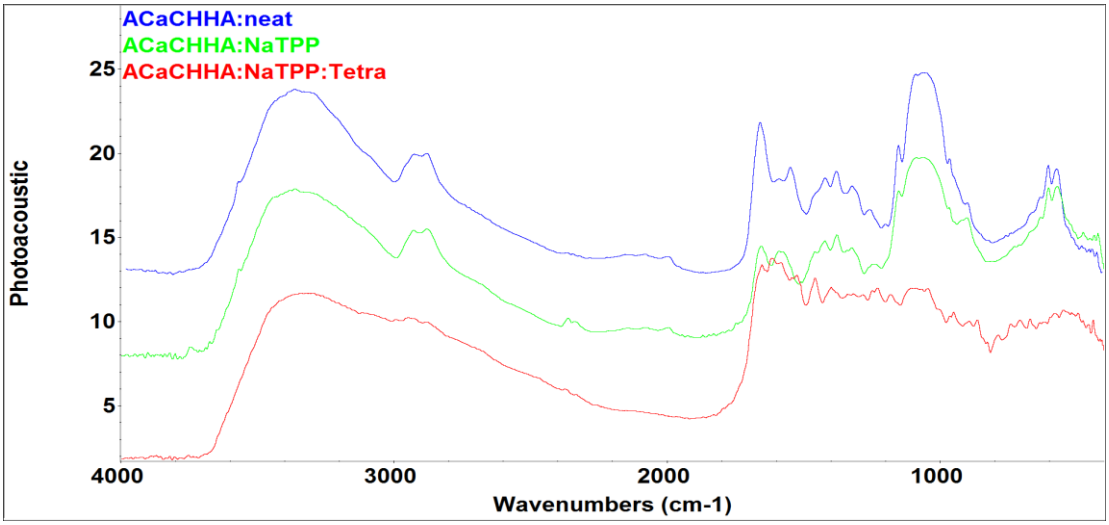

Figure 99: FTIR-PAS of ACa:CH:HA, ACa:CH:HA: 5% NaTPP and ACa:CH:HA:NaTPP:TCY.

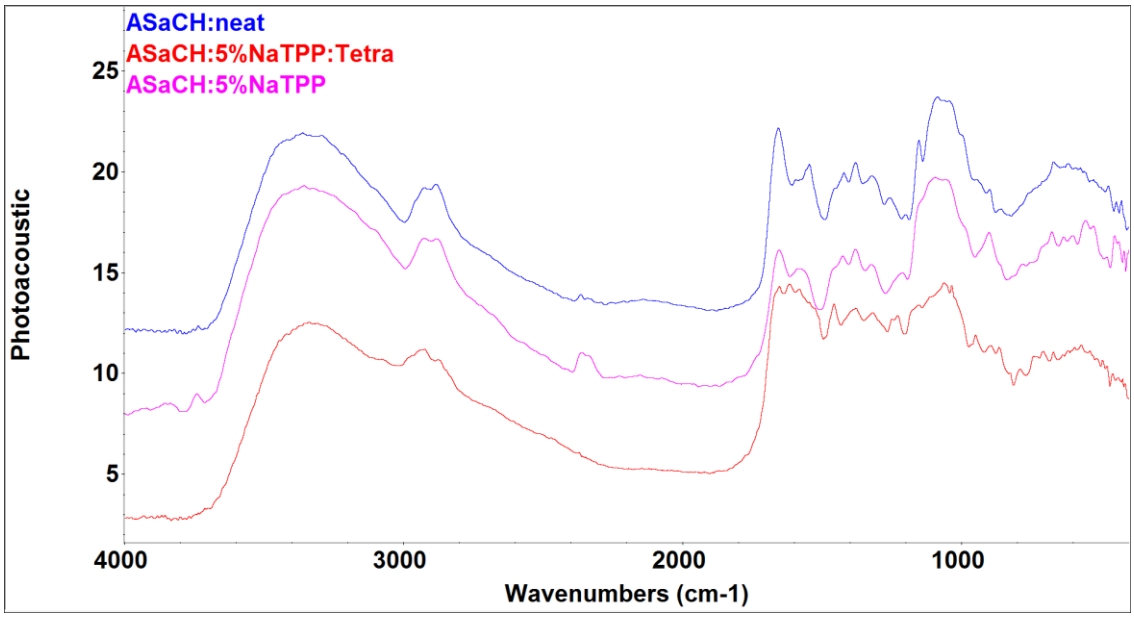

Figure 100: FTIR-PAS of, ASa:CH, ASa:CH:5% NaTPP, ASa:CH:NaTPP:TCY.

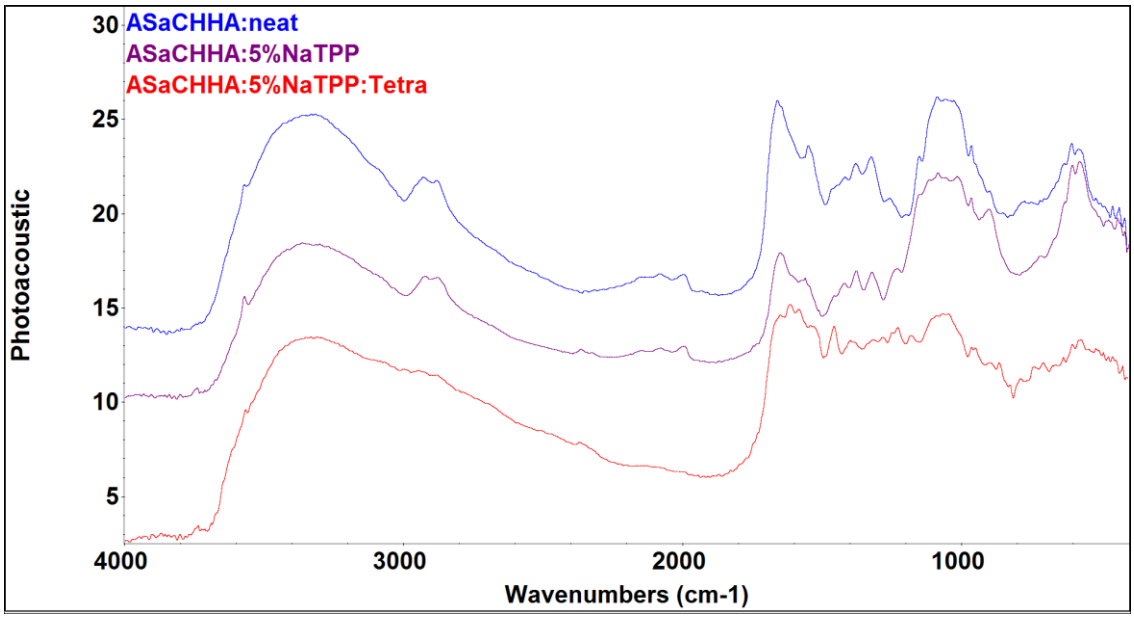

Figure 101: FTIR-PAS of ASa:CH:HA, ASa:CH:HA:5% NaTPP and ASa:CH:HA:NaTPP:TCY.

4.10.3. Swelling ratio

Results of the swelling studies obtained by over a period of 1 week (168 hrs) after varying the ratio of NaTPP are shown in Figure 102. At 0% cross-linking neat ACa-CH and ASa-CH show maximum swelling percentage of 80% within the first 15 minutes and then the trend is equilibrated. Specimens of CH in ACa and ASa with 50:50 HA show a 60 % swelling percentage and then they maintain this rate with slight fluctuation over the experimental period. In specimens cross-linked with 5% NaTPP similar trend is observed with slight reduction in values of HA incorporated specimens. At 10% NaTPP significant decrease in

swelling is observed with an overall percentage of blank CH in ACa and ASa going down to 60%, so a 20% decrease in neat scaffolds. HA reinforced scaffolds also have a decrease in swelling profile to 40% within the first 15 mins that rises to 50% after the end of 1 week experimental time.

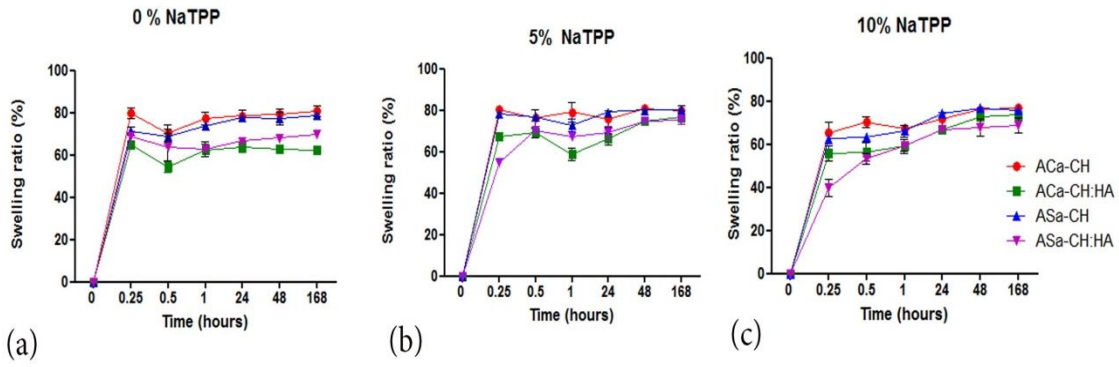

Figure 102: Swelling ratio of Freeze gelated scaffolds cross-linked with 0, 5 and 10 % wt/v NaTPP and assessed for swelling change upto 168 hours (1 week), values shown are mean ± SD (n=3).

4.10.4. Drug Loading / entrapment

Drug loading efficiency of CH FG scaffolds with and without HA at various cross linking percentages is represented in Table 22. Maximum overall loading efficiency was observed with 5% NaTPP specimens whereas neat or blank CH scaffolds regardless of the cross linking within each group showed lesser drug uptake. Least drug entrapment is seen in 0% cross linked specimens and CH in ASa with 50:50 HA has consistently shown less drug uptake within each group.

Table 22: Drug loading at 100 mg/ml Freeze gelated scaffolds cross linked at 0%, 5 % and 10% (wt/ v) of NaTPP, Values shown are mean ± SD (n=3).

FG / Scaffolds NaTPP	ACa-CH	ACa-CH:HA	ASa-CH	ASa-CH:HA
0 %	52.7 ±1.25	35.6 ±1.28	68.2 ±2.11	18.2 ±1.5
5%	78.2 ±2.1	70.8 ±1.5	78.4 ±3.0	47.9 ±3.5
10%	64 ±3.2	56.3±3.5	71.7 ±3.5	46.1 ±1.5

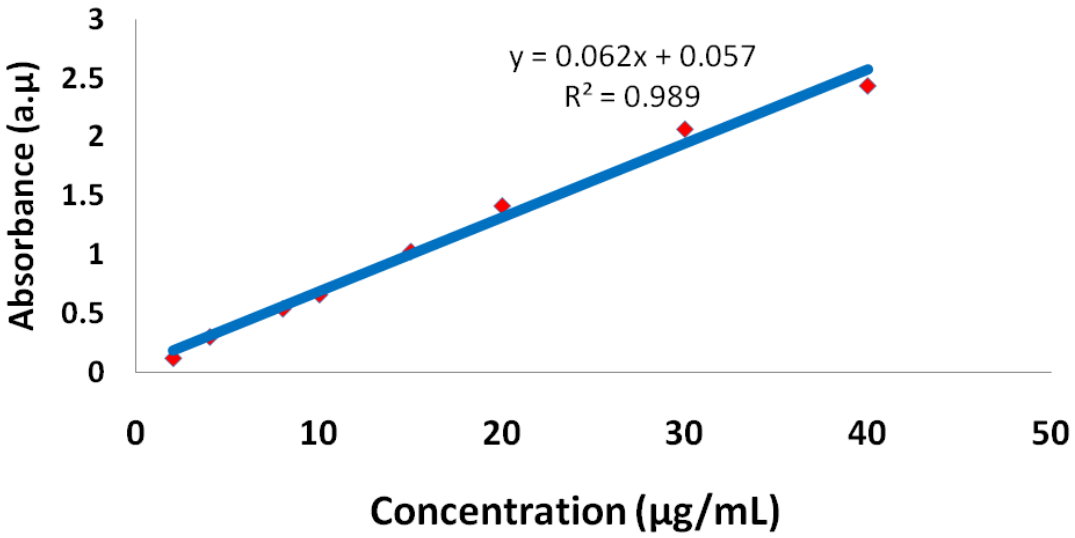

Figure 103: Tetracycline hydrochloride calibration curve prepared by using Beer's Lambert Law, repeated 5 times at 270 nm as a reference point for studying drug release from freeze gelated chitosan scaffolds.

Drug release studies carried out using a dissolution apparatus and percentage recovery graphs were plotted over 180 mins of release studies. The 0% cross-linked recovery graph (Figure 104) shows that ACa CH has a 90% recovery in the first 10 mins and comparatively ASa-CH has a lower release of 35%. A stable plateau was achieved for ACa-CH and ASa-CH, which also shows stability after 40 mins. ACa-CHHA followed a similar trend to ACa-CH. ASa-CH:HA recovery pattern shows a gradual increment from 30% at initial 10 mins to 70% at 60 minutes. At 5 wt% cross-linking (Figure 105) of NaTPP ACa CH after 10 mins shows a 80% recovery and attains a plateau till the end of the release profile. ASa CH has a 40% recovery profile in the first 10 mins of the experimental period and after 30 mins of release study it attains an equilibrium state. ACa CH HA interestingly showed an 80% recovery after 10 mins and then adopted a equilibrium profile for the rest of the release pattern. ASa CH HA showed a gradual increment in the percentage recovery of drug, which was slightly similar to that obtained for the same specimen at 0% cross-linking agent. For 10 wt % cross-linking (Figure 106) ACa CH sample showed a 70% recovery and maintained equilibrium. ASa CH also showed a similar profile with a 50% recovery after 10 mins and maintains a plateau mimicking the ACa CH release profile. ACa CH HA showed a gradual increment with time as compared to ASa CH HA showed a Figure 101 shows the calibration curve used to calculate the % recovery of TCY from FG membranes. The curve also shows the as calculated intercept and slope values.

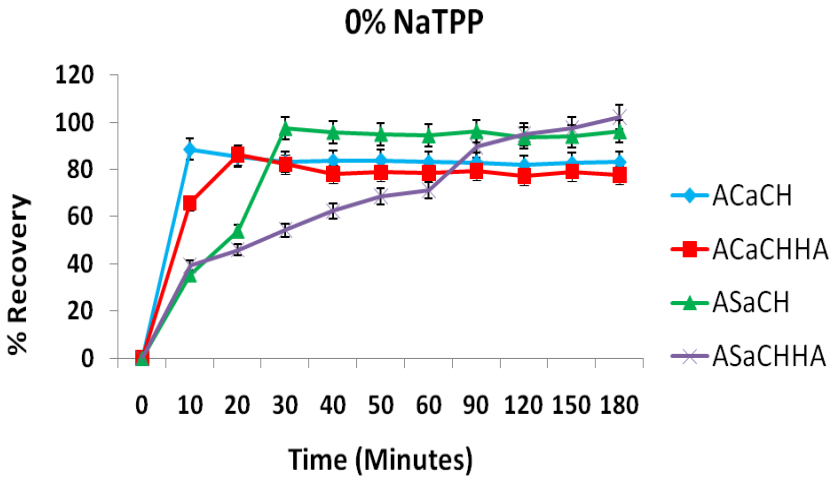

Figure 104: Percentage recovery from freeze gelated scaffolds after 0% Cross-linking with NaTPP, values shown are mean ± SEM (n=3).

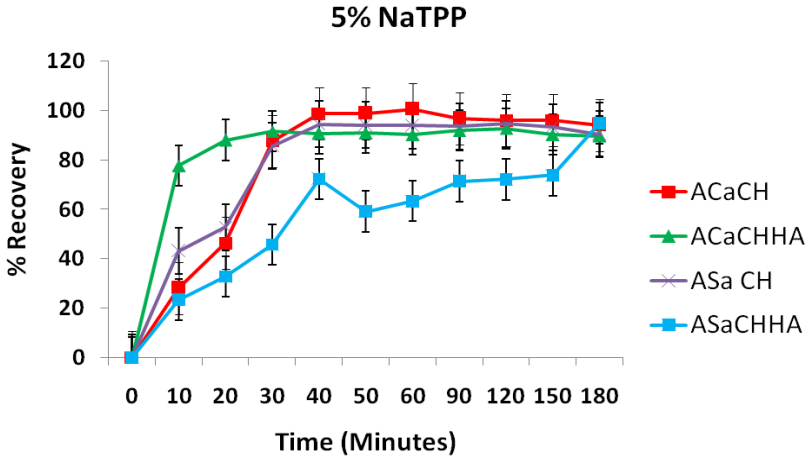

Figure 105: Percentage recovery from freeze gelated scaffolds after 5% Cross-linking with NaTPP, values shown are mean ± SEM (n=3).

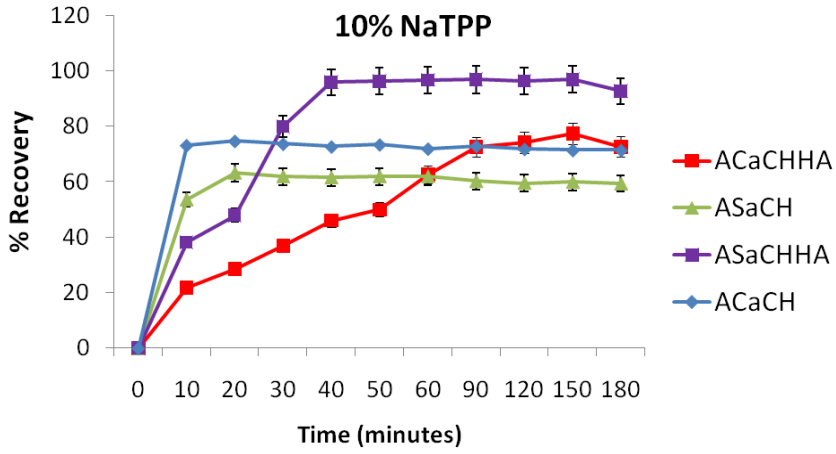

Figure 106: Percentage recovery from freeze gelated scaffolds after 10% Cross-linking with NaTPP, values shown are mean ± SEM (n=3).

SECTION III

4.11. Electrospinning chitosan

This section describes the results obtained after electrospinning CH fibres and their physiochemical, mechanical and biological characterisation. The purpose of the electrospun layer is to serve as a surface layer to the functionally graded periodontal tissue engineering constructs and face the soft tissue side when placed into the defect site.

4.11.1. SEM of Electrospun CH fibres

SEM images of electrospun mats of random and aligned CH fibres are given in Figure 107. Figure 107a show fibres with a high degree of orientation compared with figure 107b that shows fibres with no preferential direction of orientation. In Figure 107 fibres show a

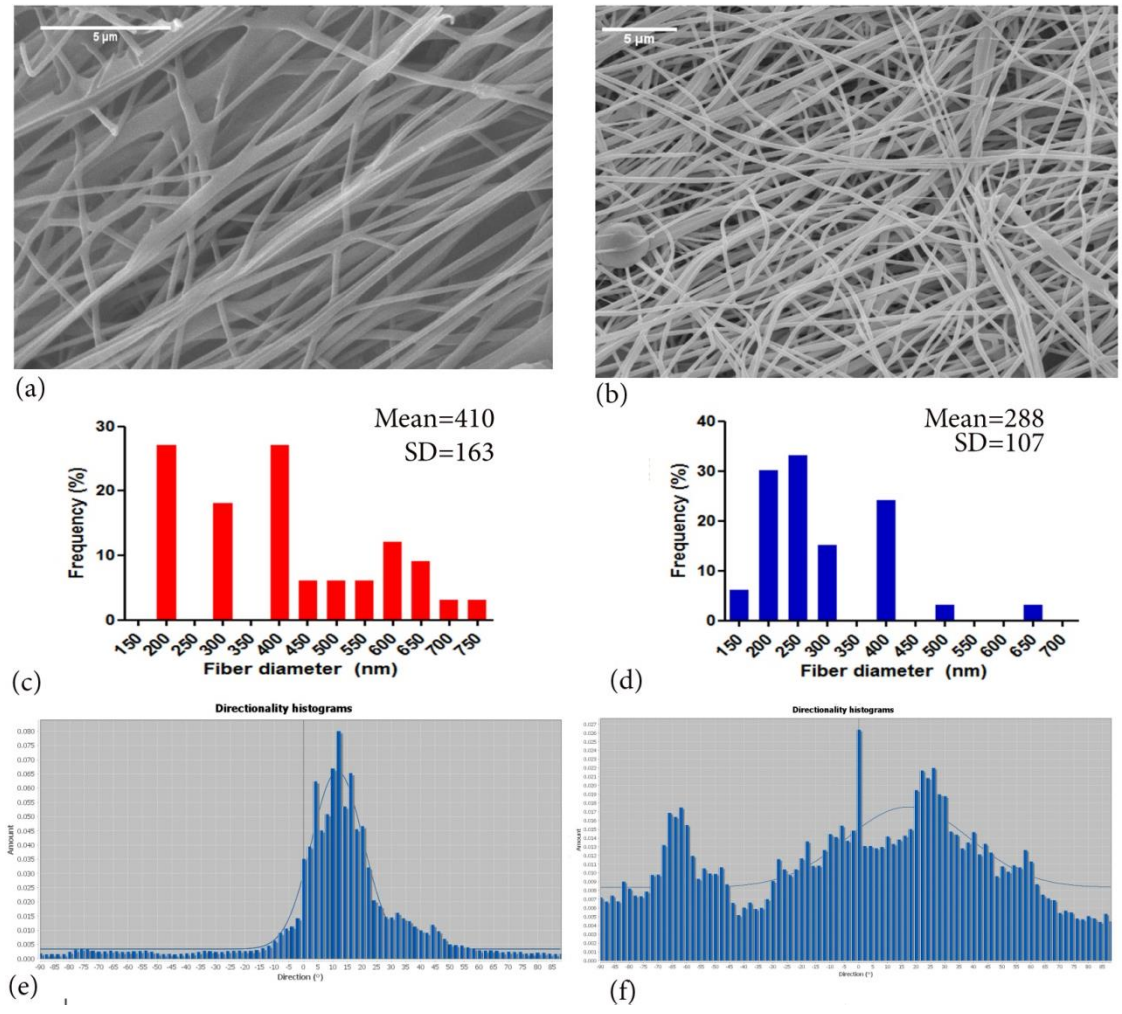

clean

Figure 107: SEM micrographs of (a) Aligned and (b) Random oriented chitosan electrospun fibres, Images scaled at 5µm, along with respected (c,d) Frequency of fibre distribution in nm plotted by

measuring 100 fibres (e, f) Directionality histograms of Aligned and Random Fibre. Frequency and Histograms plotted using graph pad Prism and Image J2 software (NIH, USA).

bead less morphology. Mean fibre diameters ranged from 410 ± 162 nm to 288 ±106 nm for aligned and random fibres respectively, with aligned fibres showing a greater variation in distribution of fibre diameters. Orientation histograms of aligned and random fibres (Figure 107 e and f) give a clearer representation of the directionality of fibres

Random fibrous scaffolds showed an even spread in all directions as compared to aligned scaffolds which had the majority of fibres orientated within 20^0 of one predominant direction indicating a much more unidirectional alignment of fibres compared to random fibres. The overall thickness of the random and aligned mats obtained was 150 ± 10 µm. Orientation histograms of aligned and random fibres (Figure 107 e and f) give a clearer representation of the directionality of fibres. Random fibres were spread in all directions as compared to aligned fibres. Figure 107 shows aligned fibres at different magnifications obtained with SEM.

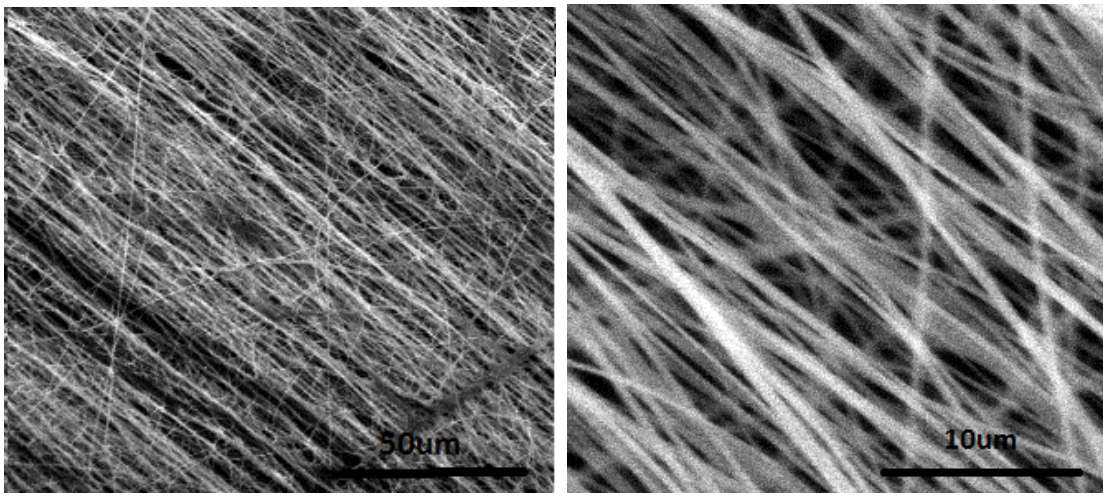

Figure 108: SEM image of Aligned CH fibres scaled at 50µm (left) and 100µm(right).

4.11.2. FTIR Spectroscopy of Random and Aligned CH Fibres

FTIR spectroscopy was carried out using ATR (Figure 109) and PAS (Figure 110) accessories for surface and bulk analysis of electrospun CH. Both random and aligned samples show a typical broad band of CH around 3366-3375cm^{-1} and another characteristic band around 1558cm^{-1}, these are commonly attributed to N-H and O-H stretching of primary amino groups, (due to the presence of hydrogen bonds with O-H group). Furthermore, N-H stretching of secondary amides (Amide II) is also visible. Very low quantity of PEO was used to make the electrospinning solution, hence, the typical triplet peak observed in plain PEO from

1150 to 1060cm^{-1} are diminished. Designated peaks identified from the FTIR ATR Spectra of PEO are listed in Table 23. The peak at 1092cm^{-1} has been attributed to typical stretching vibration of ether group (C-O-C) in PEO spectra, which showed a shift to higher wavenumber in CH PEO ATR and PAS spectra. The PEO peak at 2878cm^{-1} when observed in CH PEO fibres seem to have integrated and peak occurring in neat CH around 2800cm^{-1} due to CH_2 stretching have a more sharper peak, this is indicative of some interaction and complex formation between CH and PEO.

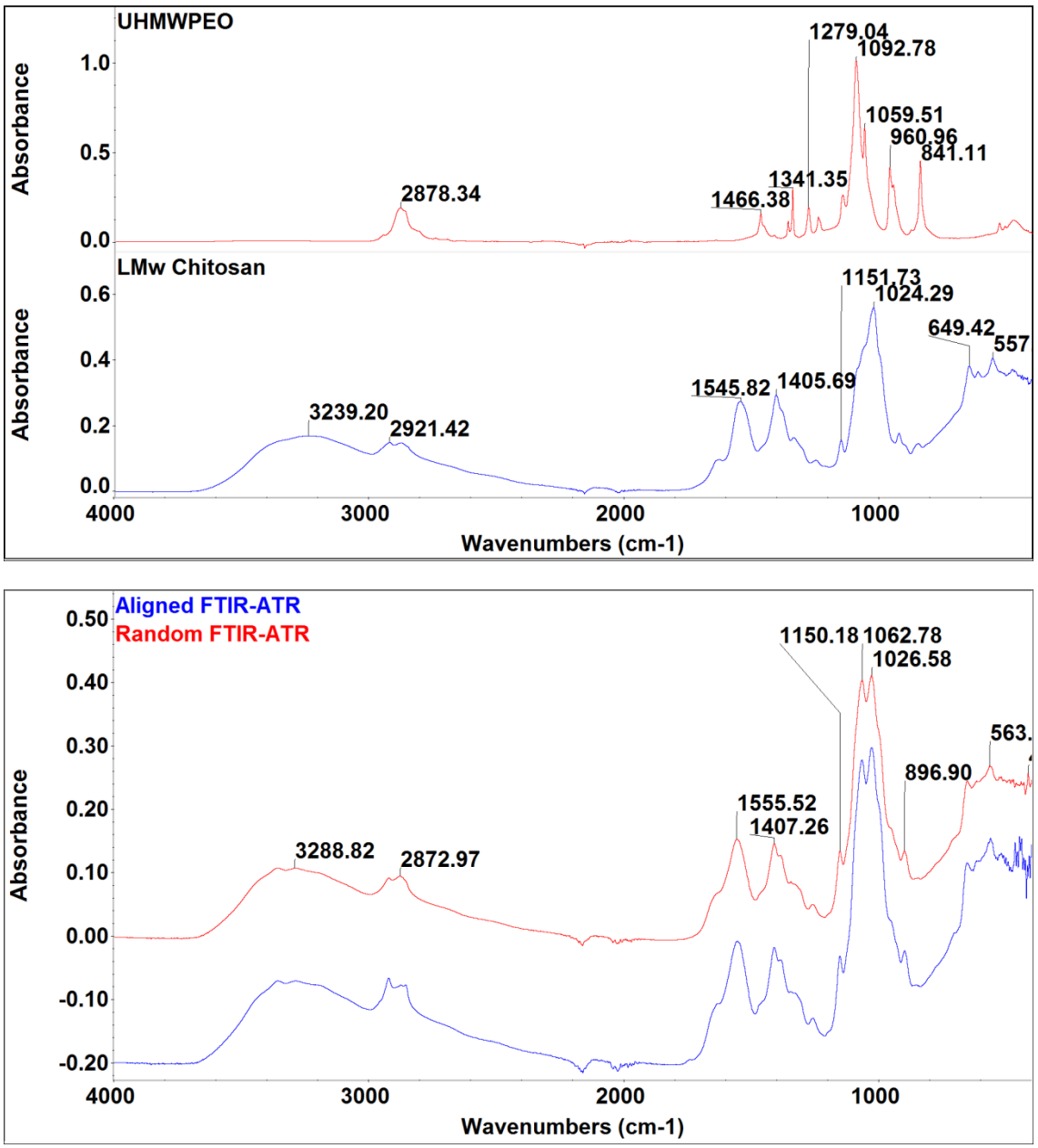

Figure 109: FTIR-ATR spectra of (Top image) neat Chitosan and neat UHMWPEO, (Bottom image) Aligned and random electrospun fibres.

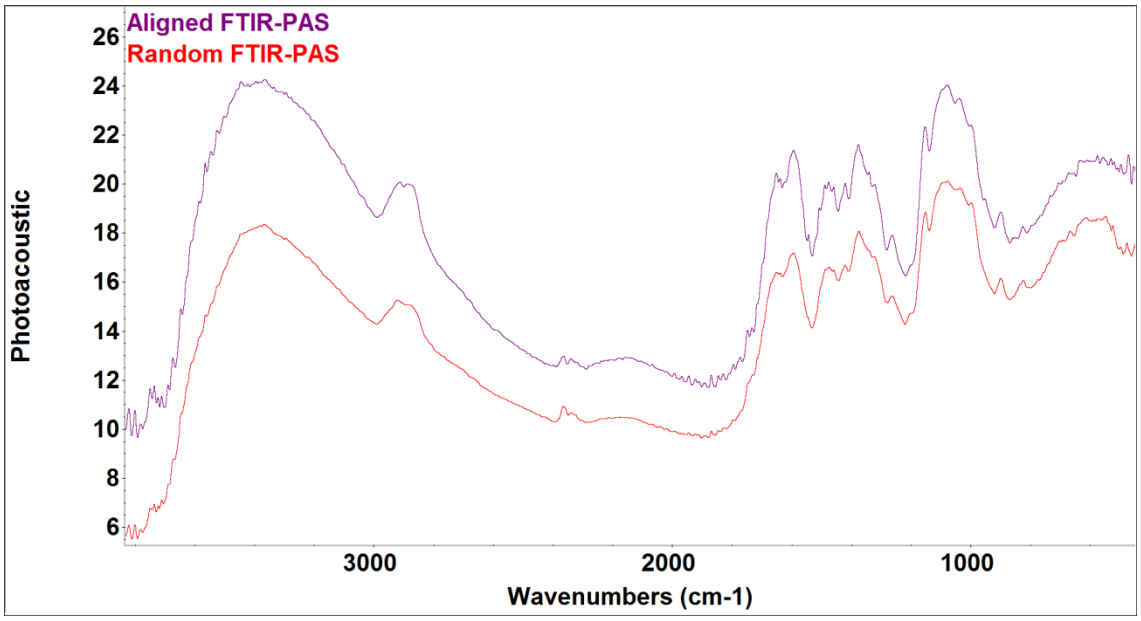

Figure 110: FTIR PAS spectra of Random and Aligned CH fibres.

Table 23: Band identification and reference of peaks identified for UHMWPEO powder.

Wavenumber (cm^{-1})	Assignment	Reference
2878	Asymmetric and symmetric vibration (CH_2)	Shen *et al.*, 2002(Shen *et al.* 2002)
1466	Asymmetric bending CH_2	
1341	Asymmetric wagging CH_2	
1279	Asymmetric twisting CH_2	
1241	Asymmetric twisting CH_2	
1144,1092,1059	Asymmetric stretching C-O-C	
960	Asymmetric rocking CH_2	
841	Symmetric rocking CH_2	

4.11.3. Tensile properties

Tensile tests conducted on dry and wet random and aligned CH fibrous mats are shown in Table 24. Dry aligned fibres showed higher modulus when compared with dry random fibres which was statistically significant. The UTS of aligned fibres was 13.58±3.68 which was statistically higher than the UTS of random fibres (7.5±3.84). Fibres showed a drop in the Elastic modulus when tested in wet conditions for Elastic modulus and UTS values. Aligned fibres are nearly 4 times stiffer and random in wet conditions and examples of the

stress strain graphs of random and aligned fibres during moist and dry conditions are shown in figure 111 (a and b).

Table 24: Tensile properties of Aligned and Random Chitosan Fibres performed in dry and moist condition. Young's Modulus (*E*= MPa) , Ultimate tensile stress (MPa), Strain (%) using 45 N load cell at a ramp rate of 1mm/sec on Bose ELF Electroforce 3200. Values shown are mean± (SD) (n=6).

Dry Fibres	YM (MPa)	UTS(MPa)	Strain (%)
Aligned	357.31±136.22	13.58±3.68	0.11±0.04
Random	259.39±192.75	7.50±3.84	0.05±0.04
Moist Fibres	**YM (*E*)**	**UTS(MPa)**	**Strain (%)**
Aligned	22.39±4.06	4.95±1.41	0.23±0.05
Random	6.25±1.01	1.95±1.15	0.13±0.11

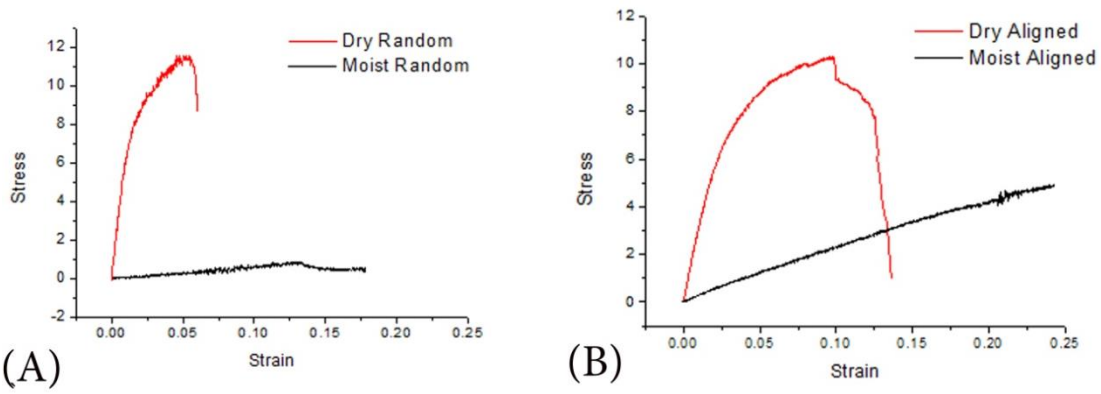

Figure 111: Example of stress strain relationship of Aligned and Random Chitosan fibres during dry and moist conditions.

4.11.4. Swelling analysis

Swelling ratio performed on CH electrospun fibres for both orientation upto 48 hrs is shown in the Figure 112. Within the first 15 mins equilibrium state was reached and a swelling of 70 to 80% is reached which plateaued with time. Random fibres showed lesser water uptake but this difference was not statistically significant

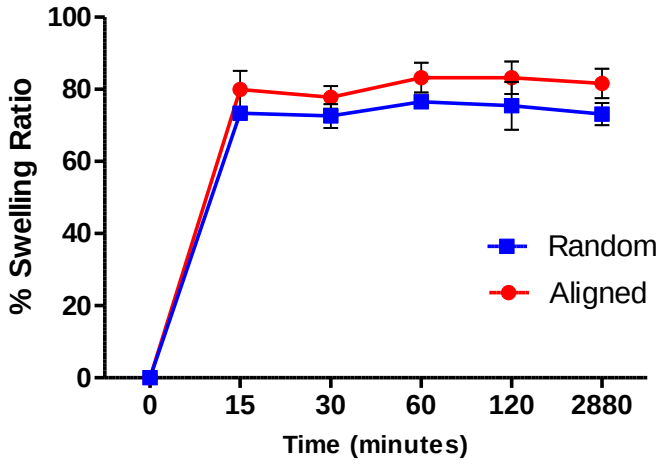

Figure 112: Swelling ratio of CH random and aligned fibres over a period of 48 hours, (n=3).

4.11.5. In-*vitro* Degradation analysis

In-*vitro* degradation of electrospun fibres were conducted by adapting the methodology described earlier. Degradation was studied by analysing the weight loss profile, FTIR spectroscopy, pH analysis and UV-Vis spectroscopy of the degraded supernatant.

4.11.5.1. Weight loss

Weight loss analysis to assess the degradation profile of CH random and aligned electrospun fibres (Figure113) reveals an initial % weight loss of 20% at day 4 for both random and aligned fibres. At day 7 random fibres show 40% weight loss which is significantly higher than weight loss of aligned fibres on the same day. Weight profile of random fibres showed a fluctuation in weight loss pattern as compared to aligned fibres that showed a gradual decrease in weight loss pattern over the 28 days of experimental period.

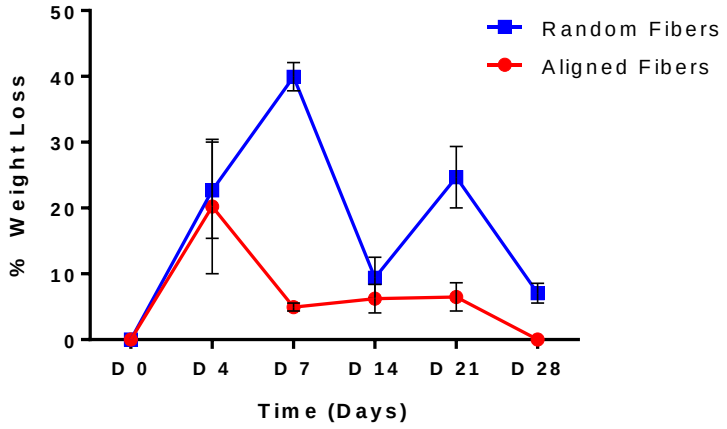

Figure 113: Degradation profile of Chitosan random and aligned fibres assessed over a period of 28 days using lysozymes. Values shown are mean ± SEM (n=3).

4.11.5.2. UV-Vis Spectroscopy

In vitro degradation assessed by analysing the degraded supernatant of CH fibres by UV-Vis Spectroscopy is shown in Figure 114. UV-Vis spectral data of degradation media gives rise to two new absorption bands at 230 and 290 nm respectively. Original CH is known to exhibit a strong absorption band at 200 which is visible in all spectra. Bands at 230 could be due to the n-σ * transition attributed to the amino group and π-π* transition denoted to carbonyl or carboxyl groups. Data collected from Day 4 to 28 showed that the bands intensity had changed with time.

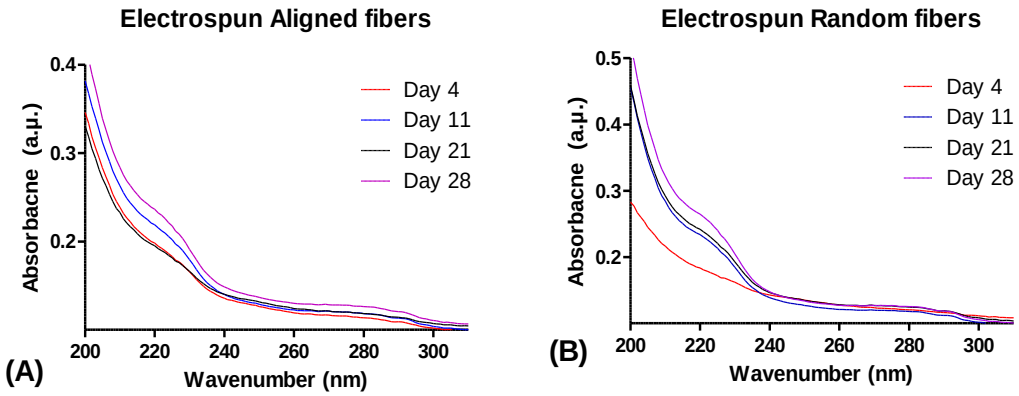

Figure 114: UV Vis spectroscopy of degraded solution conducted for degradation media of random and aligned CH fibres for day 4, 11, 21 and 28 between a range of 200 to 400nm.

4.11.5.3. pH analysis

pH change observed over the 28 day experimental period to study degradation of CH electrospun mats of random and aligned orientation is shown in Figure 115.

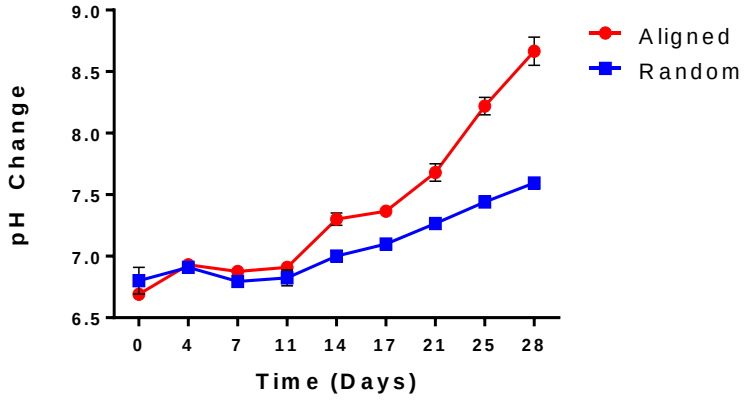

Figure 115: pH analysis of degraded media of random (ER) and aligned (EA) chitosan fibres over a period of 28 days, (n=3).

A gradual increment in the pH value was noticed from day 1 to day 28 with Aligned mats showing an increase in overall pH value from 6.7 to 8.5. Random fibres showed a similar trend although at day 28 the final pH value was 7.5.

4.11.5.4. FTIR spectroscopy

FTIR was employed to study the structural changes and degradation products as a function of time. Spectral data collected at consecutive days from day 4 to 28 to depict changes in the finger print regions of both aligned (Figure 116) and random (Figure 117) fibres. A prominent band at 1552cm^{-1} usually attributed to Amide II region and NH bending vibration in amide group was observed. The spectral bands at 2919 and 2800cm^{-1} due to CH_2 stretching vibration decreased in intensity for both fibre orientations. Shifts in the –NH and –OH stretching vibration around 3300cm^{-1} are also visible, these shifts are seen towards higher wavenumbers. The glucosamine unit of CH commonly appearing at 1150 and 1040cm^{-1} region also show subtle changes in the intensity over time, possibly indicating bond breakage in between CH and PEO with respect to time

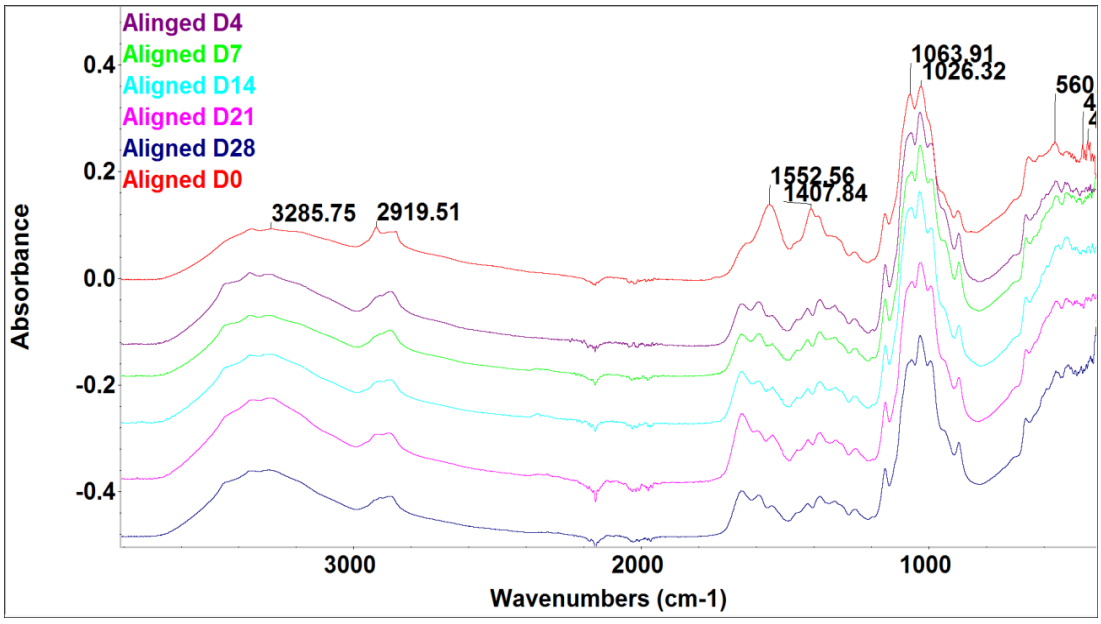

Figure 116: FTIR-ATR of Aligned Chitosan fibres on Day 0, 4, 7, 14, 21 and 28 of degradation in Lysozyme solution.

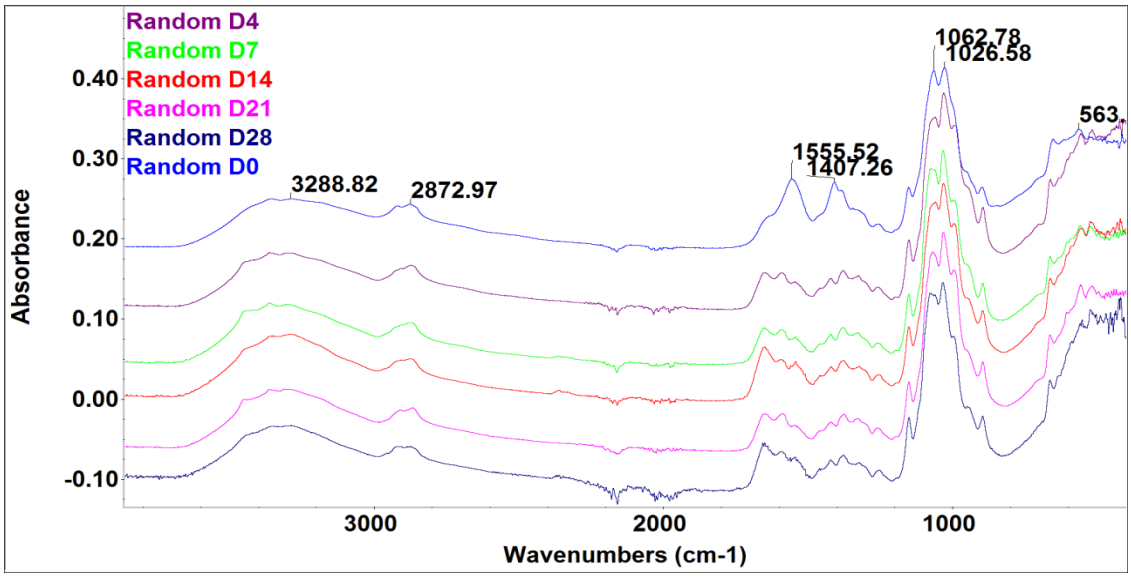

Figure 117: FTIR-ATR of Random Chitosan fibres on Day 0, 4, 7, 14, 21 and 28 of degradation in Lysozyme solution.

4.11.6. Biocompatibility assay

Alamar blue assay conducted on random and aligned CH fibres after culturing with MG63 and hES-MP cell line are shown in Figure 118 (a & b). Cells were cultured for 7 days and assessed for viability on Day 1, 4 and 7. Statistically significant results were obtained when comparing day 1 to day 7 with each type of fibre orientation. Although on day 7 within each group no significant difference was noted. For hES-MP cell line statistically significant difference was noted for day 1 values, and aligned orientation showed higher viability when compared with randomly orientated CH fibres. Mineral deposition on electrospun CH fibres was assessed by quantifying total Collagen and calcium deposited by hESMP's.

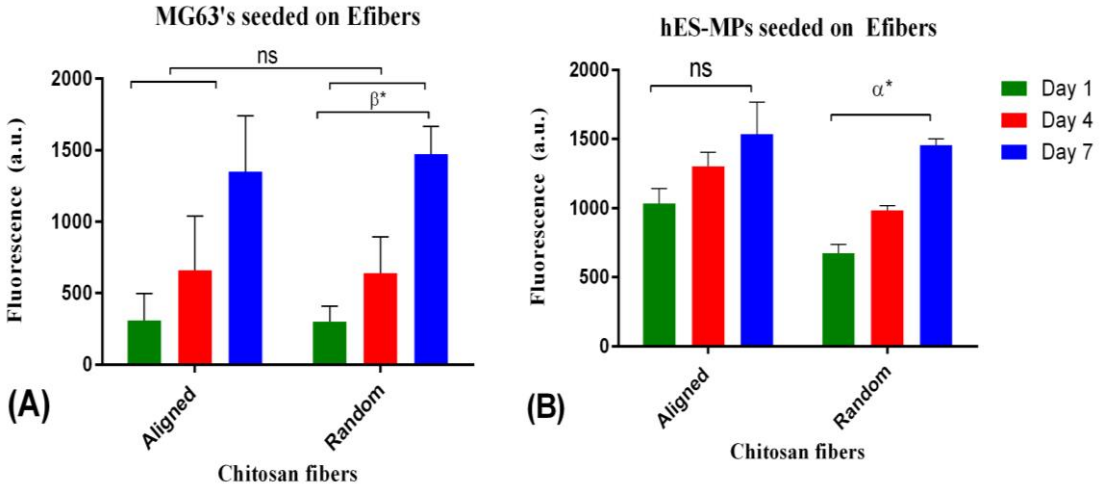

Figure 118: Cell Culturing performed on Random and Aligned CH fibres by seeding (a) MG63 and (b) hESMP's for viability on Day, 1, 4 and 7 by Alamar blue. (A) β* statistically significant difference in between D1 and 7 for random fibres. (ns) non-significant difference was

observed between Aligned and random among the two groups. (B) α* significant difference between D1 and 7 for random fibres. (ns) non-significant difference was observed between D1 and 7 for aligned fibres.

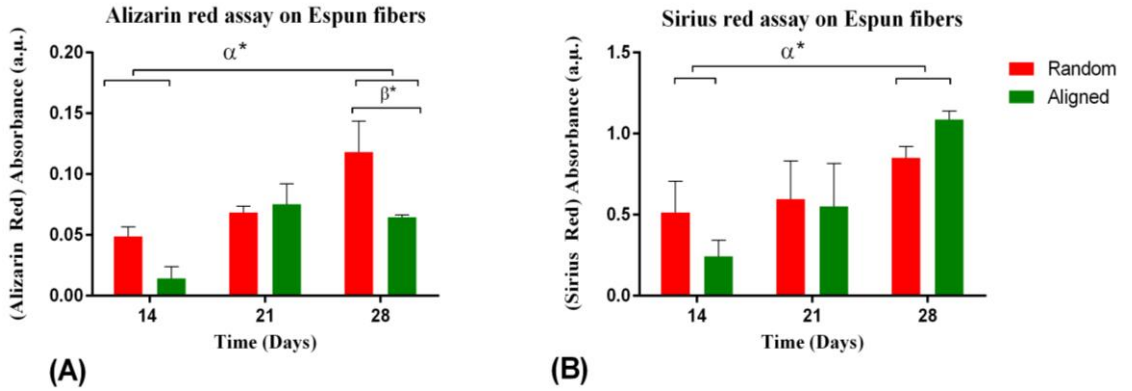

Figure 119: Matrix deposition assessed by Sirius red and Alizarin red staining at Day 14, 21, and 28 of culturing with hESMP's on random and aligned Chitosan electrospun fibres. (A) α* significant difference was observed for calcium deposited in between D14 and 28. β* significant difference was noted on D28 in between random and aligned fibres. (B) α* significant difference was observed for collagen deposited in between D14 and 28

Calcium deposited at day 14, 21 and 28 of culture with hES-MPs, shown in Figure 119. For calcium deposition random fibres showed a statistically significant difference when compared at day 14 with random fibres. At day 28 no significant difference was observed, however, at day 28 random fibres showed significantly higher values. Collagen deposition assay at day 14 showed significantly higher values. From day 14 to 28 there is an increasing trend in the absorbance values for collagen deposition. Aligned CH fibres showed a slightly higher value at day 28 but this is not significant when compared within the group.

4.11.7. Histology

Histological sections were taken to examine the extent to which hES-MP cells penetrated CH electrospun scaffolds on day 14 of culture (Figure. 120). In general, the random fibres exhibited a greater level of infiltration showing almost full coverage into the scaffolds observed via H&E. Aligned fibres had less cell penetration and separated looking layers of matrix deposition were observed within the fibres

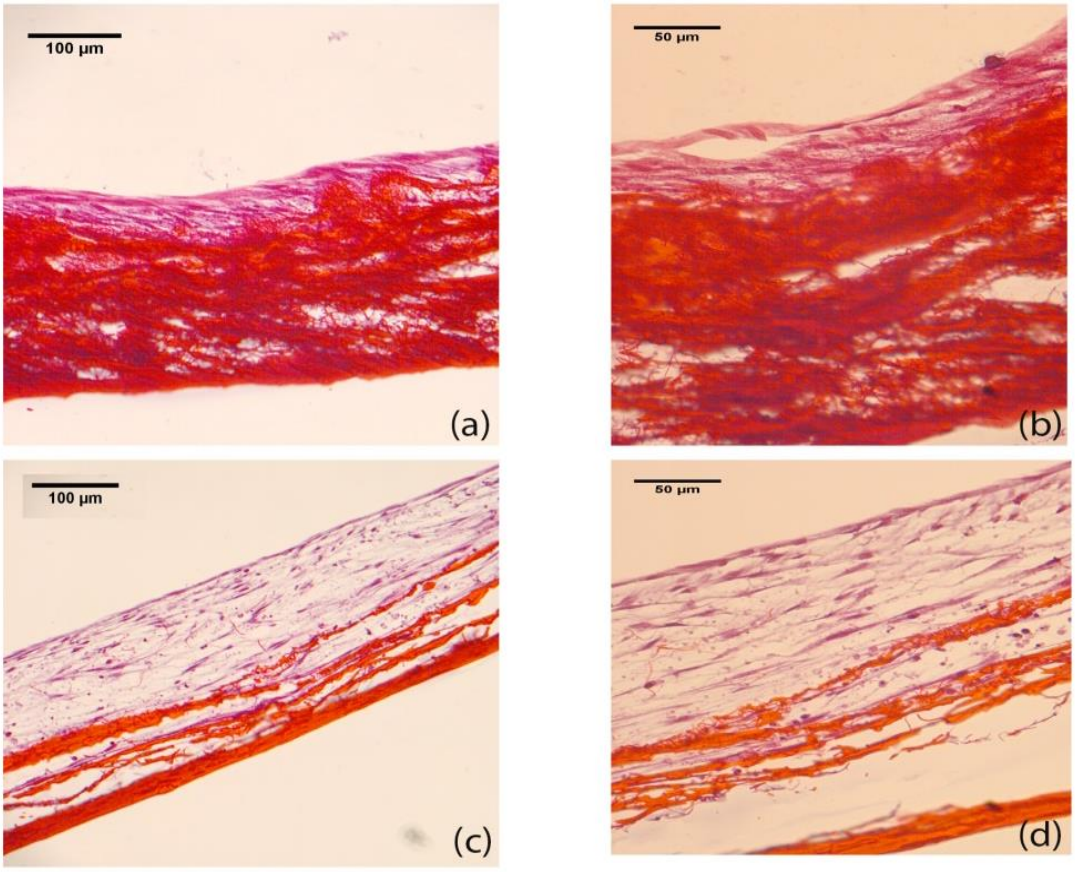

Figure 120: H&E of Random (a and b) and aligned (c and d) CH fibres performed after cryosectioning at D14 of culture with hESMP's. Images scaled at 100 and 50µm, taken at a magnification of 20x and 40x.

SECTION IV

4.12. Functionally graded membranes

4.12.1. Introduction

This section presents results obtained by combining the freeze gelation and solvent casting technique to accomplish a template for functionally graded membranes for periodontal tissue engineering. A trilayered membrane was synthesized using solvent casting of LMw 30:70 membrane on which MMw 3% (wt/v) of CH solution made up in 0.2M Acetic acid was poured. The membrane was casted according to the methodology described in the methods section 3.4. The FG solution was casted as soon as a partially rough and partially shiny surface of the membrane appeared which was taken to be indicative of some solvent evaporation. FG solution was cast with the adapted protocol for freeze gelation as mentioned in the methods section 3.5. Characterisation was carried out using SEM analysis to study morphological features of the surface and Raman Mapping was performed identify the HA distribution in the as prepared template. Figure 121 shows the handling properties of the trilayered membrane.

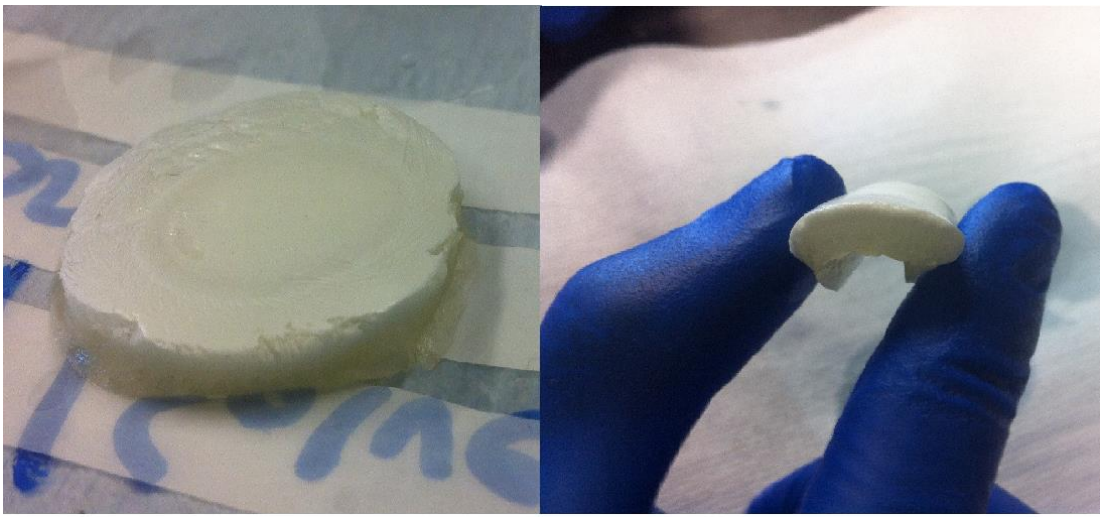

Figure 121: Macroscopic Image showing the prepared trilayered membranes. Bottom layer showing HA.

4.12.2. Scanning electron Microscopy

SEM microscopy of Trilayered template is shown in figure 122. The images depict the morphological features of the top surface, bottom surface and cross section. Pore size distribution has also been

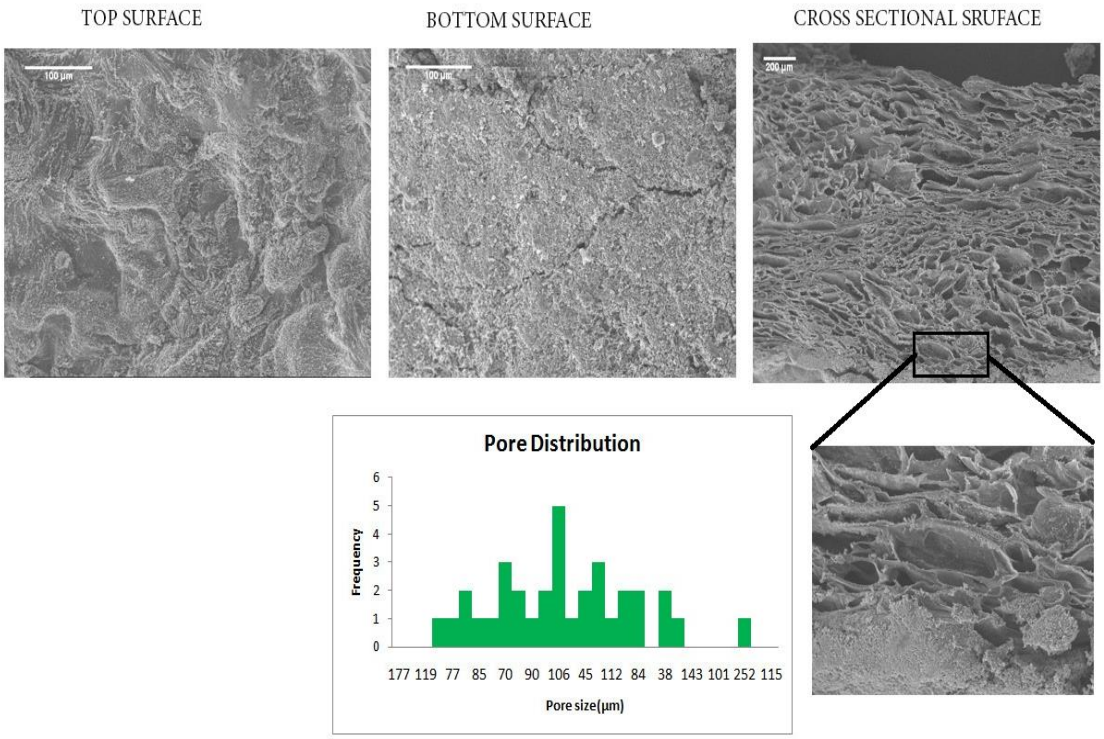

Figure 122: SEM analysis of Top, Bottom (scaled at 100µm) and Cross-sectional (scaled at 200µm) surface with a pore distribution graph. Pore size measured by using Image J software. INSET image shows a more magnified pore morphology.

plotted. With an average pore size ranging from 30 to 200µm counted by the cross sectional porous features. Top surface has an uneven profile and the bottom surface shows presence of HA particles. The cross sectional topography depicts porous features with a wide range of pore distribution. Inset image shows a more highly magnified image of the pore morphology.

4.12.3. Raman Spectroscopy

Raman Spectroscopy was adapted to perform detailed mapping and chemical imaging of the trilayered membrane. The main aim was to assess the CH and HA distribution through the cross-section of the sample. Samples were mounted on a special sample holder able to grasp the specimen and a blade was used to slice the specimen, hence, exposing the cross-sectional interfaces for more convenient mapping and imaging. Figure 123 depicts images

showing the contents of the membranes as identified by multivariate curve resolution (MCR) analysis. The ingredients/ constituents are each assigned different colours to produce a colour coded chemical image from an automatic library search built in the software. MCR analysis was specified to identify 4 components. MCR clusters all the spectra's into 4 classes according to how similar they are, and then looks up in the library to identify these components. Adjacent image shows the spectral points that were mapped (1660 points)

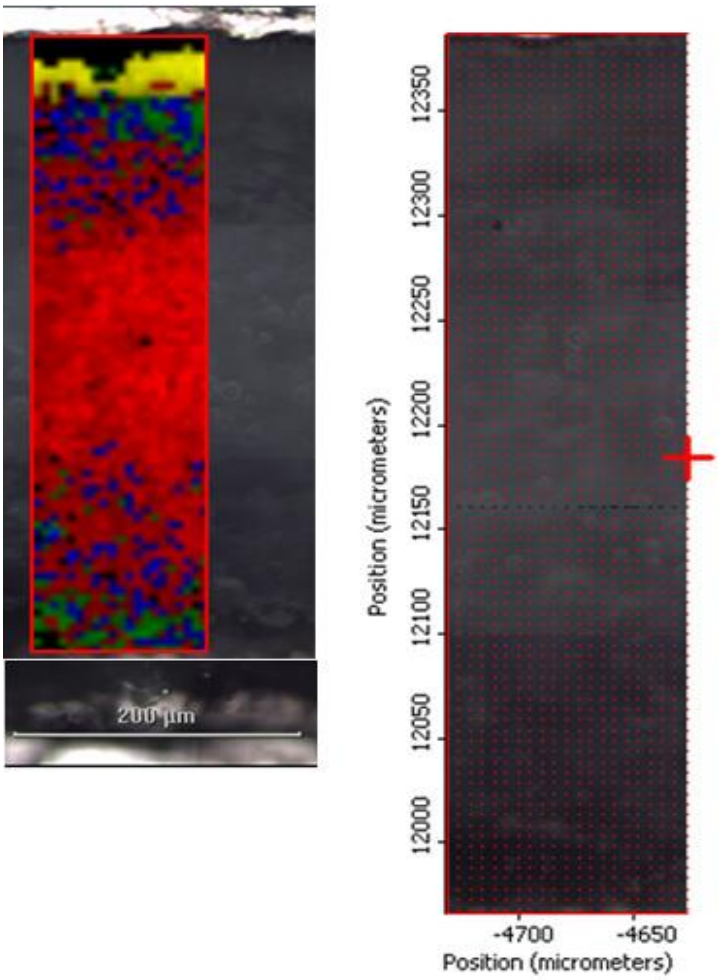

Figure 123: (Left) Image of the intensity map showing different components as picked up by the software library and (Right) Number of points collected on the spectra 1660 spectra in 5.42 minutes. Mapping of cross-sectional segment.

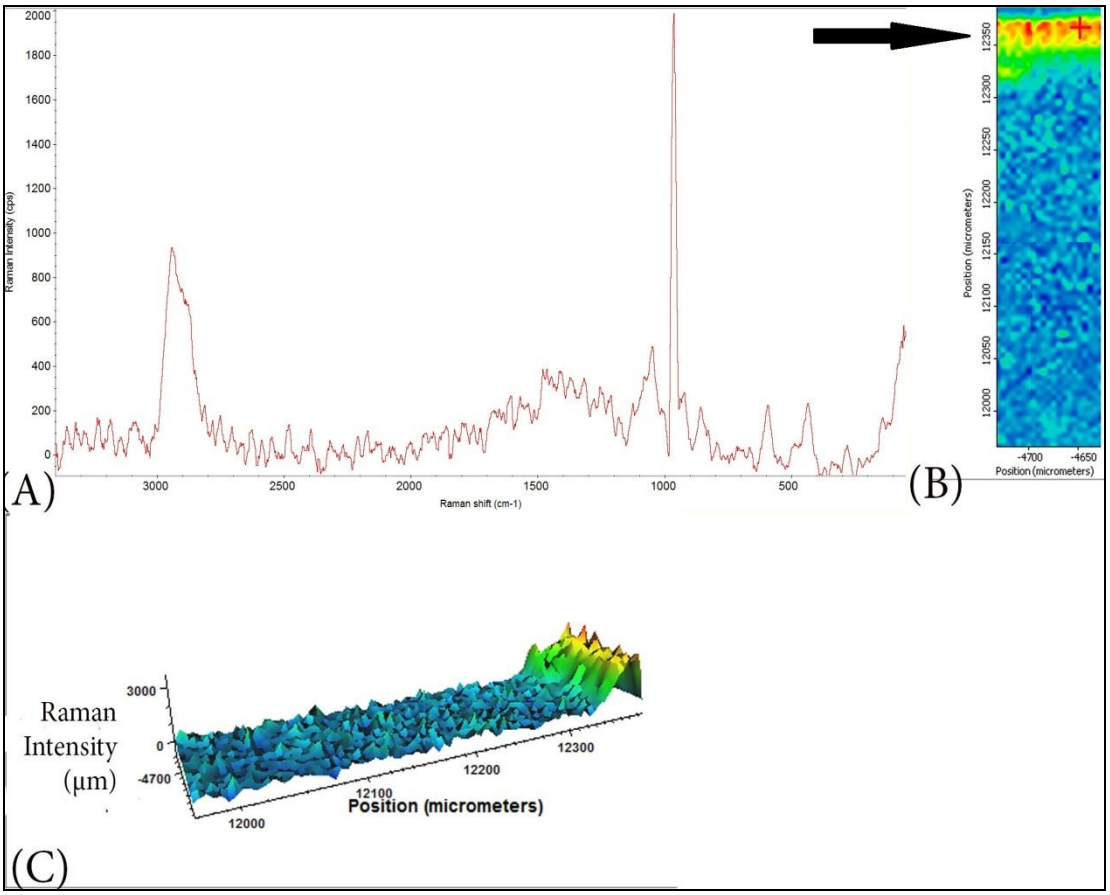

Figure 124: (A) Raman Spectra of Trilayered Membrane depicting high intensity of HA present as shown by peak at 962cm^{-1}, (B) Cross sectional image showing intensity when phosphate bad of HA selected shown by the black arrow point towards the cross hair, (C) A 3D image of the intensity map showing HA distributed only at one side of the membrane.

Figure 124 shows the results obtained by Raman spectra when selecting the phosphate peak of HA at 962cm^{-1}. Other spectral bands present at 432, 590 and 1072cm^{-1} are also due to HA presence within the scaffold. Bands in the region of 2885cm^{-1} are assigned to CH_2 stretching vibration due to CH. This shows a very high intensity which is evident in a colour coded chemical map of the spectra from the sample (B). The red region in the map shows high intensity of this particular HA peak, which is absent in the rest of the map indicating that HA is predominantly present only at one side of the scaffold. Figure (C) depicts a 3 dimensional presentation of the image (B). This gives an alternate view to how the HA is distributed with in porous scaffold.

Figure 125 (a) Depicts the Spectral bands in the region of CH_2 stretching vibration at 2894cm^{-1} and 2934cm^{-1} due to CH_3 stretching vibration appearing attributed to the presence of CH. Other bands attributed to CH which can be observed in the spectra are 488cm^{-1} attributed to in-plane bending vibrations due to C-O-C (glycosidic linkages), 853cm^{-1} stretching vibration of pyranoid ring, 925cm^{-1} ascribed to CH stretching , 1059cm^{-1} is attributed to bending vibration due to CH and OH , 1417cm^{-1} appear due to bending vibration of CH_3 and CH. When the cross-head is used to select the (B) middle 1/3 of the specimen the bands due to HA have diminished and have lower intensity as shown by the colour coded chemical 2D correlation map. (C) Shows the same colour coded 2D map plotted in form of a 3D map, representing the distribution of CH. The 3D map depicts an even distribution of CH throughout the sample with the plane declining towards the side where HA in concentrated.

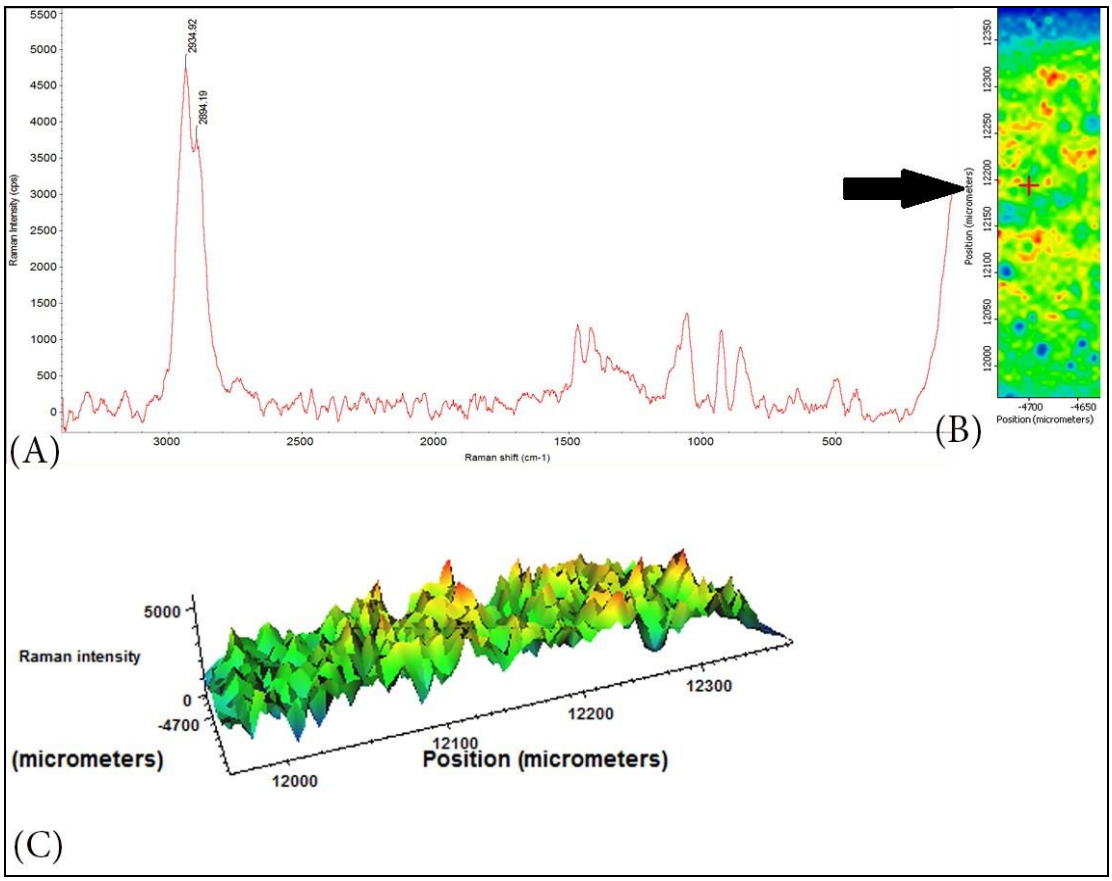

Figure 125. A) Raman Spectra of Trilayered Membrane depicting high intensity of CH present as shown by the peaks present around 2900cm^{-1} indicative of polysaccharide structure, (B) Cross sectional image showing intensity when selecting middle part as shown by the black arrow point towards the cross hair, (C) A 3D image of the intensity map.

Figure 126 (A) Shows the Raman Spectra obtained when selecting the bottom surface of the specimen. The Spectra obtained is similar to that obtained for the middle 1/3. Stretching vibrations due to CH_2 appear at 2894cm^{-1} and CH_3 stretching vibration are seen at 2934cm^{-1} , both being attributed to CH molecular structure. The colour coded map (B) shows the 2D profile of the selected region and (C) shows a 3D profile of the same 2D map showing a more descriptive image of the CH distribution within the trilayered scaffold

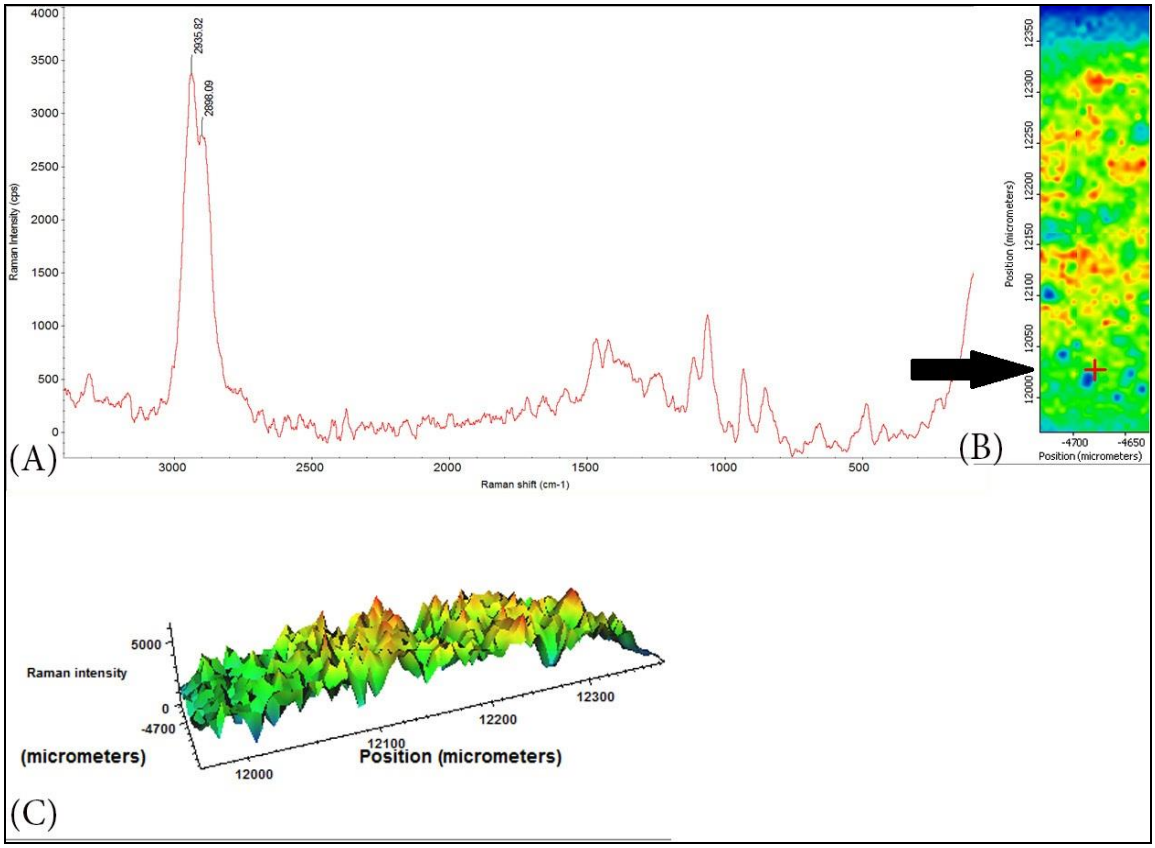

Figure 126. A) Raman Spectra of Trilayered Membrane depicting high intensity of CH present as shown by the peaks present around 2900cm-1 indicative of polysaccharide structure, (B) Cross sectional image showing intensity when selecting bottom part as shown by the black arrow point towards the cross hair, (C) A 3D image of the intensity map.

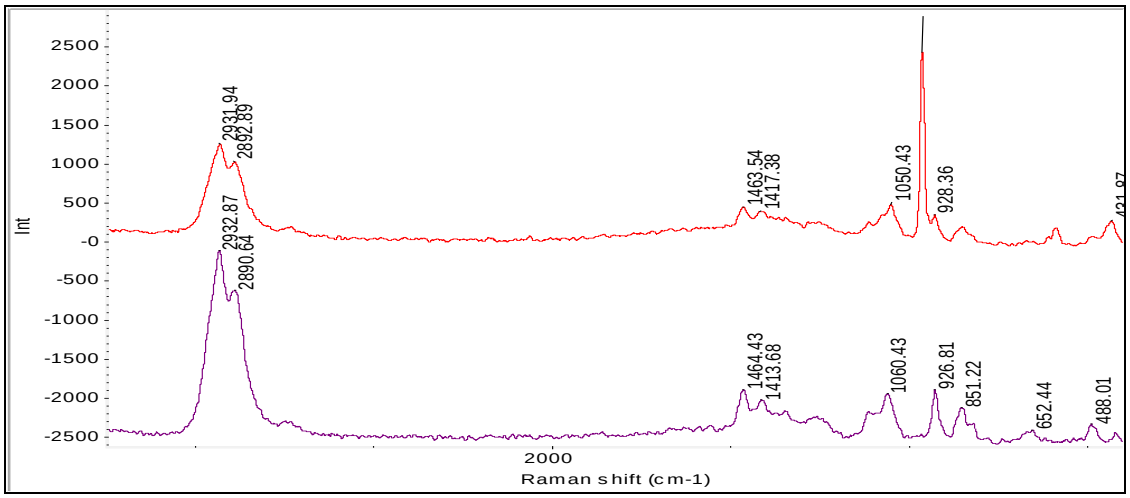

Figure 127. Stacked Raman Spectra of top surface (Red) shows high intensity of HA at 962cm^{-1} and Middle (Purple) spectra showing higher intensity if CH bands

Figure 127 shows Raman spectral data accumulated from the HA dominating surface and the core porous structure side. Difference in the spectral profile is clearly visible as a very strong and sharp peak pertaining to phosphate in HA lattice structure is indicative of presence of HA whereas the bottom image shows a strong band near 2300cm^{-1} attributed to CH structure.

5. Chapter. Discussion

5.1. Introduction

This chapter will encompass detailed description of the results obtained in Chapter 4. Each layer of the functionally graded membrane is discussed in order of the results obtained. Membranes/thin films, freeze gelated (FG) membranes and electrospun fibres were characterized using Scanning electron microscopy (SEM) to image the surface topography and morphological features, Fourier Transform infrared (FTIR) spectroscopy for chemical mapping and molecular interactions, swelling ratio, degradation profile and mechanical properties for tensile strength analysis. Degradation studies were conducted by monitoring the weight loss profile, pH change, FTIR spectroscopy and Ultraviolet visible (UV-Vis) spectroscopy of degraded supernatant. Biological characterisation was carried out by culturing human osteosarcoma (MG63) and mesenchymal progenitor cell (hES-MP) for up to 7 days and assessing for viability and proliferation by Alamar blue assay. Matrix deposition was assessed by culturing hES-MP cell line for quantifying collagen and calcium deposited for up to 28 days. Histological sections were performed to see the cellular attachment and migration. Staining was also performed for membranes to visualize cell morphology after attachment. Drug dissolution study was also carried out using FG membranes. Drug entrapment measurements were done by weight analysis and percentage recovery was performed using UV-Vis spectroscopy. Surface morphology was characterised by SEM and FTIR spectroscopy was adapted for studying surface and bulk chemical interactions of drug and cross-linking agent.

Various regenerative therapies have been pursued to engineer graded tissue interfaces that restore native tissue architecture and function. Currently available regenerative membranes rely on the amalgamation of different cell types and growth factors within multi-layered 3D scaffolds (Phillips *et al.* 2008). Engineering complex tissues is said to be the most determined goal of all tissue engineering community. The ability to harness engineering of functional interfaces with structural hierarchy and complex functional feature is emerging as an unparalleled scientific and technical challenge for the upcoming generation of tissue engineers. This has led to the concept of fabricating structures with compositional gradients or sub compartments and using different cell types to drive tissue or organ morphogenesis (Mikos *et al.* 2006). The regeneration of lost periodontal tissues after a chronic episode of periodontitis in a functional relationship with one another also remains a challenge for clinicians and tissue engineering researchers.

SECTION I

5.2. Membranes

The main aim of this study was to synthesise composite membranes that could serve as a non-porous surface layer of the functionally graded membrane. One of the crucial aspects of GTR membranes is to act as a seal to prevent the epithelium from growing into the defect which could result in formation of a long junctional epithelium and result in healing by repair. The discussion below is based in the order of the results obtained

5.2.1. Scanning Electron microscopy

An important application of the fabricated membranes is to act as an occlusive barrier. The results obtained showed that the top surface of all as prepared membranes had a dominance of CH and the bottom surface showed presence of HA in varying ratios. It was envisaged that CH side will have no osteoconductivity, hence, acting as a bioinert side, while the osteoinductive HA side will promote bone regeneration. Moreover, the HA side was intended to face the defected hard tissue side and CH was intended to face the soft tissue interface. Although there have been several previous studies involving membranes made from CH and HA (Xianmiao *et al.* 2009; Fraga *et al.* 2011; Li *et al.* 2012), they have reported on composite membranes fabricated using various ratios of bioceramics (µm to nm) and CH, a study mentioning about the high degree of segregation as achieved in this study is yet to be reported. The morphological features of the top and bottom surface showed clear discrepancies. SEM characterisation of the top surfaces of LMw and MMw membranes revealed a greater amount of CH, while the bottom surface showed HA particles and as the ratio of HA increased from 30% to 70%, more tightly packed HA particles were observed. Li *et al.,* have reported in their study; that as the concentration of nano-HA (n-HA) increased from 5 to 30%, roughness of both surfaces of the composite membrane increased. They also observed rift in the bottom surface of the membrane when nano HA content increased to 15% (Li *et al.* 2012). However, in this study the addition of HA to up to 70% was suitable, as more HA will create a more osteoconductive membrane and will be favourable for its final *in vivo* application as a GTR membrane. It would also be interesting to increase the HA content to 80% to observe the polymer ceramic interactions in future. Another recent study by Mohamed and co-workers has reported that a composite membrane of CH, gelatin and nHA content of upto 80% fabricated, there aim was to assess in-*vitro* bioactivity in SBF. The study revealed that CH, gelatin and HA of up to 70% was favourable for deposition of a carbonated apatite layer on composite membrane surfaces (Mohamed *et al.* 2014). In this study the HA surface would

eventually cover the periodontal wound site to help assist bone regeneration and the inactive CH surface will act as a gel to hold the HA particles together. This high degree of segregation was achieved by slowing the evaporation rate of the solvent and allowing the dense HA to settle to the bottom using the simple technique of solvent casting. Although this segregation was deemed enough to promote interactions of HA to CH for bond formation as reported in the next section by FTIR studies. It would also be interesting to increase the HA content to 80 or 85% to assess how much CH interacts with HA in such a high amount.

5.2.2. Fourier Transform Infrared (FTIR) Spectroscopy

FTIR spectroscopy in conjunction with a Photoacoustic sampling (PAS) accessory has been utilized to obtain detailed information on the interactions of HA with CH. This is in comparison to attenuated total reflectance (ATR) used as a sampling technique with FTIR, where more surface interactions are studied PAS provided bulk information enabling the detection of different chemical groups in detail. FTIR results obtained in this study were in agreement with work performed by previous researchers on composite membranes only (Thein-Han and Misra 2009; Maganti *et al.* 2011). Although, the clear discrepancies observed in between the spectral information of top and bottom surfaces are yet to be reported. Chemical changes were observed for either side with some degree of interaction between the two components more prominent on the spectral information collected on bottom surface of membranes. The top surface dominantly presented strong CH bands with very weak intensity of bands pertaining to HA. Other studies performed with regards to the fabrication of CH:HA composite membranes with varying ratios of CH to HA have mentioned about shifting of the absorption bands around 1654cm^{-1} and 1595cm^{-1} to lower wave numbers with increasing HA content (Teng *et al.* 2009; Xianmiao *et al.* 2009). This decrease in intensity of the band of HA is due to the gradual binding among Ca^{2+} ions of HA to $–NH_2$ groups of CH. Pointing towards the occurrence of covalent bond formation in between CH and HA as reported by Brugnerotto and co-workers (Brugnerotto *et al.* 2001; Xianmiao *et al.* 2009). Xianmiao and co-workers have reported that disappearance of –OH functional group of HA and the movement of polar groups of CH in their study was suggestive that hydroxyl ions on the surface of HA might interact with plentiful amino and hydroxyl ions of CH by formation of hydrogen bonds (Xianmiao *et al.* 2009). Furthermore, they also mentioned that there might be co-ordination bonds in between $–NH_2$ of CH and Ca^{2+} of HA. Since calcium ions have a co-ordination number of 7 and are strictly held in structure (Kikuchi *et al.* 2004; Xianmiao *et al.* 2009). These co-ordination bonds have also been confirmed by Yamaguchi and co-workers as well (Yamaguchi *et al.* 2003). In another

study based on synthesis of porous CH HA composites for TE by Kim and co-workers, it stated that during the composite process CH encloses the HA particle inside the polymer (Yamaguchi *et al.* 2003; Kim *et al.* 2007). Furthermore; they also mentioned that c-axis of HA crystal tends to align itself along the CH chains. In another similar study by Thein *et al.,* they reported that peaks around 3200 and 3400cm^{-1} underwent shifts in composite templates. They mentioned that these changes represent polar movements of polar groups of CH suggestive that –OH ion at the surface of HA could possibly have interactions with amino and hydroxyl groups on CH as mentioned earlier, hence, promoting the formation of hydrogen bonds and also hydrogen bonding in between CH and HA point towards decrease of CH crystallinity with an increment in HA content of composites (Thein-Han and Misra 2009; Xianmiao *et al.* 2009). These changes reported earlier were in accordance with our results. The Figure 127 depicts the shifts in the peaks around 3300cm^{-1}of MMw CH:HA membranes which occur due to stretching vibration of -OH group via hydrogen bonds. It can be observed, how the ratio of HA affects the regions of –NH and –OH stretching vibration (Figure 128). A subtle shift can be appreciated in the peak for 100:0 is appreciated at 3367cm^{-1}, addition of HA in a ratio of 70:30, shifts it to 3351cm^{-1},and at 50:50 at the band appears at 3361cm^{-1} at 30:70 its 3352cm^{-1}.

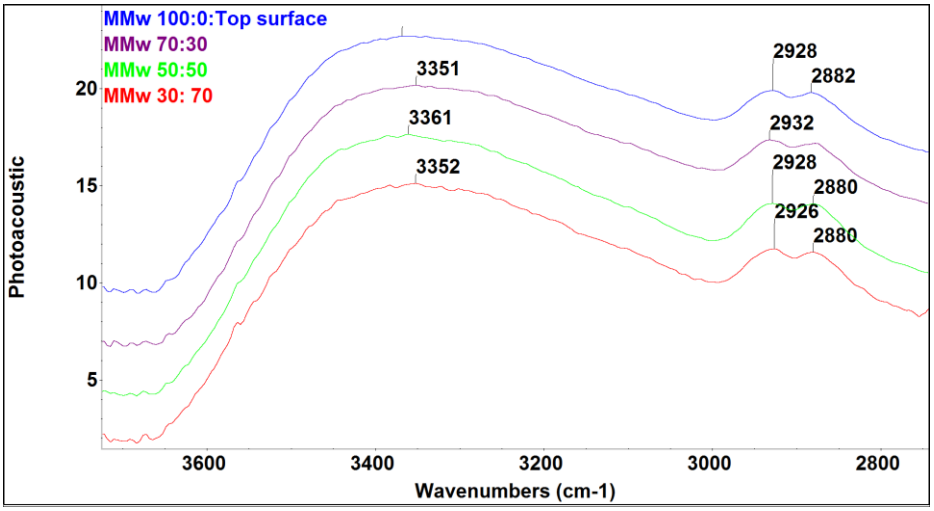

Figure 128: FTIR -PAS of MMw 100, MMw 70:30, MMw 50:50 and MMw 30:70.

Another study conducted by Wawro and Pighenilli on modified CH fibres by HA and tricalcium phosphate (TCP) nano-particles have proposed that the chemical interactions between inorganic and organic constituents of composite could probably occur due to ionic interactions (ionic bonding) between Ca^{2+} and phosphate groups and amino groups of CH. They also mentioned that CH has a high zeta potential which can enhance the colloid stability of HA. Moreover, with regards to the interactions between CH and HA, it was proposed that

strong adsorption interactions also exist in between CH and HA (Wawro and Pighinelli 2011). This adsorption of HA molecules on CH could be due to displacement of surface ions, for example, carbonate, phosphate, calcium and hydroxyl groups. HA is well known to allow not just surface interactions with other molecules but also incorporate ions into its crystal lattice structure (Wawro and Pighinelli 2011). Although the exact mode of interaction between CH and HA could not be determined in this study, composite spectra of CH and HA can be interpreted to come to a conclusion which can be summarised for further studies on CH and HA. Another study based on evaluating the structural analysis and electronic properties of CH and HA interactions by El-Sayed *et al.,* have mentioned about various possibilities in which a HA particle can form bonds with CH by modelling using FTIR analysis and thermodynamic studies, they reported that HA could be interacting through OH, and/or $Ca^{2+,}$ (El-Sayed *et al.* 2009). Closer observations of bottom surface of LMw membranes (figure 129) show how the functional group of HA (-OH peak) at 3369cm^{-1} is affected in intensity with the increasing ratios of HA from 70:30 to 30:70. This confirmed higher HA amount as the ratios increase in different membranes and possibly indicative of stronger bonding. Moreover; the peaks were in correlation to the results obtained previously by different groups (Araujo *et al.* 2009; Kithva *et al.* 2010; Fraga *et al.* 2011).

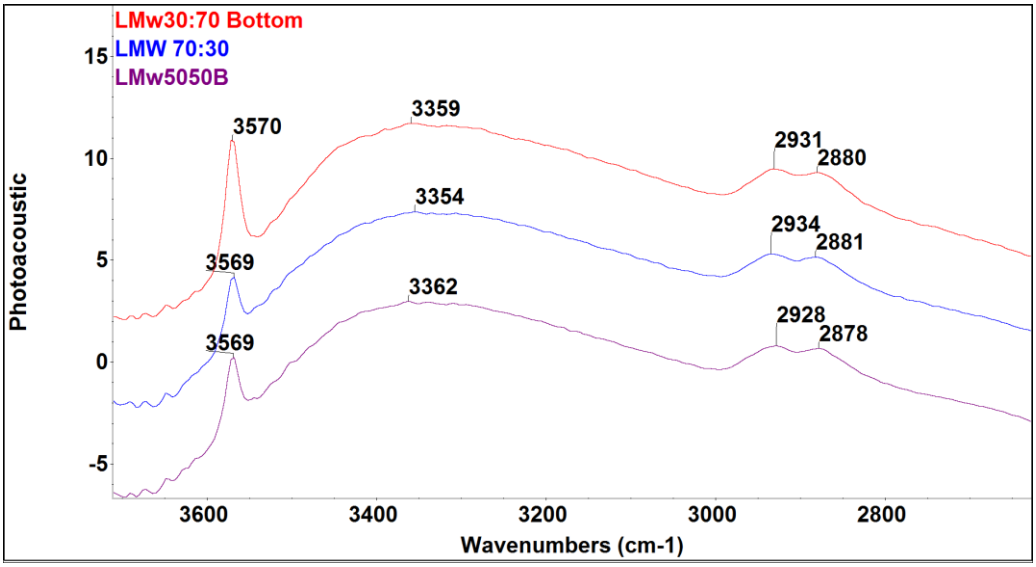

Figure 129: LMw bottom surface of 70:30, 50:50 and 30:70.

Closer observations of bottom surface of the molecular fingerprint region of LMw and MMw membranes (Figure 130) have shown differences in the intensity of bands at 1559cm^{-1} present due to –NH bending vibration in amide group and peak at 1420cm^{-1} normally attributed to C-H symmetrical deformation have shifted to 1414cm^{-1}. As the ratio of HA increases the CH bands appearing due to Amide II and C-H stretching bands shifts to lower

wave numbers. Xianmiao and co-workers report the possible interaction between CH and HA illustrated in the diagrammatic representation shown in Figure 131 (Xianmiao *et al.* 2009).

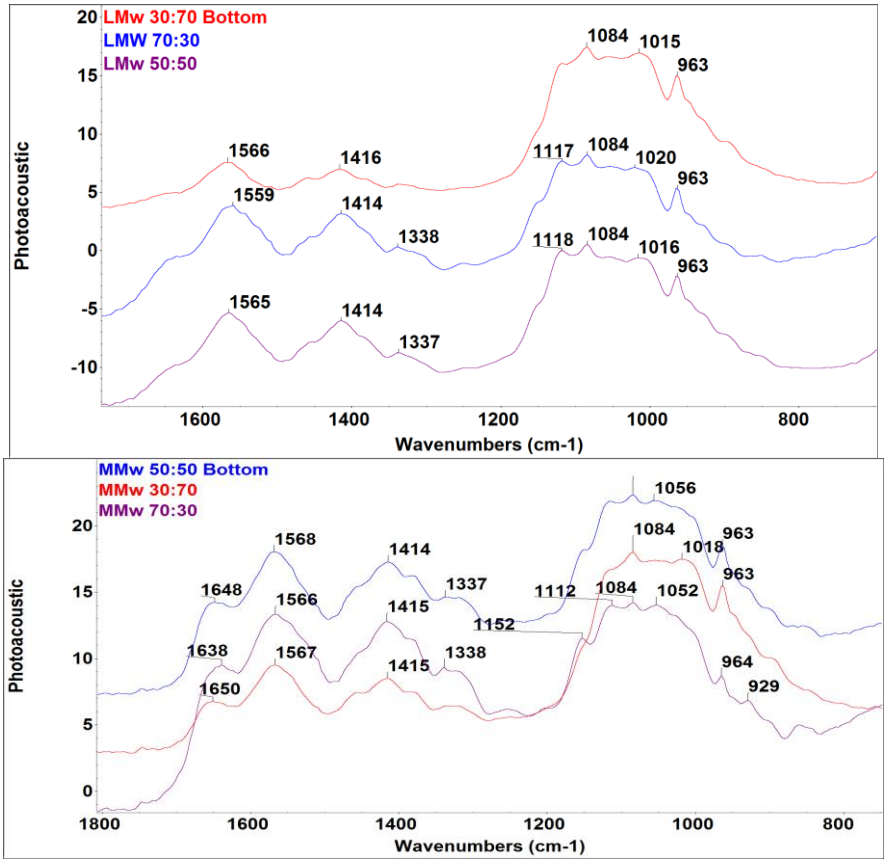

Figure 130: Molecular finger print region of (top image) LMw membranes 70:30, 50:50 and 30:70 and (bottom image) MMw membranes 70:30, 50:50 and 30:70.

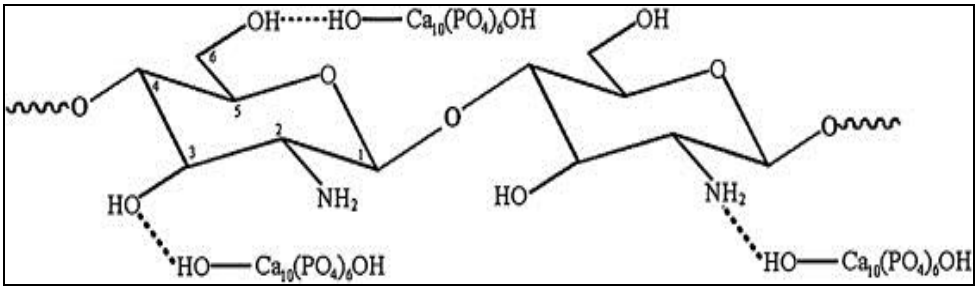

Figure 131: Chemical interactions in between CH and HA as proposed by Xianmiao *et al.*, 2009(Xianmiao *et al.* 2009) Adapted with kind permission from Publisher.

5.2.3. Tensile properties

Characterisation of tensile properties of biomaterials intended for use in periodontal tissue engineering is essential to determine the ability of scaffolds to be clinically handled during surgical procedures and be able to with stand forces when implanted against the defect site

for bone healing. Mechanical properties of CH are correlated with the degree of deacetylation (DD). Higher DD of CH will exhibit better mechanical properties. Based on the results of tensile testing performed on our membranes, it was evident that the addition of HA resulted in an overall lower tensile strength. A study conducted previously by Teng and co-workers on synthesis of CH and HA membrane by filtration process, have also reported similar findings, where the composite membranes were reported to exhibit lower tensile strength (Teng *et al.* 2009). Teng *et al.,* performed this testing under dry conditions and mentioned that the tensile strength of the membranes decreased linearly with increasing HA content. Furthermore, they mentioned that as the HA content increased, the *E* exhibited an initial rapid increase followed by gradual decrease as well. The decrease in *E* values was also observed in the current study where; addition of HA to LMw and MMw in increasing ratios showed a decline in the UTS values. Furthermore, they also mentioned that addition of 20% HA increased the *E* to 1303MPa which was significantly higher than virgin CH membranes. Interestingly further addition of HA caused a decline in properties (Teng *et al.* 2009). Studies conducted on incorporation of HA to other polymers have usually reported an increment in mechanical strength (Kim *et al.* 2005; Pandey *et al.* 2006). However, this was in contrast to the results obtained for our membranes.

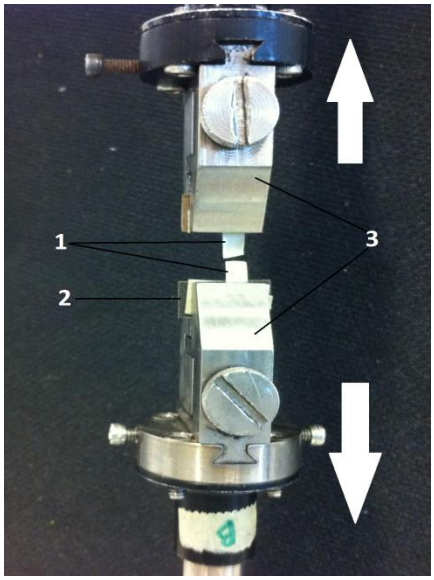

Figure 132: Tensile testing of membranes (1) Membranes mounted in clamps showing splitting in the middle due to tensile tests, (2) Sand paper used to have a tighter grip to prevent slippage. (3) Clamps holding the membranes. Arrows shows the direction of force being applied.

This behaviour can be correlated to the internal properties of this biopolymer. Unlike the other polymers CH, exhibits a brittle nature due to its rigid crystalline nature. Therefore; the incorporation of HA as a composite, which itself has a brittle nature and is used in combinations with other polymers to improve its handling will most certainly enhance the brittle feature of CH HA membranes, ultimately causing a decline in the overall properties of composite templates (Wan *et al.* 1997; Correlo *et al.* 2005; Teng *et al.* 2009). Furthermore; this decrease in properties can also be explained by inter-molecular interactions of HA to CH. As seen in the LMw 70:30 dry and wet values, addition of 30% HA increases the *E* values significantly. When HA was increased to 50 or 70%, too much HA apparently destroyed the intermolecular interactions of CH molecules, like hydrogen bonding interactions between CH networks. As a result the elastic modulus decreased after reaching a maximum level (Teng *et al.* 2009).

5.2.4. Swelling ratio analysis

To transfer nutrients and metabolites through scaffolds and absorption of physiological fluids like blood and saliva around the injury site, swelling ratio of GTR membranes is a pivotal aspect to be evaluated for barrier membranes. The results obtained were in agreement with swelling profile studies conducted earlier with CH and HA composite templates by Mohamed *et al.,* and Xianmiao *et al.,* (Xianmiao *et al.* 2009; Mohamed *et al.* 2014). Plain CH membrane and those with 70% CH swelled about 55% in case of MMw CH. Mohamed and co-workers reported that CH HA composite with 40% CH showed a swelling ratio of 180% and addition of HA lowered the swelling profile to 90%. They attributed this to the presence of polar groups. Moreover; they also mentioned that –OH of CH interacts with –OH groups of HA leading to reduction in free –OH content, which reduces hydrophilic properties for composites (Wang *et al.* 2009). In another similar study performed by XingLi and co-workers, they mentioned that water is absorbed onto the membranes by two processes; either by water binding to the material itself or water retained in the pore spaces (Li *et al.* 2012). MMw membranes showed higher swelling ratios as compared to LMw membranes and as the ratio of HA to CH increased, the swelling ratio decreased, since CH governs the water uptake ability of membranes. Ren *et al.,* studied swelling properties of CH with different DD, they reported about the inverse correlation of swelling degree with DD, they also correlated this phenomenon to reduction in polar hydroxyl groups and amino groups in the composite membrane (Ren *et al.* 2005). Moreover, other studies conducted on assessing the swelling profile have reported similar findings (Xianmiao *et al.* 2009; Li *et al.* 2012) within 15 minutes of immersion all membranes

reached an equilibrium state with slight fluctuations over the 168 hours profile. Retention of water is beneficial since it traps in between the polymer chain and gives stability to the scaffolds while performing cell viability and proliferation assays (Liu *et al.* 2004; Thein-Han and Misra 2009).

5.2.5. Degradation Studies

Bioresorption has been regarded as a critical factor in biomaterials intended to be used for regeneration of soft or hard tissues as it regulates their bioactivity after implantation. Periodontal tissue engineered cell material constructs, stability up to 4 to 6 weeks has been reported as standard degradation profile (Bottino *et al.* 2012). Comprehensive degradation studies were conducted, for studying the degradation by weight loss studies, pH change, UV-Vis spectroscopy and FTIR-PAS spectroscopy (Murugan and Ramakrishna 2004). HA is a bioresorbable material with a long term resorption profile, its ability to chemically bind with CH to form composites of different shapes and morphologies is undisputed. CH has shown to be degraded by lysozymes (Thein-Han and Misra 2009). It has been reported that N-acetyl glucosamine (NAG) groups and glycosidic bonds of CH chain are targeted by lysozymes (Saravanan *et al.* 2011). In this study MMw CH HA membranes showed stability till the 48th day. Moreover, plain LMw CH membrane started degrading after day 21. Earlier studies have shown that degradation process by lysozymes is usually determined by the DD and crystallinity of CH (Adekogbe and Ghanem 2005; Thein-Han and Kitiyanant 2007). However, the LMw and MMw CH used to fabricate the membranes in this study had the same DD (75-85%). Another study reported that high crystallinity and high DD (93%) of CH resulted in low degradation rate, (20-29% after 28 Days) (Thein-Han and Misra 2009). However, the rates of degradation were different in this study due to the difference in Mw and chain lengths. Hence, the Mw and DD are known to be the most important factors to consider when fabricating scaffolds for periodontal tissue regeneration and they can be used to tune the membrane properties (Dutta *et al.* 2004; Peniche *et al.* 2008; Martínez-Camacho *et al.* 2010).

Furthermore, swelling and degradation of CH is associated with protonation of amine / imine group and mechanical relaxation of coiled CH chains. Diffusion of water into the CH matrix is faster than degradation and the matrix tends to swell prior to triggering degradation (Ren *et al.* 2005; Thein-Han and Misra 2009). Moreover, Ren and co-workers reported that weight loss of CH occurred due to bulk erosion, and this was also reported by Gopferich and co-workers (von Burkersroda *et al.* 2002). Furthermore, they also proposed two theories of CH degradation, bi and tri-phasic degradation. Since, CH is hydrophilic and diffusion of H_2O in CH

matrix is quicker than degradation, the matrix begins to swell before triggering degradation. They further stated that initially swelling and degradation co-exist, but the former surpasses the later, as the matrix swells due to water. At stage II when swelling reaches a maximum, continual degradation leads to weight loss (Ren *et al.* 2005) (Figure 133). LMw and MMw membranes with higher CH content which in this study could behave in a way where, the amorphous regions in the CH structure could be more permeable to lysozymes than the crystalline zone, hence, amorphous regions undergo rapid degradation than the crystalline segments. Therefore, first phase of degradation involve rapid weight loss and water adsorption, followed by simultaneous static stage, in which water permeates into crystalline zones of CH which are more difficult to break (Ren *et al.* 2005).

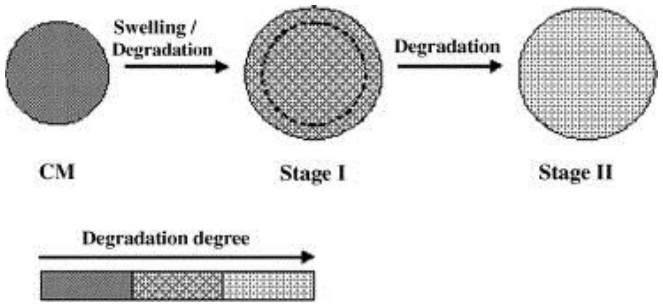

Figure 133: Swelling and degradation process of chitosan matrix illustrated by diagrammatic representation by Ren *et al.,* (Ren *et al.* 2005).

5.2.6. Weight loss analysis

Weight loss studies have been regarded as a reliable methodology to study the in-vitro degradation profiles of scaffolds over time. It has been reported by Wan *et al.,* that non-porous membrane or scaffolds only expose two surfaces to the degradation medium and hence, eventually a lower weight loss of the membrane is observed when compared to porous membranes (Wan *et al.* 2005). They also reported that the activity of lysozyme is usually high during the first few weeks during the degradation process, although in their study lysozymes were not changed after every two to three days which is in contrast to our work. In our experimental plan we infused the samples with new lysozyme solution after every 2 to 3 days. This showed an increment in weight loss profile with time. Membranes synthesized with MMw showed a more stable profile over the 48 day degradation regime which almost similar to results obtained by Liuyun *et al* (Liuyun *et al.* 2009). A comprehensive study performed by Tomihata *et al.,* on the in-*vitro* and in-*vivo* degradation of chitin and deacetylated derivates have reported that although the main degradation phenomenon is of enzymatic hydrolysis, no appreciable degradation can be observed when aqueous neutral media is brought in contact at

room temperature (RT) (20 ± 2°C) with no enzymes. Furthermore, they stated that biodegradation is not governed by the physical micro architecture, rather it's the chemical structure of the films that is responsible for its weight loss (Tomihata and Ikada 1997). The LMw membranes showed 30 % weight remaining for 30:70 and 50:50 ratios at 48th day of degradation. An extensive degradation study by Ren *et al.,* on assessing the effect of DD on degradation showed that, CH matrices with DD of 71%, 81% and 93% had a weight half-life which exceeded more than 84 days, as compared to CH matrices with 56% and 64% DD which had a weight half-life of 27 to 56 days (Ren *et al.* 2005). The DD used for in the current study were consistent for MMw and LMw CH, (75-85%). As the ratio of CH to HA varies, membranes with lower ratios of CH especially in LMw membranes due to the effect of molecular weight lost more weight as compared to MMw membranes. Another study conducted on in-*vitro* (lysozyme solution) and in-*vivo* (rats) degradation of neat CH film mentioned mass loss over a period of 16 weeks. In-*vitro* conditions led to a an overall mass loss of 40% and in-*vivo* showed 60% mass loss. Hence, showing an accelerated degradation process in in-*vivo* conditions The in-*vitro* profile showed a steady increment (Zhang and Cui 2012). The DD of CH used in their study was 85% which is similar to the one used in the present study. However, the Mw of CH used in their study was 5 x 10^5 Da (Zhang and Cui 2012). This is in contrast to the present study where we observed a LMw 100:0 to show 40 to 60 % weight remaining after 48 days and MMw showed 80% weight remaining after the incubation period.

5.2.7. pH Analysis

pH is known to have a significant effect on the wound healing process. A detailed study performed on the effect of pH and wound healing mechanism conducted by Schneider *et al.,* has mentioned that a chronic wound requires an acidic environment for adequate healing (Schneider *et al.* 2007). In this study the pH values of membranes had a peak of pH 8 after 42 days of incubation in PBS with 5mg/ml of lysozyme solution. A study performed by Murugan *et al.,* on analyzing the pH of CH and HA composites for 1000 hrs have reported that the pH values were found to decrease with increasing CH. They also mentioned that this was due to the solubility being dependant on the buffering conditions owing to the complex formation betweeen CH and HA. Furthermore, they also determined the nature of bioresorpability of composites by assessing the amount of Ca ions releases in PBS medium at pH of 7.4. They noted an increased release of Ca ions from composite membranes compared to virgin HA medium which was attributed to the less stable nature of CH macromolecules triggering the release of Ca from composite structures (Murugan and Ramakrishna 2004). However, their

study did not mentioned whether the degradation solution was renewed after every 2 to 3 days or not to simulate physiological conditions Zhang *et al.,* have reported the pH fluctuations of virgin CH over 16 week of degrdation in PBS, and showed the pH value varied from 7.4 to 7.8. This could be due to the degradation products of CH, like amino sugars (Zhang and Cui 2012). In the present study using lysozyme led to a more alkaline pH of around 8 at the end of the incubation period.

5.2.8. UV-Vis Spectroscopy

The supernatant of degraded samples was analysed by UV-Vis spectrometry to study the formation carboxylic or aldehyde groups formed after hydrolytic scission of β-1,4 glycosidic bonds of CH. Peak at 220nm might occur due to n-σ* transition of amino group and π-π* (bonding to antibonding) transition of carbonyl and carboxyl groups. Another peak at 280 nm is ascribed to n- π* (nonbonding to antibonding) transition of carbonyl or carboxyl group. Furthermore, peaks around the region of 280-300nm have been reported previously by Zhang *et al*., (Zhang and Zhang 2002). The changes in these two peaks have been correlated with carbon oxygen double bonds (carbonyl groups) occurring after the main chain cleavage of CH and hydrogen abstraction reaction followed by the ring opening as reported earlier by Ulsanki and co-worker (Ulanski and Rosiak 1992). The upward curvature of the bands with time could be due to increasing efficiency of –OH reaction with CH upon reduction of molecular weight (MW). What is interesting in this study is the variation in the bands of MMw ratios show an increasing trend as compared to LMw membranes. Two CH bands by Biskup *et al.,* have been reported at 265 and 297nm, pertaining to degraded CH, which in our case were seen at 220 and 280. Moreover, these have been regarded to be in the range for carboxylic group (Kolhe and Kannan 2002). The intensity plots for day 4, 11 and 21 also show the variations in the intensity of peaks at each time point for different specimens

5.2.9. Monitoring Degradation by Spectroscopy

FTIR spectroscopy was performed in PAS mode to study bulk profiles of degraded samples of thin films/ membranes of CH and CH:HA. Spectral data collection was carried out on top and bottom surfaces of each membrane for each time point, except a few ratios in which the membrane used to curl up after drying and mechanical agitation to flatten the membrane resulted in the HA flakes breaking off from the membranes. Hence, it was decided to analyze one side only without disrupting the sample. These were mainly LMw 70:30. 50:50 and 30:70 CH:HA. Figure 134 below depicts how the membranes curled up. The difference in the MMw at day 14 and LMw at day 7 is depicted. LMw membranes were able to curl up to

hinder the spectral data collection for CH side. As compared to the MMw ratios, they were able to remain flatten. Some HA can be seen flaking off for MMw 30:70 ratio at day 14.

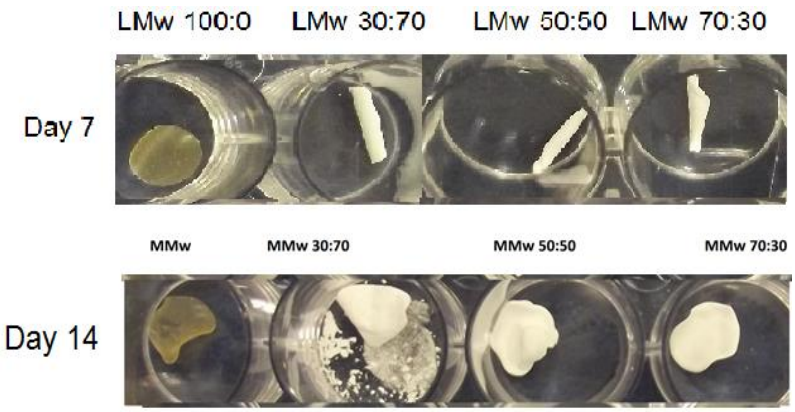

Figure 134: Optical images taken at different time points depicting LMw and MMw CH:HA membranes up after drying. Images portray the curling phenomenon of LMw and MMw ratios.

Using PAS has an added advantage compared to using ATR accessory which is restricted to surface characterisation only and PAS is well known to deliver bulk profile or molecular maps of biomaterials, in addition by controlling the velocity of the moving mirrors, it is also possible to perform depth profiling. The band positions of key peaks have been identified in a comprehensive table shown in the results section in Table 13. Typical CH spectra shows –OH and –NH stretching vibration at 3200 and 3500cm^{-1}. Absorption bands at 2800 and 2900 have been attributed to methylene (-CH_2 group), amide I band appears at 1655cm^{-1} and Amide II peak is observed at 1540cm^{-1}. Furthermore, glucosamine unit or glycosidic bonds of C-O-C appear at 1150 to 1040cm^{-1}. The –OH functional group of HA appears at 3600cm^{-1} and phosphate ν_1 , ν_2 , ν_3 and ν_4 vibration are seen at 960, 1080, 1096, 565, 603 and 472 cm^{-1} respectively. Analyzing the spectral data collected after enzymatic degradation shows varying results ranging from decrease in peak intensities to peak shifts of CH and HA when observed at both top and bottom surfaces.

It has been reported by Tachaboonyakiat *et al.,* that when lysozymes were used to assess degradation of chitin and CH, characteristic peaks were not reduced; they attributed this to the low hydrolytic activity of lysozyme relative to the high DD of CH matrix. In the same study a quantitative assessment of hydrolysis was carried out using the 1110cm^{-1} peak of HA and 1072cm^{-1} (pyranose ring) peak of CH. Correlation between absorbance ratios of pyranose of CH to the phosphate of HA were taken to be indicative of CH matrix remaining after lysozyme degradation by enzymatic hydrolysis. However, spectral data collected from the bottom surface of CH:HA membrane in this study showed that some HA was lost. This was observed

as the symmetric and asymmetric vibrations of phosphate and hydroxyl peaks visible in the spectra collected from the bottom surface showed decrease in intensity which could be indicative of the HA being resorbed or losing its bond with CH. Although this loss of HA was relatively very small, some similar studies conducted on CH:HA degradation have ignored this amount (Tachaboonyakiat *et al.* 2002). A short review performed on CH and HA composites by Pighinelli *et al.,* have reported that the bioresorption of HA is dependent on several factors, such as chemical, physical and biological conditions affecting bioceramic integrity (Pighinelli and Kucharska 2013). Comparison of virgin LMw and MMw (Figure 135) finger print region at day 1 and 36 showed clear discrepancy in the peak heights and positions. Observations of Amide I band at 1650cm^{-1} showed that the peak shifted to a higher wavenumber of 1652cm^{-1} on 28th day. The NH_2 band attributed to amide group at 1593cm^{-1} is more prominent on LMw spectra, shows a shift to a lower wavenumber at 1541cm^{-1}. Furthermore, peak at 1420cm^{-1} also shifts to a lower wave number accompanied with decrease in intensity. This is attributed to changes occurring in the methylene group. These results were also in accordance to the results obtained by Mucha and Pawlak (Mucha and Pawlak 2002).

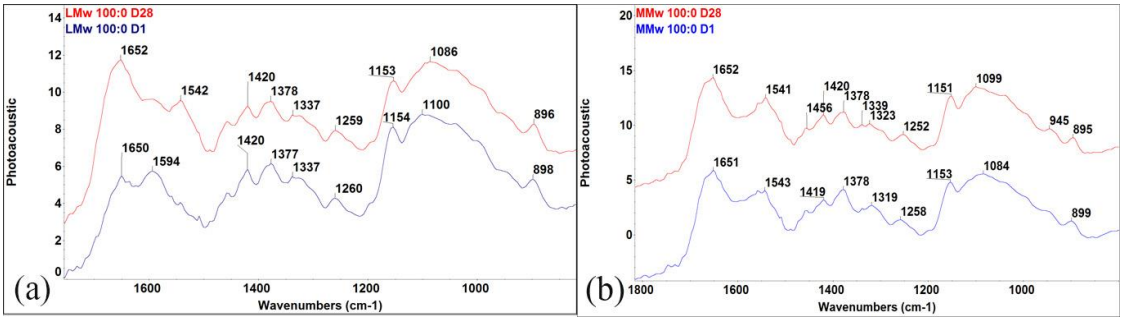

Figure 135: FTIR-PAS of finger print region of (a) LMw and (b) MMw 100:0 at day 1 and 28 after degradation

LMw and MMw membranes with CH:HA ratio of 70:30 (Figure 136), when observed closely also showed discrepancies in peak intensities, which are more prominent in spectral data of LMw membrane. Peculiar peak shifts were observed at 1649cm^{-1}, 1377cm^{-1}, 1084cm^{-1} attributed to CH structure. Furthermore, with respect to phosphate bands of HA, changes can be observed at 1120 and 1084cm^{-1}, pertaining to decrease in intensity and shifts to lower wavenumber from Day 1 to 28 of degradation. All these changes point towards the scission of CH chain structure. The vibrational band at 1100cm^{-1}, corresponds to the ether bond in the pyranose ring, its weakening is usually indicative of rupture of β-glycosidic bonds. This rupture can further effect the distribution of glycosidic bonds in the molecular chain of CH. Moreover,

it has been reported that the movement of the N-H stretching vibration towards the lower wave number is indicative of weakening of intra and inter molecular hydrogen bonds, at the same time decrease in the crystallinity after degradation has also been reported by Wang and co-workers (Wang *et al.* 2005).

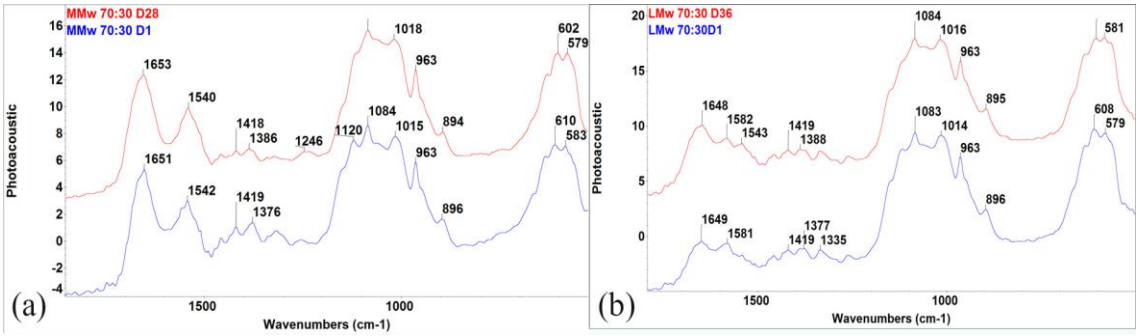

Figure 136: FTIR PAS finger print region of (a) MMw 70:30 at day 1 and day 28 (b) LMw 70:30 bottom surface at day 1 and 36

Similar findings related of peaks shifts to lower wavenumbers were observed for MMw and LMw 50:50 (Figure 137 a and b) spectra when observed from the bottom surface with decrease in intensity, peak shifts to higher and lower wavenumbers. LMw membranes showed a decrease in intensity at 1541cm^{-1} attributed to N-H bending vibration, also indicative of glycosidic bond breakage. Further, investigation of the chemical changes in the ultrastructure of LMw and MMw 50:50 ratios revealed that the peak at 960cm^{-1} (phosphate band of ν_1 in HA) showed a decrease in intensity of LMw 50:50 HA side. Which when compared to MMw 50:50 showed no signs of changes at the same region. It could be envisaged that at 28th day in lysozyme some bioresorption might be taking place in coordination with CH degradation, or HA could possibly be flaking off/debonding from the biopolymer.

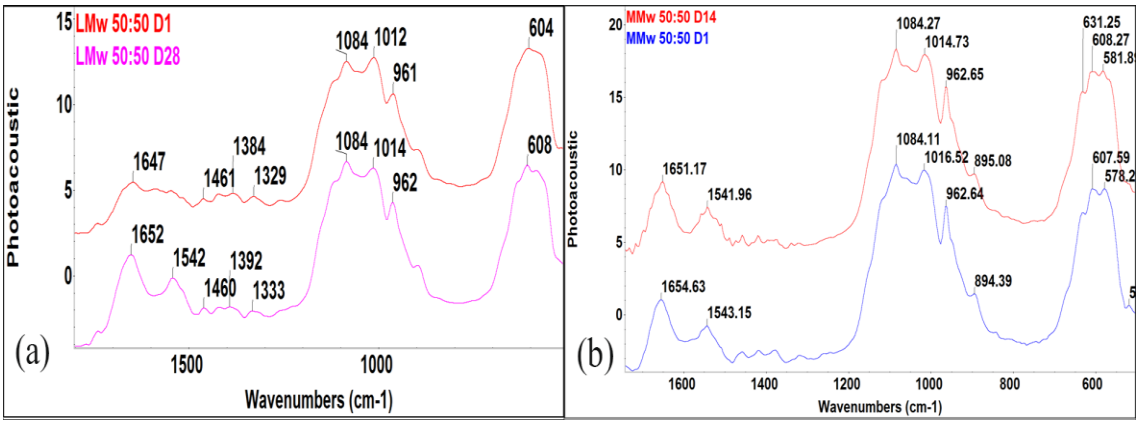

Figure 137: FTIR PAS of (a) LMw day 1 and 28 and (b) MMw 50:50 finger print region at day 1 and 14.

Comparison of MMw 30:70 membrane bearing a higher content of HA showed less changes in the HA peaks as compared to LMw 30:70 membranes. The –OH functional group peak of HA showed a gradual increment in intensity this could possibly be due to interactions between LMw and MMw CH and HA near 3560cm^{-1}. There could be a possibility that MMw CH promotes stronger interaction and LMw is conducive to weaker interactions between CH and HA. Stronger interactions eventually show higher peak intensity. Till day 28, MMw 30:70 membranes bottom surface had minuscule changes which could be indicative that HA was more strongly binding with MMw CH and is not effected by lysozyme solution (Figure 138). The hydroxyl functional peak of HA of LMw 30:70 membrane showed a gradual decrease in intensity at the 28th day of lysozyme degradation. Another study conducted by Depan *et al.,* on CH degradation performed FTIR on pure CH samples. They reported that after 1 week of immersion in PBS, no significant changes were observed in the chemical microstructure of CH. A slight decrease in the peak intensity at 1650cm^{-1} was observed during the initial hours. After 2 weeks of incubation flattening of peaks at amine region of 1590cm^{-1} and increase in intensity of peak at 1650cm^{-1} was noted (Depan *et al.* 2013). These changes or slight shifts in intensity and peaks were correlated to degraded scaffolds. Initial destruction was related to the destruction of pyranose ring. Another significant change noted was at the peak corresponding to saccharide structure at 900cm^{-1} flattened out at the end of 2 weeks, which was indicative of the rupture of glycosidic linkages between glucosamine and N-acetyl glucosamine (Depan *et al.* 2013). These results when compared to the present study tend to differ as degradation was carried out using lysozymes to mimic normal physiological conditions.

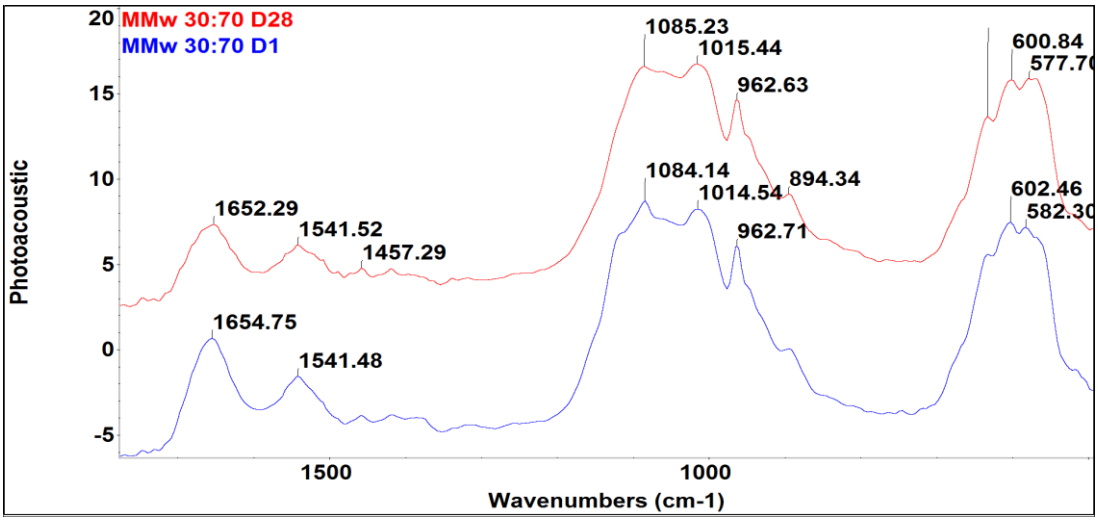

Figure 138: FTIR-PAS of MMw 30:70 depicting the finger print region at day 1 and 28 of degradation by lysozyme solutions.

Extensive in-*vitro* and in-*vivo* studies on CH and CH HA composite degradation have been carried out in the past. Analytical techniques such as FTIR spectroscopy, UV-Vis spectroscopy, gel permeation chromatography (GPC) and TGA studies were conducted by subjecting CH to lysozymes, PBS, ultrasonic degradation, thermal, radiation induced, ultraviolet light, hydrogen peroxide and hydrodynamic cavitation (Yomota *et al.* 1990; Tomihata and Ikada 1997; Mucha and Pawlak. 2002; Ren *et al.* 2005; Wang *et al.* 2005; Kim *et al.* 2011) Kim and co-workers implanted CH membranes in rats to study spinal cord repair and compared it with commercially available Gore-Tex ePTFE membrane. They reported that CH implants showed signs of degradation at 6 months after implantation (Kim *et al.* 2011). Moreover, it has also been reported that in-*vivo* degradation rate is found to be much faster than in-*vitro* degradation rate (Liu *et al.* 2012).

In future it would be interesting to carry out further characterisation of the degraded specimens by analyzing the surface topography by SEM. Assessing the decrease in molecular weight will also be beneficial for predicting the degradation profile.

5.2.10. Biocompatibility

While CH based templates are usually regarded as promising biomaterials for TE applications, there are inconsistent and conflicting reports with respect to their biological performance. This uncertainty could be due to the poor characterisation of CH HA based composites. CH properties such as DD, crystallinity and Mw could also be important while assessing the bone cell/tissue responses to study biocompatibility (Hamilton *et al.* 2007). Hamilton and co-workers have reported that the relationship between DD and attachment is attributed to attraction between the net positive charges of CH, which increases with DD due to protonation of amine groups that can attract cells carrying a net negative charge. The understanding of the adhesion kinetics of human osteosarcoma cells have shown that MG63 attachment on biomaterials is greatly dependent on the pH changes occurring during the incubation period as well. Moreover, incorporation of HA in composites assists in maintenance of this pH for macromolecular environment which in turn enhances cell adhesion and imparts cytocompatibility to the material (Sailaja *et al.* 2006). The rationale of using MG63 cell line was that this is the most commonly used cell line to assess initial biocompatibility of biomaterials and hES-MPs were used as the periodontal wound site would encounter progenitor cells, hence, this in-*vitro* study would give a good representation of in-*vivo* conditions. Culturing of MG63 and hES-MP's was performed on the bottom surface of CH HA membranes as this side was intended to be facing the hard tissue defect while acting as a GTR membrane. Studies

conducted in the past have extensively reported about composite membranes, however, to the best of the author's knowledge, the membranes synthesised for culturing in this study with a high degree of segregation in between CH and HA are yet to be reported. The overall results demonstrated that the CH HA membranes supported cellular proliferation to a greater extent. These results were in agreement to studies conducted previously (Fakhry *et al.* 2004; Bhattarai *et al.* 2005; Chesnutt *et al.* 2009) which reported the culturing of human osteoblast like cell and mesenchymal stem cells in the past on CH HA composites (Fakhry *et al.* 2004; Sailaja *et al.* 2006; Hamilton *et al.* 2007; Thein-Han and Kitiyanant 2007; Hunter and Ma 2013). Kong and co-workers have also mentioned that of CH:HA membranes showed that pre-osteoblastic cells triggered a greater rate of proliferation on composite CH:HA scaffolds compared to CH on its own (Kong *et al.* 2005; Thein-Han and Misra 2009). A gradual increment in viability for both MG63s and hES-MPs is seen for all the membranes from day 1 to 7 including those synthesized by MMw CH (only 50:50 shown). In another study by Jiang *et al.,* reported that pure CH restricted the adhesion and proliferation of osteoblast (Jiang *et al.* 2010). However, the majority of studies report initial attachment and proliferation ability of osteoblast on CH surface (Jiang *et al.* 2010). This was also the case in the present study as CH did support initial attachment and viability values increased with respect to time. The reason for this discrepancy could be the diverse nature of origin and properties of CH with respect to its Mw and DD as mentioned earlier.

Gelatin is an essential component of the membranes as it acts as a plasticizer, hence, enhancing the handling characteristics. However, in the same study D7 values showed that LMw 50:50 and 70:30 had higher viability values. Cai and co-workers reported MG63 culturing on film made with a ratio of 70:30 had much lower viability values as compared to other ratios (Cai *et al.* 2011). Furthermore, they also mentioned that with an increase in HA content the cell viability of MG63 increased significantly (Cai *et al.* 2011). In another study it has been reported about the correlation between water uptake and cellular attachment, that a higher swelling ratio capacity may provide advantages for supporting cell growth in 3D cultures (Hamilton *et al.* 2007). Although results from the swelling studies suggest that MMw 50:50 showed higher swelling profile as compared to LMw CH:HA membranes, the viability values were slightly in contrast to this. A study performed by Sailaja *et al.,* observed a dip in the viability after 24 hours, which was also noted for the viability results done with and without gelatin (Figure 48) this was explained, as it is well known that the cells need only minimum surface area during initial attachment, as the cell spreading is triggered, they acquire greater surface area, this cause a reduction in the total number of cells per specific area. Hence, the number of adhered

cells around a specific area will be reduced with time compared to the number of cells attached initially (Sailaja *et al.* 2006).

It is also recognised that surface roughness may also influence the cellular attachment. While this phenomenon was not measured in our experiment, all solvent casted membranes, based on visual inspection exhibited a smooth and uniform surface morphology with slight variations as the content of HA increased from 30 to 70%. The variations in the viability assays conducted with MG63 (with and without gelatin) and hES-MPs could also be attributed to the inconsistencies in the membrane thickness as well. The uneven thickness of CH casted membranes has been reported to play a role in mesenchymal stem cell (MSCs) attachment study performed by Uygun and co-workers. Furthermore, they mentioned that higher attachment and proliferation was noted for MSCs on thicker regions of cast CH membranes which exhibited reduced crystallinity as well (Uygun *et al.* 2010). Given that the culture was performed on both MMw and LMw CH:HA membranes, even small amount of degradation may also have resulted in large change in the film characteristics, obscuring the cellular proliferation to some extent as well (Hamilton *et al.* 2007). In another study Ohara *et al*, it is mentioned that oligosaccharide degradation products at 0.05% conc increased the gene expression of BMP over 7 days in culture of human osteosarcoma cell line (Ohara *et al.* 2004). Controlling the film thickness is a critical parameter when fabricating GTR membranes. Optimal conditions for solvent evaporation, amount of the solution poured in the petri dish and ratio of the biopolymer to bioceramic need finer tuning to tailor make GTR membrane aimed at regenerating periodontal tissues.

Hunter *et al.,* have reported about the in-*vitro* evaluation of CH HA and gelatin (G) membrane for GTR, in which they cultured human MSCs. They reported the CH:HA:G membranes supported elevated expression of bone marker proteins and genes with ability to undergo osteogenic differentiation (Hunter and Ma 2013). Moreover, as polycationic polymer CH membranes influence the adsorption of proteins such as fibronectin and vitronectin, which regulate the adhesion, proliferation and migration of mesenchymal cells (Uygun *et al.* 2010).

Matrix deposition on CH HA membranes was assessed by quantification of total calcium and collagen deposited over a culture period of 28 days. Alizarin red and Sirius red staining are common techniques to assess total calcium and collagen deposited by cells in 3D culture. The expression of collagen is known as predictive marker for new bone formation (Park *et al.* 2013). Studies in the past have shown that culturing of stem cells on composite membranes have promoted matrix deposition and differentiation of cells with time. The ability of HA to

robustly uptake Sirius red and Alizarin red stains has been rarely reported in the literature. This phenomenon was seen for the present study where HA samples were able to retain the stain even after de-staining as compared to neat CH samples. A study performed by Wang and co-workers have reported that CH HA scaffolds were able to promote calcium deposition which was assessed by Alizarin red staining up to 14 days. Furthermore, they also concluded that HA CH composites promoted higher ALP activity and mRNA expression of osteogenic differentiation markers (Wang *et al.* 2011). In another study by Park *et al.,* it was reported that CH coated apatite scaffolds promoted collagen deposition when cultured with bone marrow stromal cells (BMSCs). The deposited collagen was reported to spread throughout the entireties of the construct till day 28 (Park *et al.* 2013).

5.2.11. Conclusion

A highly segregated CH HA membrane with different ratios of HA and molecular weights was fabricated (LMw and MMw) of CH to be used as a surface layer of a functionally graded GTR membrane. Solvent casting was employed to fabricate these thin films and it is shown that this method can be a convenient way for obtaining thin films. Abundance of HA was confirmed by, visual inspection, SEM and FTIR-PAS analysis on the bottom surface of membranes. The addition of HA significantly affected swelling ratio, degradation profile, cellular viability, proliferation and matrix deposition with respect to time. Furthermore, the detailed degradation analysis showed that LMw membranes with a ratio of 30:70 could be a good candidate to be able to serve as an occlusive membrane considering the time frame known for desirable initial regeneration of the periodontal components. The results are indicative that this membrane can be used as part of a functionally graded trilayered GTR membrane for periodontal lesions. Layer by layer solvent casting could also be adapted in the future to synthesize graded membranes for use in other biomedical and dental applications.

5.2.12. Bioactivity Studies

5.2.12.1. Introduction

Ability of biomaterials reinforced with ceramics to acquire bioactive properties has been extensively studied in the past by researchers. Bioactive ceramics consist of a special class of biomaterials that have the tendency to form a mechanically strong bond to bone by means of a series of chemical reaction at the tissue-bone interface (Hench *et al.* 1998; Kokubo *et al.* 2003). In-*vitro* studies are based on immersion of specimens in SBF media and detecting the formation of a carbonated apatite (CA) layer on the surface of biomaterials (Kokubo and

Takadama 2006). In this study, CH HA membranes were assessed for their ability to be bioactive after immersion in SBF and characterized with changes in pH values, % Weight change and FTIR –PAS Spectroscopy studies with peak area analysis.

5.2.12.2. pH Analysis

It is envisaged that the formation of a CA layer will alter the pH of the medium. A gradual increment in pH was observed for both LMw and MMw CH HA membranes with respect to time. A study performed on evaluating the pH of SBF after immersion of CH and nHA composites have reported that the concentrations of Ca^{2+}, phosphorus along with pH decreased after soaking with SBF from 7.4 to 7.25. This could be due to the storage of the specimens which was done at 25, 40 and 60°C (Yoshida *et al.* 2004). In our work samples were refreshed with new SBF after every 2 to 3 days and stored in an incubator maintained at 37°C to be able to mimic normal physiological conditions. In another similar study it is mentioned that the pH value is based on the resorbability of HA, and the pH is said to decrease as the solubility increases. Rajkumar and co-workers have also reported similar results in which the pH values decreased with respect to soaking time over a 13 day experimental period. Although the pH showed a spike in between D0 to D4 but afterwards declined with time (Rajkumar *et al.* 2013). The pH increase observed for the present study could be attributed to the particle size of HA as reported in by Jebahi and co-workers. They mentioned that pH of specimens with finest particle size (<45µm) was much higher than that observed for coarser particle (800 to 1000µm) (Ashok *et al.* 2003; Jebahi *et al.* 2013). This high increase in pH could also occur, as the HA particles interact with SBF, there is possibly rapid release of alkali ions triggering the pH to increase with time. With prolonged immersion the rapid increase in the interfacial pH tends to slow down which can also be observed in our graph were the pH values shows a slight drop as well (Cerruti *et al.* 2005). Cerruti and co-workers also reported that after 2 days of full immersion there pH rise was up to 8 (Cerruti *et al.* 2005). It would be interesting to perform a long term profile to give insights into the in-*vivo* interactions of SBF and biomaterials.

5.2.12.3. Weight Analysis

According to Kokubo *et al*., the in-*vitro* immersion of bioactive materials in SBF is thought to promote the formation of bone like apatite which mimics the in-*vivo* surface structures. This bone like apatite is responsible for promoting bone bonding between the biomaterial and living tissue (Kokubo *et al.* 2004; Kokubo and Takadama 2006). Weight profiles of composite scaffolds have been investigated in the past after immersion in SBF. A study performed by Fan *et al*., conducted SBF studies on CH and nHA composites. They reported that the amount of

particles formed on the surface increased with increasing soaking time and hence, the percentage of weight increased as well (Weinberg and Bral 1998; Fan and Lü 2008). A similar study performed by Sun and co-workers on evaluating bioactivity potential of CH and HA composites have shown that after immersion in SBF solution the samples showed a weight loss until day 4, and then the weight gain was noted in the overall weight of the samples (D1=0.0192g, D7=0.0209g). Furthermore, they also mentioned that initially rapid Ca^{2+} release occurs from the specimens to the solution which is the result of initial weight loss (Sun *et al.* 2012). Weight analysis of neat CH membranes was consistent for both LMw and MMw membranes for our studies. With HA incorporated specimens weight profile showed an increment with time. Our results were similar to the finding obtained by Kong and co-workers. Kong *et al.,* (Kong *et al.* 2006) evaluated the bioactivity nature of CH HA composites by SBF media. Apatite layer formation was evaluated using FTIR, SEM and weight analysis. However, they prepared SBF with nearly five times of inorganic ion concentration of human blood plasma. The variations seen for our results, regarding the CA layer formation and disappearance could also be due to the use of a standard SBF solution. Moreover, they also reported that the weight increase in composite scaffolds was higher than to neat CH scaffolds. They also noted that the addition of nHA enhanced the mineralization bioactivity of scaffolds (Kokubo and Takadama 2006; Kong *et al.* 2006). The formation of apatite on artificial materials is induced by functional groups which could possibly reveal negative charge and further enhance the deposition of amorphous calcium apatite. Higher ratio of HA could possibly be responsible for more weight change due to the presence of more nucleation initiation sites to induce apatite formation (Kong *et al.* 2006). Once the apatite nuclei are formed they are able to grow spontaneously by consuming the Ca^{2+} and phosphate ions present in the SBF media. (Kokubo and Takadama 2006; Ghadim *et al.* 2013; Madhumathi and Kumar 2014)

5.1.1.1. FTIR-PAS Spectroscopy.

In order to evaluate the molecular and chemical alterations on the bottom surface of CH HA membranes after immersion in SBF media IR spectroscopy was employed in conjunction with PAS accessory as a tool to assess the bulk profile of specimens at each time point. Using PAS accessory for characterising the bioactive coating on bioceramics has been extensively investigated in the past (Huang *et al.* 1997; Phillips *et al.* 2008; Atala *et al.* 2012) Rehman and co-workers have reported alterations in -OH, phosphate and carbonate bands after deposition of carbonated apatite layer in SBF (Rehman and Bonfield 1997; Rehman *et al.* 2013).

It has been stated that the hydroxyl peak at 3560cm^{-1} shows a reduced intensity in the CA layer as compared to synthetic HA. This decrease in intensity of –OH peak of CA layers has been attributed to carbonate substitution whereby the –OH group competes with the carbonate groups for substitution at the interface of the growing lattice structure (Rehman and Bonfield 1997; Phillips *et al.* 2008). Similar results were obtained for the present study as well, by measuring the peak area of –OH peak at consecutive time points. A decrease in the peak area was noted around D4 to D7 which was found to increase at D14 to D21. Elliot and co-workers have also reported similar findings in which hydroxyl groups were substituted by carbonate ions (Elliott *et al.* 1985). Another explanation regarding the CA layer has been that the CA layer rapidly develops and is amorphous in nature overlaying a crystalline HA, but is weak and hence, it is washed away initially and then reappears gradually at later stage. This initial CA layer has been mentioned by Khan *et al.,* as being in an embryonic form of ideal Calcium apatite lattice (Khan 2009). The substitution of ν_2 *and* ν_3 vibrational modes of CA may be responsible for contributing to the decrease in the intensity of peaks of hydroxyl groups. Closer observations of the MMw 50:50 spectral information of the finger print region (Figure 139) revealed that the appearance of peak at 1456 and 1471 cm^{-1} which could possibly be attributed to type B carbonate substitution, this finding has been earlier reported by Fleet *et al.,* at 1455 and 1410 cm^{-1} as a doublet band (Fleet and Liu 2004).

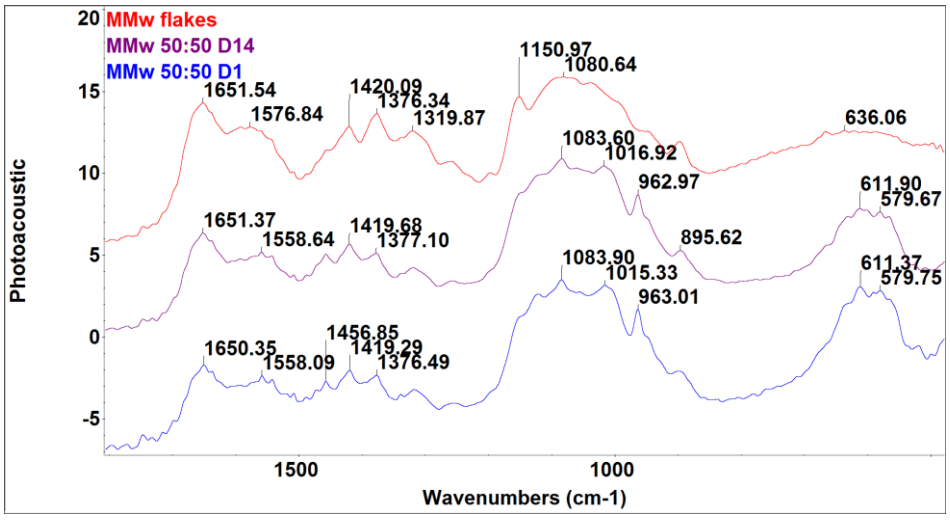

Figure 139: FTIR-PAS Spectra of MMw 50:50 Bottom surface, MMw flakes , MMw 5050 D1, D14.

Furthermore, they reported type A1 carbonate bands appear as a doublet at 1540 and 1455cm^{-1}(Fleet and Liu 2004). The ν_2 carbonate out of plane stretching mode have been reported to appear at 873cm^{-1} (Rehman and Bonfield 1997) or 875cm^{-1} (Regnier *et al.* 1994; Barralet *et al.* 1998). Regnier *et al.,* also mentions shift in this peak to 850cm^{-1} in their study.

Detailed study conducted by Barrlet and co-workers on carbonate ion substitution in HA, reports ν_3 bands occurrence at 1550-1500cm^{-1}, furthermore, they mentioned that previously bands in this region were prescribed to carbonate in the –OH of A site (Barralet *et al.* 1998) (Elliott 1964).

SBF is known to be a metastable Ca^{2+} phosphate solution supersaturated in apatite content. It is mentioned that the barrier of homogenous nucleation of apatite is too high and a stimulus is needed to trigger heterogeneous nucleation of apatite from SBF (Kong *et al.* 2006). SBF studies on CH and HA have been done in the past and identification of CA layer by have been reported consistently (Fraga *et al.* 2011; Mohamed *et al.* 2014; Siddiqui and Pramanik 2014) . However, in this study as the bands of CA and CH are obscured to some extent and peak area ratio calculations were taken to be as a definitive evidence of CA layer formation. From the spectral data collected minuscule changes were observed in the finger print region which suggests CA layer formation and disappearance with time although it could be envisaged that alterations in the peak area of hydroxyl peak point towards a CA layer formation. The apatite formation is a complex phenomenon and to some extent it is still unclear about the biological cascades occurring in the formation of a CA layer. The growth of CA layer is due to uptake of Ca^{2+} and PO_4 ions from the solution and either one can trigger this nucleation step. If Ca^{2+} ion adsorption occurs, such a surface will have negative charges whereas if a PO_4 ion adsorption occurs, this surface will have a positive charge. It has also been reported that more negative charges on the surface promote apatite formation (Li *et al.* 2002).

5.2.13. Conclusion

Formation of a carbonated apatite layer has been known be an indication of biomaterials to bear bioactive property. This was assessed by immersion of CH:HA membranes in SBF. The incorporation of HA in CH membranes affected the formation of CA layer. As the membranes had a high degree of segregation in between the two components, bottom surface or the side with higher concentration of HA which was intended to face the defect side was considered while chemical analysis. The pH analysis, weight change and FTIR-PAS spectroscopy data suggests SBF treatment of the membranes caused alterations of the bottom surface of these membranes which are intended to face the hard tissue defect site and can possibly be used as a potential GTR membranes alone or part of a functionally graded membrane.

SECTION II

5.3. Freeze gelated scaffolds

This section discusses the results obtained by using freeze gelation (FG) technique to obtain porous membranes. All types of membranes synthesized via FG have been completely characterized, by SEM for studying the micro surface topography, chemical analysis by Fourier Transform Infra-red Spectroscopy (FTIR), Swelling ratio analysis, Degradation profile by assessing the weight loss, changes in pH and chemical structural changes by FTIR.

Biological characterisation was performed using human osteosarcoma and human mesenchymal progenitor cell lines. Viability and proliferation was assessed by Alamar blue. Matrix production was characterized using Sirius red for collagen deposition and Alizarin red for calcium deposition. Histological sections have been performed to observe cell attachment onto the membranes. In order to achieve antimicrobial properties within the membranes they were loaded with Tetracycline hydrochloride after cross-linking with NaTPP. Cross linked scaffolds at various percentages for drug loading have also been studied by Scanning electron microscopy, swelling ratio at various concentrations and drug loading capacity by weight measurements.

5.3.1. Optical Images and Scanning electron micrgraphs

The regeneration of periodontal tissues lost as a consequence of destructive periodontitis remains a challenge for clinicians, and researchers have explored the possibilites of using biopolymers and bioceramics in regenerating lost periodontal apparatus. Bearing in mind the proposal by Bottino *et al.,* of having a functionally graded approch to mimic natural structural and functional conditions, we have been able to synthesize a membrane that could function as a core structure of a trilayered membrane. The use of the relatively simple technique of freeze gelation has allowed the fabrication of porous composite membranes, which support osteogenic cell viability and matrix deposition. To the best of our knowledge, the formation of porous CH:HA membranes using the reported solvent systems via freeze gelation are yet to be reported and show great potential for use as GTR membranes (Qasim *et al.* 2015).

Periodontal membranes need to serve the essential criteria of having ideal handling properties. Surgeons should be able to place it in close contact with the defect site or trim membranes considering the size of the defect varying with the location in oral cavity. FG membranes show good bending and stretching characteristics which is indicative of its ability

to be moulded while at chair side, as seen in Chapter 3, Section 4. The use of this relatively simple technique of freeze gelation has allowed the fabrication of a porous composite scaffolds. While fabricating scaffolds with porous features, criterias like pore morphology, pore size, pore distribution, interconnectivity and open or closed porous structures need to be closely looked at. A review of the literature suggests that there are conflicting reports on the ideal pore size for scaffolds. Scaffolds used in bone tissue engineering applications have used pores varying in range from 20µm to 1500µm (Murphy *et al.* 2010; Loh and Choong 2013). Another study has stated minimum pore size with respect to porous implants range from 75-100µm . Murphy *et al.,* reported that pore size of ≤ 325µm were suitable for bone tissue engineering (Murphy *et al.* 2010). Pore distribution for our FG membrane were from 75 to 250µm. ACa and formic acid have been used as the most common solvents for dissolving CH; other organic acids used include maelic acid, citric acid, tartaric acid, lactic acid and ASa or Vitamin C (Ravindra *et al.* 1998; Po Hui Chen 2007; Pillai *et al.* 2009).

The addition of HA leads to more even pore distribution. Recently Siddiqui and Pramanik have reported that, by addition of micro and nano tricalcium phosphate to CH FG scaffolds, they were able to achieve 77% to 81% porosity. These measurements were made by mercury intrusion porosimetry (Siddiqui and Pramanik 2014). They used nano TCP with CH to fabricate Freeze gelated porous templates. The ultrastructure of the specimens made with ACa was consistent with the work reported previously (Ho *et al.* 2004; Po Hui Chen 2007). It was observed that using ASa for dissolving CH also resulted in more even pores as compared to ACa. Analysis of SEM micrographs revealed different pore diameters (Qasim *et al.* 2015). It has been reported that pore size and micro architectural geometry of pores in a scaffold can be controlled by controlling thermal gradients. A sudden change or a gradual decrease in temperature will affect the geometry and morphology of pores. These slight changes can result in a membranes possessing even porous structure if the freezing temperature is gradually managed or uneven porosity if sudden changes in temperature take place (Macchetta *et al.* 2009; Qasim *et al.* 2015).

It was observed for our membranes that FG was efficient in obtaining porous features repeatedly. However, further in depth knowledge of crystallization of solvents at various freezing rates and fluid dynamics is needed when pouring non-solvent onto frozen CH:HA solution. Decreasing the temperature to -40°C or -80°C could possibly give smaller dimensions of pores. Membranes synthesized with neat CH dissolved in ACa-CH had the smallest pore diameter and highest porosity percentage as confirmed by µCT data and those made with ASa-

CH and HA showed larger but even pore sizes (Qasim *et al.* 2015). A study performed by Zoldners *et al.,* have reported the influence of ASa on sability of CH solutions and have shown that CH accelerated the ASa oxidation process in solution and tends to lower the activation energy of the of the reaction (Zoldners *et al.* 2005). Furthermore, another study conducted by Muzzarelli *et al.,* have stated that ASa is the most effective acid for dissolution of CH (Muzzarelli *et al.* 1984). Recently Siddiqui *et al* have reported that, by addition of micro and nano tricalcium phosphate to CH FG scaffolds, they were able to achieve 77% to 81% porosity, these measurements were made by mercury intrusion porosimetry (Siddiqui and Pramanik 2014; Siddiqui and Pramanik 2015).

FG scaffolds of CH synthesized by dissolving CH in ASa have shown an increase in both tensile and water uptake properties. The use of CH and ASa gel in the form of CH ascorbate for potential use in periodontal tissue regeneration has been explored earlier by Muzzarelli *et al.,* (Muzzarelli *et al.* 1989). Besides being used as a potentially suitable anti-oxidant, ASa can also react with CH to form CH derivates *v*ia Schiffs reaction. Mild oxidizing agents like iodine or air can convert ASa to dehydroascrobic acid, resulting in the carbonyl groups to react with amine (Muzzarelli *et al.* 1984). Vitamin C in biological systems plays the role of an antioxidant, simultaneously functioning as a proton donor to dissolve CH (Muzzarelli *et al.* 1984; Po Hui Chen 2007).

5.3.2. Fourier Transform Infrared (FTIR) Spectroscopy

To understand the type of chemical bonding and the functional groups interactions, FTIR in conjuntion with photoacoustic sampling accessory was employed to study chemical structural properties of bulk membranes. This is advantageous compared to other analyzing techniques such as Attenuated total reflectance (ATR) or Diffuse reflectance (DRIFT) which are routinely used to study molecular interactions and vibrations only for surface features (Rehman and Bonfield 1997). By using PAS cell, neat samples without the need of sample preparations can be analysed.

Spectral data of CH membranes synthesized with ASa-CH and ACa-CH have shown typical CH peaks at (3308, 2800, 1652, 1547, 1419, 1378, 1150 and 1040cm^{-1}) and their interpretations are summarisd in Table 1 in results chapter. A decrease in intensity of amide I band at 1547cm^{-1} was observed in the FTIR spectra of CH and HA membranes indicating that there were possible interactions between PO_4^{3-} of HA and NH of CH, which has also been reported by Cheng *et al*. (Cheng *et al.* 2009), as changes in the phosphate spectral band of

ν_1 at 962cm^{-1} (assigned to P-O symmetric stretching), 475cm^{-1} and 571 cm^{-1} denoted to phosphate (ν_2 and ν_4 bands of HA respectively) in the spectra of composite membranes point toward possible covalent interactions with CH. FTIR spectrum of HA has a strong OH band at 3568cm^{-1}), which reduces in intensity when incorporated in CH. In addition, change in wavenumber position of polar groups of CH also suggests that hydroxyl ions on the surface of HA might interact with plentiful amino and hydroxyl ions of CH by formation of hydrogen bonds (Qasim *et al.* 2015).

It has also been reported that there might be coordination bonds in between -NH_2 of CH and Ca^{2+} of HA, since Ca^{2+} ions have a coordination number of 7 and are strictly held in structure (Kikuchi *et al.* 2004; Xianmiao *et al.* 2009). These coordination bonds have also been reported by Yamaguchi and co-workers as well (Yamaguchi *et al.* 2003). In another study on synthesis of porous CH HA composites for Tissue engineering (TE) by Kim and co-workers, it has been reported that during the composite process CH encloses the HA particle inside the polymer. Furthermore, they also mentioned that the c-axis of HA crystal tends to align itself along the CH chains (Qasim *et al.* 2015). Changes in the -OH, -NH, Amide I and phosphate spectral bands confirms possible interactions between the functional groups of HA and CH (Yamaguchi *et al.* 2003; Kim *et al.* 2007).

Another evidence of possible chemical interaction in between CH and HA was observed by the appearance of weakly expressed HA functional gourp (-OH, hydroxyl group) shoulder at 3563cm^{-1} indicating possible formation hydrogen bonding interaction (Cheng *et al.* 2009) as shown in the figure 140.

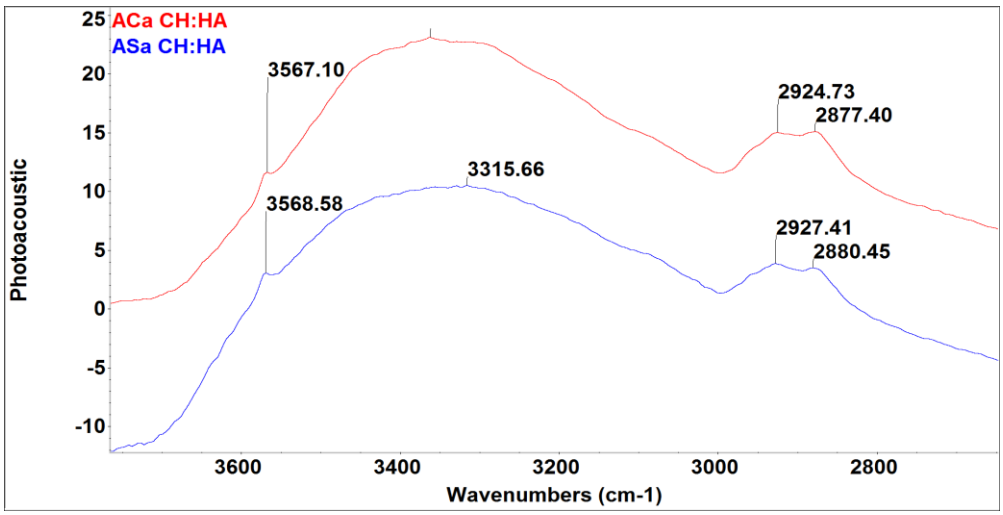

Figure 140: Shoulder of -OH group of Hydroxyapatite in FG ASa-CH:HA and ACa-CH:HA at 3563cm^{-1}

Furthermore, appearance of bands at 963cm^{-1} (assigned to P-O symmetric stretching), 601cm^{-1} and 573 cm^{-1} denoted to phosphate bands of HA in the spectra of composite scaffolds point toward the fact that HA showed covalent interactions with CH (Figure 141), which is reported earlier by Nazir and co-workers (Nazir *et al.* 2012). Superposition of peaks at 1084cm^{-1} has been attributed to the chemical interactions in between CH and HA (Danilchenko *et al.* 2011). Results obtained in this study are in agreement with previous studies performed by Rehman *et al.,*(Rehman 1997) and Van De Velde *et al.,*(Van de Velde and Kiekens 2004).

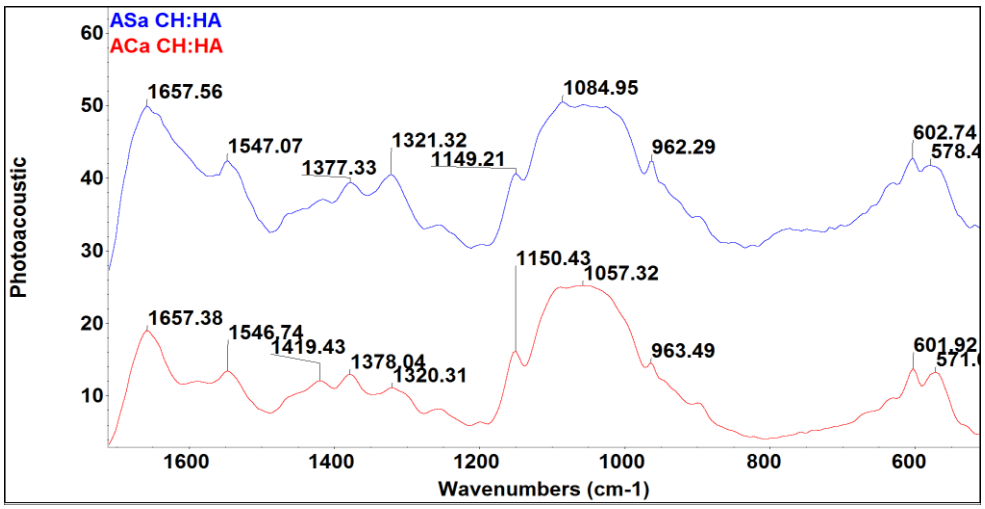

Figure 141: Finger print region of FG ACa-CH:HA and ASa-CH:HA depicting the presence of Phosphate bands.

As mentioned earlier in discussion sections of spectral data of composite membrane, it was not ascertained the type of bonding occurring in between the CH and HA molecules. Interpretations from literature were suggestive of the fact that there were possibilities of co-ordination bonds occurring as a result of mixing CH and HA in an emulsion form. Some have also pointed out towards inter and intermolecular hydrogen bond formation. HA not only allows surface adsorption of CH but also incorporates it into the molecular lattice structure, this phenomenon has also been reported previously as well (Brugnerotto *et al.* 2001).

5.3.3. Mechanical properties

The mechanical properties are known to be dependent strongly on the final form and architectural properties, such as pore size, pore morphology, pore distribution, interconnectivity and percentage porosity for porous scaffolds. Studies conducted previously on CH and HA composites have reported a decline in mechanical properties with increasing HA content (Teng *et al.* 2009; Frohbergh *et al.* 2012; Mota *et al.* 2012). A review performed by Suh and Matthew, have also reported similar findings with regards to the tensile properties of porous CH scaffolds as obtained in the current study. They mentioned that hydrated samples

have low elastic modulus around 0.1 to 0.5 MPa, which compared to nonporous membranes is significantly low (Suh and Matthew 2000). Hydrated CH scaffolds were very soft and spongy in handling, however, the overall strength was generally very low (Madihally and Matthew 1999). Tensile testing under dry conditions is indicative of the handling ability such as bending, flexibilty and ease of cutting of membranes by periodontists during manipulation into the defect site while performing a surgical procedure. Analysis in wet conditions resembles the clinical scenario once the GTR membrane is placed in a hydrated enviorment. Addition of HA to CH membranes made with ASa showed an increase in UTS and *E*, which may be due to the covalent bonding that formed between the -OH and PO_4 of HA to NH_3^+ of CH (Qasim *et al.* 2015).

Mota *et al* reported the addition of bioactive glass ceramic to CH membranes causes an increase in stiffness under both dry and wet conditions. The strength of membrane and elongation at failure also tend to decrease with the presence of Bioglass™ nanoparticles (Mota *et al.* 2012). In this study, maximum elongation at failure was seen for CH dissolved in ACa and ASa with HA. Frohberg *et al* (Frohbergh *et al.* 2012) have also reported that addition of HA reduces the mechanical strength. This decrease might not occur if HA is disperesed within the polymer chains on or near the surface of the scaffold, this is similar to what we were able to elucidate from our FTIR-PAS data that HA was dispersed through out the membrane, as HA spectral peaks were observed from different points of the samples analysed. In addition, the chemical bonding that occurs within the HA particulates and the CH is cruical in improving the mechanical strength of the composite, which was observed in the current study, as HA reinforced CH FG membranes demonstrated higher *E* values as compared to neat CH membranes. It is important to note that chemical intercations between the CH and HA were confimed by the FTIR spectral data (Qasim *et al.* 2015).

5.3.4. Swelling ratio analysis

The swelling ratio is also an important parameter for GTR membranes as in clinical use these would be placed in a periodontal defect and covered by gingival tissue during a surgical flap procedure. The swelling ratio may vary according to the percentage porosity, morphology of pores and membranes ability to uptake and hold water. For periodontal application the degree of swelling is important as the space occupied by the GTR membrane is limited. A further factor to consider is that membranes showing a higher water uptake ratio may possibly allow a greater infiltration of cells. Hydrogel type membranes have two aspects to correlate its ability of cells to migrate through the constructs, one aspect is physical barrier and another

being affinity. A negatively charged particle will struggle through a matrix that bears lots of positvely charged binding sites (like CH) due to electrostatic interactions among them (Qasim *et al.* 2015). CH membranes dissolved in ASa showed swelling profile of upto 80%, whereas, those made with ACa and HA combinations reached a maximum swelling percentage of 60 to 70% . The swelling has been attributed to the unfolding of CH molecules(Cheng *et al.* 2009). Wet membranes analysis, which mimics conditions of the membrane at the periodontal wound site, undergo hydroplastization due to the aqueous solution, this is why the elongation rate is larger and tensile strength is lower, these results are in agreement with the studies reported by Xianmiao *et al.,* in which tensile strength of wet membranes was lower than dry membranes (Cheng *et al.* 2009; Xianmiao *et al.* 2009). Swelling kinetics studied by Silva *et al.,* showed that higher cross-linking degree was effective in lowering the equilibrium hydration degree (Silva *et al.* 2004). They used gluteraldehyde as a cross-linking agent and mentioned that lower crystallinity increases the water molecules accessibility. Ren *et al.,* also studied enzymatic degradation and swelling characteristics of CH matrices and had similar findings, in which the 71% DD CH degraded to 60% by 30 days (Ren *et al.* 2005; Ren *et al.* 2005). Another study conducted by Li *et al.,* showed significant reduction in water uptake of CH and bioactive glass ceramic composite membranes, which is similar to our findings for membranes synthesized with ASa which showed a swelling rate of 90% and addition of HA resulted in decrease in swelling which we saw also (Li *et al.* 2012; Li *et al.* 2012).

5.3.5. Degradation

Weight analysis

Membrane degradation is important to avoid the need for a second surgical procedure for removal of the membrane, and to allow space for newly formed tissue. Degradation of CH occurs by hydrolysis mainly by lysozymes present in the body and β-1-4 N-acetyl glucosamine units of CH undergo chain scission. This phenomenon leads to release of aminosugars, which can be incroporated into metabolic pathway or excreted through the body (Qasim *et al.* 2015). Peter *et al.,* and Mota *et al.*, reported that addition of Bioglass™ reduces the degradation rate, they attributed this decrease in weight loss to the neutralization of the acidic products of CH by the alkali groups (Li *et al.* 2012). The current study showed similar findings and it was observed that membranes with no HA showed 50% initial weight loss whereas, with HA additions it was reduced to 35% after 21 days possibly due to the HA forming covalent bonds with polymer and delaying the degradation rate. Hydrolysis is the basic mechanism of degradation for CH, as interactions with water molecule breaks the polymer network into

smaller chains. Degradation products of the CH include saccharides and glucosamines as part of normal metabolism process (Kumar *et al.* 2004) and the breakdown of HA occurs through resorption process (Shikinami *et al.* 2005). HA interactions with CH reinforce the composite structure, which results in reduced porosity and are less prone to water uptake giving rise to decreased rate of hydrolysis. This is also evident from the results of swelling ratio, porosity decreases from 85% to 78% with the incorporation of HA. It is envisaged that by tailoring the amount and type of HA to our membrane will allow control of both the swelling ratio and as well as the degradation rate. This could be of use for preparing GTR membranes and addition of HA can reduce swelling simultaneously delaying the degradation rate (Qasim *et al.* 2015). There is a large number of degradation studies performed on CH and its derivatives. Most of them have reported similar findings although we believe that the swelling and degradation of CH as a very complex phenomenon. It is envisaged that by tailoring the amount and type of HA to our membrane will allow harnessing both the swelling ratio and the degradation rate. The conventional methods adapted to study CH degradation usually falls under two categories. One which measure and quantify the scaffolds variance with time, involved physiochemical properties and alterations in weight and morphology. Secondly, some researchers examine the degradation products of scafffolds. Weight loss analysis has been regarded as a suitable and reliable method for analyzing degradation profile of tissue engineering scaffolds. Results obtained after analysing the weight loss profile for porous CH membranes were also in agreement with study performed by Wan *et al.,* in which they correlate the weight loss with pore morphology and report that larger pore sized scaffolds with higher porosity has greater weight loss. It also mentioned that weight loss did not alter lineraly with degradation time. The cleavage of CH has been attributed to its hydrophilicity and an the initiation of degradation process has been reffered to as a superficial phenomenon rather than a bulk trend. Bigger pores have been known to offer a larger surface area and more active sites of lysozymes to react with, and hence more CH molecules are destroyed and a greater weight loss is enventually results in (Wan *et al.* 2005).

pH analysis

Wound healing has been regarded as a complicated regeneration process which is comprised of intercalating degradation and reassembly of connective tissue. The pH value has a direct and indirect relationship in all biochemical reactions occuring in the process of regeneration. It has been speculated that a low pH is favourable for healing in certain scenarios. As mentioned in the earlier section of pH change of membrane/thin film

degradation, Schneider *et al.,* conducted a detailed analysis on the effect of pH on wound healing and concluded that the final pH around a wound is a potent influential factor for the final result of any therapeutics intervention. They also concluded that chronic wounds are characterized with high bacterial colonies bearing a local pH of around 7.3 and an acidic enviroment tends to promote healing process (Schneider *et al.* 2007). With respect to our results the final pH values after degradtion of CH changes from 6.9 to 8.4. However, these are in-*vitro* results which can vary when performed in-*vivo* conditions. It would be interesting to monitor pH fluctuations without renewing the lysozyme solution after every 2 to 3 days, although this would result in deviation from the local physiological conditions. Another study reported an increase in the pH profile of pure CH scaffolds, which are similar to the finding obtained in our experiments. Wan and co-worker noticed that the magnitute of change was insignificantly altered over the incubtaion period (Wan *et al.* 2008).

UV-Vis spectroscopy

The importance of UV-Vis spectroscopy has been highlighted in previous sections. It was employed to study the degradation of FG CH membranes. Prominent bands observed appear in the range of 200 to 300nm which point towards hydrolytic scission of β, 1-4 glycosidic bonds of CH. A band at 220nm might occur due to n-σ*(nonbonding to antibonding) transition of amino group and π-π* transition of carbonyl and carboxyl groups. The second band at 280 nm is ascribed to n- π* transition of carbonyl or carboxyl group. These bands point towards bond breakage or molecular bond movement from bonding to antibonding. A study conducted by El-Sawy *et al.,* previously has reported similar findings (El-Sawy *et al.* 2010). Ulanski and co-workers conducted a study on the radiation induced changes in CH and reported that the shape and upward curve of the bands is due to carbon oxygen double bonds occurring after the bond breakage of CH and –H abstraction reaction which is followed by ring opening (Ulanski and Rosiak 1992). In research conducted by Biskup *et al.*, CH bands appear at 265 and 297nm, which they also designated to carbonyl groups. The intensity increase of these bands with time was ascribed to somewhat increasing efficiency of –OH reaction with CH on reduction of Mw. It could also be indicative of partial formation of carbonyl groups (Czechowska-Biskup *et al.* 2005).

Monitoring Degradation by Spectroscopy

FTIR spectroscopy has been used as a tool to study degradation profile of FG membranes. Bulk samples were characterized using PAS accessory. As mentioned earlier while

discussing degradation of thin films of LMw and MMw CH and HA, CH degradation is usually preceded by breakage of glycosidic bonds. Close observation of molecular finger print regions of FG samples reveals a huge amount of information which is in confirmation with the studies conducted previously by Mucha *et al.,* and Ren *et al.,*(Mucha. M and Pawlak. A 2002; Ren *et al.* 2005). The FTIR-PAS spectral information of neat ACa-CH samples when viewed at day 1 and 28 is shown in Figure 142 (finger print region). Significant decrease was observed in the intensity of amide II band and angular N-H deformation at 1419cm^{-1} and 1543cm^{-1}, indicative of CH chain breakage or scission of CH molecular structure. Similar effect has been reported earlier by de Brttio *et al.,* (de Britto and Campana 2007). They reported the spectral changes observed in their study which are similar to the findings observed for our work. Spectral changes noted were decrease in intensity and some broadening, particularly in the segment of 3440cm^{-1}, 2910cm^{-1}, 1417cm^{-1}, 1377cm^{-1} and in the range of 1153-897cm^{-1}, which were attributed to dehydration, deacetylation and depolymerzation reactions. Based on the dynamic experiments conducted on a kinetic model they also observed maximum change at 890cm^{-1} (band occurs due to glycosidic bonds, responsible for linking together alternating repeating units of CH), which was assigned to acceleratory degradation phase followed by de-acceleratory condition (de Britto and Campana 2007). Another prominent peak which shows reduction in intensity is at 1378cm^{-1}, usually attributed to CH_3 symmetrical deformation mode. A detailed study performed on CH degradation by IR spectroscopy by Mucha *et al.,* have mentioned that they were not able to observe clear structural changes when CH underwent hydrolytic degradation. Furthermore, they also observed that spectroscopic analysis of CH films subjected to biodegradation showed less structural alterations of the polymer macromolecule when compared to other forms of degradation, such as, thermal of photo-degradation. Strong spectral changes are usually reported to occur at amine, amide and glycosidic groups (Mucha. M and Pawlak. A 2002). This was also observed for the current study as well, where alterations were observed in similar regions.

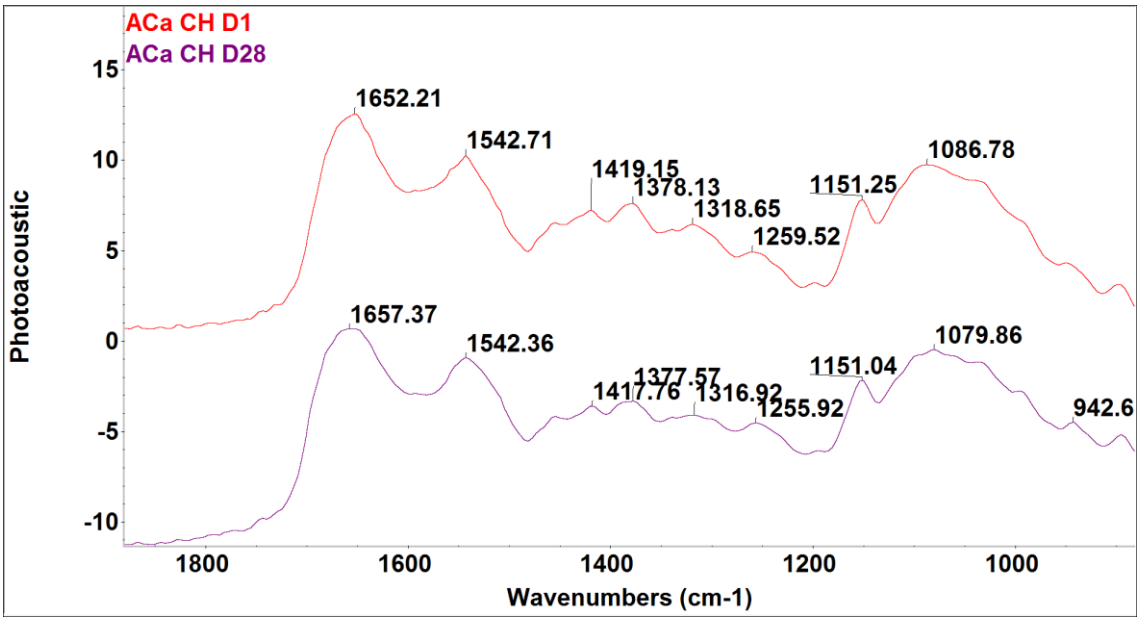

Figure 142: FTIR-PAS, neat ACa-CH finger print region at Day 1 and 28 of degradation in lysozyme solution.

Spectral data collected from ACa-CH:HA also showed subtle changes, which were indicative of CH chain breakage and scission of -C-O-C bonds. Figure 143 shows the molecular finger print region where prominent changes in the intensity of phosphate band attributed to HA can be noted. This can not necessarily be indicative of HA resorption. As mentioned earlier that HA has a prolonged resorption profile. This could possibly be indicative of CH HA bond breakage owing to loss of HA contact with CH structure. Other changes observed were reduced intensity of symmetric and asymmetric CH_2 stretching vibration and CH_3 in amide group. Similar changes observed by Mucha *et al.,* have been assigned to methylene group (Mucha and Pawlak 2002). A study conducted by Qu and co-workers on degradation of CH reports that they observed peaks in the area of 1655 and 1550cm^{-1} becoming broader, than neat CH. This finding was assigned to the CH degradation due to the formation of unsaturated structures during degradation. Moreover, they confirmed the findings from de Britto *et al.* (de Britto and Campana 2007), where, the saccharide structure peak at 897cm^{-1} and 1153cm^{-1} becomes wider (Qu *et al.* 2000). This was also observed in our spectral data in which a band at 1587cm^{-1} disappeared at day 36 of incubation. Broadening and decreased intensity are prominent for the glycosidic segment, indicative of CH degradation. Changes observed in the amide group region at 1657cm^{-1} and 1546cm^{-1} are also mentioned in the findings obtained by Mucha *et al.,* they have denoted this to scission of the main chain and destruction of the unstable amine group (Mucha and Pawlak 2002).

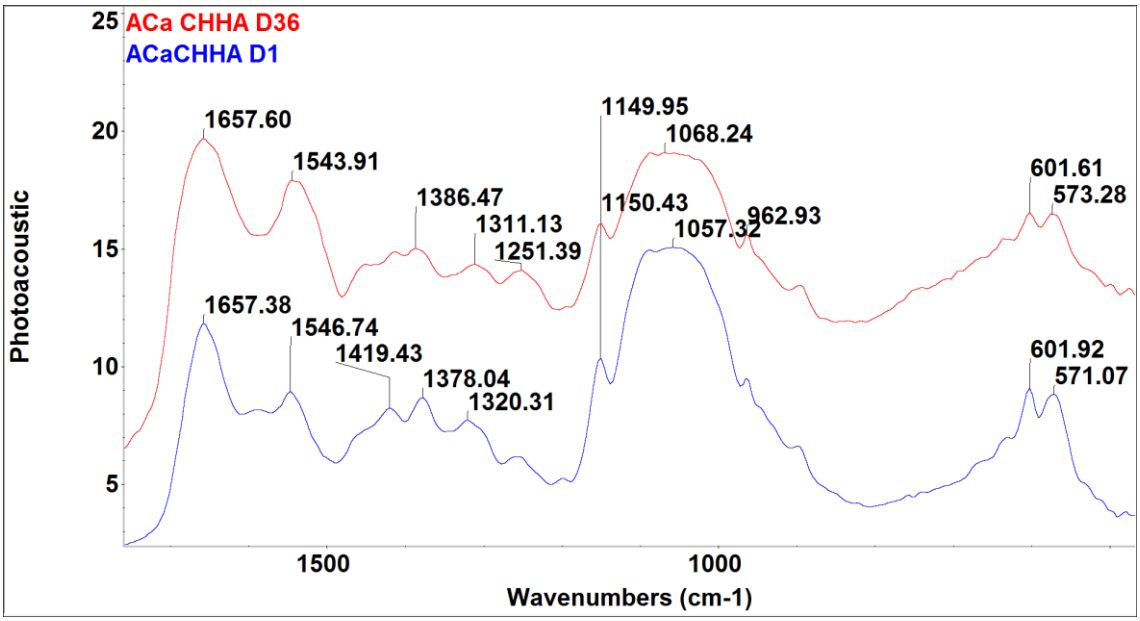

Figure 143: FTIR-PAS, neat ACa CH:HA finger print region at Day 1 and 36 of degradation in lysozyme solution.

Figure 144 depicts the molecular finger print region of neat ASa-CH, similar changes as observed previously in this region were noticed. Decrease in intensity with peak shifts were seen from 1419 to 1416cm^{-1}, peak at 1377 shifted to 1383cm^{-1} with a drop in intensity. Amide and amine region showed similar changes as reported by Mucha *et al.,* (Mucha and Pawlak 2002). An in-*vitro* study conducted by Khanna *et al.,* on CH, nHA and poly galacturonic acid reported about spectral data collected over a period of 48 days in culture medium. They stated that the degradation in culture medium was not severe, spectral changes as expected in the –C-O-C (glycosidic linkage) were not observed in soaked specimens. However, for our data glycosidic region showed slight broadening of the band in this region. Moreover, they also stated that bands pertaining to PO stretching vibration in HA structure showed no severe alterations over the incubation period (Khanna *et al.* 2010). Another recent study conducted by Corazzari and co-workers reports about the degradation of CH, that amino groups on the glucosamine structure can be released in two different ways, via ammonia release or via hetero-aromatic ring formation, confirming the biodegradation of CH can occur by random breaking of C-O-C skeletal bonds (Corazzari *et al.* 2015).

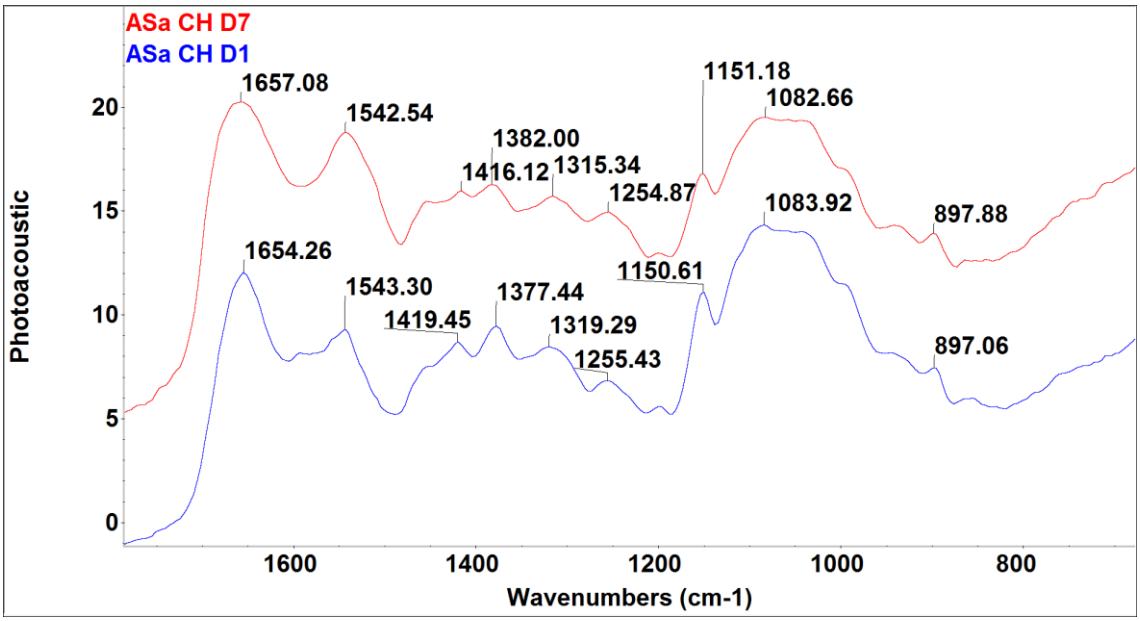

Figure 144: FTIR-PAS of neat ASa-CH Freeze gelated membrane at Day 1 and 7 in lysozyme degradation solution.

Significant decrease of absorbance intensities of symmetric and asymmetric CH_2 stretching vibration due to pyranose ring have been a consistent finding in the molecular finger print region of all CH HA scaffolds for the current study. This could possibly be indicative that apart from the typical glycosidic linkages, amine and amide regions being well known to show changes which may point towards the CH main chain scission and breakage of the macromolecules. This segment also plays a critical role which has been identified by spectral data collected by FTIR-PAS spectroscopy in this study. Figure 145 shows molecular finger print region of ASa-CH:HA and a decline in the peaks and broadening of the bands mentioned earlier can be appreciated again in the regions of glycosidic segment and amide I bands.

It would be interesting in the future to perform peak ratio of different peak as they give detailed insight into the degradation phenomenon for CH. Absorbance ratio of peaks at A_{1375}/A_{2900}, is known to increase with the degree of crystallinity, ratio of A_{1655}/A_{3450} is proportional to the acetyl groups in polysaccharide, ratio of A_{1555}/A_{2900} and A_{1555}/A_{1430} both decrease linearly as the DD increases (Penichecovas *et al.* 1993). Moreover, other characterisation techniques such as SEM analysis could show the surface morphological characteristics. It is also known that CH degradation products are known to stimulate an increased expression of osteogenic genes, such as, bone morphogenic proteins and alkaline phosphatase in *in-vivo* model (Leedy *et al.* 2011), hence, it would also be interesting to confirm this finding to establish the potential of CH use in biomaterials for use in GTR membranes.

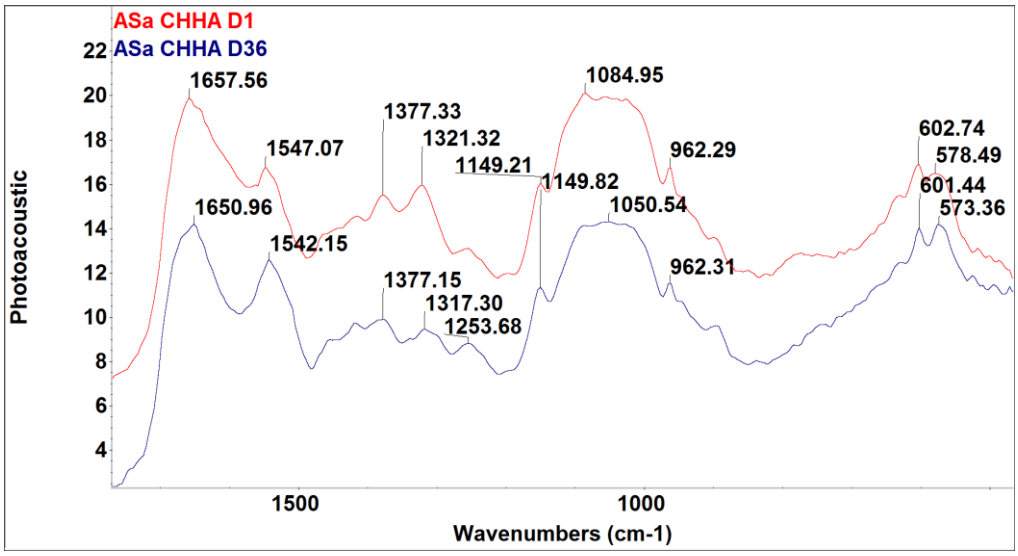

Figure 145: FTIR-PAS of neat ASa CHHA Freeze gelated membrane at Day 1 and 36 in lysozyme degradation solution

5.3.6. Tensile tests

Among the list of ideal requirements for generating new tissues, a scaffold is meant to have adequate mechanical strength to bear physiological stresses at the same time minimise stress shielding in the sourrounding host bone. Tensile testing under dry conditions is indicative of the handling ability such as bending, flexibilty and ease of cutting of membranes by periodontists during manipulation into the defect site while performing a surgical procedure (Qasim *et al.* 2015). Analysis in wet conditions resembles the clinical scenarios since biomedical implants are placed in hydrated enviorments. Addition of HA to CH membranes made with ASa showed an increase in UTS and *E*, which may be due to the covalent bonding that formed between the -OH and PO_4 of HA to NH_2 of CH (Qasim *et al.* 2015). Mota *et al.,* reported the addition of bioactive glass ceramic to CH membranes causes an increase in stiffness under both dry and wet conditions. The strength of membrane and elongation at failure also tend to decrease with the presence of bioglass nanoparticles (Mota *et al.* 2012). In this study, maximum elongation at failure was seen for CH dissolved in ACa and ASa with HA. CH membranes synthesized with ASa had equivalent elongation as HA incorporated ones. Silva *et al.,* showed that addition of small amounts of gluteraldehyde resulted in low tensile modulus (Silva *et al.* 2004; Zhang *et al.* 2010). Frohberg *et al.,* have also reported that addition of HA reduces the mechanical strength. This decrease might not occur if HA is disperesed within the polymer chains or near the surface of the scaffold, this is similar to what we were able to elucidate from the current FTIR-PAS data that HA was disperesed through out the membrane (Frohbergh *et al.* 2012) as HA spectral peaks were observed from different points

of the samples analysed. In addition, the chemical bonding that occurs within the HA particulates and the CH is cruical in improving the mechanical strength of the composite, which was observed in the current study, as HA reinforced CH FG membranes demonstrated better *E* values as compared to neat CH membranes. It is important to note that chemical intercations between the CH and HA were confimed by the FTIR spectral data (Qasim *et al.* 2015).

5.3.7. Biocompatibility

It is a widely accepted fact that cellular response to a biomaterial, such at attacment, spreading, proliferation and matrix deposition are highly dependent on a number of physcial and chemical factors. These range from surface morphology, geometry of pore architechture and porosity (Cai *et al.* 2011). Jiang and co-workers have reported that pure CH coating restrictred MG63 cell spreading and proliferation (Jiang *et al.* 2010). In contrast to this study, another study performed by Fakhry *et al.,* and Hamilton *et al.,* have reported about the initial attachment, spreading, and proliferation potential of osteoblasts on CH (Fakhry *et al.* 2004; Hamilton *et al.* 2007). This discrepancy in reported data could be due to the diverse properties of CH which vary in DD and Mw (Cai *et al.* 2011). Alamar blue results showed an increase in viability for both mature and progenitor osteogenic cells on all memrbanes over the 7 days of culture. Studies conducted previously on CH HA composites have reported that MG63, osteoblast like cells when cultured on composite templates are able to grow and migrate and showed an increase in total protein content which increased with incubation time than that of the control specimens, suggesting higher biocompatibility (Fakhry *et al.* 2004; Ohara *et al.* 2004; Hamilton *et al.* 2007; Chesnutt *et al.* 2009) (Zhang and Zhang 2002; Zhang *et al.* 2003). Our results were in agreement with previous studies based on CH HA composites, which have reported HA incorporated scaffolds to be more biocompatible. It was expected that membranes with HA would be more condusive to cellular infiltration, which was seen in our results as well.

Cai and co-workers cultured MG63 on porous CH HA scaffolds with a ratio of 40:60, they reported a rapid increase in viability during the first 7 days which slowed down subsequently. This was attributed to initial rapid proliferation and migration of cells to the inner wall of porous scaffolds during the early stages, this phenomenon was also noticed for our porous FG membranes as well. Dividing cells spread out to cover most of the inner surface area of pores and hence formed a confluent monolayer. Further, expansion of the cell population was confined to over crowding (Cai *et al.* 2011). Although it would be interesting to evaluate the effect of HA in higher ratios, for the current study a 50:50 ratio was conducive to

cell attachment and proliferation as well. In another study, in-*vitro* biological evaluation assessment after culturing MG63 and Mesenchymal stem cells (MSCs) on CH HA scaffolds also confirmed that composite specimens were both histocompatible and cytocompaible. (Wang *et al.* 2009). The osteogenic potential of CH and CH:HA membranes have been assessed in a previous study by Frohbergh *et al.,* they noticed a decrease in cell metabolic activity over time in HA membranes and attributed this decline to the increased alkaline phosphatase acitivty (Frohbergh *et al.* 2012).

The final phase for osteogenic differentiation is matrix mineralization and our analysis after 28 days of hES-MP culture showed that calcium deposition was supported by all membranes but highest on membranes prepared with HA incroporated compared to CH alone. It has been reported in literature that hES-MP cells deposit HA-like mineral *in vitro* after 3 weeks of osteogenic differentiation, which was analysed by using TOF-SIMS and depth profiling (de Peppo *et al.* 2010). Similar results were observed in this study, where increment of both the calcium and collagen deposition was observed for membranes containing HA, this could be due to the scaffold providing a more suitable balance of collagen with mineral content. Collagen production was significantly higher on ASa-CH:HA membranes compared with ACa-CH:HA while calcium deposition at day 28 was similar, this could be attributed to leaching of leftover ASa, creating more suitable environment for collagen deposition. Overall membranes with HA promoted higher mineralised-matrix deposition, and this observation has been seen previously by osteogenic cells in another three dimensional CH:HA membrane culture(Qasim *et al.* 2015) (Wang *et al.* 2011).

hES-MPs are highly representative of bone-marrow derived MSCs in terms of surface marker profile, gene expression and mesodermal differentiation ability and they express no embryonic stem cell markers. They have also been shown to deposit HA-like mineral. They show a higher degree of homogeneity than human bone marrow derived mesenchymal stem cells (h-BMSCs) giving more consistent outcomes. MG63 cells have been widely used to initially test the biocompatibility of new materials for supporting osteogenic growth (Grausova *et al.* 2011; Grausova *et al.* 2011), and it is possible that mature bone cells may be present in remaining alveolar bone (Egusa *et al.* 2012; Egusa *et al.* 2012). Periodontal ligament cells were not included in this study as the aims were to fully characterise the membranes physiochemical properties and then investigate their potential to support new bone formation, which is an important first step to then allow ligament anchorage and growth (Qasim *et al.* 2015).

Histological analysis performed 7 days after seeding the membranes with hES-MPs showed that cells penetrated deep into most membranes. hES-MPs are a more relevant cell type than MG63s in the context of the overall GTR goal, and they represent the MSC that would infiltrate the membrane in-*vivo* (Mendes *et al.* 2009), therefore histology was only performed on hES-MPs. ASa-CH membranes showed that the majority of cells formed a multilayer on the surface with few penetrating deep into the pores. This could be due to lower degree of interconnectivity or a scaffold-cell interactions hindering their migration into the membrane. ASa-CH:HA membranes showed that cells penetrated through the depth of the scaffold which may be attributed to the presence of HA or the cellular affinity for this paticular memrbanes was improved with ASa-CH and HA combination.

It would be interesting to see how nano HA affects the pore size morphology, pore distribution and porosity percentage on the overall microarchitecture of FG membranes. As it is a well etablished fact that nano-HA possesses a higher surface area to volume ratio bearing the capibility to achieve tighter interface with polymers composites. Moreover, a higher surface area will cause faster release of ions, hence, enhancing bioactivity simultaneously encouraging protein adsorption as well. Nano-HA also resembles the biological apatite due to its ultrafine structure, hence, playing a pivotal role in hard tissue replacement (Sowmya *et al.* 2013). Furthermore, directional freezing process can be employed to assist the PDL growth, by controlling the freezing orientation to fabricate sub longitudinal pores with angular similaritied to native PDL (Park *et al.* 2014).

The aim of the in-*vivo* studies was to examine the behaviour of FG CH and CH:HA membranes on cellular activity and degradation. The evaluation of bone TE templates in an in-*vivo* condition is usually the first step following from in-*vitro* characterisation (Martins *et al.* 2012). In-*vivo* studies conducted on porous CH:HA scaffolds reported in the past have mentioned that composite scaffolds are able to support more bone as compared to neat CH scaffolds (Chesnutt *et al.* 2009; Danilchenko *et al.* 2011; Jin *et al.* 2012; Martins *et al.* 2012). Jin and co-workers reported that after in-*vivo* implantation in mice, composite scaffolds provided a strong effect on bone formation. More pronounced features of newly formed bone tissue were prominent after the 8 week of implantation. Although, Danilchenko *et al.,* reported that after 10 days of implantation intense biodegradation is triggered and newly formed tissue completely replaces the CH:HA composite on the 24th day of implanation (Danilchenko *et al.* 2011). Furthermore, they also mentioned that the newly formed tissue had not only osteoblasts but also osteoclasts and Howship's Lacunae present within its structure (Jin *et al.*

2012). In our case, histological images and morphometirc data results from the first time point were suggestive of CH:HA membranes to be a favourable membrane for cellular infiltration which is in agreement with previous studies. As HA addition is known to have a stimulatory effect on cell migration and osteoblastic acitivity, it is probably a key factor for bone ingrowth. In another study conducted by Chesnutt and co-workers, they reported that CH nHA scaffolds induce osteocalcin production by osteoblasts in-*vitro* and support bone formation in-*vivo* (Chesnutt *et al.* 2009).

It could be concluded that pure CH membranes allow cell migration after implantation to only the superficial zone. CH:HA composite membranes have significant increase in conductive properties of the graft and stimulate new ingrowth after 7 days of implanation. Biological properties of the graft are independent of the solvent used for fabricating the memrbanes. In future it would be interesting to conduct long term in-vivo time points to assess the degradation and new tissue formation which would give us more insight when fabricatin functionally graded GTR membrane.

5.3.8. Conclusion

In this study, porous CH-based membranes with and without HA were prepared using ACa or ASa as solvents systems via the novel and efficient technique of freeze gelation. The CH:HA composites have shown potential for use as a core layer in a functionally graded GTR membrane for periodontal tissue engineering, fullfilling a number of key requirements of satisfactory handling properties for clinicians. Choice of solvent used to dissolve CH and amount of incorporated HA helps in tailor making the physical and chemical properties of membranes. Membranes were resilient to handle during dry and wet conditions that may simulate clinical use. A favourable cellular response was also seen for CH:HA composite membranes suggesting that HA incorporation effects cellular activity. Therefore; this study shows that these porous membranes have a potential to be used as a core layer of a functionally graded structure in periodontal regeneration membranes. Furthermore, freeze gelation technique may be employed in future to create tissue engineering scaffolds for other biomedical applications.

5.4. Bioactivity Analysis on Freeze gelated Membranes

The innovation in the field of bioactive substances has significantly enhanced the integration of biomaterials with surrounding tissue. The capability of a material to bond with bone by forming a carbonated apatite (CA) layer has been regarded as Bioactivity (Hench 1998;

Jones 2013). It is an essential criteria for HA incorporated scaffolds to be bioactive to encourage this bone bonding. FG CH membranes have been deployed in simulated body fluid (SBF) and characterized using pH analysis, weight profile studies and FTIR-PAS Spectroscopy.

5.4.1. pH and weight analysis

Fluctuations in the pH value are known to be triggered during the deposition of CA layer. The pH analysis showed an increment in pH over the course of the experimental period. It has been reported by Tasselli *et al.,* that pH of a solution is one of the most critical parameters affecting the adsorption process (Tasselli *et al.* 2013). An increment in the local pH could be due to the particle size of HA, as reported earlier by Jebahi *et al.,* which stated that the pH of specimens with a fine particle size was higher than coarser particle size specimens (Samira Jebahi *et al.* 2013). pH values of all membranes have a linear correlation and rise from Day 1 to 21. In another study, increase in pH was also attributed to the interaction between HA and SBF media, whereby a possible release of alkali ions can elicit the pH rise. Moreover, in another study they mentioned that an increase could also be ascribed due to the leaching of cations and exchange of H^+ ions from the solution (Cerruti *et al.* 2005). Longer immersion times can adversely affect the surrounding environment which can also result in decreased pH, as mentioned by Cerruti *et al.,* (Cerruti *et al.* 2005). CA layer formation kinetics is strongly affected by the surrounding pH of the media. Moreover, pH is indirectly controlled by the ionic strength and carbonate concentration in SBF solution. Results observed for the current study are coinciding with a previous study conducted by Xiao and co-workers. They also observed a rise in the local pH which was ascribed to the release of alkaline ions arising from the partial dissolution of HA. Furthermore, the degradation of CH can also effect this pattern of pH rise as well (Xiao *et al.* 2009). Maachou and co-workers have conducted a similar study on studying the SBF activity of FG CH scaffolds with different ratios of HA. They performed water absorption capacity tests and noted a decrease in the absorption percentage with time up to 28 days. This was reported to be due to the Ca^{2+} phosphate deposition in the porosities of the membrane or due to the biodegradation of CH in the presence of SBF, possibly responsible for collapse of the membrane structure. Moreover, it was mentioned that both phenomenon may occur simultaneously. Weight loss studies performed by Maachou *et al*., noted a weight loss during the first week of contact in SBF (Maachou *et al.* 2008). For our results neat ASa-CH and ACa-CH were only assessed till day 7 as compared to HA ones, which were possible to evaluate till day 21 due to the condition of the sample. It could be due the higher porosity percentage of neat CH samples allowing more SBF solution to penetrate into the porous structure and assist

the natural polymer degradation process. This physiochemical degradation is achieved either by breaking of electrostatic interactions and the intermolecular bonds, depolymerisation of the membrane or by hydrolysis of the membrane, which could form other compounds such as CO_2, H_2O or carbohydrates (Maachou *et al.* 2008). Weight profiles of samples with 70% HA in the study conducted by Maachou *et al*., showed a plateau during the initial 7 days and then increased after this time point. FG samples with HA in the current study showed a weight increase as well till day 21.

5.4.2. FTIR-PAS Spectroscopy

FTIR-PAS characterisation is a useful technique to assess the formation of a CA layer indicative of the ability of biomaterials to bond to living tissue (Hench 1998; Jones 2013). In the past Rehman and co-workers have reported in detail on the spectroscopic studies of HA and carbonated apatite layers by using FTIR- PAS technique along with peak area measurements to quantify the alterations in the peaks position and intensities (Rehman and Bonfield 1997). Other studies that report about treating porous CH HA composites with SBF have also mentioned about the formation of a carbonated apatite layer (Maachou *et al.* 2008) and exaggerated response has also been evaluated by immersion in 1.5 SBF (Chesnutt *et al.* 2007; Fraga *et al.* 2011).

It is known that the CA layer formation proceeds initially as being amorphous and weak in nature overlaying a crystalline HA, nevertheless, it is washed away and then develops again when suitable physiochemical conditions are available (Elliott 1964). The results obtained in this study were suggestive of a weak layer formation to start with and developing into crystalline phase at a later stage. A decrease in the intensity of hydroxyl peak at 3560cm^{-1} has been reported as a distinctive feature by Rehman *et al.,* this phenomenon has been ascribed due to the competition between the carbonate and -OH ion to occupy a position in the crystal lattice structure. Moreover, they also mentioned that this change occurs at the interface of the growing crystal. A larger decrease in the intensity could be attributed to increased substitution (Elliott 1964; Rehman and Bonfield 1997). Similar observations were observed in this study, and peak area measurements ACa-CH:HA showed a decline after day 1 till day 14 indicative of an immature layer formation of CA, which is also reported earlier as an embryonic form of the ideal calcium apatite layer (Khan 2009). Maachou (Maachou *et al.* 2008) *et al.,* have reported about the characterisation and in-*vitro* bioactivity of CH:HA composite membranes synthesized by Freeze gelation. They mentioned that after immersion in SBF medium the absorption band at 1596cm^{-1} and 1380cm^{-1} disappeared, these bands have been ascribed to -C-O primary

alcohol and secondary amide. Disappearance was indicative that both amide and alcoholic groups contributing towards the formation of Ca-P layer at the surface. However, for our studies these bands were present at 1559cm^{-1} attributed to free primary amino group (Wawro and Pighinelli 2011; Pighinelli and Kucharska 2013) and 1376cm^{-1}, and showed decrease in intensity with time for both ACa-CH:HA and ASa-CH:HA specimens. In another study performed by Siddiqui and co-worker (Siddiqui and Pramanik 2014), FG scaffolds were prepared with varying ratios of β-TCP. Biodegradation studies of these composite FG membranes was performed in SBF for up to 4 weeks [CH: TCP (70:30) and (80:20)] (Siddiqui and Pramanik 2014), formation of apatite layers was reported to be initiated after 7 days of soaking in SBF. For the current study the peak area calculations were suggestive of layer formation at D21. Furthermore, they also mentioned that amount of CA layer formed gradually showed an increment with time and entire surface area of the scaffolds was coated after 18 days of immersion (Siddiqui and Pramanik 2014). Although the study mentioned about agreement with previous studies it only showed an SEM as an evidence of apatite layer formation (Siddiqui and Pramanik 2014). Siddiqui *et al.*, also mentioned that CH:nHA (80:20) was a more suitable candidate for bioactive layer formation as increase in apatite layer for these samples was due to the uniform distribution of nano sized bioceramic, which lead to enhanced nucleation sites (Causa *et al.* 2006; Siddiqui and Pramanik 2014). In this study peak area analysis was also performed at consecutive days for peak at 3650cm^{-1} and 960cm^{-1}. Peak area measurements were also performed for phosphate peak $\nu 1$ at 960cm^{-1} to assess the alterations in the intensity. A study conducted by Rehman *et al* have mentioned that carbonated apatite have two well defined peaks ($\nu 3$) appearing at 1649 and 1470cm^{-1} (Rehman and Bonfield 1997). In composite spectra of FG membranes these peaks are obscured due to the presence of peaks at 1651cm^{-1} which is also present in neat CH spectra.

It would be interesting to assess long term bioactivity studies for further in depth characterisation of freeze gelated membranes by XRD analysis, EDX analysis to determine the elemental components. Moreover, addition of nano HA to FG membranes can also be promising for other GTR and biomedical applications (Zhao and Chang 2004). It is envisaged that HA favours the nucleation of bone like apatite, and a more homogenous distribution or higher amount of HA inclusion could have the potential to provide more nucleation sites and further improve the bioactivity (Hong Li *et al.* 2010).

5.4.3. Conclusion

The ability of porous FG membranes to be conducive to CA layer formation was analysed after SBF immersion. The changes in the pH and weight suggest that a CA layer formation increased the overall weight profile and pH with time. FTIR-PAS spectroscopy confirmed the existence of carbonate moiety FG membranes.

5.5. Drug incorporation

Drug incorporation into the FG core layer was achieved using a cross linking agent at various concentrations and assessing the effect of this on the loading capacity of each FG membrane. Scanning electron microscopy was performed after cross linking membranes and FTIR spectroscopy was used in both ATR and PAS mode to study surface and bulk chemical properties of the drug. Effect of cross-linking on the swelling ratio of these membranes was conducted over a period of 1 week and loading capacity was calculated using the formula described previously in methods section. A calibration curve of the drug was made using Beer's Lambert Law to assist calculation of the % recovery of drug studies (Chapter 4, Figure 102, Page 172).

5.5.1. Scanning electron microscopy

Scanning electron microscopy of the FG core layer structures after cross-linking with 5 wt/v % Sodium tripolyphosphate (NaTPP) and drug loaded by adsorption is shown in Chapter 4, Figure 91. The importance of porous templates have been highlighted and emphasized in previous sections. Pores are critical for vascularization, cell adhesion, penetration and proliferation within the scaffold for bone tissue engineering (Nguyen *et al.* 2012). Cross sectional micrographs of the cross-linked membranes depict that the porous structure was retained. However, the pores became slightly compressed, this could be due to the samples required complete drying while performing SEM studies and water uptake could possibly show some extent of swelling which is evident in the swelling analysis data discussed in a later section of 5.5.3. Cross-linking could also be responsible for such pore microarchitecture. Pores became slightly elongated as well and drug crystals were could be observed on the lamella and top surface of the membranes. These observations when compared to the blank FG membranes presented in Figure 64 show significant changes. Membranes comprising of HA and drug showed less pores emerging on the top surface of the composite membranes.

5.5.2. Fourier Transform Infrared spectroscopy (ATR-PAS)

Spectroscopic methods have been adapted in characterisation of biopolymers with drug interactions due to their non-destructive nature. They can be adapted alongside other solid-state techniques for quantitative determination of pharmaceutical excipients. In order to achieve this by using the least destructive technique, FTIR spectroscopy can serve the purpose to study the inter / intramolecular bond formation in between polymers and drugs. Appropriate characterisation of the surface and bulk characteristic of scaffolds is necessary for predicting the performance of composite biomaterials (Ahmed *et al.* 2013).

FTIR studies were performed in both ATR and PAS modes to study bulk and surface interaction of tetracycline hydrochloride (TCY) and Chitosan (CH). Characterisation of samples using PAS has been reported extensively by Rehman *et al.,* for analysis of polymers, ceramics and composite or hybrid materials (Rehman *et al.* 1995; Rehman and Bonfield 1997). The inclusion of phosphate group into CH is of particular interest in bone TE applications as these moieties may act as templates for HA growth through complexation with Ca^{2+} and enhance the osteoinduction and osteoconduction properties (Pati *et al.* 2011). Moreover, the ion pairs, liberated through negatively charged Sodium Tripolyphosphate (NaTPP) with protonated amine functionality of CH, via ionotropic gelation are also expected to give CH an amphoteric nature, which may enhance protein adhesion and simultaneously accelerate the attachment of anchorage dependant cells (Pati *et al.* 2011).

Results obtained from surface characterisation by using ATR accessory of neat 0 wt%, 5 wt% and 10 wt% cross-linked specimens are shown in Chapter 4, section 4.10.2. Non cross-linked spectra showed a strong and broad band at 3354 cm^{-1} pertinent to overlapping of the -OH and N-H stretching vibration of functional group engaged in hydrogen bonds. Peaks at 2921 and 2877 cm^{-1} are denoted to C-H stretching, peaks ascribed to glucosamine units are present at 1150, 993 and 1027cm^{-1}. Other characteristic peak of amide I band (C=O stretching) are observed at 1649cm^{-1} and amide II bands appear at 1581cm^{-1}(N-H in plane deformation) (Mucha and Pawlak. 2002; Siddiqui and Pramanik 2014). Furthermore, peaks present at 1376, 1320 and 1421cm^{-1} are attributed to CH_2 wagging with -OH in plane deformation (Teng *et al.* 2009; Thein-Han and Misra 2009). The presence of free amino group in CH ($-NH_2$) gives it the diversity of interacting with functional groups with these moieties. In a study conducted by Tiwary *et al.*(Tiwary and Rana 2010), on evaluating the effect of NaTPP on CH membranes, cross-linking at 4% w/v with NaTPP showed peaks at 1060-1300cm^{-1}, which were suggestive of phosphonate linkages between -NH of CH and PO_3 . At 5 % w/v, they noticed two peaks at 1140 and 1280 cm^{-1} (due to restricted rotation) which were indicative of symmetric and anti-

symmetric stretching of phosphonate linkages respectively (Tiwary and Rana 2010). Furthermore, they also mentioned that terminal -PO_3 moieties of NaTPP seem to be linked to –NH_3^+ moieties of CH monomer on each side. Spectral information for our samples when cross-linked with 5% w/v and 10% w/v revealed a peak around 1223 and 1224cm^{-1} which is ascribed to P=O stretching vibration in phosphate ions. In another detailed study on cross-linking of CH via NaTPP by Bhumkar *et al.,* they mentioned that after cross-linking, P=O peak at 1150cm^{-1} appeared, another peak at 1655cm^{-1} disappeared and 2 new peaks at 1645 and 1554 cm^{-1} appeared. This disappearance was attributed to the linkages between phosphoric and ammonium ions. Moreover, a decrease in the amide II bands was also indicative of ionic cross-linking between CH and NaTPP according to Bhumkar and co-worker (Bhumkar and Pokharkar 2006). Similar observations were also noted in this study (Figure 146 and 147). It has also been reported by Knaul *et al.,* that amide II peak at 1588cm^{-1} is indicative of possible interactions at the amine group of CH and this could point towards the binding of phosphate to this site (Knaul *et al.* 1999).

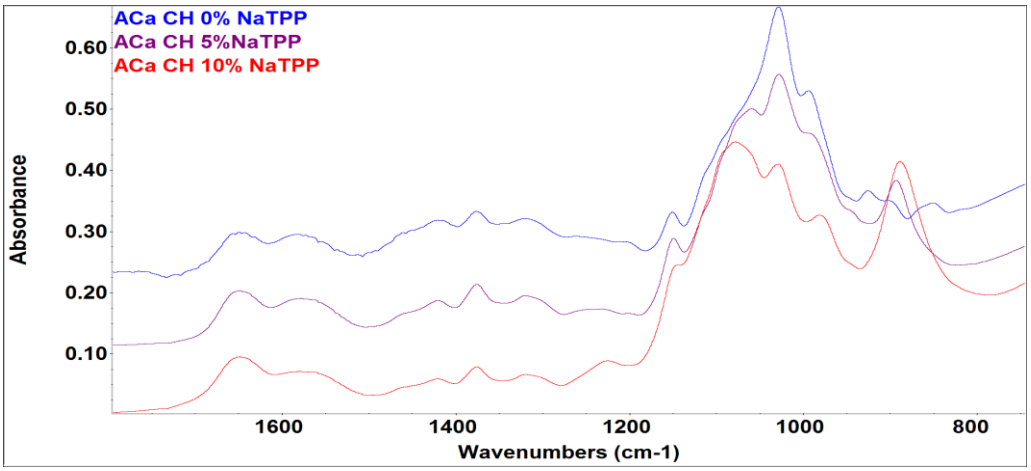

Figure 146; Finger print region of FTIR-ATR of ACa-CH 0%, 5%, 10% wt/v NaTPP.

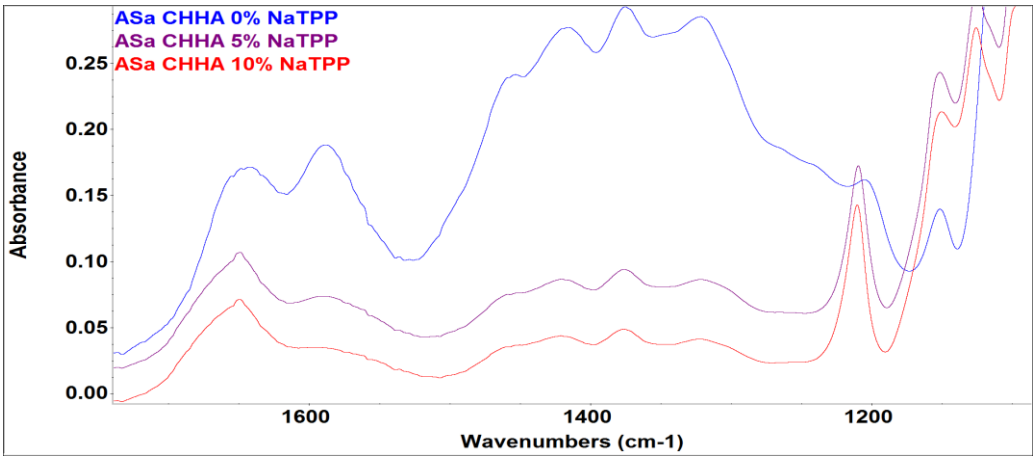

Figure 147; Finger print region of FTIR-ATR of ASa -CH:HA 0%, 5%, 10% wt/v NaTPP

FTIR analysis of Amide II bands in both ATR and PAS accessory mode has shown that peaks at 1540 to 1588cm^{-1} subside as the percentage of the cross-linking agent is increased. In addition, a small shoulder at 3600cm^{-1},which is seen in HA incorporated spectra particularly attributed to the functional group (-OH) of HA molecule, is also present in the spectra of FG membranes. Phosphate modes of ν_1 at 960cm^{-1}, ν_3 at 1057cm^{-1} and ν_4 at 571 and 601cm^{-1} are also more prominent in FTIR spectra collected using PAS (Rehman and Bonfield 1997). A significant finding seen for the 5 and 10% cross-linked spectra is the appearance of a peak at 3626cm^{-1} which is also present in the neat NaTPP spectra in Figure 91. The increasing intensity of this peak is suggestive that there is possibly stronger bonding of NH of CH and NaTPP molecules with higher percentages. Similar results were observed by Rodrigues and co-workers (Rodrigues *et al.* 2012). As shown in the Figure 148, Bhumkar *et al.,* proposed two mechanisms of bonding, either ionic cross-linking (Figure 147) or deprotonation.

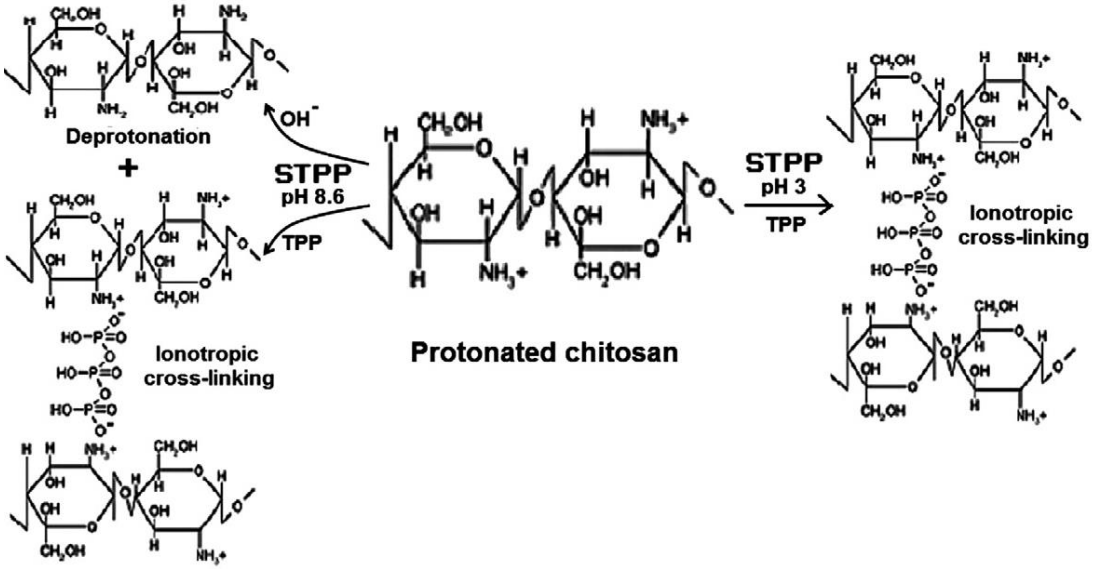

Figure 148; Possible interaction of CH with NaTPP as proposed by Bhumkar *et al.,* 2006 (Bhumkar and Pokharkar 2006) and F.Pati *et al.,* (Pati *et al.* 2011)

When cross-linking the FG membranes with 10 wt% NaTPP, very prominent shifts and peaks are observed in the molecular fingerprint region. Especially in the glyosidic segment of the FTIR spectra. These shifts in peaks are indicative of the ionic cross-linking in between CH and NaTPP

Pati and co-workers reported a shift in the peak position from 1340cm^{-1}, pertaining to C-N stretching coupled with NH in plane deformation to 1330cm^{-1}, this shift was attributed to the ionic inter actions of NaTPP ions. Furthermore, they also observed a decreased intensity of bands at 1450cm^{-1}, 1390cm^{-1} (due to CH_2 wagging coupled with OH in plane deformation). Similar observations were seen for our samples cross-linked with 10% w/v of NaTPP and this

could be attributed to the formation of hydrogen bonding with phosphate group of NaTPP. The degree of cross-linking has been referred to as the percentage of free amino groups (Pati *et al.* 2011). It would be interesting to study the degree of cross-linking in detail by utilizing the Ninhydrin essay reported by F.Pati *et al.,* (Pati *et al.* 2011). Cross-linking of CH with NaTPP has shown to give better stability of CH template prepared in dilute acids, PBS and SBF. This stability was attributed to the strong intra and inter-molecular ionic cross-linking of protonated amines with PO_4 groups of NaTPP. It would be interesting to see if lower concentrations of NaTPP can cause the same chemical and physical characteristics of CH membranes (Pati *et al.* 2011).

The interactions between bioactive molecules and biopolymers are of interest in development of polymeric devices for controlled drug delivery. In particular, CH due to its versatility in the ability to undergo various forms of structural chemical modifications is of special interest. FTIR-PAS spectra of samples after drug uptake show peaks in the molecular finger print region which are similar to the peaks seen in neat TCY. These are assigned to the crystalline bands of TCY. Results from the ATR data were suggestive of drug interactions via adsorption. It has been mentioned in a study conducted on the kinetics of adsorption of TCY on CH particles, that adsorption occurs at a solid-liquid interface and since adsorption is a surface effect, it tends to selectively remove or store one or more type of adsorbate molecules present in the solution. This could be either by physical interactions (physisorption) or through chemical process (chemisorptions). This uptake is affected by pH, ionic strength and temperature (Caroni *et al.* 2009; Caroni *et al.* 2012). Spectral information obtained by using ATR and PAS accessory for TCY loaded samples showed subtle changes. A ring carbon-carbon stretching vibrations occur in the region of 1625 and 1530cm^{-1}. Reports from a detailed study suggests that these bands are variable in intensity and are observed at 1625-1590 cm^{-1}, 1590-1575 cm^{-1}, 1525-1470 cm^{-1} and 1465-1430cm^{-1}. Several aromatic phenyl ring vibrations are also observed which are ascribed to C-C ring stretch. Furthermore, they also mentioned that the bands in the aromatic ring vibration are sensitive to alterations in the nature and position substituent's (Gunasekaran S *et al.* 1996). Peaks observed in the FG membranes pertaining to TCY were present at, 1643, 1576, 1513, 1450 cm^{-1} and more detailed information regarding the peak identification has been described earlier in Chapter 4, table 21. It can be observed in Figure 149 that the peaks in PAS and ATR give variable information. Peaks at 1650 , 1651 (νC=C of aromatic ring), 1455, 1376, 1316 (δOH, δC-C, νC-C, δN-H) , 1060, and 1033 cm^{-1} occur in the spectral profile obtained by PAS whereas spectral information obtained by ATR show peaks at 1641, 1577, 1514, 1451, and 1395cm^{-1}. This confirms that chemical structure of the surface of

the membrane is different to the one in the bulk of the membrane. Similar results were also reported by Caroni and co-workers in their study based on tetracycline adsorption on CH (Caroni *et al.* 2012). Results obtained from using ATR and PAS accessory were suggestive that TCY was able to penetrate the porous membranes and possibly had some inter molecular bond formation to CH *via* NaTPP. CH being a cationic polymer was able to cross-link with anions of NaTPP, which might have led to the formation of inter/intra molecular ionic bonds with cationic nature of TCY.

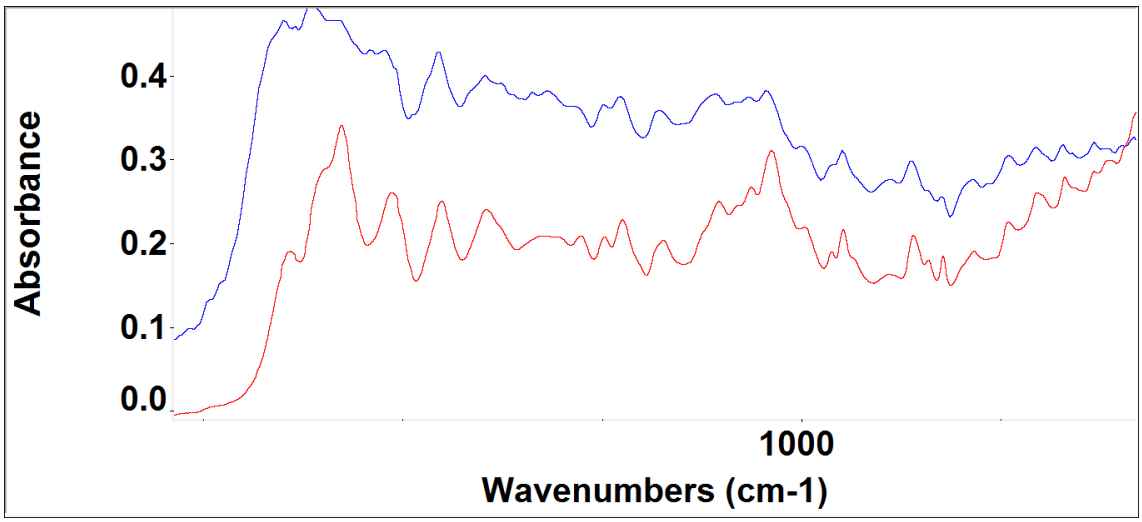

Figure 149: FTIR spectra of finger print region of ASa-CH, using PAS and ATR accessory

5.5.3. Swelling ratio of cross linked FG membranes

Swelling ability of CH is influenced by the ionic interactions in between CH chains. It is reported by Tiwary and co-worker, to be dependent on the cross-linking density achieved. Generally an increase in the cross-linking density is reported to decrease the swelling equilibrium (Tiwary and Rana 2010). Another key factor responsible for swelling of cross-linked CH hydrogels is the ionization of functional groups along the polymer chain and the ionization of crosslinking agent (Giri *et al.* 2012). Swelling ratio of cross-linked membranes evaluated over a period of 168 hrs using 0%, 5% and 10 % (wt/v) is shown earlier in Figures 100. The swelling ratio of cross-linked CH membranes has been correlated to the hydrophilicity of the whole network. Hydrophilic nature of CH tends to decline due to loss of amino binding sites.

Results obtained for this study were also suggestive of a similar phenomenon, where a higher cross-linking percentage reduced the water uptake in FG membranes. It has been reported by Tasselli *et al.,* that as the concentration of the cross-linking agent increases, more amine groups in CH are consumed due to the reaction. Hence, the cross-linked CH becomes less capable of hydrogen bonding with water molecules, resulting in a decreased degree of

swelling at equilibrium. In the current study at 10wt% the swelling was reduced to 40 %. Furthermore, swelling is likely to decrease due to elastic restrictions imposed by the cross-linker that prevents expansion in water as well as the indicated reduced hydrogen bonding that accompanies structure modification of the amines (Tasselli *et al.* 2013).

Another study conducted on cross-linking porous CH scaffolds with Genipin by Gorczyca and co-workers have reported about the water uptake of scaffolds after cross-linking with 0.5, 1, and 2 %. They stated that 0.5% cross-linked scaffolds had a slightly higher swelling capacity compared to neat scaffolds; this was due to weak mechanical properties of non-cross linked scaffold. Further increase in cross-linking concentration resulted in reduced swelling capacity. This could be attributed to increased hydrophilicity of the material due to increased cross-linking degree. Swelling ratio of biopolymers is greatly dependent on the ionic strength of the medium. Most studies report performing swelling studies in PBS or distilled water. This media is void of multivalent cations, the presence of which is linked with ionic cross-linking at the interface of materials, ultimately causing a decrease in the swelling capacity of wound exudates (Gorczyca *et al.* 2014).

5.5.4. Drug release

The aim of the drug release studies was to assess the effect of cross-linking on loading and release profile of FG membranes. CH HA composites are promising candidates for periodontal tissue regeneration, however, their in-vivo utilization sometimes requires adjuvant antibiotic therapy (Teng *et al.* 2009). In order to enhance the structural integrity of CH products, researchers have attempted to chemically cross-link CH. This has notably resulted in enhanced flexibility, reduction in swelling index and effecting the release of pharmaceutical excipients (Phaechamud and Charoenteeraboon 2008). Studies have been conducted in the past, based on loading porous CH scaffolds with Tetracycline (TCY) and doxycycline hyclate (Shen *et al.* 2008; Teng *et al.* 2009), (Phaechamud and Charoenteeraboon 2008; Tiwary and Rana 2010; Caroni *et al.* 2012). A study conducted on drug loading of cross-linked CH films at various percentages reports that at 5% w/v of NaTPP appeared to be optimum for CH, however, at higher concentrations (10-20% NaTPP w/v) the drug had enhanced passage across the films (Tiwary and Rana 2010). This behavior could possibly be indicative of higher amount of negative charges occurring due to the presence of $-PO_3$ moieties at the surface. This is in contrast to our results as higher percentage of drug entrapment was noted for samples cross-linked at 5% w/v as compared 10%w/v. Although the entrapment efficiency for 5% NaTPP was higher for ACa-CH (85% Porosity) and ASa-CH (78% porosity) membranes as compared to 0%

and 10% in this study, there are several other factors that need to be considered when analyzing drug entrapment, % release and % recovery such as swelling, degradation and porosity percentage of scaffolds. The TCY adsorption on CH has been investigated earlier by Caroni and co-workers. They reported that process of adsorption on TCY involves surface protonation of CH. As its concentration is increased it tends to disrupt the CH surface (Caroni *et al.* 2009; Caroni *et al.* 2012). With regards to the % recovery profile, initial rapid recovery from the ACa-CH in 0% NATPP could be explained due to the less surface interaction of the drug, or it could be more concentrated on the surface, and as the surface drug dissolves, the rate of release slows down (Caroni *et al.* 2009).This surface and bulk uptake of drug is explained earlier by the spectral information collected by FTIR utilizing ATR and PAS accessory.

This higher loading could be due to the membranes having a more favorable interaction with TCY and cross-linking agent at 5% NaTPP. Surprisingly it was unexpected to see 10% NaTPP group showing lower entrapment efficiency. This could be due to the cross-linking agent closing the pores and increasing the rigidity of polymer chain, hence, causing less drug uptake. These membranes also showed a steady increment in % recovery profile. A study conducted by Teng *et al.*, reported the loading and release studies of CH and HA FG scaffolds with TCY in a functionally graded scaffold prepared by freeze drying (Teng *et al.* 2009). They noticed that increase in HA content decreased the pore size and porosity of the scaffolds, similar findings were observed for our FG membranes. Moreover, they mentioned that decreased pore size and porosity rendered the fluid access more difficult, therefore, retarding the diffusion process and release rate of TCY. It could be envisaged that cross-linking membranes at 10% w/v (NaTPP) resulted in more shrinkage of the pore morphology and lead to less drug uptake as compared to 5% NaTPP, which provided a more suitable balance in between the drug adsorption and pore size. The recovery behaviour has also been partially dependent on the hydrolytic behaviour of the membrane. The % recovery ACa-CH:HA and ASa-CH:HA showed variations in the recovery profile for 0, 5 and 10% NaTPP. As mentioned earlier this could also be correlated to the porosity percentage and pore size variations of CH:HA membranes. Swelling and degradation kinetics can further affect the release or recovery pattern. Neat ASa-CH:HA membranes showed a steady increment in recovery. This behavior can be ascribed to the entrapment of the drug and its interaction with CH network *via* hydrogen bonding and ionic interactions or it could also be adsorbed onto the HA particles due to the strong affinity with calcium ions, as reported earlier by Teng and co-workers (Teng *et al.* 2009). To achieve fine tuning of the release properties of porous CH HA based scaffolds,

designing carriers with porous structures or functionally gradient approach could be of essence in future.

Due to the anionic property of NaTPP, it interacts with polycationic CH through electrostatic forces. The electrostatic forces between cross-linked CH and NaTPP leads to decrease intermolecular spaces and consequently results in suspension of the release of tetracycline and prolonged disintegration of sponges as reported in an earlier study by Shen and co-workers (Shen *et al.* 2008). Furthermore, they also mentioned that disintegration of non-cross-linked sponges could be due to gradual release of mild acids. Nevertheless, the higher drug loading achieved for 5% NATPP membranes observed for the current study needs further investigation. Moreover, the % recovery pattern observed with 0%, 5% and 10% NaTPP cross-linking with and without HA also needs further in-depth characterisation to establish a baseline data for adding it as a component in GTR membrane. It would also be interesting to look into cross-linking with lower percentages of the cross-linking agent in the future. Long term release profile for up to 24 hrs can also be beneficial for predicting *in-vivo* release pattern.

5.5.5. Conclusion

Drug loaded freeze gelated porous membranes were prepared after cross-linking at different concentrations to study the effect of cross-linking on release profile. Chemical interactions of Sodium tripoly phosphate and tetracycline were studied by both surface and bulk characterisation techniques. FTIR spectral information revealed the NaTPP caused both surface and bulk alterations in the spectral information of FG membranes. In addition, the surface and bulk analysis of drug loaded cross-linked membranes was also indicative of some bonding between composite membranes. Swelling profile indicated a decrease in water uptake of membranes at 10% wt/v of NaTPP showing that, cross-linking FG membranes can harness the water uptake behaviour depending upon the application. It was revealed that maximum entrapment efficiency was achieved at 5% w/v of NaTPP. % Recovery profile of 0% and 10% w/v of NaTPP showed an initial burst and 5% showed a steady recovery over the experimental period. The possibility of properly tuning the ideal cross-linking percentage and loading efficiency of drug onto the membranes suggests that these porous freeze gelated membranes can be used as a drug delivery vehicle in GTR membranes for periodontal tissue engineering.

SECTION III

5.6. Chitosan Electrospinning

This section discusses the results obtained by electrospinning CH fibres in both random and aligned orientations. Physiochemical, mechanical and biological characterisation have been discussed in detail. Degradation was assessed using FTIR analysis, assessing the changes in pH values and UV-Vis spectra of the degraded media.

5.6.1. Scanning Electron Microscopy

Electrospinning is an attractive technique to fabricate scaffolds that could mimic extracellular matrix (ECM). This promising technique has shown the capability to achieve micro to nanofibres that will more closely resemble native ECM in which cells normally exist in physiological conditions (Jeong *et al.* 2011). We have demonstrated that CH fibres with both random and overly aligned orientation can be obtained using very low concentrations of polyethylene oxide (PEO). Although the use of fibre forming agent such as PEO have been discussed in the literature before (Jankovic *et al.* 2013; Sarkar *et al.* 2013; Toskas *et al.* 2013), this agent was used at a low concentration in the current study and the total CH concentration was 4.5 wt% with a 95:5 ratio to PEO. It is well known that PEO exhibits a biologically inert nature and hence, it is commonly used as copolymer in electrospinning. Moreover, it is frequently considered when using natural polymers to obtain fibres (Jeong *et al.* 2011). It is known to act as a plasticizer in electrospinning procedure (Pakravan *et al.* 2011). The use of Triton X 100 ™ has also been mentioned as an additive (surfactant) to the polymer solutions to enhance electrospinning. A study conducted by Jeong *et al.,* have reported that PEO inclusion of up to 50% are required for uniform nanofibre production (Jeong *et al.* 2011). This is in contrast to what we were able to achieve, as bead less fibres were generated using low conc of PEO. The ability to obtain aligned fibres has interesting implications in the field of TE. Higher degree of alignment can be achieved by modulating the electric field configuration or by depositing fibres in a restricted area. A study conducted on obtaining aligned CH fibres reports the use of copper wire. The copper wire was winded as an electrode onto the insulating cylinder (Bhattarai *et al.* 2005). Although, in the current study no such electrode was used therefore, the fibres obtained were not highly aligned. The rigid D-glucosamine units of CH are highly crystalline in nature and its ability to form hydrogen bonds leads to poor solubility in organic solvents making the electrospinning of neat CH even more complex. Hence, studies performed in the literature discuss about cross-linking CH with various other polymers and cross linking agents such as gluteraldehyde and/or genipin (C.K.S. Pillai *et al.* 2009; Frohbergh

et al. 2012; Norowski *et al.* 2012). The use of toxic solvents such as trifluoroacetic acid (TFA) ($C_2HF_3O_2$) and hexafluoro isopropanol (HFIP) for CH electrospinning have been extensively discussed in the literature (Frohbergh *et al.* 2012). TFA is known to be environmentally harmful, very toxic and corrosive, therefore, from an industrial point of view the use of TFA is very limited (Pakravan *et al.* 2011). Frohbergh *et al.,* have reported that they were able to optimize conditions for production on beadles CH fibres. Conditions such as humidity, temperature and DD of CH were looked into and a CH solution with 7wt% was used for electrospinning random fibres (Frohbergh *et al.* 2012). However, they used TFA and genipin as cross-linking agent in their study. Studies performed on electrospinning CH report an average fibre diameter within the range of 40 to 200 nm (Bhattarai *et al.* 2005; Jessica D. Schiffman 2007; Jeong *et al.* 2011; Pakravan *et al.* 2011; Sarkar *et al.* 2013). Sarkar *et al.,* (Sarkar *et al.* 2013) and Spasova *et al.,* reported that they were able to achieve fibre diameter in the range of 80 to 180 nm using PEO / CH composite (Spasova *et al.* 2004). In the current study fibre dimensions varied from 288 to 400nm, which could be due to restricted ratio of CH:PEO. Another study performed by Lou *et al.,* used PEO CH ratio of 60:40 to obtain fibres ranging from a few nm to µm (approximately 30nm) (Sailaja *et al.* 2006). Klossner *et al.,* in their study demonstrated that as polymer concentration is increased consecutively number of beads and fibre diameter decreased (Klossner *et al.* 2008). The polycationic nature causes the fibres to repel which was observed during our electrospinning process. It has been hypothesized by Dilamian *et al.,* that repulsive forces present in between ionic groups within the polymer backbone increases due to high electric field while performing electrospinning, this inhibits fibre formation and produces particles only; this phenomenon was also observed in the current study during optimization time for fibre production (Dilamian *et al.* 2013). The fibre directionality graphs also confirmed that random fibres were spread at different angles and aligned orientation had significantly lesser range of distribution.

5.6.2. Fourier Transform Infrared Spectroscopy (FTIR) (ATR-PAS)

FTIR spectra of fibres collected by electrospinning using ATR and PAS accessory to investigate surface and bulk molecular interactions of the mats showed that PEO had successfully integrated with CH. Strong broad spectral band at 3500 to 3100 cm^{-1} are allocated to N-H and O-H stretching vibration and intermolecular hydrogen bonding of CH structure. Three spectral peaks at 1150, 1029 and 1023 cm^{-1} are attributed to stretching vibrations of the glycosidic bonds (C-O-C), peak at 1591cm^{-1} is ascribed to amide II (N-H in plane deformation), other significant bands were 1420 cm^{-1}, owing to CH_2 wagging coupled with –OH in plane

deformation, 1375cm^{-1} due to amide III. Peak at 892cm^{-1} is pertinent to saccharide structure (Sarkar *et al.* 2013). Furthermore, the appearance of band at 2885cm^{-1} is attributed to CH_2 stretching in CH structure. A detailed study conducted by Kriegel and co-workers on CH and PEO nanofibres reported the peak at 2885cm^{-1} to be ascribed to CH_2 stretching vibration, and its increased intensity resulted in decrease of $-NH_2$ stretching at 1590cm^{-1} (Kriegel *et al.* 2009). Peaks observed at 1063, 1026 and 1150cm^{-1} in spectral data of random and aligned fibres are suggestive that PEO formed a complex with CH. PEO spectra shows a strong triplet at 1144, 1092 and 1059cm^{-1}, associated with asymmetric C-O-C stretching vibration (Figure 150) (Sarkar *et al.* 2013; Toskas *et al.* 2013). Figure 150 also shows the shifts and changes in the peak numbers after PEO inclusion in the finger print region (a). Peaks at 1460cm^{-1} are ascribed to asymmetric CH_2 bending and 1341cm^{-1} in neat PEO spectra correspond to symmetric CH_2 wagging. Changes in the molecular finger print region are also indicative of that CH chains were encouraged to form hydrogen bonds with PEO, by reducing the polyelectrolyte effect. The triplet peaks of PEO due to -C-O-C- bands are strongly dependant on the crystallinity of PEO and intermolecular interactions in between C-O-C groups of CH as reported previously by Mehrali and co-workers (Talebian *et al.* 2014). Although the spectra of CH:PEO fibres shows subtle differences, within the -C-O-C region to have peaks at 1026 and 1062cm^{-1}, reports from a study conducted by Kolhe *et al.,* on combinations of PEO and CH also mentioned that absence of peaks at 843, 1280 and 947cm^{-1} were suggestive that intermolecular interactions were absent (Kolhe and Kannan 2002). The shifts of the peaks in the –NH and –OH stretching vibrations regions are suggestive of partial miscibility which is in agreement with the literature (Kolhe and Kannan 2002).

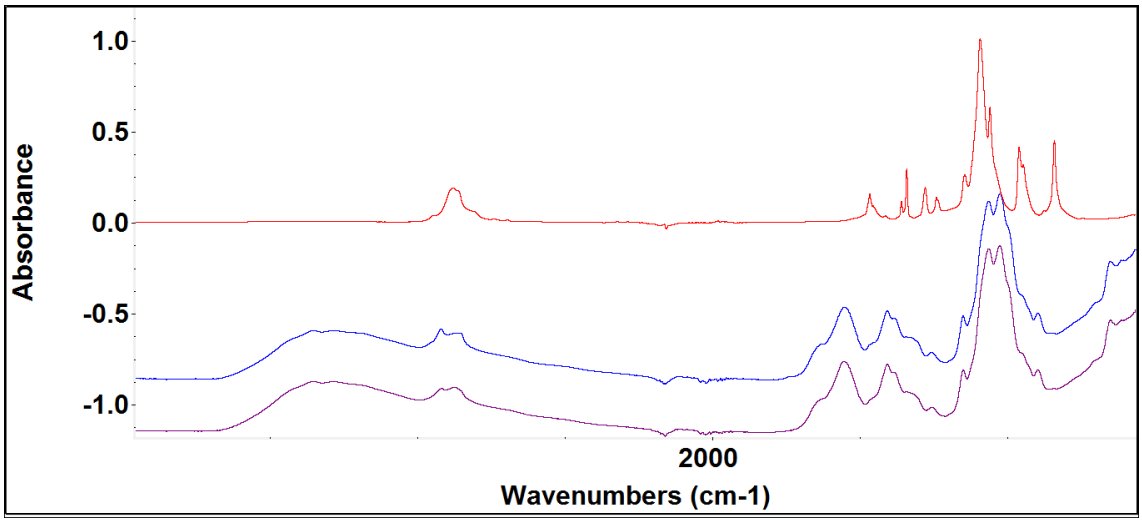

Figure 150: ATR FTIR, of Aligned, Random and virgin PEO spectra, Showing the molecular finger print region and –NH and –OH stretching vibrations.

Few other studies performed on CH and PEO have demonstrated that that using PEO as a copolymer tends to disrupt the self-association of CH chains by creation of H-bonding between its -OH groups and H_2O molecules (Kriegel *et al.* 2009). Consequently this results in reduced repulsive forces between polycationic groups of CH and promotes chain entanglements which encourage fibre formation (Bhattarai *et al.* 2005; Dilamian *et al.* 2013). Pakravan and co-workers added PEO in varying percentages and stated that in their studies absorption peak at 1112cm^{-1} attributed to ether band shift to lower wavenumbers as the CH was added. They also mentioned that PEO addition helps in decreasing the viscosity by breaking inter and intramolecular interactions of CH chain through new interactions with PEO. Another mechanism proposed, suggests that flexible PEO chains occupy themselves in between the rigid CH structure (Pakravan *et al.* 2011). An extensive study performed by Pakravan *et al.,* on CH PEO electrospinning have reported that the interaction of CH PEO is caused by strong hydrogen bonds forming between hydroxyl and amino groups present of CH and ether groups present on PEO (Pakravan *et al.* 2011). As shown in the figure 151 illustrates the molecular interactions.

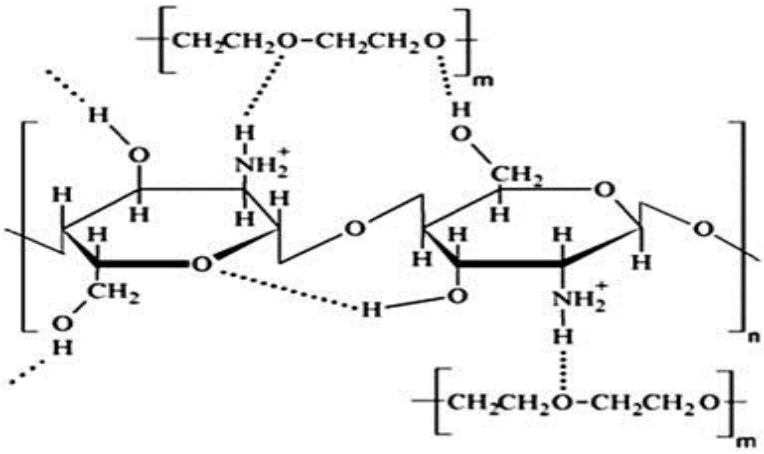

Figure 151: Propose Hydrogen bonding interaction in between CH and PEO as suggested by Pakravan *et al.,*(Pakravan *et al.* 2011), Adapted with kind permission from Elsevier.

When blank LMw CH film (Figure 152) spectra was compared with PEO blended fibres for the current study, the glucosamine unit showed absorption peak at 1024cm^{-1}, which when compared with ATR spectra of CH PEO showed a doublet formation appearance of peaks at 1062 and 1026cm^{-1}, furthermore, amide II peak at 1545 shifted to 1555cm^{-1} (Figure 152). Shifts in peaks at amine, hydroxyl and ether segment may be attributed to the formation of hydrogen bonds in between polyether oxygen and amino hydrogen in PEO and CH respectively

(Deyao *et al.* 1993; Chen *et al.* 2008) (Dilamian *et al.* 2013). Furthermore, when aligned and random CH PEO mats were assessed by PAS accessory, neat CH showed a strong peak attributed to amine band at 1559cm^{-1} which shifted to a higher wavenumber at 1592cm^{-1} in electrospun CH. This is also indicative of hydrogen bonds formation in between polyether oxygen and amino hydrogen of PEO and CH molecules (Dilamian *et al.* 2013). Over all spectral data obtained by ATR-FTIR and PAS-FTIR were suggestive of changes in the molecular finger print region, which were indicating that CH chains were encouraged to form hydrogen bonds with PEO, by reducing the polyelectrolyte effect. It would have been interesting to analyse the rheological properties of the electrospinning solution made and by subjecting it to various shear rates to correlate the effect of its flow behaviour on spin ability, but non availability of the rheometer capable for analysing such a sample become a barrier.

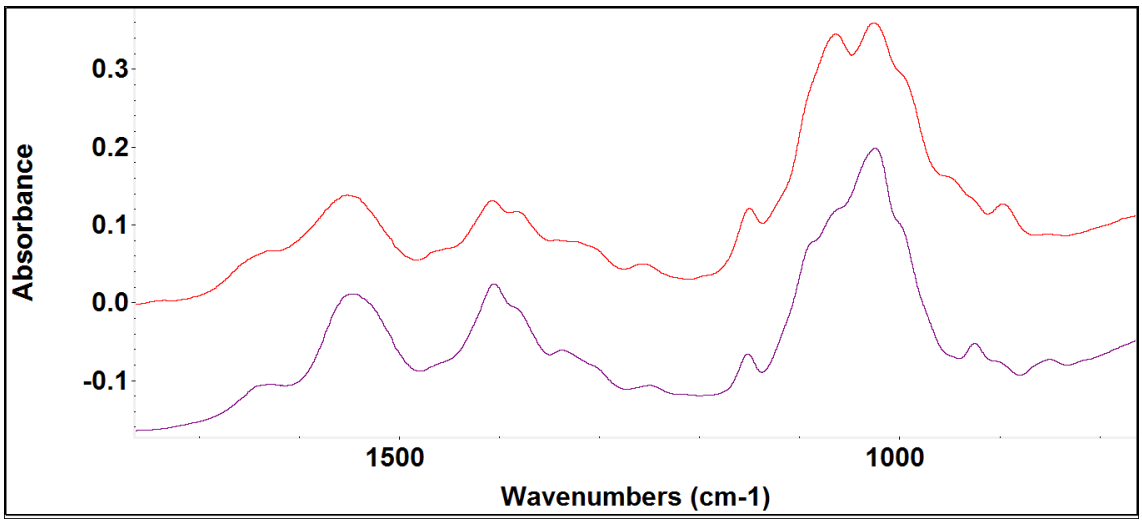

Figure 152: Amide I, Amide II and C-O-C region of neat LMw CH film and CH PEO electrospun fibre.

5.1.2. Mechanical tests

The results from the mechanical testing showed that aligned CH fibres, were not only easier to handle but also had a higher modulus of elasticity (stiffer) and a higher ultimate tensile strength. When compared to other commercially available resorbable GTR membranes (Bottino *et al.* 2012), random fibres performed poorly when subjected to tensile loads. Dry random fibres failed at 7.5 MPa while wet random fibres failed at 1.95 MPa. However, aligned fibres exhibited a much higher tensile strength. Dry aligned fibres exhibited a tensile strength of 28.76MPa which is higher than that of collagen GTR membranes (Bottino *et al.* 2012). On the other hand, although wet fibres were considerably weaker when compared to dry aligned

fibres, they still performed better than wet random fibres by having a tensile strength of 13.77MPa. It has been reported in another study that cross-linking CH fibres can enhance the mechanical strength and inhibit the swelling ratio to some extent (Kolhe and Kannan 2002). Other methods that could be adapted to increase the mechanical properties could be spinning random and aligned layer by layer or as mentioned earlier, using a cross-linking agent such as genipin, gluteraldehyde (GA) or NaTPP could have a positive effect on the physiochemical properties such as enhanced stiffness (Pillai *et al.* 2009; Tasselli *et al.* 2013).

5.6.3. Swelling Ratio

Swelling ratio of CH scaffolds as mentioned previously in discussions is usually dependant on the amount (conc) and type (Mw and DD) of CH present. This is due to the ability of CH to uptake water and swell, which has been reported extensively in literature (Qu *et al.* 1999; Ren *et al.* 2005; Thein-Han and Misra 2009; Tiwary and Rana 2010). In order for the fibres to be able to maintain a favourable environment for cell attachment differentiation, matrix deposition and transfer of nutrients swellability has been regarded as essential parameter for success of a tissue engineering construct. It has been reported by Tasseli *et al.,* that CH fibres swells most in acidic conditions when compared with saline solution or distilled water. They mentioned that CH is a weak base with a pKa or 6.4, at a lower pH amine groups of CH are ionized to ammonium ions (NH_3^+) , hence, the cationic charges present in the fibre structure act as repulsive forces in between the polymer chains inducing more swelling (Tasselli *et al.* 2013). Jankovic *et al.,* reported swelling profile of CH PEO fibres over 60 mins and mentioned that within the first 15 mins swelling profile reached 100% and after 60 minutes a reduced profile was observed at an overall swelling ratio of 80% (Jankovic *et al.* 2013).

The addition of PEO to CH fibres decreases the repelling interactions of CH molecular chains in the electrospinning solution, hence, improving molecular interactions. As mentioned earlier in the FTIR spectroscopy discussion section intermolecular hydrogen bonding between CH and PEO also play a critical role in swellability of CH fibres.

5.6.4. In-*vitro* degradation

The rate of scaffolds degradation plays a critical role for biomaterials intended to be used as a biodegradable device and should be able to match up with the rate of new tissue formation in tissue engineering. Therefore, it is essential to understand the mechanism underlying electrospun fibre degradation in order to tailor make scaffolds for periodontal applications (Cunha-Reis *et al.* 2007). It is known that CH degradation occurs under the action of 8 different

enzymes. Lysozyme is the most commonly used enzyme for studying degradation of CH based scaffolds for in-*vitro* analysis. To study CH degradation, samples were assessed for Weight profile, pH change, UV-Vis analysis of the supernatant and FTIR-ATR spectroscopy of fibres at each time point.

5.6.5. Weight Loss

As mentioned previously degradation rate is inversely proportional to the degree of deacetylation. The degradation of CH electrospun fibres in such detail as performed in the current study by weight loss, pH and FTIR spectroscopy has not yet been reported. Studies conducted previously on assessing the effect of orientation on degradation of other polymers have been reported (Subramanian *et al.* 2013). Similar results were also obtained for this study as aligned fibres showed a more stable profile as compared to random fibres. Results were also suggestive that random fibres showed a higher degradation rate as compared to the aligned ones. Subramanian and co-workers have also reported the degradation of aligned fibres to be slower than randomly oriented fibres (Subramanian *et al.* 2013). However, they used poly (lactide-co-glycolide) fibres for their study and carried out the degradation study using PBS as the degradation media. In the present study we used lysozyme solution in PBS as the degradation media which was rejuvenated after every 2 to 3 days to mimic normal physiological conditions. Another similar study conducted by the same author on studying the degradation rates of random and aligned fibres have also supported similar phenomenon (Subramanian *et al.* 2011). The mass loss percentage of random fibres was significantly higher than aligned fibres. Subramanian *et al.,* have postulated that this is due to decreased pore sizes found in aligned mats, hence, decreasing the diffusion rate of lysozyme solution. Furthermore, they stated that axial alignment improves the compactness of fibres and results in decreased pore size (Subramanian *et al.* 2011). This is also indicative that randomly CH fibres in the present study might have higher porosity as compared to aligned orientation.

5.6.6. UV-Vis Spectroscopy

UV-Vis Spectroscopy has been used whilst performing CH degradation studies to identify certain functional groups in molecules. The absorption of ultraviolet or visible light by organic molecules is restricted to specific functional groups or chromophores that exhibit valence electrons of low excitation energy (Kumirska *et al.* 2010). Studies performed on characterisation of degraded supernatant in the past have reported two absorption bands within the range of 200 to 300 nm (Ulanski and Rosiak 1992) (El-Sawy *et al.* 2010). A band at 220nm might occur due to n-σ* (n= nonbonding, σ*= Antibonding) transition of amino group

and π-π*(π=Bonding to π*=antibonding, pi to pi transitions) transition of carbonyl and carboxyl groups. Another band at 280 nm is ascribed to n- π* transition of carbonyl or carboxyl group. The increase in intensity of these bands with respect to time as observed for random and aligned fibres has been ascribed to scission of 1-4 glycosidic bonds caused by rearrangement of radicals. Moreover, it is due to the formation of carbonyl and carboxyl groups as reported by Ulsanki *et al.,* (Ulanski and Rosiak 1992). Furthermore, correlation of these bands was explained by Ulsanki and co-workers to occur due to carbon oxygen double bonds (carbonyl groups) occurred after the main chain cleavage of CH and hydrogen abstraction reaction followed by the ring opening. The upward curvature of the bands with time could be due to increasing efficiency of –OH reaction with CH upon reduction of molecular weight (MW) (Ulanski and Rosiak 1992).

5.6.7. pH Analysis

pH value has been reported to be as a key element for metabolism during wound healing. It is also regarded as a pivotal parameter for therapeutic interventions in wound care procedures (Schneider *et al.* 2007). Chronic wounds are known to exhibit a high bacterial load resulting in an eventual pH above 7.3 (Schneider *et al.* 2007). pH analysis showed an gradual increment with respect to time for random and aligned CH fibres, reaching a peak of 8.5 at 28th day of degradation. In this study the aim was to mimic normal physiological conditions by rejuvenating the specimens with fresh lysozyme solution after every 2 to 3 days. Recently, Wang and co-workers reported monitoring pH profile for degradation of CH fibres reinforced by PLLA. They observed a decline in pH with time for PLLA CH fibres from 6.8 to 5.9. This was ascribed to acidic self-catalytic effect causing hydrolysis of PLLA. CH acting as a alkalescent polysaccharide, bears amino groups which neutralizes acidic PLLA products (Wang *et al.* 2009). This was in contrast to our results were we had neat CH fibres showing a gradual increment in pH value. Wei *et al.,* conducted extensive degradation studies by loading lysozymes on CH films incorporated with Calcium alginate micro particles. They mentioned that rate of CH degradation with lysozymes could be changed with the surrounding conditions, because lysozymes ability to cause chain breakage is highly sensitive to pH (Wei *et al.* 2011). In another study conducted by Zhang and co-workers, reported about change in pH and mass loss of plain CH. The results obtained were slightly similar to what we observed in the present study. At the end of 16 weeks of degradation by using PBS solution the pH value remained around 7.4 to 7.6 with no drastic changes seen during the overall experimental period (Zhang and Cui 2012).

5.6.8. Monitoring Degradation by Spectroscopy

Spectroscopic analysis of degradation profile of electrospun fibres was performed by FTIR-ATR. ATR accessory was adapted to acquire surface chemical alterations resulting due to degradation. A comparative spectrum displayed in Figure 153 showing day 0 and day 7 after immersion in lysozyme solution depicts reduction in overall intensity and shifts of spectral bands at 1562 and 1407cm^{-1}. A diminution in the intensity and peak shifts have been reported earlier to be indicative of bond breakage and chain scission in the CH ultra-structure (Ren *et al.* 2005). Significant changes can be observed for -C-O-C- region pertaining to glycosidic bonds, where peak at 1063cm^{-1} shifts to a higher wavenumber of 1067cm^{-1} with a decrease in intensity, another peak at 1028cm^{-1} shows an increase in intensity at day 7. Furthermore, alterations in the intensity of band at 894cm^{-1} attributed to CH deformation have also been reported in study performed by Kriegel and co-workers (Kriegel *et al.* 2009). Results obtained in this study depict similar alterations. Figure 153 shows the decrease in the intensity of the band attributed to typical absorption bands for PEO at 2869cm^{-1}, this could also be indicative of bonds breakage between CH and PEO. Bhattarai and co-workers observed the integrity of CH fibres after immersion in water over a period of 7 days. They synthesized CH nanofibres with a ratio of 90:10 and 60:40 CH:PEO. Since PEO is water soluble they observed the PEO in 40% ratio affected the integrity of fibres. No significant change in morphology was observed for fibres made with 10% PEO and the micro structural integrity was retained in water. Furthermore; they also mentioned that a prolonged immersion time led to slight swelling of the fibres but the fibrous morphology remained unchanged (Bhattarai *et al.* 2005). Spectral data collected for Random and aligned fibres after immersion in lysozyme degradation solution showed changes in the in glycosidic linkages, which could be indicative of bond breakages within the molecular structure of CH. These miniscule changes could also suggest that the fibres were able to maintain the integrity in lysozyme solution to a certain extent. Since the amount of PEO used in the present study was 5% as compared to 95% LMw CH. The slight changes reported by Bhattari *et al.,* could also be due to the use of 2 % CH solution for making the CH PEO complex (Bhattarai *et al.* 2005).

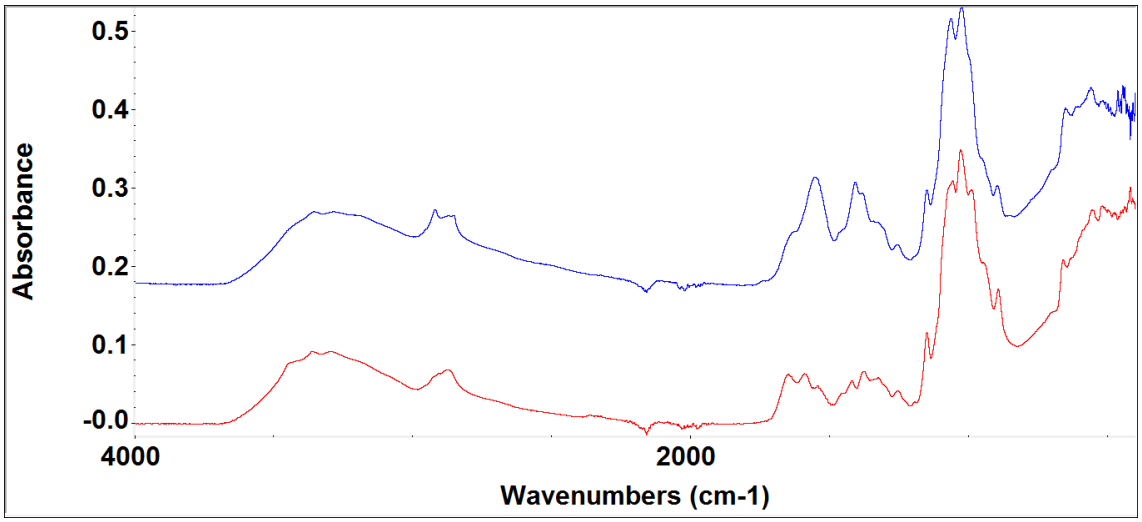

Figure 153: FTIR-ATR of CH aligned fibres at Day 0 and Day 7, image showing the CH_2 stretching vibration.

A study conducted by Norowski *et al.,* on synthesizing nano CH fibres with and without cross-linking with genipin has reported that neat CH fibres fragmented after 4 weeks in solution (Norowski *et al.* 2012). Results obtained in the present study showed that random fibres had a higher weight loss as compared to aligned fibres. Chemical mapping of samples till day 28 were suggestive that the samples maintained their structure and hence, morphological features could have been slightly affected as evident by the decrease in intensity of the bands observed. In another study performed on CH fibres by Sangsanoh and Supaphol on CH fibres degradation using PBS only reported a slower degradation rate and showed a 14% mass loss after 4^{th} week and 16.5% mass loss after 12^{th} week (Sangsanoh *et al.* 2007). Example of the intensity decrease is shown in Figure 154 of random CH fibres where spectral data represent molecular finger print region after day 4 and 21 of degradation in lysozyme solution. These changes in the spectral profile are indicative of changes in the molecular structure of CH. It could be envisaged that CH fibres can be used for periodontal TE and the degradation of the fibres can possibly assist in the new tissue formation.

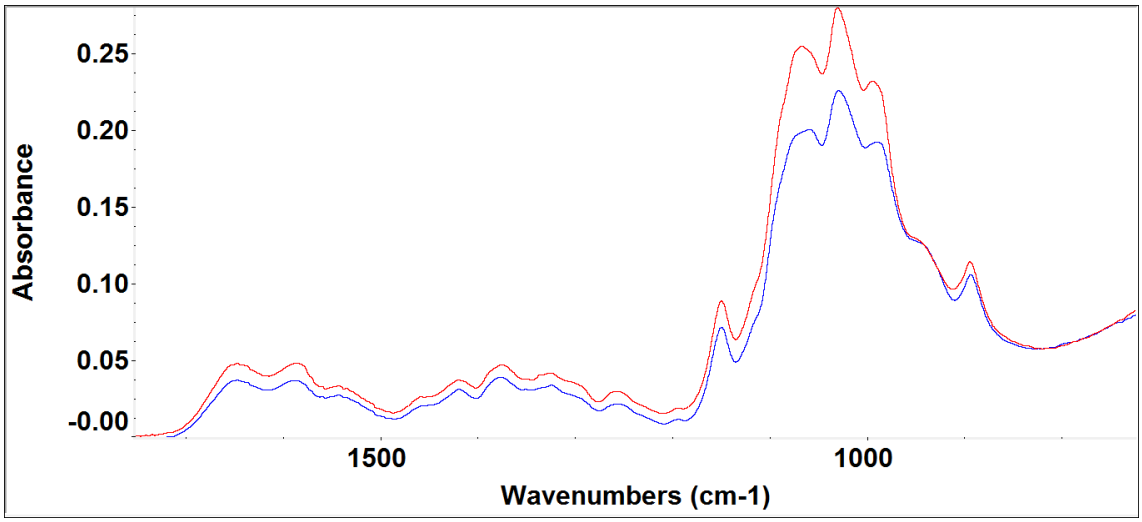

Figure 154: FTIR-ATR of CH Random fibres at Day 4 and Day 21.

5.6.9. Biocompatibility

Electrospun fibres are reported to mimic extracellular matrix and be conducive to support cell attachment, proliferation and matrix deposition. Culturing of human osteosarcoma (MG63) and progenitor cell (hES-MP) line on the random and aligned CH fibres showed that the templates supported cellular attachment and proliferation over the culture period on both orientations obtained. A study conducted by Fakhry and co-workers on culturing osteoblast cells on CH scaffolds have shown favourable results in the past (Fakhry *et al.* 2004; Hamilton *et al.* 2007). In another study by Norowski *et al.*, randomly oriented CH fibres were reported to be more conducive to osteoblastic proliferation over the 5 day culturing period (Norowski *et al.* 2012). There was no significant difference observed in the values obtained at day 7 in between the random and aligned groups. Bhattarai and co-workers reported culturing of MG63 on aligned CH PEO fibres. They observed better cell attachment on aligned fibres which was attributed to the availability of large surface area promoting higher attachment sites. After 5 day culturing of MG63 they noted cell attachment on the surface due to discrete filopodia and long, numerous microvilli on their surface. Interesting finding of the study was that the microvilli of cells tend to attach and grow along the polymer nanofibres whose diameter was similar to that of microvilli seen in SEM imaging (Bhattarai *et al.* 2005). In the current study MG63 culturing on random and aligned fibres did show a gradual increment in viability with time however, there was no difference in the overall attachment level at D7. Culturing for longer time periods might be able to give us more insights on the type of orientations supporting higher proliferation and viability.

Mesenchymal stem cells (MSC) are known to be able to differentiate into bone tissue, neural tissue, cartilage, muscle and fat (El-Amin *et al.* 2006). Kim and co-workers have reported culturing of human MSC's on CH and CH HA fibres. They also observed that the cells were able to adhere, attach and spread over the surface. A confluent multilayer was reported on both CH and CH HA fibres (Kim *et al.* 2013). This study is in agreement with the results obtained in this study, where both orientations promoted cellular attachment and proliferation with time. Total collagen and calcium deposition assessed by Alizarin red and Sirius red assays also showed favourable results on both fibre orientations. Calcium deposition on randomly oriented fibres was performed previously by Kim *et al.,* They reported that calcium accumulation in cell grown on CH HA fibres was greater than neat CH fibre. Furthermore; they also reported higher ALP activity on composite fibres with HA (Kim *et al.* 2013). It would have been interesting to culture both cell lines for longer time periods, possibly till day 28 to find out the weather random or aligned fibres promote higher proliferation. It would also be interesting to evaluate the ability of human periodontal ligaments (hPDL) cell line against CH fibres and its effect on the fibre orientation. It has been reported that fibre orientation does play a significant role in cellular attachment. Histological sections performed after culturing mesenchymal stem cells showed that the cells were able to from mono and multilayers. Results of H & E sectioning were indicative that the CH fibres were conducive to cellular attachment and proliferation.

5.6.10. Conclusion

In the current study, a solution of chitosan and PEO in a ratio of 95:5 was successfully electrospun to obtain a thin fibrous membrane in both aligned and random configurations. These electrospun chitosan fibrous mats may have the potential to be used as a surface layer of a functionally graded membrane but this hypothesis needs further investigation. Detailed orientation analysis by SEM demonstrated aligned and random morphologies which could also be further tuned to develop structural gradients when designing a trilayered construct with structural and functional gradients for periodontal regeneration. The results from the mechanical data propose that fibre can be handled with ease at chair side in a clinical setup. Degradation studies were suggestive that the rate of fibre breakdown could possible match the rate of regeneration of periodontal tissues. Cellular viability and mineral deposition response indicate that randomly orientated fibres promoted proliferation of osteoblastic cells and matrix turnover. Additionally, in future a combination of layered alternating random and

aligned fibres can also be used to fabricate tissue engineering templates for various other biomedical applications.

SECTION IV

5.7. Functionally graded templates

5.7.1. Scanning electron microscopy

The use of a bi or trilayered scaffold for bone tissue and periodontal engineering have been looked into in the past (Teng *et al.* 2009), however, certain critical aspects of occlusivity, degradation, bioactivity and handling are still undermined. Recently Bottino and co-workers have envisioned that a trilayered membrane that mimics natural tissue structure and function can be the future of ideal GTR membrane (Bottino *et al.* 2011; Bottino *et al.* 2012). This vision can lead to the next generation of GTR membranes for Periodontal TE. The study conducted by Bottino *et al.,* reported the use of a combination of natural and synthetic polymers and bioceramic like HA to fabricate a trilayered membrane using electrospinning. Similarly Liao and co-workers also reported the fabrication of a trilayered GTR membrane using nHA, collagen and PLGA. They mentioned that the membrane was prepared by simple biomimetic method and casting technique to achieve a non-porous and porous morphology (Liao *et al.* 2005). The fabrication of a trilayered membrane using CH, HA and collagen for GBR purpose has also been reported earlier. Teng and co-workers adapted a layer by layer filtration process to overcome the issues with interfacial bonding (Teng *et al.* 2008). The trilayered template made in the present study was a combination of solvent casting and freeze gelation. This resulted in a non-porous interface of high HA accumulated at one end of the membrane, intended to face the periodontal defect side and a CH porous interface intended to act as a bioinert side to face soft tissue defect side. Transverse section of the scaffolds revealed presence of porosities within the core of the membrane. Although this is the first attempt to combine solvent casting and freeze gelation to achieve a trilayered membrane further investigation into the stability of the membrane and its ability to act as a selective cellular infiltration device still needs to be evaluated comprehensively.

5.7.2. Raman Spectroscopy

Raman spectroscopy has evolved drastically over the past years due to the technological advances for analyzing molecular composition of substrates. This technique has the ability to non-destructively obtain Raman scattering spectral maps and images of specimens giving spatial information and showing detailed distribution and orientation of chemical constituents

on a biomaterials interface (Okulus *et al.* 2014). The aim of this study was to assess the distribution of HA and CH within the scaffold. Spectroscopic data obtained was indicative of a functionally graded structure with different morphology obtained by adapting two different techniques of solvent casting and freeze gelation. The spectral peaks of HA obtained in the present study were coinciding with study conducted by Rehman *et al.,* (Rehman *et al.* 1995; Rehman I U *et al.* 2013). Rehman and co-workers have extensively reported the use of vibrational spectroscopy for biological tissues such as bone. They mentioned that HA spectrum is dominated by the asymmetric P=O bands. The peaks of the phosphate moiety were centered at 952cm^{-1} (PO stretching mode) and 584cm^{-1} (PO bending mode) (Rehman *et al.* 1995; Rehman I U *et al.* 2013). The figure 155 depicts the raman spectra extracted from the collected map of trilayered membrane showing the middle region with CH dominance, observed by the presence of CH peaks at the higher wavenumbers and a sharp peak at 960cm^{-1} pertaining to the phosphate vibration of HA is indicative of higher HA amount at this surface.

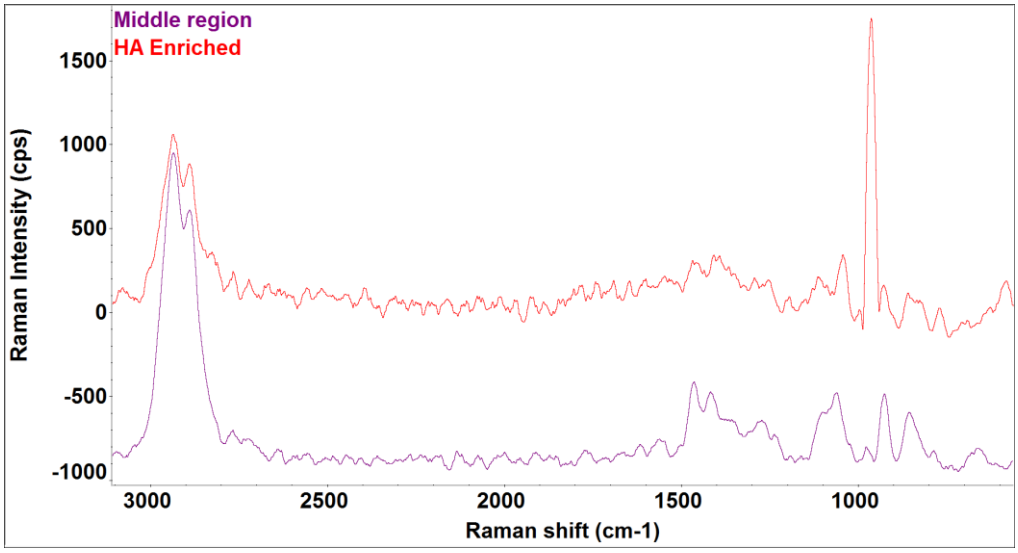

Figure 155: Raman Spectra of the trilayered Membrane collected from the top HA enriched region showing high intensity of HA peak at 960cm^{-1} and Middle region with high CH content.

Furthermore, HA was listed as an intense Raman scatterer due to the intense signal to noise ratio variations. In the present study this PO stretching mode of HA was observed at 962cm^{-1}. The peaks obtained for CH structure were similar to the results reported by Zajac and co-workers (Zajac *et al.* 2015). This very recent study reported the use of Raman to determine the DD of CH. The presence of a band at 2885cm^{-1} was assigned to CH stretching vibration of the pyranose ring. Furthermore; they reported about the presence of bands at 1654, 1591 and 936cm^{-1} (Zajac *et al.* 2015), which were all assigned to -CH structure. Although the weak intensity these Amide I and Amide II bands could be indicative of bonding between the CH and

HA of LMw CH and MMw CH. Since the membrane was synthesized with LMw CH and freeze gelated component was made by MMw CH. Spectral information obtained after mapping is indicative that HA concentration is high on one side of the membrane. On selection of bands pertaining to CH, it was evident that the CH distribution was dominant in the rest of the scaffold. It is worth mentioning here that the trilayered membranes were synthesized following the protocol for solvent casting and just when the solvent was partially evaporated. Freeze gelation solution of CH was poured on top of the membrane and then protocol for freeze gelation was followed.

5.7.3. Conclusion

A functionally graded membrane was prepared using two different techniques of solvent casting and freeze gelation to obtain a nonporous and porous surface with higher HA present at the nonporous side and CH forming the porous segment of the membrane. The chemical mapping performed with Raman Spectroscopy was instrumental in obtaining the interactions in between HA and CH throughout the membrane. Further insights into the fabrication techniques are required to tune the properties of such functionally graded membrane to be used in other tissue engineering and regenerative medicine applications.

6. Conclusions and Future Work

6.1. Conclusions

In summary the present study have shown that,

- Membranes / thin films based on chitosan and hydroxyapatite were successfully prepared in different ratios from Low and medium molecular weight chitosan using the simple technique of solvent casting to serve as the surface layer of a GTR membrane. SEM studies showed clear discrepancy between the top and bottom surface. FTIR spectroscopy also confirmed high degree of segregation between the top and bottom surface. Swelling ratio studies showed that the swelling was governed by the amount of Chitosan present and HA restricted the swelling.

- In-*vitro* Degradation studies performed by weight analysis showed MMw membranes were stable till 48th day and LMw membranes showed 20-30% weight remaining after 48th day in lysozyme solution. Spectral data collected from FTIR showed alterations of the peak intensity and shifts in wavenumbers of glycosidic linkages of chitosan. This confirmed that LMw membranes showed chain scission of Chitosan to smaller fragments and signs of bond breakage between Chitosan and hydroxyapatite were also present. pH studies showed an increment in pH value with time and UV-Vis spectroscopy performed on the degraded supernatant also showed typical bands pertaining to ring opening occurring after hydrolytic scission of 1-4 glycosidic bonds of Chitosan confirming the degradation of Chitosan.

- Biocompatibility studies performed on the bottom surface of the membranes using human osteosarcoma and mesenchymal progenitor cell lines to assess for viability and proliferation by Alamar Blue showed that LMw 30:70(CH:HA) membranes had higher viability with culture time. Matrix deposition conducted by culturing mesenchymal progenitor up to day 28 also showed hydroxyapatite incorporated membranes promotes collagen and calcium deposition.

- In-*vitro* bioactivity studies conducted by weight analysis, pH profile and FTIR showed that the presence of hydroxyapatite on the bottom surface intended for facing the defect site showed initial signs of carbonated apatite layer formation which disappeared with time. Peak area analysis performed on spectral data collected by FTIR showed typical hydroxyl peak decrease indicative of immature or embryonic form of

CA layer formation. Weight changes also showed an increment in weight confirming that the layer formation affected the weight profile as well.

- Porous CH-based membranes with and without HA were prepared using acetic acid or ascorbic acid as solvent systems *via* the novel and efficient technique of freeze gelation. The CH:HA composites have shown potential for use as a core layer in a functionally graded GTR membrane for periodontal tissue engineering, fulfilling a number of key requirements of satisfactory handling properties for clinicians. Choice of solvent used to dissolve CH and amount of incorporated HA helps in tailor making the physical and chemical properties of membranes. Membranes were resilient to handling during dry and wet conditions that may simulate clinical use. A favourable cellular response was also seen for CH:HA composite membranes suggesting that HA incorporation effects cellular activity. Therefore; this study shows that these porous membranes have a potential to be used as a core layer of a functionally graded structure in periodontal regeneration membranes. Furthermore, freeze gelation technique may be employed in future to create tissue engineering scaffolds for other biomedical applications.

- Swelling and degradation studies performed by weight analysis, pH profile and FTIR showed that neat Chitosan membranes had higher swelling ratio and faster degradation. With Hydroxyapatite inclusion in the membrane the swelling and degradation was restricted. In-*vitro* bioactivity studies were also suggestive that the carbonated apatite layer in these membranes was also formed and was washed away by analysing the peak area ratio of hydroxyl peak at 3560cm^{-1}.

- In-*vivo* studies performed after implanting these specimens in rabbits also showed that HA inclusion promote more cellular infiltration in the deep zones of the membranes.

- Freeze gelated samples were cross-linked with sodium tripolyphosphate in two different concentration which was confirmed by FTIR analysis showing the tripolyphosphate peaks appearing more strongly in higher concentration samples. SEM showed that after cross-linking and drug loading pores were more compressed. Drug loading and % recovery studies up to 180 minutes were performed by Tetracycline hydrochloride. FTIR analysis after drug loading showed peaks pertaining to tetracycline showing strong bonding with chitosan. Recovery studies conducted up to 180 minutes, non-cross-linked samples showed an initial burst with neat Chitosan membranes and

HA inclusion caused a delay in the % recovery profile. After cross-linking the recovery showed a gradual increment with time.

- Chitosan was successfully electrospun by using PEO in a ratio of 95:5 to obtain a thin fibrous membrane in both aligned and random configurations. These electrospun chitosan fibrous mats may have the potential to be used as a surface layer of a functionally graded membrane. Detailed orientation analysis by SEM demonstrated aligned and random morphologies which could also be further tuned to develop structural gradients when designing a trilayered construct with structural and functional gradients for periodontal regeneration. The results from the mechanical data propose that fibrous mats can be handled with ease at chair side in a clinical setup. Degradation studies were suggestive that the rate of fiber breakdown could possibly match the rate of regeneration of periodontal tissues. Cellular viability and mineral deposition response indicate that randomly orientated fibres promoted proliferation of osteoblastic cells and matrix turnover.

- A functionally graded membrane was prepared by combining solvent casting and freeze gelation techniques to form a trilayered template. SEM analysis showed porous features. Raman mapping performed showed HA concentration on one side of the membrane and no HA was detected

6.2. Future Work

The dire need to fabricate functionally graded membranes for periodontal tissue engineering is needed to improve the regeneration of periodontal tissues lost as a consequence of periodontal diseases. Despite the advances in membrane technology for treating Periodontitis, it is still a challenging disease for clinical specialists to treat such conditions. A functional gradient provides a graded approach to mimic the natural tissue structure and function in order to meet local systemic and bio-functional requirements. A bioactive degradable membrane with growth factors and drugs can not only assist the formation of alveolar bone but also guide and trigger periodontal ligaments and cementum to regenerate in their natural orientations. This PhD work demonstrates that chitosan and hydroxyapatite can be combined together to obtain different morphological templates of a

spatially designed functionally graded membrane that can be combined together to form a trilayered membrane.

- In future it would be interesting with respect to solvent casted membranes to assess higher percentages of Hydroxyapatite incorporation. Simultaneously substituted HA with either carbonate, fluoride, magnesium or strontium ions will be valuable. Nanoscale HA addition to this composite membrane may further improve the properties of the resulting composite. Layer by layer solvent casting with different bioactive agents can also be a fascinating approach to investigate the efficiency of the method in future.

- Freeze gelation is a very promising technique for fabricating porous membranes. It would be valuable to incorporate higher ratios of hydroxyapatite in combination with other bioactive molecules in future. Adding substituted HA to this segment would also be an interesting option for future studies. Directional freezing to control the pores size and morphology can also be an attractive option. Layer by layer freeze gelation on its own can also assist in fabricating a trilayered membrane with porous gradient.

- Although electrospinning chitosan is difficult, but it would be interesting to fabricate a layer by layer electrospinning to achieve micro fibre mats over nanofibre mats. Fibre layers can have HA or drug incorporated in either layer to meet the functionally graded criteria.

- It has been demonstrated in this work that the scaffolds showed biocompatibility with human osteosarcoma and mesenchymal progenitor cell line, therefore, it would be interesting to investigate the effect of culturing human periodontal ligament cell line to assess viability and matrix deposition over long term cultures to closely mimic in-vivo conditions.

- Initial studies of combining freeze gelated and solvent casted layers in this work demonstrated that a composite membrane using two different fabrication procedures is possible and it would be interesting to tri-layer electrospun membrane over solvent casted or freeze gelated membrane with solvent casting.

The work performed in this PhD has contributed significantly towards the prospects of 4th generation of membranes for periodontal tissue engineering. This would certainly be a stepping stone towards the possibilities of functionally graded membranes being implemented for guided tissue regeneration. Until today the search for an ideal membrane by researchers is the ultimate goal which remains unmet, due to the existing limitations in handling and bio-

functionality. A trilayered functionally graded membrane can overcome these limitations and become the first choice for regenerating lost support when treating chronic periodontal conditions.

References

Abbas, A. O. M. (2010). Chitosan for biomedical applications. Pharmacy. Iowa, University of Iowa. **DPhil**.

Adekogbe, I. and A. Ghanem (2005). "Fabrication and characterization of DTBP-crosslinked chitosan scaffolds for skin tissue engineering." Biomaterials **26**(35): 7241-7250.

Agarwal, S., J. H. Wendorff, et al. (2008). "Use of electrospinning technique for biomedical applications." Polymer **49**(26): 5603-5621.

Aggarwal S P, Aggarwal, Ankur, et al. (2014). "Subgingival microbiota and chronic periodontal disease: Culpability in causation of systemic pathologies." Practice changing continuing education: preventive medicine **1**(2): 100-103.

Ahmed, S., M. Sheraz, et al. (2013). "Studies on Tolfenamic Acid–Chitosan Intermolecular Interactions: Effect of pH, Polymer Concentration and Molecular Weight." AAPS PharmSciTech **14**(2): 870-879.

Aichelmann-Reidy, M. E. and R. A. Yukna (1998). "Bone replacement grafts. The bone substitutes." Dental Clinics of North America **42**(3): 491-503.

Akizuki, T., S. Oda, et al. (2005). "Application of periodontal ligament cell sheet for periodontal regeneration: a pilot study in beagle dogs." Journal of Periodontal Research **40**(3): 245-251.

AlGhamdi, A. S. and S. G. Ciancio (2009). "Guided tissue regeneration membranes for periodontal regeneration--a literature review." Journal of International Academy of Periodontology **11**(3): 226-231.

Ana Pejčić, Ljiljana Kesić, et al. (2010). "Antibiotics in the Management of Periodontal Disease." Scientific Journal of the Faculty of Medicine in Niš **27**(2): 85-92.

Araujo, A. B., A. F. Lemos, et al. (2009). "Rheological, microstructural, and in vitro characterization of hybrid chitosan-polylactic acid/hydroxyapatite composites." Journal of Biomedical Materials Research A **88**(4): 916-922.

Armitage, G. C. (1999). "Development of a classification system for periodontal diseases and conditions." Annals of Periodontology **4**(1): 1-6.

Armitage, G. C. and M. P. Cullinan (2010). "Comparison of the clinical features of chronic and aggressive periodontitis." Periodontology 2000 **53**: 12-27.

Ashok, M., N. M. Sundaram, et al. (2003). "Crystallization of hydroxyapatite at physiological temperature." Materials Letters **57**(13-14): 2066-2070.

Atala, A., F. K. Kasper, et al. (2012). "Engineering Complex Tissues." Science Translational Medicine **4**(160).

Atout, R. and S. Todescan (2013). "Managing Patients with Necrotizing Ulcerative Gingivitis." Journal of Canadian Dental Association **79**.

Aurer, A. and K. JorgiÊ-Srdjak (2005). "Membranes for Periodontal Regeneration." Acta Stomatol Croatia, **39**: 107-112.

Azab, A. K., B. Orkin, et al. (2006). "Crosslinked chitosan implants as potential degradable devices for brachytherapy: In vitro and in vivo analysis." Journal of Controlled Release **111**(3): 281-289.

Balmayor, E. R., H. S. Azevedo, et al. (2011). "Controlled delivery systems: from pharmaceuticals to cells and genes." Pharm Res **28**(6): 1241-1258.

Barralet, J., S. Best, et al. (1998). "Carbonate substitution in precipitated hydroxyapatite: An investigation into the effects of reaction temperature and bicarbonate ion concentration." Journal of Biomedical Materials Research **41**(1): 79-86.

Bhardwaj, N. and S. C. Kundu (2010). "Electrospinning: A fascinating fiber fabrication technique." Biotechnology Advances **28**(3): 325-347.

Bhattarai, N., D. Edmondson, et al. (2005). "Electrospun chitosan-based nanofibers and their cellular compatibility." Biomaterials **26**(31): 6176-6184.

Bhumkar, D. R. and V. B. Pokharkar (2006). "Studies on effect of pH on cross-linking of chitosan with sodium tripolyphosphate: a technical note." AAPS PharmSciTech **7**(2): E50.

Blomlof, L., B. Jonsson, et al. (2000). "A clinical study of root surface conditioning with an EDTA gel. II. Surgical periodontal treatment." International Journal of Periodontics Restorative Dentistry **20**(6): 566-573.

Bosshardt, D. D. and A. Sculean (2009). "Does periodontal tissue regeneration really work?" Periodontology 2000 **51**(1): 208-219.
Bostanci, N. and G. N. Belibasakis (2012). "Doxycycline inhibits TREM-1 induction by Porphyromonas gingivalis." FEMS Immunol Med Microbiol.

Bottino, M. C., V. Thomas, et al. (2011). "A novel spatially designed and functionally graded electrospun membrane for periodontal regeneration." Acta Biomaterialia **7**(1): 216-224.

Bottino, M. C., V. Thomas, et al. (2012). "Recent advances in the development of GTR/GBR membranes for periodontal regeneration-A materials perspective." Dental Materials **28**(7): 703-721.

Brugnerotto, J., J. Lizardi, et al. (2001). "An infrared investigation in relation with chitin and chitosan characterization." Polymer **42**(8): 3569-3580.

Buchmann R, Conrads G, et al. (2010). "Short-term effects of systemic antibiotics during periodontal healing." Quintessence International. **41**(4): 303-312.

Burg, K. J. L., S. Porter, et al. (2000). "Biomaterial developments for bone tissue engineering." Biomaterials **21**(23): 2347-2359.

Cai, X., L. Chen, et al. (2011). "Facile synthesis of anisotropic porous chitosan/hydroxyapatite scaffolds for bone tissue engineering." Journal of Materials Chemistry **21**(32): 12015-12025.

Caroni, A. L., C. R. de Lima, et al. (2009). "The kinetics of adsorption of tetracycline on chitosan particles." Journal of Colloid Interface Science **340**(2): 182-191.

Caroni, A. L. P. F., C. R. M. de Lima, et al. (2012). "Tetracycline adsorption on chitosan: A mechanistic description based on mass uptake and zeta potential measurements." Colloids and Surfaces B-Biointerfaces **100**: 222-228.

Causa, F., P. A. Netti, et al. (2006). "Poly-epsilon-caprolactone/hydroxyapatite composites for bone regeneration: in vitro characterization and human osteoblast response." Journal of Biomedical Materials Research A **76**(1): 151-162.

Cerruti, M. G., D. Greenspan, et al. (2005). "An analytical model for the dissolution of different particle size samples of Bioglass® in TRIS-buffered solution." Biomaterials **26**(24): 4903-4911.

Chandra, R. and R. Rustgi (1998). "Biodegradable polymers." Progress in Polymer Science **23,**: 1273-1335.

Chen, F.-m., Y.-m. Zhao, et al. (2006). "Enhancement of periodontal tissue regeneration by locally controlled delivery of insulin-like growth factor-I from dextran–co-gelatin microspheres." Journal of Controlled Release **114**(2): 209-222.

Chen, F-M, Shelton R-M, Chapple, I.L.C, (2009) Localized delivery of growth factors for periodontal tissue regeneration: Role strategies and prespectives, Medicinal Research reviewes **29** (3)472-513.

Chen, F.M, Jin Y, (2010) Periodontal tissue engineering and regeneration: current approches and expanding opportunities Tissu Engineering part B reviews **16** (2) 219-255

Chen F.M, Zhang J, Zhang M, An, Y, Chen, F, Wu Z -F, (2010) A review of endogenous regenerative technology in periodontal regenerative medicine, Biomaterials 31 (31) 7892-7927.

Chen, M.-C., F.-L. Mi, et al. (2011). Chitosan: Its Applications in Drug-Eluting Devices. Chitosan for Biomaterials I. R. Jayakumar, M. Prabaharan and R. A. A. Muzzarelli, Springer Berlin Heidelberg. **243:** 185-230.

Chen, Z., X. Mo, et al. (2008). "Intermolecular interactions in electrospun collagen–chitosan complex nanofibers." Carbohydrate Polymers **72**(3): 410-418.

Cheng, X. M., Y. B. Li, et al. (2009). "Properties and in vitro biological evaluation of nano-hydroxyapatite/chitosan membranes for bone guided regeneration." Materials Science & Engineering C-Biomimetic and Supramolecular Systems **29**(1): 29-35.

Chesnutt, B. M., Y. Yuan, et al. (2007). "Characterization of biomimetic calcium phosphate on phosphorylated chitosan films." Journal of biomedical materials research. Part A **82**(2): 343-353.

Chesnutt, B. M., Y. Yuan, et al. (2009). "Composite chitosan/nano-hydroxyapatite scaffolds induce osteocalcin production by osteoblasts in vitro and support bone formation in vivo." Tissue Engineering Part A **15**(9): 2571-2579.

Cho, E. H., J. C. Park, et al. (2011). "Dimensional change of the healed periosteum on surgically created defects." Journal of Periodontal Implant Sci **41**(4): 176-184.

Choi, B.-K., K.-Y. Kim, et al. (2001). "In vitro antimicrobial activity of a chitooligosaccharide mixture against Actinobacillus actinomycetemcomitans and Streptococcus mutans." International Journal of Antimicrobial Agents **18**(6): 553-557.

Christgau, M., G. Schmalz, et al. (1995). "Clinical and Radiographical Split-Mouth Study on Resorbable Versus Non-Resorbable Gtr-Membranes." Journal of Clinical Periodontology **22**(4): 306-315.

Christgau, M., G. Schmalz, et al. (1997). "Periodontal regeneration of intrabony defects with resorbable and non-resorbable membranes: 30-month results." Journal of Clinical Periodontology **24**(1): 17-27.

Christgau M., B. N., Felden A., Gradl J., Wenzel A., Schmalz G (2002). "Guided tissue regeneration in intrabony defects using an experimental bio resorbable polydioxanon (PDS) membrane." Journal of Clinical Periodontology **29**(710-723).

Corazzari, I., R. Nisticò, et al. (2015). "Advanced physico-chemical characterization of chitosan by means of TGA coupled on-line with FTIR and GCMS: Thermal degradation and water adsorption capacity." Polymer Degradation and Stability **112**(0): 1-9.

Correlo, V. M., L. F. Boesel, et al. (2005). "Hydroxyapatite reinforced chitosan and polyester blends for biomedical applications." Macromolecular Materials and Engineering **290**(12): 1157-1165.

Correlo, V. M., E. D. Pinho, et al. (2007). "Water absorption and degradation characteristics of chitosan-based polyesters and hydroxyapatite composites." Macromol Bioscience **7**(3): 354-363.

Cosyn, J. and M. M. Sabzevar (2005). "A systematic review on the effects of subgingival chlorhexidine gel administration in the treatment of chronic periodontitis." Journal of Periodontology **76**(11): 1805-1813.

Crout, R. J., H. M. Lee, et al. (1996). "The "cyclic" regimen of low-dose doxycycline for adult periodontitis: a preliminary study." Journal of Periodontology **67**(5): 506-514.

Cunha-Reis, C., K. TuzlaKoglu, et al. (2007). "Influence of porosity and fibre diameter on the degradation of chitosan fibre-mesh scaffolds and cell adhesion." Journal of Materials Science-Materials in Medicine **18**(2): 195-200.

Czechowska-Biskup, R., B. Rokita, et al. (2005). "Degradation of chitosan and starch by 360-kHz ultrasound." Carbohydrate Polymers **60**(2): 175-184.

Dalton, P. D., D. Grafahrend, et al. (2007). "Electrospinning of polymer melts: Phenomenological observations." Polymer **48**(23): 6823-6833.

Danilchenko, S. N., O. V. Kalinkevich, et al. (2011). "Characterization and in vivo evaluation of chitosan-hydroxyapatite bone scaffolds made by one step coprecipitation method." Journal of Biomedical Materials Research Part A **96A**(4): 639-647.

Darby, I. B. and K. H. Morris (2012). "A Systematic Review of the Use of Growth Factors in Human Periodontal Regeneration." Journal of Periodontology **21**: 21.
Darnell Kaigler, Gustavo Avila, et al. (2011). "Platelet-derived growth factor applications in periodontal and peri-implant bone regeneration." Expert Opin Biol Therapy **11**(3): 375-385.

de Britto, D. and S. P. Campana (2007). "Kinetics of the thermal degradation of chitosan." Thermochimica Acta **465**(1-2): 73-82.

de Peppo, G. M., P. Sjovall, et al. (2010). "Osteogenic Potential of Human Mesenchymal Stem Cells and Human Embryonic Stem Cell-Derived Mesodermal Progenitors: A Tissue Engineering Perspective." Tissue Engineering Pt A **16**(11): 3413-3426.

Delaine-Smith, R. M. (2013). Mechanical and physical guidance of osteogenic differentiation and matrix production. Materials Science and Engineering. Sheffield, University of Sheffield. PhD thesis, University of Sheffield.

Dentino, A., S. Lee, et al. (2013). "Principles of periodontology." Periodontology 2000 **61**(1): 16-53.

Depan, D., J. S. Shah, et al. (2013). "Degradation mechanism and increased stability of chitosan-based hybrid scaffolds cross-linked with nanostructured carbon: Process–

structure–functional property relationship." Polymer Degradation and Stability **98**(11): 2331-2339.

Deville, S. and R. K. Nalla (2006). "Freezing as a path to build complex composites (vol 312, pg 515, 2006)." Science **312**(5778): 1312-1312.

Deville, S., E. Saiz, et al. (2006). "Freezing as a path to build complex composites." Science **311**(5760): 515-518.

Deyao, K., P. Tao, et al. (1993). "Ph-Sensitivity of Hydrogels Based on Complex-Forming Chitosan - Polyether Interpenetrating Polymer Network." Journal of Applied Polymer Science **48**(2): 343-354.

Dilamian, M., M. Montazer, et al. (2013). "Antimicrobial electrospun membranes of chitosan/poly(ethylene oxide) incorporating poly(hexamethylene biguanide) hydrochloride." Carbohydrate Polymers **94**(1): 364-371.

Domb, A. J., N. K. (2011). Biodegradable Polymers in Clinical Use and Clinical Development, Wiley Publishers.

Dutta, P. K., J. Dutta, et al. (2004). "Chitin and chitosan: Chemistry, properties and applications." J Sci Ind Res India **63**(1): 20-31.

Egusa, H., W. Sonoyama, et al. (2012). "Stem cells in dentistry--Part II: Clinical applications." Journal of Prosthodont Research **56**(4): 229-248.

El-Amin, S. F., E. Botchwey, et al. (2006). "Human osteoblast cells: isolation, characterization, and growth on polymers for musculoskeletal tissue engineering." Journal of Biomedical Materials Research Part A **76**(3): 439-449.

El-Sawy, N. M., H. A. Abd El-Rehim, et al. (2010). "Radiation-induced degradation of chitosan for possible use as a growth promoter in agricultural purposes." Carbohydrate Polymer **79**(3): 555-562.

El-Sayed, E. M., A. Omar, et al. (2009). "On the Structural Analysis and Electronic Properties of Chitosan/Hydroxyapatite Interaction." Journal of Computational and Theoretical Nanoscience **6**(7): 1663-1669.

Elliott, J. C. (1964). The crystallographic structure of dental enamel and related apatites. Departm eit of Dental Histology and Pathology. London, University of London. **PhD:** 203.

Elliott, J. C., D. W. Holcomb, et al. (1985). "Infrared determination of the degree of substitution of hydroxyl by carbonate ions in human dental enamel." Calcif Tissue International **37**(4): 372-375.

Fakhry, A., G. B. Schneider, et al. (2004). "Chitosan supports the initial attachment and spreading of osteoblasts preferentially over fibroblasts." Biomaterials **25**(11): 2075-2079.

Fan, Y.-b. and X.-y. Lü (2008). "A study of apatite formation on natural nano-hydroxyapatite/chitosan composite in simulated body fluid." Frontiers of Materials Science in China **2**(1): 91-94.

Fathi, M. H., A. Hanifi, et al. (2008). "Preparation and bioactivity evaluation of bone-like hydroxyapatite nanopowder." Journal of Materials Processing Technology **202**(1-3): 536-542.

Fleet, M. E. and X. Y. Liu (2004). "Location of type B carbonate ion in type A-B carbonate apatite synthesized at high pressure." Journal of Solid State Chemistry **177**(9): 3174-3182.

Formhals. (1934). U. patent. US. **1:** 503-508.
Fraga, A. F., E. d. A. Filho, et al. (2011). "Synthesis of chitosan/hydroxyapatite membranes coated with hydroxycarbonate apatite for guided tissue regeneration purposes." Applied Surface Science **257**(9): 3888-3892.

Frohbergh, M. E., A. Katsman, et al. (2012). "Electrospun hydroxyapatite-containing chitosan nanofibers crosslinked with genipin for bone tissue engineering." Biomaterials **33**(36): 9167-9178.

Garg, K, Bowlin, G, (2011) "Electrospining jets and nanofibrous strucures" Biomicrofluidics **(5**)1:013403

Garrett, S., A. M. Polson, et al. (1997). "Comparison of a bioabsorbable GTR barrier to a non-absorbable barrier in treating human class II furcation defects. A multi-center parallel design randomized single-blind trial." Journal of Periodontology **68**(7): 667-675.

Gates, K. A. (1999). Controlled Drug Delivery Using Bioerodible Polymeric Systems for the Treatment of Periodontitis, Thesis (Ph.D.)--University of Toronto.

Gentile, P., V. Chiono, et al. (2011). "Polymeric membranes for guided bone regeneration." Biotechnology Journal **6**(10): 1187-1197.

Gestrelius S, A. C., Lidström D, Hammarström L, Somerman M (1997). " In vitro studies on periodontal ligament cells and enamel matrix derivative. ." Journal Clincal Periodontol **24**(685-692).

Gestrelius, S., S. P. Lyngstadaas, et al. (2000). "Emdogain--periodontal regeneration based on biomimicry." Clinical Oral Investig **4**(2): 120-125.

Ghadim, E. E., F. Manouchehri, et al. (2013). "Adsorption Properties of Tetracycline onto Graphene Oxide: Equilibrium, Kinetic and Thermodynamic Studies." Plos One **8**(11).

Giannobile, W. V. (1996). "Periodontal tissue engineering by growth factors." Bone **19**(1, Supplement 1): S23-S37.

Giri, T. K., A. Thakur, et al. (2012). "Modified chitosan hydrogels as drug delivery and tissue engineering systems: present status and applications." Acta Pharmaceutica Sinica B **2**(5): 439-449.

Golub, L. M., N. S. Ramamurthy, et al. (1991). "Tetracyclines Inhibit Connective-Tissue Breakdown - New Therapeutic Implications for an Old Family of Drugs." Critical Reviews in Oral Biology and Medicine **2**(3): 297-322.

Golub, L. M., K. Suomalainen, et al. (1992). "Host modulation with tetracyclines and their chemically modified analogues." Curr Opin Dent **2**: 80-90.

Gorczyca, G., R. Tylingo, et al. (2014). "Preparation and characterization of genipin cross-linked porous chitosan–collagen–gelatin scaffolds using chitosan–CO2 solution." Carbohydrate Polymer **102**(0): 901-911.

Grandin, H. M., A. C. Gemperli, et al. (2012). "Enamel matrix derivative: a review of cellular effects in vitro and a model of molecular arrangement and functioning." Tissue Engineering Part B Rev **18**(3): 181-202.

Grausova, L., A. Kromka, et al. (2011). "Enhanced Growth and Osteogenic Differentiation of Human Osteoblast-Like Cells on Boron-Doped Nanocrystalline Diamond Thin Films." Plos One **6**(6).

Gunasekaran S, Varadhan SR, et al. (1996). "Qualitative analysis on the infrared bands of Tetracycline and ampicillin." Proc Indian Nan Sci Acad **62**(4): 309-316.

Haghi, A. K. and M. Akbari (2007). "Trends in electrospinning of natural nanofibers." physica status solidi (a) **204**(6): 1830-1834.

Hamilton, V., Y. L. Yuan, et al. (2007). "Bone cell attachment and growth on well-characterized chitosan films." Polymer International **56**(5): 641-647.

Hammarström L, H. L., Gestrelius S (1997). "Periodontal regeneration in a buccal dehiscence model in monkeys after application of enamel matrix proteins. 24:669-677." Journal of Clinical Periodontol **24**: 669-677.

Hench, L., D. Wheeler, et al. (1998). "Molecular Control of Bioactivity in Sol-Gel Glasses." Journal of Sol-Gel Science and Technology **13**(1-3): 245-250.

Hench, L. L. (1998). "Biomaterials: a forecast for the future." Biomaterials **19**(16): 1419-1423.

Hench, L. L. and J. M. Polak (2002). "Third-generation biomedical materials." Science **295**(5557): 1014-1017.
Herrera, D., M. Sanz, et al. (2002). "A systematic review on the effect of systemic antimicrobials as an adjunct to scaling and root planing in periodontitis patients." Journal of Clinical Periodontology **29**: 136-159.

Hirsch, R., H. Deng, et al. (2012). "Azithromycin in periodontal treatment: more than an antibiotic." Journal of Periodontal Research **47**(2): 137-148.

Ho, M.-H., P.-Y. Kuo, et al. (2004). "Preparation of porous scaffolds by using freeze-extraction and freeze-gelation methods." Biomaterials **25**(1): 129-138.

Hong Li, Chang-Ren Zhou, et al. (2010). "Preparation and Characterization of Homogeneous Hydroxyapatite/Chitosan Composite Scaffolds via In-Situ Hydration." Journal of Biomaterials and Nanobiotechnology **1**: 42-49.

Honga H., W. J. a. L. C. (2007). "Development of asymmetric gradational-changed porous chitosan membrane for guided periodontal tissue regeneration." Journal of Bio-engineered Composites, **38**: 311-316.

Hou, L. T., J. J. Yan, et al. (2004). "Polymer-assisted regeneration therapy with Atrisorb barriers in human periodontal intrabony defects." Journal of Clinical Periodontology **31**(1): 68-74.

Hsieh, C-Y, Tsai, S-P, H0 M.W et al (2007) Analysis of freeze gelation and crosslinking processes for preparing porous chitosan scaffolds." Carbohydrate Polymers 6 (1): 124-132.

Huang, J., L. D. Silvio, et al. (1997). "Evaluation of in vitro bioactivity and biocompatibility of Bioglass®-reinforced polyethylene composite." Journal of Materials Science: Materials in Medicine **8**(12): 809-813.

Huang, Z.-M., Y. Z. Zhang, et al. (2003). "A review on polymer nanofibers by electrospinning and their applications in nanocomposites." Composites Science and Technology **63**(15): 2223-2253.

Hudson, S. M., D. W. Jenkins. (2001). "Chitin and Chitosan." Encyclopedia of Polymer Science and Technology,, Wiley Interscience.

Hughes, F. J., M. Ghuman, et al. (2010). "Periodontal regeneration: A challenge for the tissue engineer?" Proceedings of the Institution of Mechanical Engineers, Part H: Journal of Engineering in Medicine **224**(12): 1345-1358.

Hunter, K. T. and T. Ma (2013). "In vitro evaluation of hydroxyapatite–chitosan–gelatin composite membrane in guided tissue regeneration." Journal of Biomedical Materials Research Part A **101A**(4): 1016-1025.

Illueca, F. M. A. P. B. V., Cabanilles P. de G., Fernandez V. F., Francisco José Gil Loscos (2006). "Periodontal regeneration in clinical practice." Med Oral Patol Oral Cir Bucal **11**: 382-392.

Intini G, (2010) Future approches in periodontal regeneration:Gene therapy, stem cells and RNA interfaces. Dental Clinical of North America **54** (1)141-155.

Jain, N., G. K. Jain, et al. (2008). "Recent approaches for the treatment of periodontitis." Drug Discovery Today **13**(21–22): 932-943.

Jankovic, B., J. Pelipenko, et al. (2013). "The design trend in tissue-engineering scaffolds based on nanomechanical properties of individual electrospun nanofibers." International Journal of Pharmaceutics **455**(1-2): 338-347.

Javed, F., M. Al-Askar, et al. (2011). "Significance of the platelet-derived growth factor in periodontal tissue regeneration." Archives of Oral Biology **56**(12): 1476-1484.
Jayakumar, R., M. Prabaharan, et al. (2010). "Novel chitin and chitosan nanofibers in biomedical applications." Biotechnology Advances **28**(1): 142-150.

Jebahi, S., Oudadesse H., et al. (2013). "Effect of pH and Ionic Exchange on the Reactivity of Bioglass/Chitosan Composites Used as a Bone Graft Substitute." International Journal of Chemical, Nuclear, Materials and Metallurgical Engineering **7**: 142-148.

Jeong, S. I., M. D. Krebs, et al. (2011). "Electrospun chitosan-alginate nanofibers with in situ polyelectrolyte complexation for use as tissue engineering scaffolds." Tissue Eng Part A. **17**(1-2): 59-70. doi: 10.1089/ten.TEA.2010.0086. Epub 2010 Sep 1021.

Jiang, T., Z. Zhang, et al. (2010). "Surface functionalization of titanium with chitosan/gelatin via electrophoretic deposition: characterization and cell behavior." Biomacromolecules **11**(5): 1254-1260.

Jin, H. H., D. H. Kim, et al. (2012). "In vivo evaluation of porous hydroxyapatite/chitosan-alginate composite scaffolds for bone tissue engineering." International Journal of Biological Macromolecules **51**(5): 1079-1085.

Jones, J. R. (2013). "Review of bioactive glass: from Hench to hybrids." Acta Biomaterialia **9**(1): 4457-4486.

Jones, J. R. and L. L. Hench (2001). "Materials perspective - Biomedical materials for new millennium: perspective on the future." Materials Science and Technology **17**(8): 891-900.

Karring, T., S. Nyman, et al. (1993). "Development of the biological concept of guided tissue regeneration--animal and human studies." Periodontology 2000 **1**: 26-35.

Kassebaum, N. J., E. Bernabe, et al. (2014). "Global burden of severe periodontitis in 1990-2010: a systematic review and meta-regression." J Dent Res **93**(11): 1045-1053.

Khan, A. S. (2009). A Novel Bioactive Nano-Composite: Synthesis and Characterisation with Potential Use as Dental Restorative Material. School of Engineering and Materials Science London, Queen Mary University of London. **PhD:** 350.

Khanna, R., K. S. Katti, et al. (2010). "In Situ Swelling Behavior of Chitosan-Polygalacturonic Acid/Hydroxyapatite Nanocomposites in Cell Culture Media." International Journal of Polymer Science **2010**.

Khor, E. and L. Y. Lim (2003). "Implantable applications of chitin and chitosan." Biomaterials **24**(13): 2339-2349.

Kikuchi, M., T. Ikoma, et al. (2004). "Biomimetic synthesis of bone-like nanocomposites using the self-organization mechanism of hydroxyapatite and collagen." Composites Science and Technology **64**(6): 819-825.

Kikuchi, M., Y. Koyama, et al. (2002). "In vitro change in mechanical strength of beta-tricalcium phosphate/copolymerized poly-L-lactide composites and their application for guided bone regeneration." Journal of Biomedical Materials Research **62**(2): 265-272

Kim, B. S., J. S. Kim, et al. (2013). "Growth and osteogenic differentiation of alveolar human bone marrow-derived mesenchymal stem cells on chitosan/hydroxyapatite composite fabric." Journal of Biomedical Materials Research A **101**(6): 1550-1558.

Kim, H., C. H. Tator, et al. (2011). "Chitosan implants in the rat spinal cord: biocompatibility and biodegradation." Journal of Biomedical Materials Research A **97**(4): 395-404.

Kim, H. S., J. T. Kim, et al. (2007). "Preparation of a porous chitosan/fibroin-hydroxyapatite composite matrix for tissue engineering." Macromolecular Research**15**(1): 65-73.

Kim, H. W., J. H. Song, et al. (2005). "Nanofiber Generation of Gelatin–Hydroxyapatite Biomimetics for Guided Tissue Regeneration." Advanced Functional Materials **15**(12): 1988-1994.

Kinane, D. F. and G. J. Marshall (2001). "Periodontal manifestations of systemic disease." Australian Dental Journal **46**(1): 2-12.

King, R. N. and D. J. Lyman (1975). "Polymers in Contact with the Body." Environmental health prespectives. **11**: 71-74.

Kithva, P., L. Grondahl, et al. (2010). "Biomimetic synthesis and tensile properties of nanostructured high volume fraction hydroxyapatite and chitosan biocomposite films." Journal of Materials Chemistry **20**(2): 381-389.

Klossner, R. R., H. A. Queen, et al. (2008). "Correlation of Chitosan's Rheological Properties and Its Ability to Electrospin." Biomacromolecules **9**(10): 2947-2953.

Knaul, J. Z., S. M. Hudson, et al. (1999). "Improved mechanical properties of chitosan fibers." Journal of Applied Polymer Science **72**(13): 1721-1732.

Kokubo, T., M. Hanakawa, et al. (2004). "Apatite formation on non-woven fabric of carboxymethylated chitin in SBF." Biomaterials **25**(18): 4485-4488.

Kokubo, T., H. M. Kim, et al. (2003). "Novel bioactive materials with different mechanical properties." Biomaterials **24**(13): 2161-2175.

Kokubo, T. and H. Takadama (2006). "How useful is SBF in predicting in vivo bone bioactivity?" Biomaterials **27**(15): 2907-2915.

Kolhe, P. and R. M. Kannan (2002). "Improvement in Ductility of Chitosan through Blending and Copolymerization with PEG: FTIR Investigation of Molecular Interactions." Biomacromolecules **4**(1): 173-180.

Kong, L., Y. Gao, et al. (2005). "Preparation and characterization of nano-hydroxyapatite/chitosan composite scaffolds." Journal of Biomedical Materials Research Part A **75A**(2): 275-282.

Kong, L. J., Y. Gao, et al. (2006). "A study on the bioactivity of chitosan/nano-hydroxyapatite composite scaffolds for bone tissue engineering." European Polymer Journal **42**(12): 3171-3179.

Kriegel, C., K. M. Kit, et al. (2009). "Electrospinning of chitosan–poly(ethylene oxide) blend nanofibers in the presence of micellar surfactant solutions." Polymer **50**(1): 189-200.

Kumar, M. N. V. R., R. A. A. Muzzarelli, et al. (2004). "Chitosan chemistry and pharmaceutical perspectives." Chemical Reviews **104**(12): 6017-6084.

Kumar, S. T. S. (2013). Physical and Chemical Characterization of Biomaterials. Characterization of Biomaterials. A. Bandhyopadhya and S. Bose, Elsevier**:** 11-47.

Kumirska, J., M. Czerwicka, et al. (2010). "Application of Spectroscopic Methods for Structural Analysis of Chitin and Chitosan." Marine Drugs **8**(5): 1567-1636.

Lang NP, Hammerle CH, Bragger U , et al. Guided tissue regeneration in jawbone defects prior to implant placement. Clinical Oral Implants Research. 1994**;5**:92–7.

Langer, R. S. and N. A. Peppas (1981). "Present and future applications of biomaterials in controlled drug delivery systems." Biomaterials **2**(4): 201-214.

Lee, H. M., S. G. Ciancio, et al. (2004). "Subantimicrobial dose doxycycline efficacy as a matrix metalloproteinase inhibitor in chronic periodontitis patients is enhanced when combined with a non-steroidal anti-inflammatory drug." Journal of Periodontology **75**(3): 453-463.

Lee, D. W., H. L., Chong H. N., Shim W. S. (2009). "Advances in Chitosan Material and its Hybrid Derivatives: A Review." The open Biomaterials Journal **1**: 10-20.
Lee, J. Y., Y. M. Lee, et al. (2004). "Effect of subantimicrobial dose doxycycline as an effective adjunct to scaling and root planing." Journal of Periodontology **75**(11): 1500-1508.

Leedy, M. R., H. J. Martin, et al. (2011). "Use of Chitosan as a Bioactive Implant Coating for Bone-Implant Applications." Chitosan for Biomaterials Ii **244**: 129-165.

Leong, K. F., C. K. Chua, et al. (2008). "Engineering functionally graded tissue engineering scaffolds." Journal of the Mechanical Behavior of Biomedical Materials **1**(2): 140-152.

Levitt, S. R., Crayton, P. H., Monroe, E. A., Condrate, R. A. (1969). "Forming methods for apatite prostheses." Journal of Biomedical Materials Research**. 3:** 683–684.

Li, F., Q. L. Feng, et al. (2002). "A simple biomimetic method for calcium phosphate coating." Surface & Coatings Technology **154**(1): 88-93.

Li, X. Y., K. H. Nan, et al. (2012). "Preparation and characterization of nano-hydroxyapatite/chitosan cross-linking composite membrane intended for tissue engineering." International Journal of Biological Macromolecules **50**(1): 43-49.

Liang, D., B. S. Hsiao, et al. (2007). "Functional electrospun nanofibrous scaffolds for biomedical applications." Advanced Drug Delivery Reviews **59**(14): 1392-1412.

Liao, S., W. Wang, et al. (2005). "A three-layered nano-carbonated hydroxyapatite/collagen/PLGA composite membrane for guided tissue regeneration." Biomaterials **26**(36): 7564-7571.

Liao, S., F. Watari, et al. (2007). "The degradation of the three layered nano-carbonated hydroxyapatite/collagen/PLGA composite membrane in vitro." Dental Materials **23**(9): 1120-1128.

Lim, L. Y., E. Khor, et al. (1998). "Gamma irradiation of chitosan." Journal of Biomedical Materials Research **43**(3): 282-290.

Lim, L. Y., E. Khor, et al. (1999). "Effects of dry heat and saturated steam on the physical properties of chitosan." Journal of Biomedical Materials Research **48**(2): 111-116.

Lin, N. H., S. Gronthos, et al. (2008). "Stem cells and periodontal regeneration." Australian Dental Journal **53**(2): 108-121.

Liu, H., J. Mao, et al. (2004). "A study on a chitosan-gelatin-hyaluronic acid scaffold as artificial skin in vitro and its tissue engineering applications." Journal of Biomaterials Science, Polymer Edition **15**(1): 25-40.

Liu, X., L. Ma, et al. (2011). Chitosan-Based Biomaterials for Tissue Repair and Regeneration. Chitosan for Biomaterials II. R. Jayakumar, M. Prabaharan and R. A. A. Muzzarelli, Springer Berlin Heidelberg. **244:** 81-127.

Liu, Y. G., C. R. Zhou, et al. (2012). "A biomimetic strategy for controllable degradation of chitosan scaffolds." Journal of Materials Research **27**(14): 1859-1868.

Liuyun, J., L. Yubao, et al. (2009). "Preparation and biological properties of a novel composite scaffold of nano-hydroxyapatite/chitosan/carboxymethyl cellulose for bone tissue engineering." J Biomed Sci **16**: 65.

Loh, Q. L. and C. Choong (2013). "Three-Dimensional Scaffolds for Tissue Engineering Applications: Role of Porosity and Pore Size." Tissue Engineering Part B-Reviews **19**(6): 485-502.

Lommer, M. J., R. B. Wiggs, et al. (2012). Chapter 20 - Osteoconductive and osteoinductive agents in periodontal surgery. Oral and Maxillofacial Surgery in Dogs and Cats. Oxford, W.B. Saunders**:** 185-192.

Lundgren AK, Sennerby L, Lundgren D, Taylor A, Gottlow J, Nyman S. Bone augmentation at titanium implants using autologous bone grafts and bioresorbable barrier. An experimental study in the rabbit tibia. Clinical Oral Implants Res. 1997 Apr; **8**(2):82-9

Lyman, D. (2002). Characterization of Biomaterials. Integrated Biomaterials Science. R. Barbucci, Springer US**:** 325-337.

Lyman, D (1974) Polymers in Medicine, Angewandte International edition Chemie 13(2)

Lynch, S. E., G. R. de Castilla, et al. (1991). "The effects of short-term application of a combination of platelet-derived and insulin-like growth factors on periodontal wound healing." Journal of Periodontology **62**(7): 458-467.

Maachou, H., Bal, KE, et al. (2008). "Characterization and In Vitro Bioactivity of Chitosan/Hydroxyapatite Composite Membrane Prepared by Freeze-Gelation Method." Trends in Biomaterials and Artificial Organs **22**(16-26).

Macchetta, A., I. G. Turner, et al. (2009). "Fabrication of HA/TCP scaffolds with a graded and porous structure using a camphene-based freeze-casting method." Acta Biomaterialia **5**(4): 1319-1327.

Madhumathi, K. and T. S. S. Kumar (2014). "Regenerative potential and anti-bacterial activity of tetracycline loaded apatitic nanocarriers for the treatment of periodontitis." Biomedical Materials **9**(3).

Madihally, S. V. and H. W. Matthew (1999). "Porous chitosan scaffolds for tissue engineering." Biomaterials **20**(12): 1133-1142.

Maganti, N., P. K. C. Venkat Surya, et al. (2011). "Structure–Process–Property Relationship of Biomimetic Chitosan-Based Nanocomposite Scaffolds for Tissue Engineering: Biological, Physico-Chemical, and Mechanical Functions." Advanced Engineering Materials **13**(3): B108-B122.

Martínez-Camacho, A. P., M. O. Cortez-Rocha, et al. (2010). "Chitosan composite films: Thermal, structural, mechanical and antifungal properties." Carbohydrate Polymers **82**(2): 305-315.

Martins, A. M., J. D. Kretlow, et al. (2012). "Gradual pore formation in natural origin scaffolds throughout subcutaneous implantation." Journal of Biomedical Materials Research A **100**(3): 599-612.

McKee, M. G., M. T. Hunley, et al. (2005). "Solution Rheological Behavior and Electrospinning of Cationic Polyelectrolytes." Macromolecules **39**(2): 575-583.

Mellonig, J. T. (1992). "Autogenous and allogeneic bone grafts in periodontal therapy." Crit Rev Oral Biol Med **3**(4): 333-352.

Mendes, P. N., S. C. Rahal, et al. (2009). "In vivo and in vitro evaluation of an Acetobacter xylinum synthesized microbial cellulose membrane intended for guided tissue repair." Acta Vet Scand **51**.

Mi, F.-L., C.-Y. Kuan, et al. (2000). "The study of gelation kinetics and chain-relaxation properties of glutaraldehyde-cross-linked chitosan gel and their effects on microspheres preparation and drug release." Carbohydrate Polymers **41**(4): 389-396.

Mi, F.-L., H.-W. Sung, et al. (2000). "Synthesis and characterization of a novel chitosan-based network prepared using naturally occurring crosslinker." Journal of Polymer Science Part A: Polymer Chemistry **38**(15): 2804-2814.

Mi, F.-L., H.-W. Sung, et al. (2002). "Drug release from chitosan–alginate complex beads reinforced by a naturally occurring cross-linking agent." Carbohydrate Polymers **48**(1): 61-72.

Mikos, A. G., S. W. Herring, et al. (2006). "Engineering complex tissues." Tissue Engineering **12**(12): 3307-3339.

Mohamed, K. R., H. H. Beherei, et al. (2014). "In vitro study of nano-hydroxyapatite/chitosan–gelatin composites for bio-applications." Journal of Advanced Research **5**(2): 201-208.

Mota, J., N. Yu, et al. (2012). "Chitosan/bioactive glass nanoparticle composite membranes for periodontal regeneration." Acta Biomater **8**(11): 4173-4180.

Mucha. M and Pawlak. A (2002). "Complex study on chitosan degradability." Polymer **47**: 519-516.

Muniz, F. W. M. G., C. C. de Oliveira, et al. (2013). "Azithromycin: A new concept in adjuvant treatment of periodontitis." Eur J Pharmacol **705**(1-3): 135-139.

Murphy, C. M., M. G. Haugh, et al. (2010). "The effect of mean pore size on cell attachment, proliferation and migration in collagen-glycosaminoglycan scaffolds for bone tissue engineering." Biomaterials **31**(3): 461-466.

Murugan, R. and S. Ramakrishna (2004). "Bioresorbable composite bone paste using polysaccharide based nano hydroxyapatite." Biomaterials **25**(17): 3829-3835.

Muzzarelli, R., G. Biagini, et al. (1989). "Reconstruction of parodontal tissue with chitosan." Biomaterials **10**(9): 598-603.

Muzzarelli A.A.R., (2009) Chitins and chitosans for the repair of wounded skin, nerve, cartilage and bone, Carbohydrate Polymers, **76,** 167-182

Muzzarelli, R. A. (2011). New Techniques for Optimization of Surface Area and Porosity in Nanochitins and Nanochitosans. Chitosan for Biomaterials II. R. Jayakumar, M. Prabaharan and R. A. A. Muzzarelli, Springer Berlin Heidelberg. **244:** 167-186.

Muzzarelli, R. A. A., F. Tanfani, et al. (1984). "Chelating derivatives of chitosan obtained by reaction with ascorbic acid." Carbohydrate Polymers **4**(2): 137-151.

Nair, L. S. and C. T. Laurencin (2007). "Biodegradable polymers as biomaterials." Progress in Polymer Science **32**(8-9): 762-798.

Nanci, A. and D. D. Bosshardt (2006). "Structure of periodontal tissues in health and disease." Periodontology 2000 **40**(1): 11-28.

Nazir, R., N. Iqbal, et al. (2012). "Rapid synthesis of thermally stable hydroxyapaptite." Ceramics International **38**(1): 457-462.

Neto, C. G. T., T. N. C. Dantas, et al. (2005). "Permeability studies in chitosan membranes. Effects of crosslinking and poly(ethylene oxide) addition." Carbohydrate Research **340**(17): 2630-2636.

Nevins, M., W. V. Giannobile, et al. (2005). "Platelet-derived growth factor stimulates bone fill and rate of attachment level gain: results of a large multicenter randomized controlled trial." Journal of Periodontology **76**(12): 2205-2215.

Newman, M. G., H. H. Takei, et al. (2012). Carranzas clinical periodontology, St Louis Mo, Elsevier Saunders.

Nguyen, L. H., N. Annabi, et al. (2012). "Vascularized bone tissue engineering: approaches for potential improvement." Tissue Engineering Part B Rev **18**(5): 363-382.

Nieminen, T., I. Kallela, et al. (2006). "In vivo and in vitro degradation of a novel bioactive guided tissue regeneration membrane." Int J Oral Maxillofac Surg **35**(8): 727-732.

Norowski, P. A., T. Fujiwara, et al. (2012). "Novel naturally crosslinked electrospun nanofibrous chitosan mats for guided bone regeneration membranes: material characterization and cytocompatibility." Journal of Tissue Engineering and Regenerative Medicine:

Nyman, S., J. Gottlow, et al. (1987). "New attachment formation by guided tissue regeneration." Journal Periodontal Research **22**(3): 252-254.

O'Brien, J., I. Wilson, et al. (2000). "Investigation of the Alamar Blue (resazurin) fluorescent dye for the assessment of mammalian cell cytotoxicity." European Journal of Biochem **267**(17): 5421-5426.

Ohara, N., Y. Hayashi, et al. (2004). "Early gene expression analyzed by cDNA microarray and RT-PCR in osteoblasts cultured with water-soluble and low molecular chitooligosaccharide." Biomaterials **25**(10): 1749-1754.

Ohkawa, K., D. Cha, et al. (2004). "Electrospinning of Chitosan." Macromolecular Rapid Communications **25**(18): 1600-1605.

Okulus, Z., T. Buchwald, et al. (2014). "Study of a new resin-based composites containing hydroxyapatite filler using Raman and infrared spectroscopy." Materials Chemistry and Physics **145**(3): 304-312.

Owens KW, Yukna RA. Collagen membrane resorption in dogs a comparative study. Implant Dentistry. 2001;10:49–58

Pachence, J. M. and Kohn, J. (2000). Biodegradable Polymers. Principles of Tissue engineering. R. L. Robert L Panza, Joseph Vacanti., Academic Press.

Pakravan, M., M. C. Heuzey, et al. (2011). "A fundamental study of chitosan/PEO electrospinning." Polymer **52**(21): 4813-4824.

Palumbo, A. (2011). The Anatomy and Physiology of the Healthy Periodontium. Gingival Diseases - Their Aetiology, Prevention and Treatment. F. S. P. a. R. M. Davies, InTech,.

Pandey, A., E. Jan, et al. (2006). "Physical and mechanical behavior of hot rolled HDPE/HA composites." Journal of Materials Science **41**(11): 3369-3376.

Pandit, N., R. Malik, et al. (2011). "Tissue engineering: A new vista in periodontal regeneration." J Indian Soc Periodontology **15**(4): 328-337.

Park, C. H., K. H. Kim, et al. (2014). "Spatiotemporally controlled microchannels of periodontal mimic scaffolds." J Dent Res **93**(12): 1304-1312.

Park, H., B. Choi, et al. (2013). "Anionic carbohydrate-containing chitosan scaffolds for bone regeneration." Carbohydrate Polymers **97**(2): 587-596.
Pati, F., B. Adhikari, et al. (2011). "Development of chitosan-tripolyphosphate fibers through pH dependent ionotropic gelation." Carbohydrate Research **346**(16): 2582-2588.

Peniche, C., W. Arguelles-Monal, et al. (2008). "Chitin and Chitosan: Major Sources, Properties and Applications." Monomers, Polymers and Composites from Renewable Resources: 517-542.

Penichecovas, C., W. Arguellesmonal, et al. (1993). "A Kinetic-Study of the Thermal-Degradation of Chitosan and a Mercaptan Derivative of Chitosan." Polymer Degradration and Stability **39**(1): 21-28.

Phaechamud, T. and J. Charoenteeraboon (2008). "Antibacterial Activity and Drug Release of Chitosan Sponge Containing Doxycycline Hyclate." AAPS PharmSciTech **9**(3): 829-835.

Phillips, J. E., K. L. Burns, et al. (2008). "Engineering graded tissue interfaces." Proceedings of the National Academy of Sciences of the United States of America **105**(34): 12170-12175.

Pighinelli, L. and M. Kucharska (2013). "Chitosan-hydroxyapatite composites." Carbohydrate Polymers **93**(1): 256-262.

Pihlstrom, B. L., B. S. Michalowicz, et al. (2005). "Periodontal diseases." The Lancet **366**(9499): 1809-1820.

Pillai, C. K. S., W. Paul, et al. (2009). "Chitin and chitosan polymers: Chemistry, solubility and fiber formation." Progress in Polymer Science **34**(7): 641-678.

Po Hui Chen, H. Y.-H., Ting-Yun Kuo , Fang- Hsuan Liu, Juin Yih Lai, Hsyue-jen, Hsieh (2007). "Improvement in properties of chitosan membranes using natural organic acid solutions as solvents for chitosan dissolution. ." Journal of medical and biological engineering. **27**(1): 23-28.

Pompe, W., H. Worch, et al. (2003). "Functionally graded materials for biomedical applications." Materials Science and Engineering: A **362**(1–2): 40-60.

Pontoriero, R., J. Lindhe, et al. (1988). "Guided tissue regeneration in degree II furcation-involved mandibular molars. A clinical study." Journal of Clinical Periodontology **15**(4): 247-254.

Pontoriero, R., J. Lindhe, et al. (1989). "Guided tissue regeneration in the treatment of furcation defects in mandibular molars. A clinical study of degree III involvements." Journal of Clinical Periodontology **16**(3): 170-174.

Preshaw, P. M., A. L. Alba, et al. (2012). "Periodontitis and diabetes: a two-way relationship." Diabetologia **55**(1): 21-31.
Qasim, S. B., R. M. Delaine-Smith, et al. (2015). "Freeze gelated porous membranes for periodontal tissue regeneration." Acta Biomaterialia **23**: 317-328.

Qu, X., A. Wirsén, et al. (1999). "Structural change and swelling mechanism of pH-sensitive hydrogels based on chitosan and D,L-lactic acid." Journal of Applied Polymer Science **74**(13): 3186-3192.

Qu, X., A. Wirsen, et al. (2000). "Effect of lactic/glycolic acid side chains on the thermal degradation kinetics of chitosan derivatives." Polymer **41**(13): 4841-4847.

Queen, H. (2006). Electrospinning chitosan based nanofibers for biomedical applications. Graduate Faculty of, North Carolina State University. **MSc Tissue engineering**.

Raafat, D. and H.-G. Sahl (2009). "Chitosan and its antimicrobial potential – a critical literature survey." Microbial Biotechnology **2**(2): 186-201.

Rajkumar, M., K. Kavitha, et al. (2013). "Nanohydroxyapatite-chitosan-gelatin polyelectrolyte complex with enhanced mechanical and bioactivity." Mater Sci Eng C Mater Biol Appl **33**(6): 3237-3244.

Ramakrishna, S., J. Mayer, et al. (2001). "Biomedical applications of polymer-composite materials: a review." Composites Science and Technology **61,**: 1189-1224.

Ramakrishna, SeeramK. F., Wee-Eong Teo , Teik-Cheng Lim , Zuwei Ma (N (2005). An Introduction To Electrospinning And Nanofibers, World scientific publishing.

Ramseier, C. A., G. Rasperini, et al. (2012). "Advanced reconstructive technologies for periodontal tissue repair." Periodontology 2000 **59**(1): 185-202.

Ramseier, C. A., G. Rasperini, et al. (2012). "Advanced reconstructive technologies for periodontal tissue repair." Periodontology 2000 **59**(1): 185-202.

Rashi Chaturvedi, A. S. G., Poonam Sikri (2008). "Evaluation of the regenerative potential of 25% doxycycline-loaded biodegradable membrane vs biodegradable membrane alone in the treatment of human periodontal infrabony defects: A clinical and radiological study." Indian Journal of Dental research **19**(2): 116-123.

Ratner, B. D. (2004). Biomaterials Science; An Introduction to materials in Medicine Elsevier.

Ravindra, R., K. R. Krovvidi, et al. (1998). "Solubility parameter of chitin and chitosan." Carbohydrate Polymers **36**(2–3): 121-127.

Regnier, P., A.C.Lasaga, et al. (1994). "Mechanism of CO substitution in carbonate-fluorapatite: Evidence from FTIR spectroscopy, C NMR, and quantum mechanical calculations." American Mineralogist **79**: 809-818.

Rehman, I. and W. Bonfield (1997). "Characterization of hydroxyapatite and carbonated apatite by photo acoustic FTIR spectroscopy." Journal of Materials science:Materials in Medicine **8**: 1-4.

Rehman, I., R. Smith, et al. (1995). "Structural evaluation of human and sheep bone and comparison with synthetic hydroxyapatite by FT-Raman spectroscopy." Journal of Biomedical Materials Research **29**(10): 1287-1294.

Rehman, I. U, Movasaghi Z, et al. (2013). Chemical and structural Analysis of bone by Spectroscopy. Vibrational spectroscopy for tissue analysis. I. u. Rehman, CRC Press, Taylor and Francis group.**:** 190.

Rehman, I. B., W. (1997). "Characterization of hydroxyapatite and carbonated apatite by photo acoustic FTIR spectroscopy." Journal of materials sciecne: Materials in medicine **8**: 1-4.

Rehman, I. U., Z. Movasaghi, et al. (2013). Chemical and structural Analysis of bone by Spectroscopy. Vibrational spectroscopy for tissue analysis. I. u. Rehman. Sheffield, CRC Press, Taylor and Francis group.**:** 190.

Ren, D., H. Yi, et al. (2005). "The enzymatic degradation and swelling properties of chitosan matrices with different degrees of N-acetylation." Carbohydrate Research **340**(15): 2403-2410.

Reynolds, M. A., M. E. Aichelmann-Reidy, et al. (2003). "The efficacy of bone replacement grafts in the treatment of periodontal osseous defects. A systematic review." Ann Periodontology **8**(1): 227-265.

Rinaudo, M. (2006). "Chitin and chitosan: Properties and applications." Progress in Polymer Science **31**(7): 603-632.

Riva, R., H. Ragelle, et al. (2011). Chitosan and Chitosan Derivatives in Drug Delivery and Tissue Engineering. Chitosan for Biomaterials II. R. Jayakumar, M. Prabaharan and R. A. A. Muzzarelli, Springer Berlin Heidelberg. **244:** 19-44.

Rodrigues, S., A. M. da Costa, et al. (2012). "Chitosan/carrageenan nanoparticles: effect of cross-linking with tripolyphosphate and charge ratios." Carbohydrate Polymers **89**(1): 282-289.

Roeder, R. K. (2013). Mechanical Characterization of Biomaterials. Characterization of Biomaterials. A. Bandhyopadhya and S. Bose, Elsevier**:** 49-104.

Roskos, K. V., B. K. Fritzinger, et al. (1995). "Development of a drug delivery system for the treatment of periodontal disease based on bioerodible poly(ortho esters)." Biomaterials **16**(4): 313-317.

Sabokbar, A., R. Pandey, et al. (2001). "Hydroxyapatite particles are capable of inducing osteoclast formation." J Materials Science: Materials in Medicine **12**(8): 659-664.

Sailaja, G. S., P. Ramesh, et al. (2006). "Human osteosarcoma cell adhesion behaviour on hydroxyapatite integrated chitosan-poly(acrylic acid) polyelectrolyte complex." Acta Biomaterialia **2**(6): 651-657.

Sakallıoğlu, U., G. Açıkgöz, et al. (2004). "Healing of periodontal defects treated with enamel matrix proteins and root surface conditioning—an experimental study in dogs." Biomaterials **25**(10): 1831-1840.

Sakallioglu, U., U. Yavuz, et al. (2007). "Clinical outcomes of guided tissue regeneration with Atrisorb membrane in the treatment of intrabony defects: a 3-year follow-up study." Int J Periodontics Restorative Dent **27**(1): 79-88.

Sangsanoh, P., S. Waleetorncheepsawat, et al. (2007). "In vitro biocompatibility of schwann cells on surfaces of biocompatible polymeric electrospun fibrous and solution-cast film scaffolds." Biomacromolecules **8**(5): 1587-1594.7

Saravanan, S., S. Nethala, et al. (2011). "Preparation, characterization and antimicrobial activity of a bio-composite scaffold containing chitosan/nano-hydroxyapatite/nano-silver for bone tissue engineering." International Journal of Biological Macromolecules **49**(2): 188-193.

Sarkar, S. D., B. L. Farrugia, et al. (2013). "Physico-chemical/biological properties of tripolyphosphate cross-linked chitosan based nanofibers." Mater Sci Eng C Mater Biol Appl **33**(3): 1446-1454.

Schiffman, J. D., C. L. S. (2007). "One-Step Electrospinning of Cross-Linked Chitosan Fibers." Biomacromolecules **8**(9): 2665-2667.

Schmalz, G. (2009). Determination of Biocompatibility. Biocompatibility of Dental Materials. G. Schmalz and D. A. Bindslev, Springer.

Schneider, L. A., A. Korber, et al. (2007). "Influence of pH on wound-healing: a new perspective for wound-therapy?" Arch Dermatol Res **298**(9): 413-420.

Seymour, R. A. and P. A. Heasman (1995). "Pharmacological control of periodontal disease. II. Antimicrobial agents." J Dent **23**(1): 5-14.

Shen, E. C., C. Wang, et al. (2008). "Tetracycline release from tripolyphosphate-chitosan cross-linked sponge: a preliminary in vitro study." Journal of Periodontal Research **43**(6): 642-648.
Shen, Z., G. P. Simon, et al. (2002). "Comparison of solution intercalation and melt intercalation of polymer–clay nanocomposites." Polymer **43**(15): 4251-4260.

Shi, C., Y. Zhu, et al. (2006). "Therapeutic potential of chitosan and its derivatives in regenerative medicine." J Surg Res **133**(2): 185-192.

Shikinami, Y., Y. Matsusue, et al. (2005). "The complete process of bioresorption and bone replacement using devices made of forged composites of raw hydroxyapatite particles/poly L-lactide (F-u-HA/PLLA)." Biomaterials **26**(27): 5542-5551.

Shoichet, M. S. (2010). "Polymer Scaffolds for Biomaterials Applications." Macromolecules **43**: 581-591.

Shue, L., Z. Yufeng, et al. (2012). "Biomaterials for periodontal regeneration: A review of ceramics and polymers." Biomatter **2**(4): 271-277.

Siddiqui, N. and K. Pramanik (2014). "Effects of micro and nano β-TCP fillers in freeze-gelled chitosan scaffolds for bone tissue engineering." Journal of Applied Polymer Science **131**(21): n/a-n/a.

Siddiqui, N. and K. Pramanik (2015). "Development of fibrin conjugated chitosan/nano β-TCP composite scaffolds with improved cell supportive property for bone tissue regeneration." Journal of Applied Polymer Science:

Silva, R. M., G. A. Silva, et al. (2004). "Preparation and characterisation in simulated body conditions of glutaraldehyde crosslinked chitosan membranes." Journal of Materials Science-Materials in Medicine **15**(10): 1105-1112.

Slots, J. and T. E. Rams (1990). "Antibiotics in periodontal therapy: advantages and disadvantages." Journal of Clinical Periodontology **17**(7 (Pt 2)): 479-493.

Sowmya, S., J. D. Bumgardener, et al. (2013). "Role of nanostructured biopolymers and bioceramics in enamel, dentin and periodontal tissue regeneration." Progress in Polymer Science **38**(10-11): 1748-1772.

Spasova, M., N. Manolova, et al. (2004). "Preparation of chitosan-containing nanofibres by electrospinning of chitosan/poly(ethylene oxide) blend solutions." E-Polymers.

Struszczyk, M.H, Struszczyk, K. J, (2007) Medical applications of chitin and its derivatives, Polish Chitin society, Monograph XII

Subramanian, A., U. M. Krishnan, et al. (2011). "Fabrication of uniaxially aligned 3D electrospun scaffolds for neural regeneration." Biomedical Materials **6**(2): 025004.

Subramanian, A., U. M. Krishnan, et al. (2013). "In vivo biocompatibility of PLGA-polyhexylthiophene nanofiber scaffolds in a rat model." Biomed Research International **2013**: 390518.

Suh, J. K. and H. W. Matthew (2000). "Application of chitosan-based polysaccharide biomaterials in cartilage tissue engineering: a review." Biomaterials **21**(24): 2589-2598.
Suha, J.-K F., H. W. T. M. (2000). "Application of chitosan-based polysaccharide biomaterials in cartilage tissue engineering: a review." Biomaterials **21**(24): 2589-2598.

Sukigara, S., M. Gandhi, et al. (2003). "Regeneration of Bombyx mori silk by electrospinning - Part 1: Processing parameters and geometric properties." Polymer **44**(19): 5721-5727.

Sun, F., K. Koh, et al. (2012). "Biocompatibility of Nanoscale Hydroxyapatite-embedded Chitosan Films." Bulletin of the Korean Chemical Society **33**(12): 3950-3956.

Sun, H. H., T. J. Qu, et al. (2012). "Designing biomaterials for in situ periodontal tissue regeneration." Biotechnol Progress **28**(1): 3-20.

Sung, H. W., R. N. Huang, et al. (1999). "In vitro evaluation of cytotoxicity of a naturally occurring cross-linking reagent for biological tissue fixation." J Biomater Sci Polym Ed **10**(1): 63-78.

Tachaboonyakiat, W., T. Serizawa, et al. (2002). "Inorganic-organic polymer hybrid scaffold for tissue engineering - II: Partial enzymatic degradation of hydroxyapatite-chitosan hybrid." Journal of Biomaterials Science-Polymer Edition **13**(9): 1021-1032.

Takata, T., H. L. Wang, et al. (2001). "Attachment, proliferation and differentiation of periodontal ligament cells on various guided tissue regeneration membranes." Journal of Periodontal Research **36**(5): 322-327.

Talebian, S., M. Mehrali, et al. (2014). "Chitosan (PEO)/bioactive glass hybrid nanofibers for bone tissue engineering." Rsc Advances **4**(90): 49144-49152.

Tan, A. E. (1993). "New ideas and advancing technologies in periodontology: surgical options with advancing technologies." Int Dent J **43**(6): 567-577.

Tasselli, F., A. Mirmohseni, et al. (2013). "Mechanical, swelling and adsorptive properties of dry–wet spun chitosan hollow fibers crosslinked with glutaraldehyde." Reactive and Functional Polymers **73**(1): 218-223.

Teng, S.-H., E.-J. Lee, et al. (2009). "Chitosan/nanohydroxyapatite composite membranes via dynamic filtration for guided bone regeneration." Journal of Biomedical Materials Research Part A **88A**(3): 569-580.

Teng, S. H., E. J. Lee, et al. (2009). "Functionally Gradient Chitosan/Hydroxyapatite Composite Scaffolds for Controlled Drug Release." Journal of Biomedical Materials Research Part B-Applied Biomaterials **90B**(1): 275-282.

Teng, S. H., E. J. Lee, et al. (2008). "Three-layered membranes of collagen/hydroxyapatite and chitosan for guided bone regeneration." Journal of Biomedical Materials Research B Appl Biomater **87**(1): 132-138.

Tetteh, G., A. S. Khan, et al. (2014). "Electrospun polyurethane/hydroxyapatite bioactive Scaffolds for bone tissue engineering: The role of solvent and hydroxyapatite particles." Journal of the Mechanical Behavior of Biomedical Materials **39**: 95-110.
Thasneem, Y. M. and C. P. Sharma (2013). In Vitro Characterization of Cell–Biomaterials Interactions. Characterization of Biomaterials. A. Bandhyopadhya and S. Bose, Elsevier**:** 175-205.

Thein-Han, W. W. and Y. Kitiyanant (2007). "Chitosan scaffolds for in vitro buffalo embryonic stem-like cell culture: An approach to tissue engineering." Journal of Biomedical Materials Research Part B: Applied Biomaterials **80B**(1): 92-101.

Thein-Han, W. W. and R. D. K. Misra (2009). "Biomimetic chitosan–nanohydroxyapatite composite scaffolds for bone tissue engineering." Acta Biomaterialia **5**(4): 1182-1197.

Thomas, V. and Y. K. Vohra (2012). Functionally-Graded Biomimetic Vascular Grafts for Enhanced Tissue Regeneration and Bio-integration. Integrated Biomaterials in Tissue Engineering, John Wiley & Sons, Inc.**:** 235-273.

Tiwary, A. K. and V. Rana (2010). "Cross-linked chitosan films: effect of cross-linking density on swelling parameters." Pak J Pharm Sci **23**(4): 443-448.

Toffey, A. and W. G. Glasser (1999). "Chitin derivatives. II. Time–temperature–transformation cure diagrams of the chitosan amidization process." Journal of Applied Polymer Science **73**(10): 1879-1889.

Tomihata, K. and Y. Ikada (1997). "In vitro and in vivo degradation of films of chitin and its deacetylated derivatives." Biomaterials **18**(7): 567-575.

Toskas, G., C. Cherif, et al. (2013). "Chitosan(PEO)/silica hybrid nanofibers as a potential biomaterial for bone regeneration." Carbohydrate Polymers **94**(2): 713-722.

Ulanski, P. and J. Rosiak (1992). "Preliminary Studies on Radiation-Induced Changes in Chitosan." Radiation Physics and Chemistry **39**(1): 53-57.

Uygun, B. E., T. Bou-Akl, et al. (2010). "Membrane thickness is an important variable in membrane scaffolds: Influence of chitosan membrane structure on the behavior of cells." Acta Biomaterialia **6**(6): 2126-2131.

Van de Velde, K. and P. Kiekens (2004). "Structure analysis and degree of substitution of chitin, chitosan and dibutyrylchitin by FT-IR spectroscopy and solid state 13C NMR." Carbohydrate Polymers **58**(4): 409-416.

van Winkelhoff, A. J. and E. G. Winkel (2009). "Antibiotics in Periodontics: Right or Wrong?" Journal of Periodontology **80**(10): 1555-1558.

Vishakha Patil, R. M., Amita Mali (2013). "Systemic anti-microbial agents used in periodontal therapy." Journal of Indian Society of Periodontology **17**(2): 1662-1168.

von Burkersroda, F., L. Schedl, et al. (2002). "Why degradable polymers undergo surface erosion or bulk erosion." Biomaterials **23**(21): 4221-4231.

Walker, C. and K. Karpinia (2002). "Rational of use of Antibiotics in Periodontics." Journal of Periodontology **73**(10): 1188-1196.

Walters, M.A, Leung , Y.C, et al (1990)"A raman and infrared spectroscopic investigation of biological hydroxyapatite." Journal of inorganic biochemistry **39**(3): 193-200.

Wan, A. C. A., E. Khor, et al. (1997). "Hydroxyapatite modified chitin as potential hard tissue substitute material." Journal of Biomedical Materials Research **38**(3): 235-241.

Wan, Y., H. Wu, et al. (2008). "Compressive mechanical properties and biodegradability of porous poly(caprolactone)/chitosan scaffolds." Polymer Degradation Stability **93**(10): 1736-1741.

Wan, Y., A. Yu, et al. (2005). "Porous-conductive chitosan scaffolds for tissue engineering II. in vitro and in vivo degradation." Journal of Materials Science Materials in Medicine **16**(11): 1017-1028.

Wang, G. C., L. Zheng, et al. (2011). "In Vitro Assessment of the Differentiation Potential of Bone Marrow-Derived Mesenchymal Stem Cells on Genipin-Chitosan Conjugation Scaffold with Surface Hydroxyapatite Nanostructure for Bone Tissue Engineering." Tissue Engineering Pt A **17**(9-10): 1341-1349.

Wang, H. L. and H. Greenwell (2001). "Surgical periodontal therapy." Periodontology 2000 **25**: 89-99.

Wang, S. M., Q. Z. Huang, et al. (2005). "Study on the synergetic degradation of chitosan with ultraviolet light and hydrogen peroxide." Carbohydrate Research **340**(6): 1143-1147.

Wang, X., G. Song, et al. (2009). "Fabrication of nano-fibrous PLLA scaffold reinforced with chitosan fibers." Journal of Biomaterials Science Polymer Ed **20**(14): 1995-2002.

Wang, X., X. Wang, et al. (2009). "Synthesis and evaluation of collagen–chitosan–hydroxyapatite nanocomposites for bone grafting." Journal of Biomedical Materials Research Part A **89A**(4): 1079-1087.

Wawro, D. and L. Pighinelli (2011). "Chitosan fibers modified with HAp/beta-TCP nanoparticles." International Journal of Mol Science **12**(11): 7286-7300.

Wei, L., C. H. Cai, et al. (2011). "Degradation controllable biomaterials constructed from lysozyme-loaded Ca-alginate microparticle/chitosan composites." Polymer **52**(22): 5139-5148.

Weinberg, M. A. and M. Bral (1998). "Tetracycline and its analogues: A therapeutic paradigm in periodontal diseases." Critical Reviews in Oral Biology & Medicine **9**(3): 322-332.

Wikesjö, U. M. E., M. Qahash, et al. (2009). "Bone morphogenetic proteins for periodontal and alveolar indications; biological observations – clinical implications." Orthodontics & Craniofacial Research **12**(3): 263-270.

Windisch, P., A. Sculean, et al. (1999). "GTR with three different types of membranes in the treatment of intrabony periodontal defects: three-year results in sixty consecutive cases." J Long Term Eff Med Implants **9**(3): 235-246.

Xianmiao, C., L. Yubao, et al. (2009). "Properties and in vitro biological evaluation of nano-hydroxyapatite/chitosan membranes for bone guided regeneration." Materials Science and Engineering: C **29**(1): 29-35.

Xiao, X., R. Liu, et al. (2009). "Preparation and characterization of hydroxyapatite/polycaprolactone-chitosan composites." Journal of Materials Science: Materials in Medicine **20**(12): 2375-2383.

Yamaguchi, I., S. Itoh, et al. (2003). "The chitosan prepared from crab tendons: II. The chitosan/apatite composites and their application to nerve regeneration." Biomaterials **24**(19): 3285-3292.

Yan, X. Z., F. Rathe, et al. (2012). "The effect of enamel matrix derivative (Emdogain(R)) on gene expression profiles of human primary alveolar bone cells." Journal of Tissue Engineering Regenerative Medicine **11**(10).

Yao FL, C. W., Wang H, Liu HF, Yao KD, Sun PC, (2003). "A study on cytocompatible poly (chitosan-g-L-lactic acid)." Polymer **44**: 6435-6441.

Yi, H., L. Q. Wu, et al. (2005). "Biofabrication with chitosan." Biomacromolecules **6**(6): 2881-2894.

Yomota, C., T. Komuro, et al. (1990). "[Studies on the degradation of chitosan films by lysozyme and release of loaded chemicals]." Yakugaku Zasshi **110**(6): 442-448.

Yoshida, A., T. Miyazaki, et al. (2004). "Preparation of bioactive chitosan-hydroxyapatite nanocomposites for bone repair through mechanochemical reaction." Materials Transactions **45**(4): 994-998.

Yun, Y.-R., J. E. Won, et al. (2010). "Fibroblast Growth Factors: Biology, Function, and Application for Tissue Regeneration." Journal of Tissue Engineering **1**(1).

Zajac, A., J. Hanuza, et al. (2015). "Determination of N-acetylation degree in chitosan using Raman spectroscopy." Spectrochimica Acta Part a-Molecular and Biomolecular Spectroscopy **134**: 114-120.

Zakaria, S. M., S. H. Sharif, et al. (2013). "Nanophase Hydroxyapatite as a Biomaterial in Advanced Hard Tissue Engineering: A Review." Tissue Engineering Part B-Reviews **19**(5): 431-441.

Zellin G., Gritli-Linde A., Linde A. Healing of mandibular defects with differen biodegradable and non-biodegradable membranes: an experimental study in rats Biomaterials, **16** (1995), 601–609

Zhang, Y., M. Ni, et al. (2003). "Calcium phosphate-chitosan composite scaffolds for bone tissue engineering." Tissue Engineering. **9**(2): 337-345.

Zhang, Y. and M. Zhang (2002). "Calcium phosphate/chitosan composite scaffolds for controlled in vitro antibiotic drug release." Journal of Biomedical Materials Research **62**(3): 378-386.

Zhang, Y. Z., V. J. Reddy, et al. (2010). "Enhanced Biomineralization in Osteoblasts on a Novel Electrospun Biocomposite Nanofibrous Substrate of Hydroxyapatite/Collagen/Chitosan." Tissue Engineering Pt A **16**(6): 1949-1960.

Zhang, Z. and H. Cui (2012). "Biodegradability and biocompatibility study of poly(chitosan-g-lactic acid) scaffolds." Molecules **17**(3): 3243-3258.

Zhao, L. and J. Chang (2004). "Preparation and characterization of macroporous chitosan/wollastonite composite scaffolds for tissue engineering." Journal of Materials Science: Materials in Medicine **15**(5): 625-629.

Zoldners, J., T. Kiseleva, et al. (2005). "Influence of ascorbic acid on the stability of chitosan solutions." Carbohydrate Polymers **60**(2): 215-218.

Zuo, W., M. Zhu, et al. (2005). "Experimental study on relationship between jet instability and formation of beaded fibers during electrospinning." Polymer Engineering and Science **45**(5): 704-709.

Appendix 1

Mentoring MSc (Biomaterials and Regenerative Medicine and Dental Biomaterials) and Undergraduate Students for final year Project

- Adim De

  (Undergrad and MSc 2012-14)

- Jithendra Ratnayake

  (Undergrad 2012-13)

- Niranjan Ramesh (MSc 2012-13)
- Rebecca Kalvanes (MSc 2012-13)
- Shariq Najeeb (MSc 2013-14)
- Shehriar Hussain (MSc 2013-14)
- Ying Huang (MSc 2013-14)
- Nathan Kucko (MSc 2013-14)
- Didar Dousiken (MSc 2014-15)
- Arqam Najmi (MSc 2014-15)
- Nisha Nair (MSc 2014-15)
- Daniella (MSc 2014-15)
- Ahmed Rafikan (MSc 2014-15)

The morphometric analysis was made using SEO Image Lab Bio (Sumy, Ukraine, license number 27335). We made 10 histological slides from each samples (5 from deep zone and 5 – from superficial). Each slide was divided into 6 zones that were captured using the light microscope "OLYMPUS".We measured the square of empty pores, as well as fibrous tissue and osteoid that filled pores in each from 6 zones. Than we calculated the percentage of these parameter in each slide and sample in total. Cells and fibroblast density was calculated for 1 mm^2 in each slide and calculated for sample in total. Data are expressed as mean ± SEM. Statistical significance was defined as □ ≤ 0.05, and these values were calculated using SPSS software, version 21.0.

First time point

	ASa-CH	ASa-CH:HA	ACa-CH	ACa-CH:HA
Empty pores	58.6±2.6	42.5±3.1 *p=0.002*	54.1±1.8	38.6±2.3 *p=0.0003*
Fibrous tissue	24.8±1.6	21.7±0.9 *p=0.12*	22.3±1.2	19.4±1.4 *p=0.14*
Osteoid	-	12.9	-	13.7
Cell density	23.5±1.2	45.2±3.7 *p=0.0002*	19.8±2.5	39.6±4.1 *p=0.002*
Fibroblast	4.6±0.4	11.6±0.8 *p=0.0001*	3.9±0.5	13.3±1.2 *p=0.0001*

Morphometric parameters of Chitosan scaffolds in 30 days after the bone implantation. Bone, fibrous tissue and remnant of scaffold - % from slide surface, osteoblast, osteocyte and fibroblast – number per 1 mm^2.

	ASa-CH	ASa-CH:HA	ACa-CH	ACa-CH:HA
Bone tissue	35.6±2.8	49.2±1.4 *p=0.001*	31.8±1.9	46.3±4.2 *p=0.01*
Fibrous tissue	11.5±1.3	3.9±0.7 *p=0.0004*	9.4±0.9	4.3±0.5 *p=0.0006*
Remnant of scaffold	-	5.9±0.3	-	3.5±0.4
Osteoblast	16.5±1.2	27.4±1.6 *p=0.0003*	19.3±2.1	31.9±4.2 *p=0.02*
Osteocyte	4.3±0.8	3.7±0.5 *p=0.53*	5.7±0.8	4.6±0.4 *p=0.45*
Fibroblast	5.3±0.5	2.8±0.4 *p=0.002*	4.8±0.3	3.2±0.7 *p=0.06*

Low molecular weight CH: HA 50:50 stained at Day 7 of seeding with hES-MP's Cells on scaffolds labelled with DAPI (conc.) and FITC (conc.) for (incubation period). Both DAPI and FITC excited with 800nm and emission collected with two filter BP 435-485 for DAPI and BP 500-550 for FITC. (Images are taken using water dipping lenses at 40X magnification

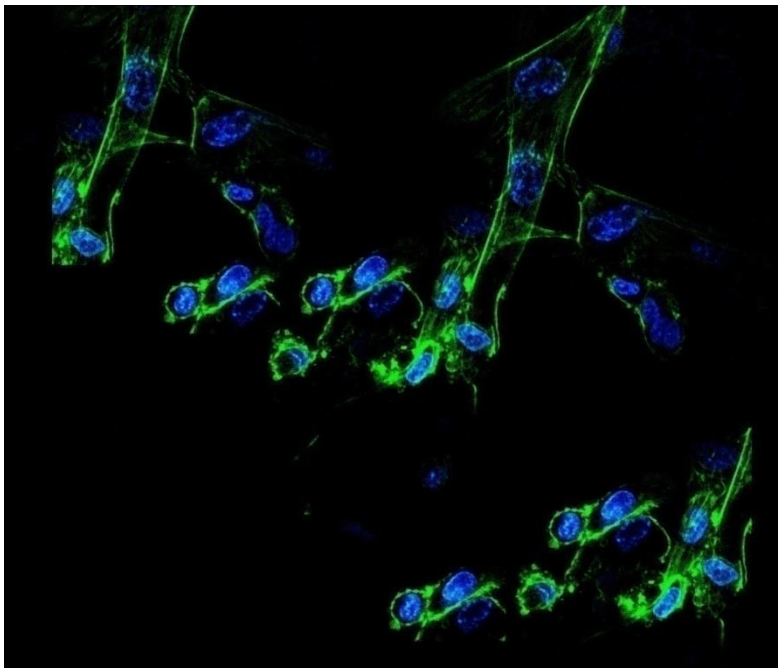

Commercial Hydroxyapatite used in the project, SEM images of HA flower taken from the bottom surface of CH HA solvent casted membranes. SEM analysis for particle size (Plasma Biotal, batch No P220) and

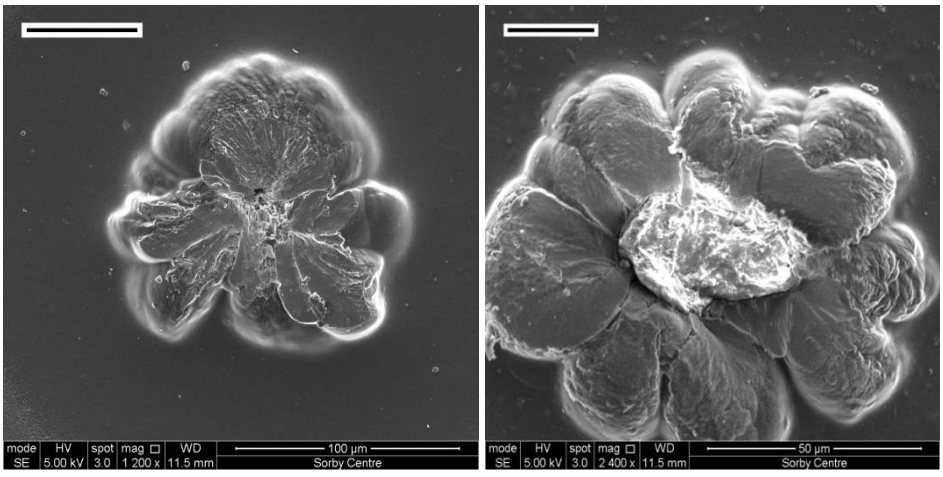

Particle size analysis of the Hydroxyapatite used, range can be seen from 0.5 ±2 to 12±1 µm conducted on Malvern MAstersizer 3000® Hydro EV wet dispersion unit, UK.

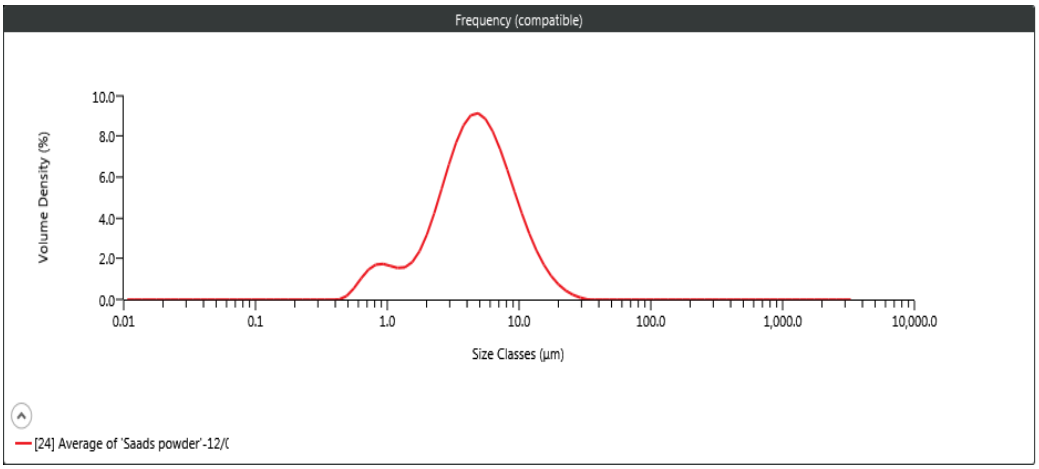

Spread of collagen on random aligned and control scaffolds at different time points

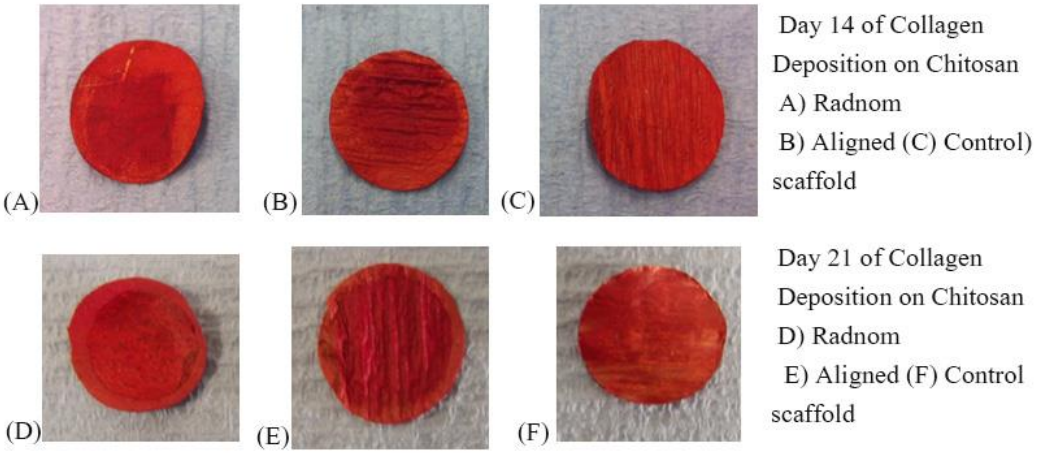

Example of the Drug release graphs, Absorbance plotted against Wavenumbers (nm), Reading measured at 270 nm

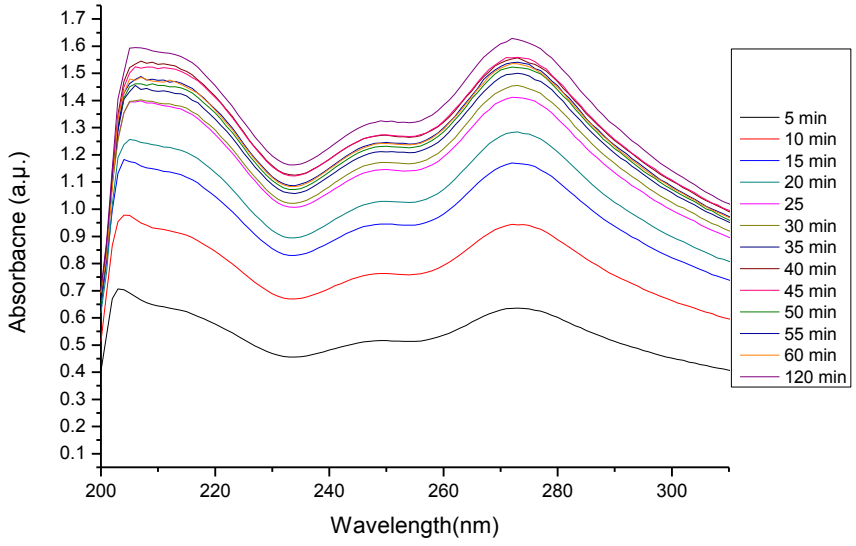

MG63 seeded on NaTPP cross linked FG samples at 0, 5 and 10 wt/v % , Results shown are 24hrs absorbance value taken by conducting Alamar blue.

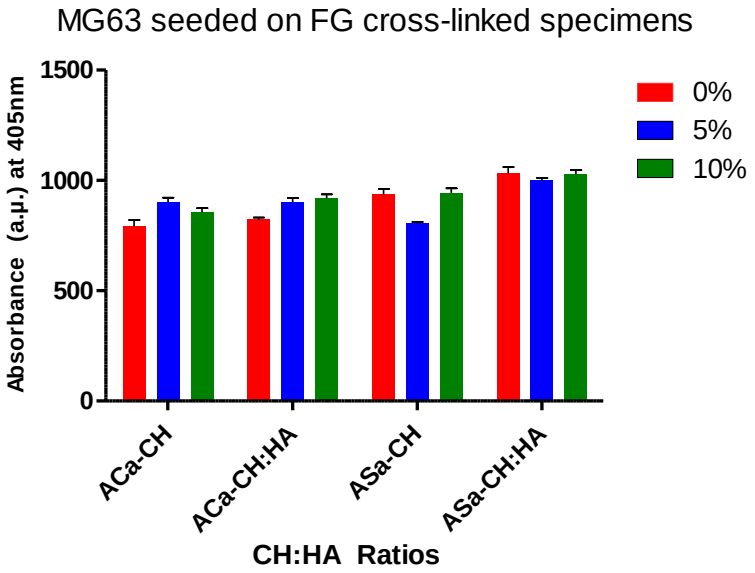

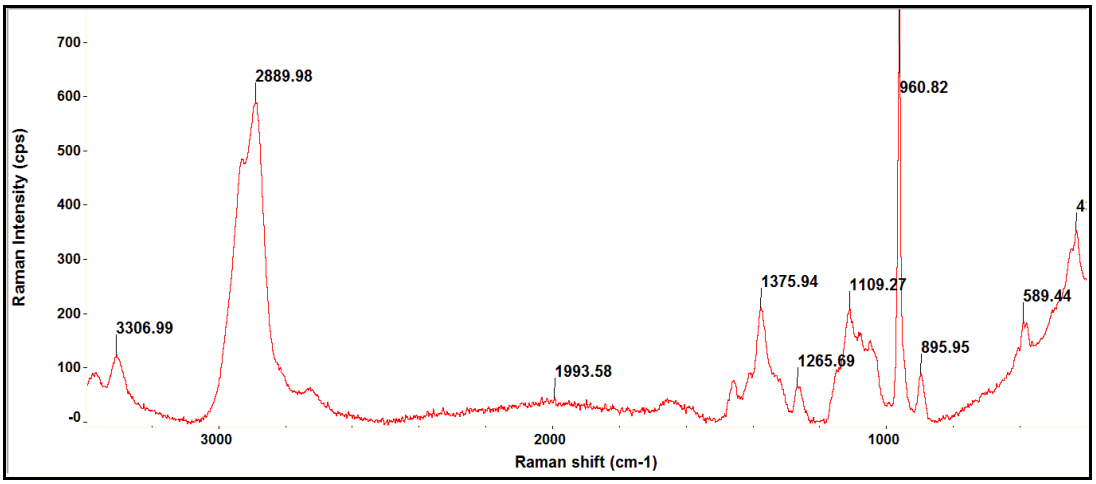

Raman Spectra of chitosan hydroxyapatite composite membrane, HAp shows a strong and narrow adsorption band at 962-964 cm-1. This band appears also in IR since it is given by the -P-O stretching bond. For the biological apatites or for synthetic ones this band is more or less shifted to higher or lower wavenumber. The shift in peaks can be used to study structural conformations, kinetic investigations and formation of new apatite phases could also be detected by these changes.

Colony forming unit (CFU) counted while performing antimicrobial tests with Porphyronomas gingivalis

Uncountable	Uncountable	Uncountable	uncountable
44 (144)	5 0 (32)	23 (75)	32(104)
5	17	14	8
4	5	2	-

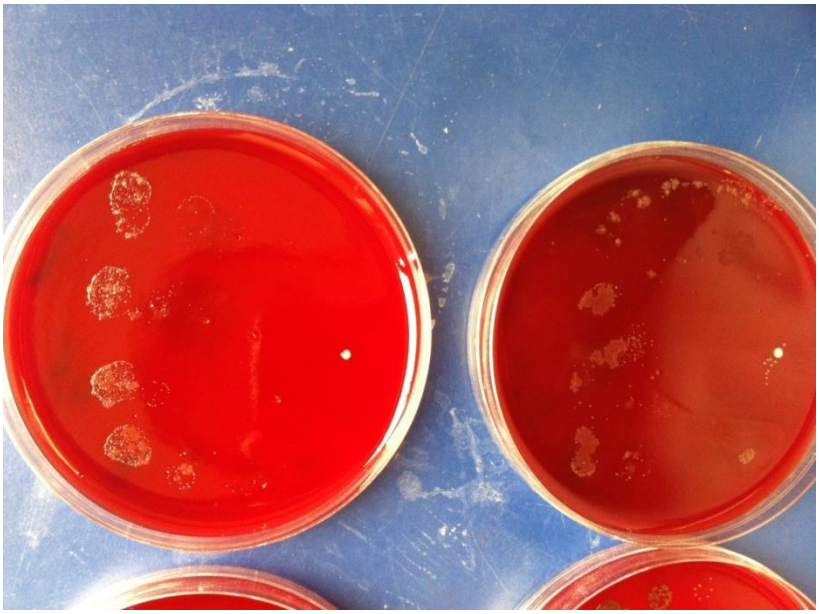

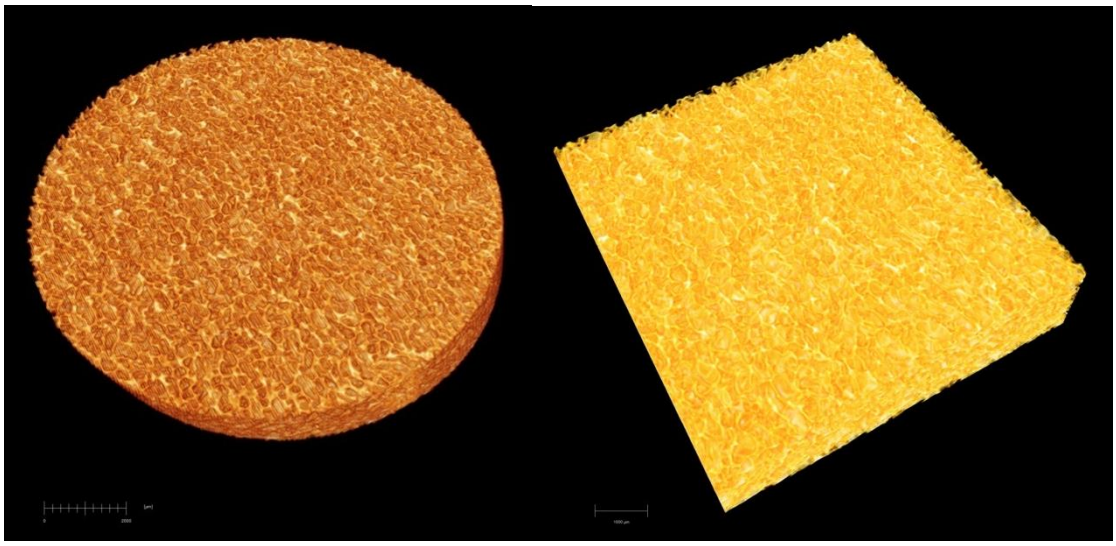

ASa-CH full sample and Cutt of region middle

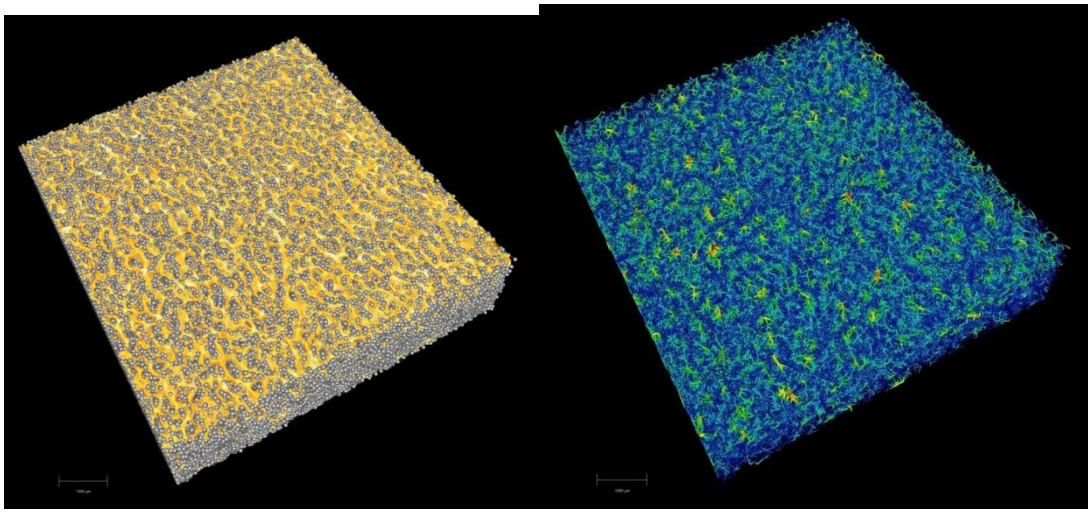

Regional materials and pores and pore structure network

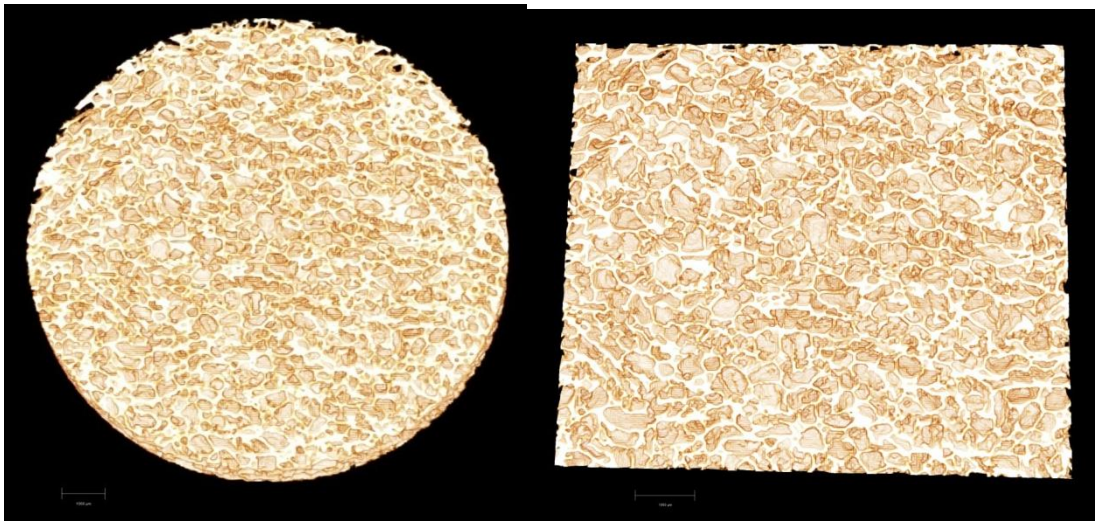

ASa-CH:HA full sample and Cutt of region middle

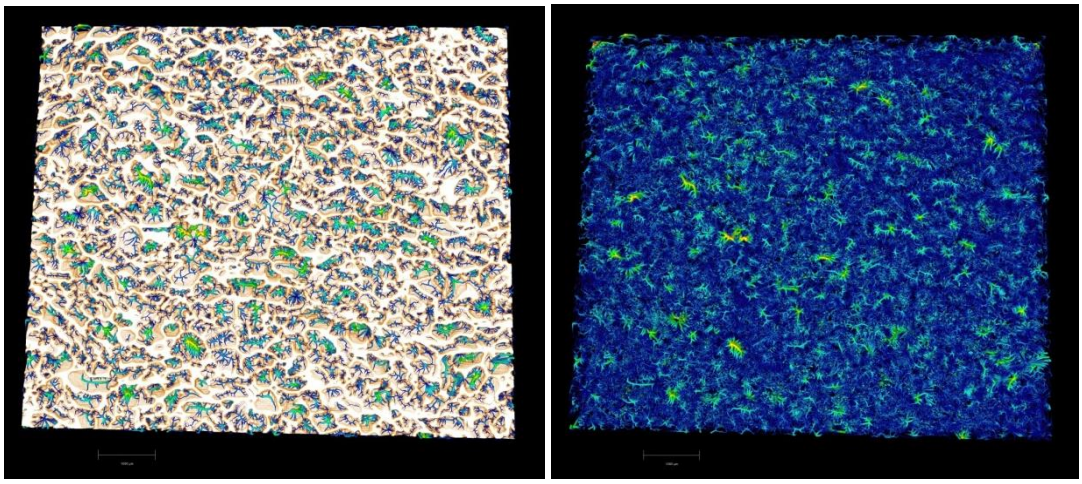

Regional materials and pores and pore structure network

Appendix II

Accepted Manuscript

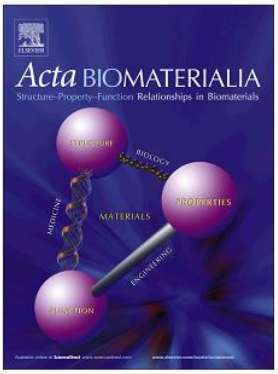

Freeze gelated porous membranes for periodontal tissue regeneration

Saad B. Qasim, Robin M. Delaine-Smith, Tobias Fey, Andrew Rawlinson, Ihtesham-Ur- Rehman

PII: S1742-7061(15)00218-4
DOI: http://dx.doi.org/10.1016/j.actbio.2015.05.001
Reference: ACTBIO 3694

To appear in: *Acta Biomaterialia*

Received Date: 11 January 2015
Revised Date: 2 April 2015
Accepted Date: 4 May 2015

Please cite this article as: Qasim, S.B., Delaine-Smith, R.M., Fey, T., Rawlinson, A., Rehman, I-U., Freeze gelated porous membranes for periodontal tissue regeneration, *Acta Biomaterialia* (2015), doi: http://dx.doi.org/10.1016/j.actbio.2015.05.001

Acta Biomaterialia 23 (2015) 317–328

Contents lists available at ScienceDirect

Acta Biomaterialia

journal homepage: www.elsevier.com/locate/actabiomat

Freeze gelated porous membranes for periodontal tissue regeneration

Saad B. Qasim [a], Robin M. Delaine-Smith [b], Tobias Fey [c], Andrew Rawlinson [d], Ihtesham Ur Rehman [a,*]

[a] Materials Science and Engineering Department, Kroto Research Institute, University of Sheffield, Sheffield S3 7HQ, United Kingdom
[b] Institute of Bioengineering, School of Engineering and Materials Science, Queen Mary University of London, Mile End Road, E1 4NS London, United Kingdom
[c] Department of Materials Science (Glass and Ceramics), University of Erlangen-Nuernberg, Martensstr. 5, 91058 Erlangen, Germany
[d] Academic Unit of Restorative Dentistry, School of Clinical Dentistry, University of Sheffield, Sheffield S10 2SZ, United Kingdom

ARTICLE INFO

Article history:
Received 11 January 2015
Received in revised form 2 April 2015
Accepted 4 May 2015
Available online 9 May 2015

Keywords:
Ascorbic acid
Guided tissue regeneration
Resorbable
Bioactivity
Osteoblasts

ABSTRACT

Guided tissue regeneration (GTR) membranes have been used for the management of destructive forms of periodontal disease as a means of aiding regeneration of lost supporting tissues, including the alveolar bone, cementum, gingiva and periodontal ligaments (PDL). Currently available GTR membranes are either non-biodegradable, requiring a second surgery for removal, or biodegradable. The mechanical and biofunctional limitations of currently available membranes result in a limited and unpredictable treatment outcome in terms of periodontal tissue regeneration. In this study, porous membranes of chitosan (CH) were fabricated with or without hydroxyapatite (HA) using the simple technique of freeze gelation (FG) via two different solvents systems, acetic acid (ACa) or ascorbic acid (ASa). The aim was to prepare porous membranes to be used for GTR to improve periodontal regeneration. FG membranes were characterized for ultra-structural morphology, physiochemical properties, water uptake, degradation, mechanical properties, and biocompatibility with mature and progenitor osteogenic cells. Fourier transform infrared (FTIR) spectroscopy confirmed the presence of hydroxyapatite and its interaction with chitosan. μCT analysis showed membranes had 85–77% porosity. Mechanical properties and degradation rate were affected by solvent type and the presence of hydroxyapatite. Culture of human osteosarcoma cells (MG63) and human embryonic stem cell-derived mesenchymal progenitors (hES-MPs) showed that all membranes supported cell proliferation and long term matrix deposition was supported by HA incorporated membranes. These CH and HA composite membranes show their potential use for GTR applications in periodontal lesions and in addition FG membranes could be further tuned to achieve characteristics desirable of a GTR membrane for periodontal regeneration.

1. Introduction

Destructive forms of periodontal disease such as chronic periodontitis affect the supporting tissues of teeth causing loss of gingival tissue, connective tissue, alveolar bone and periodontal ligaments. Initial treatment of these diseases includes the elimination of the primary causative factor (the dental plaque biofilm) by effective patient performed oral hygiene procedures and non-surgical treatment provided by a dentist or hygienist. While treatment usually halts disease progression, healing is characterized by repair of affected tissues with a long junctional epithelium, bone remodeling, and limited regeneration of the cementum and the lost periodontal ligaments that normally attach the tooth to the alveolar bone.

For these reasons, there has been much interest in developing methods for enhancing the regeneration of lost tissues in order to restore dental function and esthetics. This has been met with limited success using biologically active agents and guided tissue regenerative (GTR) or guided bone regeneration (GBR) membranes [1,2]. The ideal requirements for a GTR membrane include; a cell isolating occlusive biomaterial which meets minimum mechanical, physical, structural and biocompatibility requirements; ability to support organized and vascularized ingrowth and wound stabilization; protecting the underlying blood clot and thereby limiting the epithelial and unwanted connective tissue growth into the defect; promoting functional tissue regeneration from the relevant cells in the defect (avoiding healing by repair); and degrading in adequate time to provide space for newly formed periodontal tissue. The membrane surface facing the soft tissue should support cell attachment, growth and differentiation while the surface facing the defect acts as a biological seal [3].

A number of resorbable GTR/GBR membranes have now replaced the conventional non-resorbable membrane (expanded

* Corresponding author at: The Kroto Research Institute, North Campus, University of Sheffield, Broad Lane, Sheffield S3 7HQ, United Kingdom. Tel.: +44 (0) 114 222 5946; fax: +44 (0) 114 222 5943.
E-mail address: i.u.rehman@sheffield.ac.uk (I.U. Rehman).

http://dx.doi.org/10.1016/j.actbio.2015.05.001
1742-7061/